STUDIES ON THE EFFECT OF ADDITIVES ON HIGH TEMPERATURE SUPERCONDUCTOR $YBa_2Cu_3O_{7-\delta}$

K. V. PAULOSE

THESIS SUBMITTED TO
COCHIN UNIVERSITY OF SCIENCE AND TECHNOLOGY
FOR THE AWARD OF THE DEGREE
OF

DOCTOR OF PHILOSOPHY IN PHYSICS

REGIONAL RESEARCH LABORATORY
(C S I R)
TRIVANDRUM-695 019

AUGUST 1992

वैज्ञानिक एवं औद्योगिक अनुसंधान परिषद्
COUNCIL OF SCIENTIFIC & INDUSTRIAL RESEARCH
क्षेत्रीय अनुसंधान प्रयोगशाला, तिरुवनन्तपुरम
REGIONAL RESEARCH LABORATORY, TRIVANDRUM.
तिरुवनन्तपुरम-695019
TRIVANDRUM-695 019.
भारत
INDIA

Dr. K. Ravindran Nair
Scientist

CERTIFICATE

This is to certify that the thesis entitled "**STUDIES ON THE EFFECT OF ADDITIVES ON HIGH TEMPERATURE SUPERCONDUCTOR** $YBa_2Cu_3O_{7-\delta}$ " is an authentic record of the research work carried out by Mr. K.V. Paulose, M.Sc., M.Tech., under my supervision in partial fulfilment of the requirements for the **Degree of Doctor of Philosophy** of the Cochin University of Science and Technology, Cochin, and further that no part of this thesis has been presented before for any other degree.

K. Ravindran Nair

(K. Ravindran Nair)

Grams: 'CONSEARCH' Telex: 0435-232 Phones: PABX 76774/76769/76851/76852/70811

C O N T E N T S

		Page
	SUMMARY	i
	LIST OF PUBLICATIONS	vii
CHAPTER 1	GENERAL INTRODUCTION	1
1.1	Classification of materials based on band theory	1
1.2	The salient features of superconductors	2
1.3	Brief survey of conventional superconductors	3
1.4	The discovery of high T_c superconductivity in cuprates	3
1.5	N-type superconductors	10
1.6	The non-copper oxide superconductors	10
1.7	Preparative aspects of YBCO	11
1.8	Some basic parameters of YBCO	13
1.9	The crystal structure of $YBa_2Cu_3O_{7-\delta}$ and the importance of oxygen stoichiometry	14
1.10	Experimental studies on YBCO	19
1.11	Substitution studies in YBCO	27
1.12	Fabrication of YBCO for practical applications	29
	References	32
CHAPTER 2	EXPERIMENTAL METHODS	48
2.1	Preparation of ceramic samples	48
2.2	Resistivity measurements	49
2.3	Current density measurements	53
2.4	Thermoelectric power measurements (TEP)	55
2.5	X-ray powder diffraction studies	59
2.6	Scanning electron microscopy	59
2.7	Measurement of dielectric properties	61
	References	62

		Page
CHAPTER 3	EFFECT OF VARIOUS ADDITIVES ON HIGH TEMPERATURE SUPERCONDUCTOR $YBa_2Cu_3O_{7-\delta}$: (ADDITIVES Nb_2O_5, Sb_2O_3, SnO_2, ZrO_2 OR BeO)	63
3.1	Introduction	63
3.2	Studies on Nb_2O_5 added YBCO	66
3.3	Studies on Sb_2O_3 added YBCO	83
3.4	Studies on SnO_2 added YBCO	95
3.5	Studies on ZrO_2 added YBCO	103
3.6	Studies on BeO added YBCO	110
3.7	Discussion	116
3.8	Conclusion	122
	References	124
CHAPTER 4	SYNTHESIS OF Ba_2YAO_6 : A NEW CLASS OF CERAMIC COMPOUNDS FORMED IN $YBa_2Cu_3O_7$- A_xO_y SYSTEMS (A = Nb, Sb, Sn or Zr)	127
4.1	Synthesis and characterisation of Ba_2YNbO_6 (BYNO)	127
4.2	Synthesis and characterisation of Ba_2YSnO_6 (BYSnO)	139
4.3	Synthesis and characterisation of Ba_2YZrO_6 (BYZO)	150
4.4	Synthesis and characterisation of Ba_2YSbO_6 (BYSbO)	164
4.5	Discussion	172
4.6	Scope for future investigations on new compounds Ba_2YAO_6	177
	References	181

		Page
CHAPTER 5	**TRANSPORT PROPERTIES OF CERAMIC INSULATOR-SUPERCONDUCTOR COMPOSITES: A PERCOLATION STUDY**	183
5.1	Introduction	183
5.2	What is a percolation model	185
5.3	Studies on Ba_2YNbO_6-$YBa_2Cu_3O_{7-\delta}$ (BYNO-YBCO) composites	187
5.4	Studies on Ba_2YSnO_6-$YBa_2Cu_3O_{7-\delta}$ (BYSnO-YBCO) composites	199
5.5	Studies on Ba_2YSbO_6-$YBa_2Cu_3O_{7-\delta}$ (BYSbO-YBCO) composites	211
5.6	Studies on Ba_2YZrO_6-$YBa_2Cu_3O_{7-\delta}$ (BYZO-YBCO) composites	221
5.7	Discussion	232
	References	237
CHAPTER 6	**STUDIES ON NOBLE METAL-SUPERCONDUCTOR COMPOSITES Ag-YBCO**	238
6.1	Introduction	238
6.2	Preparation	239
6.3	Resistivity studies	241
6.4	Thermoelectric power	246
6.5	X-ray diffraction studies	251
6.6	Silver-YBCO composite system: A discussion	251
	References	254
CHAPTER 7	**CONCLUSION**	255

****

SUMMARY

The discovery of high temperature superconductivity in copper oxide based materials have generated enormous amount of activities on these materials because of their high scientific and technological potential. One of the immediate approaches towards search for new and better materials is made through doping studies. Doping studies can provide information about the fundamental mechanism behind the observed properties, improve the properties of existing materials, provide new materials and compounds with superior properties and tailor the properties of existing materials for specific technological applications. During doping, the dopants can go into the lattice of the host material or can react with the host material to form a secondary phase or can remain as an impurity. In conventional superconductors, additives and second phase along with the parent phase have prominent role in enhancing the current densities to several times especially in applied magnetic field through flux pinning. The presence of minor quantities of additives and impurities acts as flux trapping centers, so that extremely high values of current passes through the superconductor in presence of applied magnetic field. In the present investigation attempts have been made to study the effect of additives such as BeO, Nb_2O_5, Sb_2O_3, SnO_2 and ZrO_2 on high temperature superconductor $YBa_2Cu_3O_{7-\delta}$ (YBCO). The resultant variations on superconducting transition temperature, crystal structure, current density and the nature of secondary phases due to the additives were studied by XRD, SEM and resistivity measurements.

The thesis is divided into seven chapters. The first chapter gives a general introduction to superconductivity, the salient features of superconductors compared to conventional conductors, evolution of superconducting materials through the years till date. A brief survey of the important studies on $YBa_2Cu_3O_{7-\delta}$ compound and its crystal structure is also included.

The second chapter deals with the experimental methods and techniques such as solid state reaction to form compounds, XRD and SEM for characterisation, measurement techniques of current density, resistivity, thermopower etc. which have been used to study in the present investigation.

The effect of dopants such as BeO, Nb_2O_5, Sb_2O_3, SnO_2 and ZrO_2 on the structure of YBCO as well as its superconducting properties are described in chapter 3. It was found that the above dopants are not going appreciably into the lattice of YBCO. Also these dopants do not reduce the superconducting transition temperature of YBCO, if small quantities of the dopants are added. But x-ray powder diffraction studies have shown that all the above dopants except BeO react with YBCO and form a second phase during processing at 950^{o} C. The current densities of Nb_2O_5 and SnO_2 added YBCO increase by two to three times whereas the current densities of Sb_2O_3 and ZrO_2 added YBCO remain more or less same as that for pure YBCO. The most important finding observed in doped YBCO is the enhanced oxygen absorption compared to undoped YBCO. Usually the YBCO absorbs oxygen at a slow rate and in order to get

a superconducting orthorhombic phase, slow cooling of processed YBCO in an oxygen atmosphere is essential. If we quench the undoped YBCO from temperatures above 800°C, it will always result in tetragonal structure. But in the case of YBCO doped with Nb_2O_5, Sb_2O_3, SnO_2 and ZrO_2, it is found that a superconducting orthorhombic phase could be obtained even if we quench the processed YBCO from 950°C to room temperature in oxygen atmosphere. The enhanced oxygen absorption in doped YBCO is attributed to the modified microstructure with the formation of a second phase.

Experiments have been carried out to identify the secondary phase formed in YBCO due to the addition of different dopants. Chapter 4 describes the synthesis of a new class of ceramic compounds Ba_2YNbO_6, Ba_2YSbO_6, Ba_2YSnO_6 and Ba_2YZrO_6 from its constituent oxides. These compounds originally appeared as a secondary phase in $YBa_2Cu_3O_{7-\delta}$ due to the additives Nb_2O_5, Sb_2O_3, SnO_2 and ZrO_2. It has been reported by other researchers that the secondary phase formed due to the dopants Sb_2O_3, SnO_2 and ZrO_2 as Sb_2O_5, $BaSnO_3$ and $BaZrO_3$ respectively. But the present investigation proved that the secondary phases are Ba_2YAO_6 and not $BaAO_3$ where A = Nb, Sn, Sb or Zr. The above four compounds have been synthesised as a single phase material, optimised the processing conditions to get a highly sintered body with good mechanical strength. The crystal structure has been identified as cubic perovskite with relatively high value of lattice parameter $a \simeq 8.43$ A. The dielectric properties of the sintered bulk materials have been evaluated as a function of frequency at room temperature. The

chemical reactivity of the above ceramic compounds with the superconductor $YBa_2Cu_3O_{7-\delta}$ have been studied and found to be non-reactive. The thermal conductivity and the specific heat of the compounds have also been measured.

Almost all the known ceramic insulators react with YBCO at elevated temperatures of processing so that there was no attempt to prepare a ceramic insulator-superconductor composite. Thin film of $YBa_2Cu_3O_{7-\delta}$ has been prepared on single crystals of MgO, $LaAlO_3$ $SrTiO_3$ etc. But if we powder these and mix with $YBa_2Cu_3O_{7-\delta}$ and heat at 950^oC and above, we can see that the superconducting properties are destroyed. Due to the non-reactivity of the new compounds Ba_2YAO_6 with the superconductor $YBa_2Cu_3O_{7-\delta}$ ceramic insulator-superconductor composites have been prepared successfully for the first time. Chapter 5 deals with the preparation and characterisation of the insulator-superconductor composites. The composite systems studied at present are

$$Ba_2YNbO_6 - YBa_2Cu_3O_{7-\delta}$$

$$Ba_2YSbO_6 - YBa_2Cu_3O_{7-\delta}$$

$$Ba_2YSnO_6 - YBa_2Cu_3O_{7-\delta}$$

$$Ba_2YZrO_6 - YBa_2Cu_3O_{7-\delta}$$

The normal state percolation and superconducting state percolation behaviour of the ceramic insulator-superconductor composites have been studied extensively based on conductivity measurements. The

present investigation proved that YBCO forms composites with Ba_2YSnO_6 and Ba_2YNbO_6 throughout the entire volume range. The percolation theory for insulator-metal composites holds fairly good for the ceramic insulator-superconductor composites, Ba_2YSnO_6-$YBa_2Cu_3O_{7-\delta}$ and Ba_2YNbO_6-$YBa_2Cu_3O_{7-\delta}$ systems. In the case of Ba_2YSbO_6-$YBa_2Cu_3O_{7-\delta}$ and Ba_2YZrO_6-$YBa_2Cu_3O_{7-\delta}$ systems, the percolation theory holds good for low volume percentage of insulating phase. But for higher volume percentages, the model deviates considerably. The percolation threshold values obtained for the normal state transport properties and superconducting states are in the same range. In the case of Ba_2YNbO_6-$YBa_2Cu_3O_{7-\delta}$ and Ba_2YSnO_6-$YBa_2Cu_3O_{7-\delta}$, the threshold values are around 20 vol % of $YBa_2Cu_3O_{7-\delta}$ whereas for Ba_2YSbO_6-$YBa_2Cu_3O_{7-\delta}$ composite it is around 30 vol % and for Ba_2YZrO_6-$YBa_2Cu_3O_{7-\delta}$ composite, the threshold volume is around 35 vol % for $YBa_2Cu_3O_{7-\delta}$. XRD and SEM studies were carried out to see the phase combatibility and reactivity of the composites. The studies have proved that practically there is no reaction between YBCO and Ba_2YAO_6 if the processing temperatures are optimised below 1000^oC.

In chapter 6 the preparation of a normal metal-ceramic superconductor composite Ag-$YBa_2Cu_3O_{7-\delta}$ has been described. Its superconducting properties, normal state transport properties were studied and explained by the percolation theory.

Finally chapter seven gives a conclusion of the above investigation, the identification of the secondary phases formed

in $YBa_2Cu_3O_{7-\delta}$ due to the dopants Nb_2O_5, Sb_2O_3, SnO_2 and ZrO_2, preparation of the compounds as a single phase material from their constituent oxides and confirmation of the secondary phase as it is by studying the phase combatibility etc. Further it is suggested that the new compounds synthesised in chapter 4 can be used as a possible substrate for the deposition of thin films of $YBa_2Cu_3O_{7-\delta}$ primarily due to the non-reactivity.

LIST OF PUBLICATIONS

1. **Effect of Beryllia substitution and addition in $YBa_2Cu_3O_{7-\delta}$ compound**
   Appl. Phys. Lett., 58 (2) 176 (1991)

2. Observation of superconductivity in Nb_2O_5 doped $YBa_2Cu_3O_{7-\delta}$ compound by Rapid Quenching
   Jpn. J. Appl. Phys.,30, L 458 (1991)

3. Enhanced oxygen absorption in SnO_2 doped $YBa_2Cu_3O_{7-\delta}$
   Solid State Commun., 79, 815 (1991)

4. Superconductivity in $YBa_2Cu_3O_{7-\delta}$-ZrO_2 systems
   Supercond. Sci. Technol., 4, 98 (1991)

5. High temperature superconductivity in air quenched $YBa_2Cu_3O_{7-\delta}$ doped with Sb_2O_3
   Appl. Phys. Lett., 59 (10), 1251 (1991)

6. Thermopower of $YBa_2Cu_3O_{7-\delta}$ -Ag composite
   J. American Ceram. Society, 74, 2679 (1991)

7. Synthesis of YBa_2SbO_6 : A possible new substrate for $YBa_2Cu_3O_7$ thin films
   Supercond. Sci. Technol., 5, 31 (1992)

8. YBa_2NbO_6 : Synthesis, properties and compatibility with $YBa_2Cu_3O_7$
   Physica C, 193, 273 (1992)

9. $YBa_2SnO_{5.5}$: A new phase in $YBa_2Cu_3O_{7-\delta}$ -SnO_2 system
   Jpn. J. Appl. Phys. Pt. 1, 31, 1323 (1992)

10. Synthesis of Ba_2YZrO_6 : A new phase in $YBa_2Cu_3O_7$-ZrO_2 system and its suitability as a substrate material for YBCO films
Solid State Commun. (In press)

11. Thermal and elastic properties of Ba_2YZrO_6
Physica Status Solidi (communicated)

12. Transport properties of $YBa_2Cu_3O_7$ - YBa_2SnO_6 percolation system
Phys. Rev. Lett. (communicated)

13. Percolation and superconducting properties of ceramic-insulator-superconductor composite Ba_2YNbO_6-$YBa_2Cu_3O_7$
(to be communicated)

14. Preparation and properties of Ba_2YZrO_6-$YBa_2Cu_3O_7$ composites
(to be communicated)

15. Ceramic insulator-superconductor composite Ba_2YSbO_6-$YBa_2Cu_3O_7$: A percolation study
(to be communicated)

CHAPTER 1

GENERAL INTRODUCTION

The discovery of high temperature superconducting transition (1-8) in copper oxide based materials, has generated enormous amount of activities in the field of superconductors because of its high scientific and technological potential. The special features of superconductors compared to conventional conductors are the dissipationless current carrying capacity in presence of strong magnetic field and the Josephson phenomenon observed in weakly-coupled junctions. These two features of superconducting materials have been exploited into technological devices where the efficiency is several orders higher compared to conventional materials and in certain cases we cannot expect an equal par in normal conductors and materials. But the main difficulty with the classical superconductors are that they exhibit superconductivity only at extremely low temperatures, where cooling to such lower temperatures is very expensives and have lot of practical limitations. But the break through achieved in increasing the superconducting transition to relatively higher temperatures has widened the scope for its use into reality.

1.1 CLASSIFICATION OF MATERIALS BASED ON BAND THEORY

Band theory of solids explains the electrical conductivity in solids (9-11). Accordingly materials are classified into

(i) insulators, (ii) semi-conductors and (iii) metals. In insulators there exists a wide energy gap between the conduction band and valence band whereas in metals, the valence band and conduction band overlap together, thus there is no energy gap. In semiconductors the energy gap lies in between insulators and metals.

Superconductors belong to the group of metallic materials (10, 11). The important determinant of the properties of the superconducting state is the energy gap that exists between the lowest excitation state and the energy levels of the ground state of the system. For electrons in metals, the allowed states form a continuous spectrum in energy, so that any arbitrarily small amount of energy added to a system in its ground state can cause an excitation from ground state. The energy gap plays an important role in determining the properties of a superconductor compared to normal metals.

1.2 THE SALIENT FEATURES OF SUPERCONDUCTORS

Superconductors have four important characteristics (9-12). (i) Zero resistivity which means that a superconductor is an electrically perfect conductor. In addition, superconductors have three critical parameters; critical temperature T_c, critical magnetic field H_c and critical current density J_c. It has been recognised that the most difficult parameter to be developed is high critical current density J_c. (ii) The Meissner effect, i.e. superconductors show perfect diamagnetism. (iii) The Josephson effect, an electric property in the superconductor/insulator/superconductor triple layers and weakly coupled junctions. If we apply the current through the

insulator, tunnelling effect is observed. We can use this effect for switching systems. (iv) Quantization of magnetic field occurs. A magnetic flux is measured digitally by the minimum amount of flux ($\frac{2\ h}{e}$) . Zero resistivity and Meissner effect are related to electric power applications where large values of current and magnetic fields are coming into picture. The Josephson effect and quantization are related to the microelectronic applications.

1.3 BRIEF SURVEY OF CONVENTIONAL SUPERCONDUCTORS

Superconductivity was first observed (13) by Kamerlingh Onnes in mercury in 1911, three years after he first liquified the He gas. Then the phenomenon was observed in many metals and alloys and inorganic compounds. Tables 1.1 and 1.2 list the important superconducting metals, alloys and inorganic compounds (9, 14). It is now believed (10, 11) that supercurrents are being carried by Cooper pairs and have been explained by BCS theory.

1.4 THE DISCOVERY OF HIGH T_c SUPERCONDUCTIVITY IN CUPRATES

Eventhough superconductivity was observed in perovskite materials (15) and some tungsten bronze compounds (16) long before, the superconducting transition temperatures in those materials were very low. In 1986 Bednorz and Müller first announced (1) the discovery of high T_c superconductivity in $La_{2-x}\ Ba_x CuO_4$ with a transition temperature of 30 K. T_c further increased to 35 K when Ba was replaced with Sr. Soon after superconductivity was observed in $YBa_2Cu_3O_{7-\delta}$ compound with T_c of 92 K (2, 3), bismuth alkaline earth cuprates with T_c of 110 K (4, 5) and thallium alkaline earth

Table 1.1: Superconductivity of some selected metals and alloys (After 9)

Compound	T_c (K)
$(SN)_x$ polymer	0.26
Ti_2Co	3.44
La_3In	10.4
NbN	16.0
V_3Ga	16.5
V_3Si	17.1
Nb_3Al	17.5
Nb_3Sn	18.05
Nb_3Ge	23.2

Table 1.2: Superconductivity of some selected inorganic compounds (After 14)

Compounds	T_c (K)
$SrTiO_3$ (perovskite)	0.7
A_xWO_3 (tungsten bronze)	6
A_xReO_3 (bronze)	4
A_xMoO_3 (bronze)	4
$Li_xTi_2O_4$ (perovskite)	13.7
Ba(Pb Bi)O_3 (perovskite)	13
TiO	2.3
$LiTi_{1.1}S_2$	10-15
$Mo_{6-x}A_xS_6$ (A = Ag,Cu)	2.5-13
$CuRh_2S_4$	4.8
$CuRh_2Se_4$ (chalcogenides)	3.5

cuprates with T_c of 125 K (6-8). The compound $La_{2-x}Sr_xCuO_4$ discovered by Müller with the general formula A_2BO_4 (A = La) and (B = Cu) possess K_2NiF_4 structure where the B ions interact only in the a-b plane. The structure of the A_2BO_4 complex oxides is related to the perovskite structure which is that of the ABO_3 complex oxide. In the K_2NiF_4 structure (see Fig. 1.1), the B atoms have the same environment as in perovskite, ie., six oxygen atoms arranged octahedrally, but A atoms have an unusual arrangement of nine oxygen atoms instead of the original twelve neighbours in perovskite ABO_3. The structure of $La_{2-x}Sr_xCuO_4$ is same as that shown in Fig. 1.1. La(Sr) occupies A site in the K_2NiF_4 structure and Cu the B sites. The unit cell parameters are a = 3.78 A and c = 3.23 A (16 A). The compound $YBa_2Cu_3O_{7-\delta}$ has an orthorhombic unit cell (a = 3.816 A, b = 3.883 A, c = 11.698 A) with an oxygen deficient perovskite structure (Fig. 1.3) (34). The structure is discussed in detail in section 1.9.

The important rare earth cuprate superconductors are listed in Table 1.3 and bismuth and thallium compounds are listed in Table 1.4 with their corresponding transition temperatures. All the above compounds are P type conductors (17, 18) and have CuO planes with layer structure.

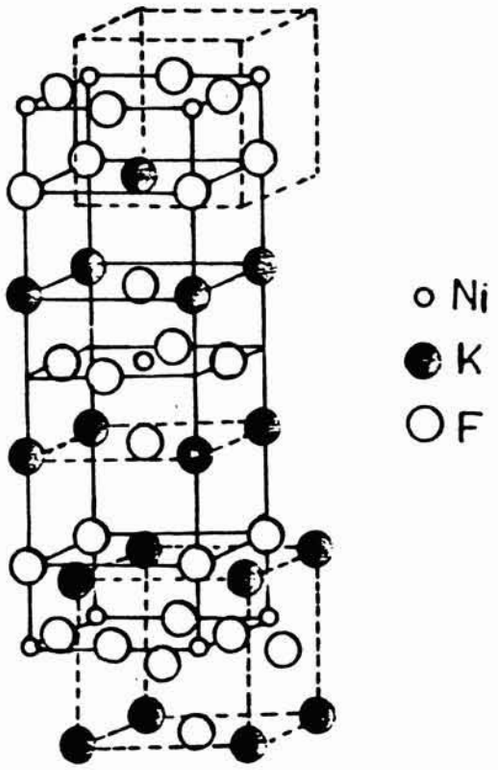

Fig. 1.1: Crystal structure of K_2NiF_4 type of oxides A_2BO_4

Table 1.3: Crystal symmetry and unit cell parameters of rare earth cuprate superconductors along with T_c

Oxide	Symmetry	Lattice parameter A			T_c K
		a	b	c	
$La_{1.85}Sr_{.15}CuO_4$	Tetragonal	3.78		13.23	35
$YBa_2Cu_3O_{7-\delta}$	Orthorhombic	3.816	3.883	11.698	92
$YBa_2Cu_4O_{10}$	Tetragonal	3.86		27.24	80
*$Pb_2Sr_2ACu_3O_{8-\delta}$	Orthorhombic	5.40	5.43	15.74	70

*(A = Lanthanide or Lanthanide + Sr or Ca)

Table 1.4: Crystal symmetry and unit cell parameters of bismuth and thallium cuprates along with T_c

Oxide	Symmetry	Lattice parameter (A)			T_c
		a	b	c	(K)
$Bi_2Sr_2CuO_6$	Orthorhombic	5.36	5.37	24.62	20
$Bi_2Sr_2CaCu_2O_8$	Orthorhombic	5.40	5.41	30.78	85
$Bi_2Sr_2Ca_2Cu_3O_{10}$	Orthorhombic	5.40	5.41	37.18	110
$Tl_2Ba_2CuO_6$	Tetragonal	3.86		23.24	6-80
$Tl_2Ba_2CaCu_2O_8$	Tetragonal	3.86		29.39	105
$Tl_2Ba_2Ca_2Cu_3O_{10}$	Tetragonal	3.85		35.6	125
$Tl_2Ba_2Cu_3Cu_4O_{12}$	Tetragonal	3.85		42.0	105
$TlBa_2CaCu_2O_7$	Tetragonal	3.83		12.68	65
$TlBa_2Ca_2Cu_3O_9$	Tetragonal	3.84		15.88	120
$TlBa_2Ca_3Cu_4O_{11}$	Tetragonal	3.85		19.10	70

1.5 N-TYPE SUPERCONDUCTORS

In early 1989, Tokura et al. (19) reported n-type superconductivity in the Nd-Ce-Sr-Cu-O system. The general formula of the compound is $Nd_{2-x-y}\ Ce_xSr_yCuO_4$ with T_c = 28 K. In these compounds the carriers are electrons. The $Nd_{1.4}Ce_{0.2}Sr_{0.4}CuO_4$ has tetragonal structure with a = 3.85 A and c = 12.50 A. Some new compounds with n-type superconductivity have been reported (20). According to Markert et al. (20) $Pr_{1.85}Th_{.15}CuO_{4-y}$ and $Eu_{1.85}Ce_{.15}\ CuO_{4-y}$ with a T_c of 23 K and 13 K respectively are electronic superconductors.

1.6 THE NON-COPPER OXIDE SUPERCONDUCTORS

Superconductivity was observed in ceramic perovskite material $BaPb_{1-x}\ Bi_xO_3$ (x = 0.0-0.35) by Sleight et al. (21) with a T_c of 13 K. In 1988 Cava et al. (22) discovered superconductivity in $Ba_{1-x}\ k_xBiO_3$ with a T_c of 30 K and many groups have reproduced superconductivity in $Ba_{1-x}\ K_xBiO_3$ with same T_c (23, 24). It has a cubic structure and the superconducting properties are highly isotropic in contrast to the copper oxide superconductors.

Kroto et al. (25) synthesised the cluster form of carbon, named fullerene of which C_{60} is the archetype. The alkali metal intercalation products of fullerenes show superconducting transition in K_3C_{60} with T_c = 20 K (26) and Rb_3C_{60} with T = 30 K (27). The superconductivity characteristic for these materials are very similar to those of $Ba(Pb/Bi)O_3$ and $(K/Ba)BiO_3$ with large

penetration depth λ = 2500 A^{o}, a short coherence length (ξ = 25 A^{o}), Landau Ginzberg parameter k = 100 expressing extreme type II behaviour (28) .

1.7 PREPARATIVE ASPECTS OF YBCO

1.7.1 Phase diagram of Y_2O_3-BaO-CuO system

Many workers have carried out the phase diagram studies of Y_2O_3-BaO-CuO system (29-31). These preliminary phase diagram studies established phase stability fields below liquidus temperature (around 950 ^{o}C) and among the many phases only YBCO has been clearly established to be a high T_c superconductor. The known compounds in this system have been given by Frase et al. (29). Karpinski et al. (32) carried out investigations on the high pressure phase diagram (1-3000 bar oxygen) in Y-Ba-Cu-O system. They found the existence of a multiphase region consisting of $YBa_2Cu_4O_8$ (124), $Y_2Ba_4Cu_7O_{14}$ (247) and $YBa_2Cu_3O_{7-\delta}$ (123) in the pressure range 50-2000 bar oxygen. The compound $YBa_2Cu_4O_8$ is also superconducting and has a T_c of 80 K (32).

1.7.2 Synthesis of $YBa_2Cu_3O_{7-\delta}$

Preparation of homogeneous and well defined single phase materials with uniform oxygen stoichiometry are necessary for evaluation of accurate physical parameters and for technological applications. YBCO has been prepared as a single phase material by solid state reaction method starting from stoichiometric amount of constituent oxides/carbonates or nitrates (33). In this method the powders

of different components in the appropriate ratio are mixed and heated at 900-950^{o} C in an oxygen atmosphere. YBCO obtained in this manner is oxygen defficient and non-superconducting. This compound is annealed in an oxygen atmosphere at 450-500^{o} C when it absorbs more oxygen and acquires the superconducting properties.

YBCO has been successfully synthesised from precursor powders made by co-precipitation of mixtures of hydroxides, carbonates, nitrates, oxalates, citrates and acetates (14,33-36). The sol-gel method also has been used to synthesise YBCO (37, 38). The advantage of these methods are that they yield fine powders having particle size less than 1 micron and a better homogeniety of phase. A major drawback of these processes are the side reactions of the constituent metal ions.

Large quantities of YBCO have been prepared by molten oxide process (39), hot compaction (40), rapid solidification processing (41) and aerosol flow reactor production (33).

1.7.3 Single crystal growth

To study the intrinsic properties of YBCO one should use single crystals. Many groups have tried to grow single crystals of YBCO (42-44). YBCO melts incongruently above 970^{o}C. So single crystals cannot be obtained by solidification of the melt. Only the flux method can be used to grow single crystals. The fluxes used are $BaCuO_2$ /CuO mixtures. Phase diagram studies (30,31,45) give an idea about the temperature at which YBCO is formed. Alkali

chlorides have also been used as fluxes (33). It is difficult to prepare large single crystals of YBCO. Usually flaky crystals of a few mm size are obtained by the flux method.

1.8 SOME BASIC PARAMETERS OF YBCO

Some of the important properties of YBCO have been summarized by Malozemoff et al. (46) and are as follows:

1. It is a type II superconductor

2. It is highly anisotropic

3. Hall carrier density = 4 x 10^{21} cm^{-3} (for a material of resistivity 400 $\mu\Omega$-cm just above T_c)

4. $$\frac{d\ H_{c2}}{dT} = \frac{2T}{K}$$

   BCS coherence length = 1.4 nm

   London penetration depth = 200 nm

   Mean freepath = 1.2 nm

5. $H_{c(0)}$ = 1 Tesla

6. $H_{c2(0)}$ = 120 Tesla

7. Critical current density (J_c)

   In bulk ceramic samples 10^3 A/cm^2 at 77 K

   In thin films 10^6 to 10^7 A/cm^2 at 77 K

   In melt textured ceramics 10^4 A/cm^2 at 77 K

8. Absolute thermopower at 303 K 3 μV/K

In the following, structure, oxygen stoichiometry, phase transition, superconducting transition temperature, resistivity and thermopower are discussed briefly.

1.9 THE CRYSTAL STRUCTURE OF $YBa_2Cu_3O_{7-\delta}$ AND THE IMPORTANCE OF OXYGEN STOICHIOMETRY

1.9.1 Structure

The structure of $YBa_2Cu_3O_{7-\delta}$ was deduced by x-ray powder diffraction method (47, 48) and also by neutron diffraction studies (49-53). YBCO has an oxygen defficient perovskite structure with orthorhombic symmetry (a = 3.816 A, b = 3.883 A and c = 11.698 A). The x-ray diffraction pattern with Cu-Kα radiation of YBCO is given in Fig. 1.2 and the lattice spacing with corresponding indices are given in Table 1.5. The XRD pattern for tetragonal $YBa_2Cu_3O_6$ is also given in Fig. 1.2 and the lattice spacing in Table 1.5.

Later more detailed studies on structure have been reported (54-56) using single crystals (Fig. 1.3). There are two crystallographically inequivalent sites for Cu atoms Cu (1) and Cu (2). The Cu (1) atoms are surrounded by four oxygen atoms, two at 1.942 A and two at 1.845 A. Here the oxygen atoms form near rectangles connected by vertices, and resulting in the Cu-O chains along b-axis. On the other hand Cu (2) is surrounded by four oxygen atoms two at 1.929 A and two at 1.96 A. A fifth oxygen is located at 2.30 A giving rise to a square pyramidal coordination for Cu forming puckered CuO_2 layers (57). The 01 and 05 oxygens are missing

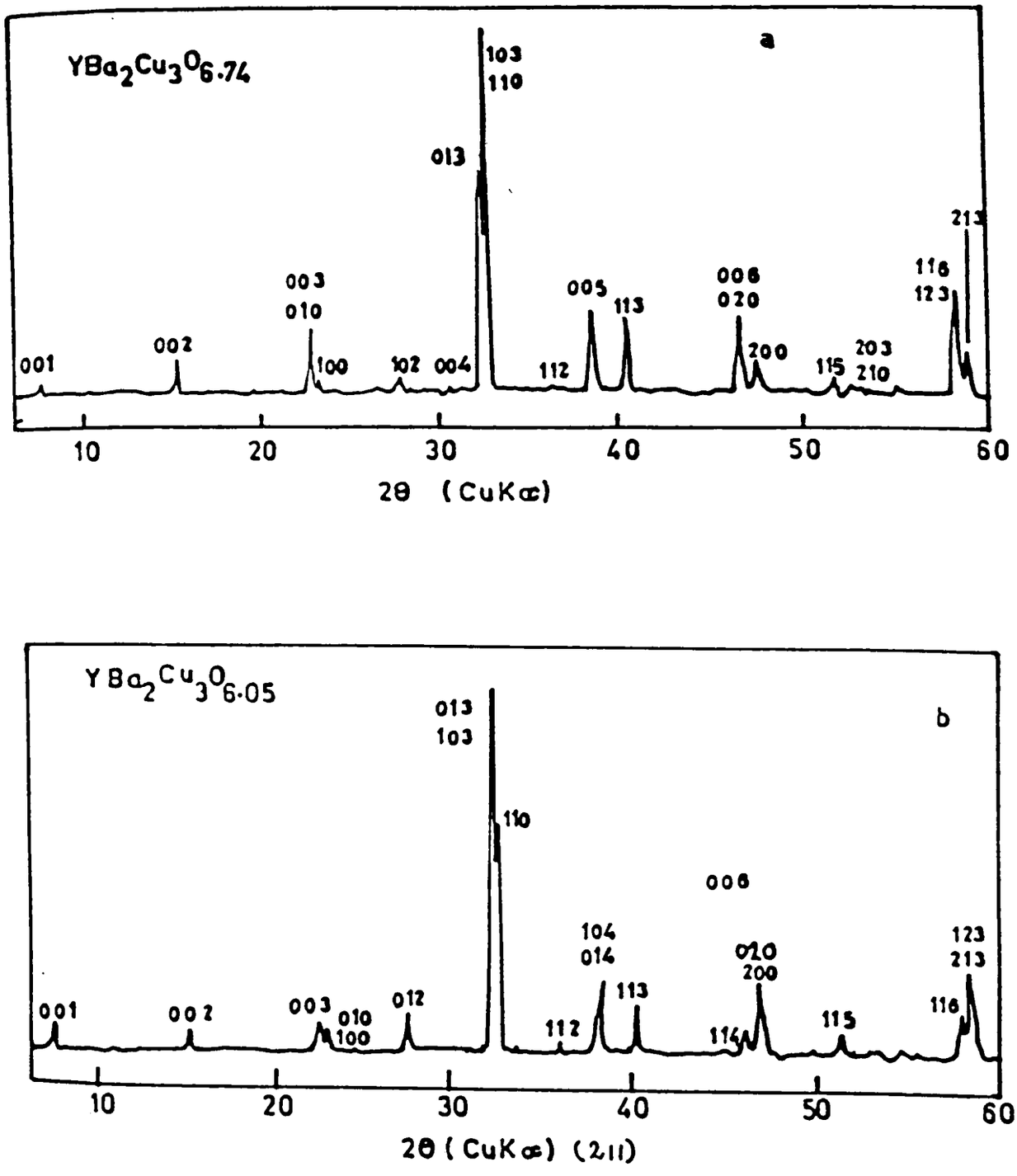

Fig. 12: X ray powder diffraction patterns of the orthorhombic phase (a) and the tetragonal phase (b) of $YBa_2Cu_3O_{7-\delta}$.

Table 1.5: X-ray Powder Data for $Ba_2YCu_3O_x$

$Ba_2YCu_3O_7$ a=3.816Å b=3.883Å c=11.698Å Pmmm						$Ba_2YCu_3O_6$ a=3.853Å c=11.780Å P4/mmm					
2θ obs	2θ calc	d_{calc}	I/I_o obs	I/I_o calc	hkl	hkl	I/I_o obs	I/I_o calc	d_{calc}	2θ obs	2θ calc
	7.56	11.70		2	0 0 1						
	15.15	5.849		3	0 0 2						
22.86	22.81	3.899	8	10	0 1 0						
	22.90	3.883		8	0 0 3	0 0 3	5	2	3.927	22.70	22.64
23.30	23.31	3.816	2	6	1 0 0	1 0 0	6	11	3.853	23.18	23.08
27.73	27.57	3.235	2	5	0 1 2						
27.90	27.92	3.196	4	9	1 0 2	1 0 2	10	8	3.221	27.76	27.67
32.60	32.54	2.751	50	89	0 1 3	1 0 3	100	100	2.750	32.65	32.56
32.88	32.84	2.727	100	96	1 1 0	1 1 0	49	36	2.725	32.95	32.87
	32.91	2.722		100	1 0 3						
33.75	33.81	2.651	1	2	1 1 1						
36.46	36.41	2.468	3	5	1 1 2	1 1 2	3	2	2.473	36.37	36.33
38.57	38.48	2.340	17	6	0 1 4						
	38.54	2.336		11	0 0 5	0 0 5	11	6	2.356	38.14	38.20
38.75	38.79	2.321	1	4	1 0 4	1 0 4	10	3	2.340	38.57	38.48
40.16	40.41	2.232	19	28	1 1 3	1 1 3	15	12	2.238	40.31	40.29
46.68	46.58	1.950	33	17	0 0 6	0 0 6	13	8	1.963	46.22	46.21
	46.79	1.941		31	0 2 0						
47.63	47.66	1.908	17	29	2 0 0	2 0 0	32	26	1.927	47.20	47.18
51.58	51.51	1.774	5	6	1 1 5	1 1 5	8	2	1.782	51.28	51.26
52.68	52.52	1.742	4	2	0 1 6	1 0 6	1	2	1.749	52.31	52.29
	52.66	1.738		2	0 2 3						
52.87	52.91	1.730	3	2	1 2 0	2 1 0	3	3	1.723	53.07	53.15
53.43	53.46	1.714	6	2	2 0 3						
	53.51	1.712		2	2 1 0						
55.00	54.91	1.671	3	2	0 0 7						
55.37	55.37	1.659	2	3	1 2 2	2 1 2	5	2	1.654	55.55	55.57
55.88	55.95	1.643	1	2	2 1 2						
58.26	58.21	1.585	49	37	1 1 6	1 1 6	16	13	1.593	57.85	57.89
	58.31	1.582		32	1 2 3						
58.87	58.90	1.568	25	32	2 1 3	2 1 3	45	35	1.578	58.42	58.49

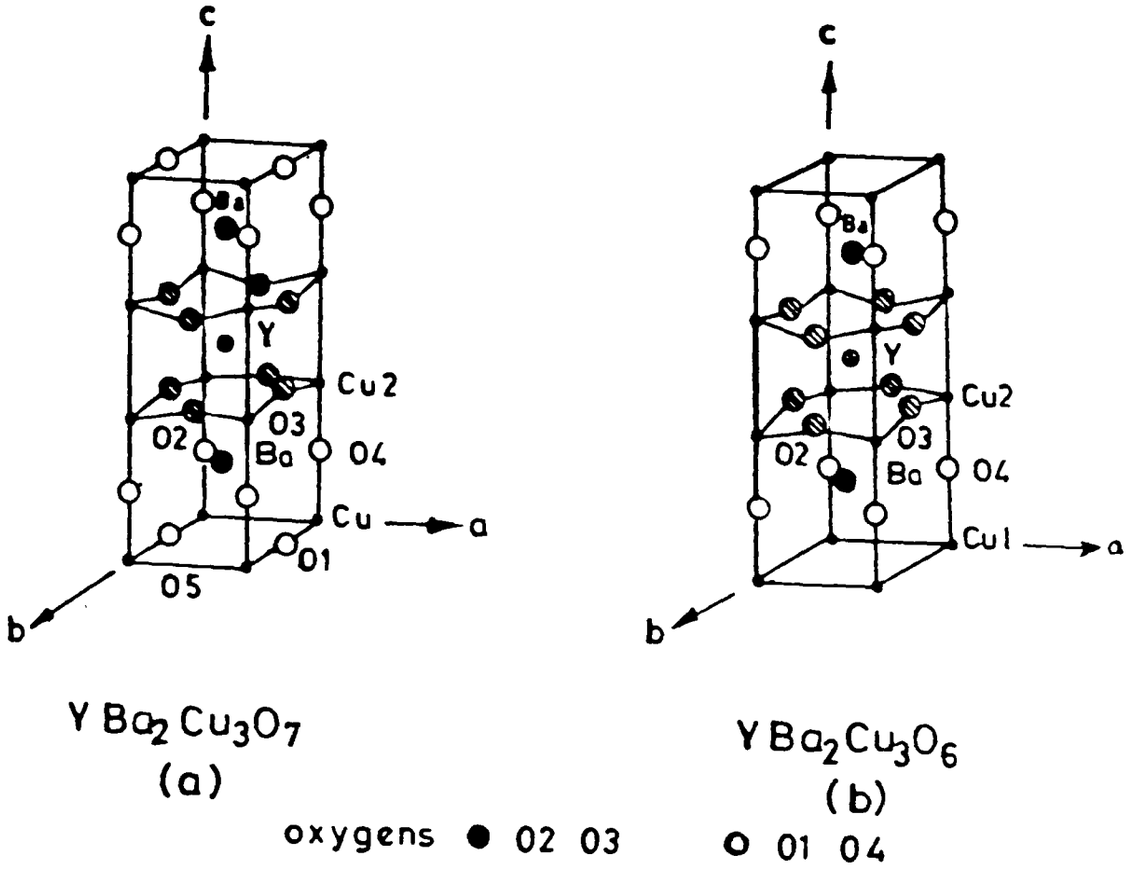

Fig. I.3 Structure of $YBa_2Cu_3O_{7-\delta}$ compounds

as shown in Fig. 1.3 b and hence Cu-O chains along the b-axis are absent. The Cu (1) atoms are two fold coordinated (57). The Cu (1)-04 bond in this oxide is very short (1.80 A) as in Fig. 1.3 b.

1.9.2 Phase transition and oxygen stoichiometry

The compound $YBa_2Cu_3O_{7-\delta}$ undergoes phase transition from superconducting state to non-superconducting tetragonal structure as the oxygen content changes from 7 to 6.0. At higher temperatures the structure is tetragonal and at lower temperatures it absorbs oxygen from atmosphere and become orthorhombic and these transformations are reversible. In the range 6 to 6.5 of oxygen content, the compound is tetragonal and above 6.5 the compound is orthorhombic upto oxygen content 7 (58). In the orthorhombic form all the 01 sites are occupied and in the tetragonal form 01 sites are empty (59). On quenching YBCO from high temperature ie. above $950^{o}C$ results in oxygen defficiency and the compound is tetragonal. If the compound is slowly cooled in oxygen from a high temperature of $950^{o}C$, more oxygen is absorbed (60) and the associated tetragonal to orthorhombic transition occurs in the 620-700 K range depending on the oxygen partial pressure.

The structural transformations and the dependence of superconducting properties on the oxygen content of YBCO have been studied by many workers (61-65). Chen et al. (66) reported the possible existence of orthorhombic I and orthorhombic II forms. For orthorhombic I, the oxygen content is 6.7 to 7.0 and for

orthorhombic II, it is 6.50 to 6.70. The three forms tetragonal, orthorhombic I and II differ in their cell parameters.

The superconducting transition temperature of $YBa_2Cu_3O_{7-\delta}$ varies with oxygen content (61,63,67,68). The variation of T_c with δ is shown in Fig. 1.4. For δ = 0 to 0.2, T_c remains almost 90 K leading to a pleateau in the curve, but falls suddenly to 60 K for δ = 0.25 to 0.50. Beyond δ = 0.5, T_c falls suddenly to 4 K and is due to the orthorhombic to tetragonal transition. The dependence of oxygen content in $YBa_2Cu_3O_{7-\delta}$ on temperature and partial pressure of oxygen have been studied by several groups (63,67,69-71). Gallagher et al. (34) carried out many experiments on the equilibrium relationship between PO_2 and temperature for the single phase region of YBCO over the range of 10^{-3} atm. $\leq PO_2 \leq$ 1 atm. and $400^oC < T < 1000^oC$. The melting point of YBCO is dependent upon the atmosphere because of the pronounced change in the oxygen content at the melting temperature (72).

1.10 EXPERIMENTAL STUDIES ON YBCO

1.10.1 Resistivity measurements

The temperature-resistance measurements on high T_c superconductors show a metallic behaviour (47, 73, 74) with room temperature resistivity of 0.8 to 1.12 mΩ-cm. Pure YBCO shows (47) superconducting transition at 92 K (see Fig. 1.5). During cooling the resistivity decreases gradually and just above T_c it starts to decrease rapidly at the onset temperature. The difference between

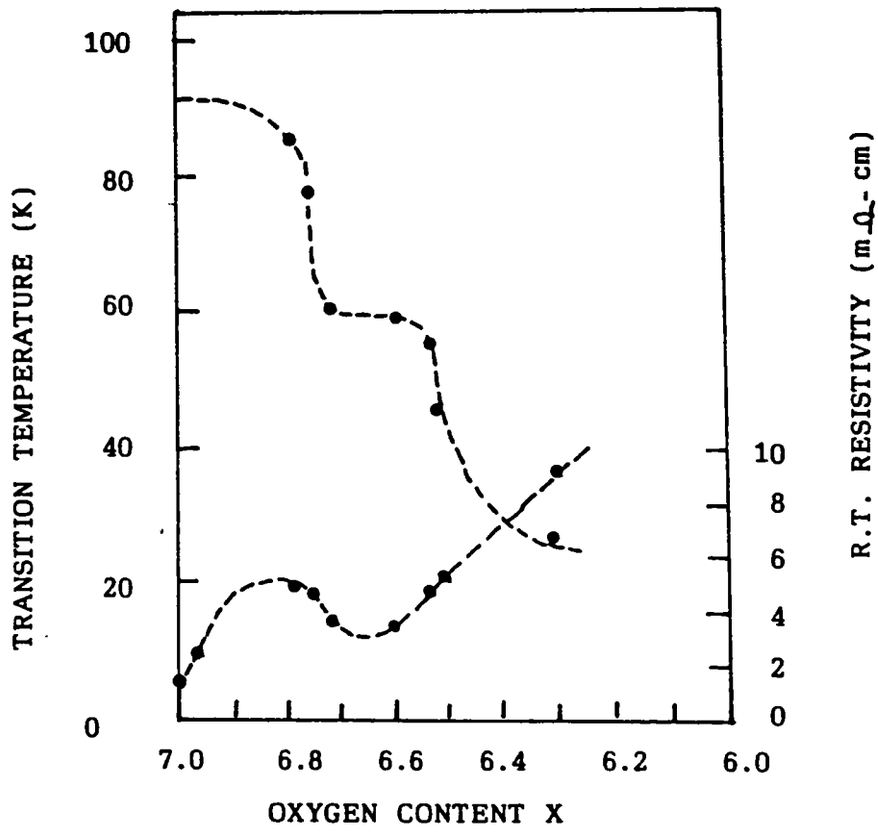

Fig. 1.4: Oxygen stoichiometry dependance of the resistive superconducting transition temperature in $YBa_2Cu_3O_x$ for x = 6.3 to 7.0.
Also shown are the room temperature resistivities.

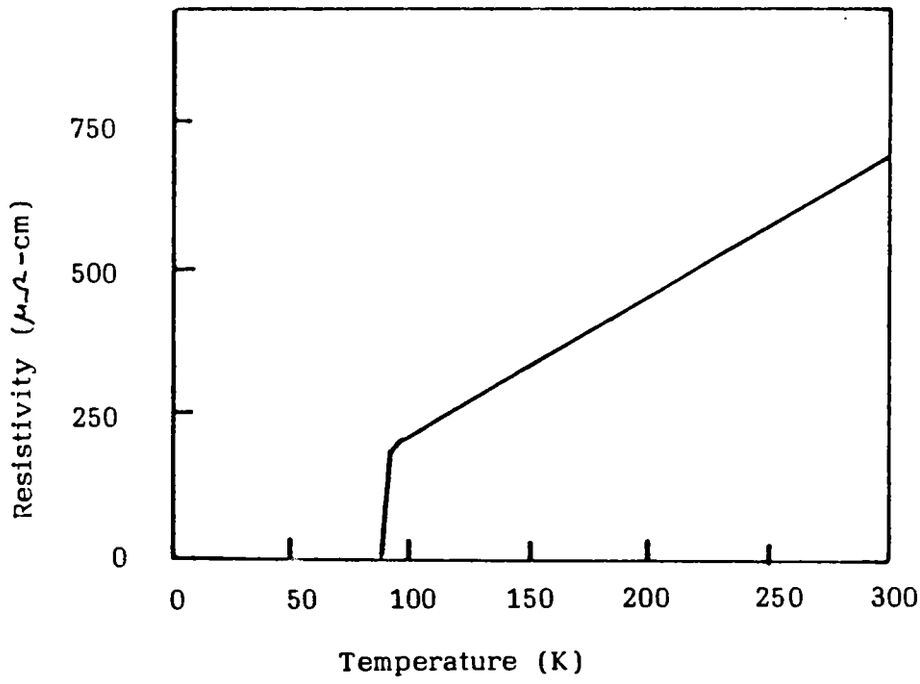

Fig. 1.5: Temperature-resistance curve for $YBa_2Cu_3O_{7-\delta}$

the onset temperature and the temperature at which the resistivity becomes zero ie. the off set temperature is called the transition width ΔT and is usually about 1 to 2 K. For polycrystalline materials ΔT depends on the sample history.

The resistivity measurements on single crystals showed that it is highly anisotropic but has temperature dependence similar to polycrystalline samples (74, 75). It is found (76) that the room temperature resistivity parallel to the c-axis is thirty times higher than the resistivity along the a-b plane.

The variations of resistivity with temperature and partial pressure of oxygen have been studied by many groups (63,65,76,77) . Fisher et al. (77) interpreted their data in terms of a narrow band gap model which is full for $\delta = 1$ and half filled for $\delta = 0$ in $YBa_2Cu_3O_{7-\delta}$. The contribution of electron-phonon interaction to the transport properties is discussed by Horng et al. (79).

The peculiarities of the resistive state in YBCO has been studied by Pau et al. (80). I-V curves and their first order derivatives have been investigated. Non-linear behaviour of I-V curves in a magnetic field is shown to be due to the weak coupling of the superconductor current channels. The intergrain resistivity is higher than the resistivity of individual grains and has been studied by Hal Britter et al. (81).

The metal-insulator transition in YBCO has been studied by many groups (82-84). The lower oxygen concentration destroys

the superconductivity, causes removal of the orthorhombic distortion in the perovskite system and results in a metal-insulator transition. The presence of variable range hopping-conductivity in the insulator region strongly suggests that the metal-insulator transition is of Anderson type (83).

1.10.2 Thermoelectric power measurements (TEP)

The absolute thermopower of YBCO has been studied by several groups from room temperature to superconducting transition temperature (85-88). It is found that YBCO shows a large enhancement of thermopower in the range 150-100 K (89, 90). According to Uher and Kaiser (86) the enhancement in TEP in the range 100 K is due to phonon drag effect. Uher et al. (89) have suggested mechanisms that could enhance phonon drag just above T_c, (a decrease in effective carrier density and an increase in phonon current due to superconducting fluctuations) but the normal effect of superconducting fluctuations is to reduce the thermopower as they short out the thermoelectric voltage. The enhancement may also be due to the disorder effects (89). Ausloos et al. (91) explained the phonon drag effect as due to the electron phonon interaction and many other groups (89-93) explained the phonon drag effect.

The dependence of TEP on temperature and oxygen partial pressure were studied by many groups (86,87,94-96). Disorder effects on TEP have been studied by elemental substitution at both the Y site as well as the Cu site (97-99).

1.10.3 Thermal properties

The knowledge of the temperature dependence of thermal parameters like specific heat, thermal expansion and thermal conductivity are of fundamental significance for the understanding of physical systems. The specific heat studies of YBCO show two unusual features. There is a linear term and also an upturn in C/T at low temperatures (100, 101). The measurements on specific heat show that $\frac{\Delta c}{Tc}$ is 48 mJ/Mol K^2 giving rise to a $\frac{\Delta c}{\gamma Tc}$ of 1.33, where γ and Δc are the linear coefficient and the jumb in specific heat respectively. The overall temperature dependence of thermal expansion of YBCO has been studied by several groups (102-105). The coefficient of thermal expansion found to be of 12 to 14 x 10^{-6} K^{-1} at 300 K. The effect of oxygen content as well as substitution on Cu and Y sites have also been discussed by different groups (104, 105).

The thermal conductivity K provides information on the dynamical behaviour, ie. on the different type of scattering mechanism of electrons phonons and other quasi-particles (89). An unexpected strong increase in thermal conductivity of YBCO just below T_c is reported (85, 106, 107). The thermal conductivity is of the order of 3 to 4 (w $M^{-1}K^{-1}$).

1.10.4 Magneto-resistance and Hall effect measurements

The high temperature superconductor YBCO is highly anisotropic. The dimensionality of YBCO has been determined as being three dimensional from the fluctuation excess conductivity determined

by magneto-resistance measurements above T_c with sintered samples (108-110).

The Hall coefficient Rh is often used as an indicator of carrier sign and density. For YBCO, Rh is strongly temperature dependent (111). A detailed study of the Hall effect has been done by Gottwick et al. (112). According to them Rh is positive and essentially linear with temperature (T) in the range 4 K - 350 K. The dependence of Rh on oxygen content and temperature has been studied by different groups (113, 114).

1.10.5 Spectroscopic studies

Various spectroscopic studies have been carried out on high T_c superconductors to characterise the materials and its superconducting properties and to understand the mechanism behind high T_c superconductivity.

Microwave absorption studies (115-117) are useful (i) for the detection of superconducting phase by contactless mechanism, (ii) for the determination of critical fields and (iii) to study the Josephson tunnel junctions. Infra-red and Raman spectroscopy have been used to study (118-123) the lattice vibrations of the superconducting material and their dependence on oxygen content, element substitution, isotope exchange and impurity phases. The temperature dependence of the optical phonon spectrum and the superconducting gap have also been investigated (124).

Nuclear magnetic resonance (NMR) and nuclear quadrupole

resonance specroscopy are useful techniques for studying the changes occurring in the electronic and magnetic properties of the material under test when it passes from its normal to the superconducting state (125-129). In the YBCO structure there are two crystallographically non-equivalent copper sites Cu(1) and Cu(2) and therefore there are two distinct electric field gradient for copper and NQR spectra reveal such information. Copper NMR/ NQR measurements have been carried out in doped $YBa_2Cu_{3-x}M_xO_{7-\delta}$ (M = Mg, Zn, Al, Ga, V). The NMR/NQR of samples with Y replaced by magnetic rare earth ions such as Gd, Er, Ho etc. have also been carried out. The results from these studies have been used (125) to discuss the mutual magnetic interaction between the substituent ions and the magnetic moment in Cu(2) ions.

X-ray photoelectron spectroscopy (XPS) can give the chemical state or valence state of the atoms in the sample surface. The major conclusion arising from the studies on XPS valence band spectra of YBCO compound is that there is dimerisation of oxygen ions at low temperatures (130). The available experimental data on valence bands and theoretical calculations have not yet succeeded in relating the mechanism of superconductivity in the electronic structure of the high T_c superconductors.

The occupied and unoccupied electronic states of matter can be probed by x-ray spectroscopic method. The XANES (X-ray absorption near edge structure) region contains information about the binding energies, the symmetries and multiplicities of the low

lying resonant electric states in the continuum of the absorbed atoms. A discussion of XANES and EXAFS (X-ray absorption fine structure) is given by Bianconi et al. (131). Many workers have carried out XANES and EXAFS studies on CuK and CuL-3 and oxygen K absorption edge and XPS measurements on Cu2P and 013 (132-134).

Different types of disorders such as twinning, oriented domains, oxygen non-stoichiometry, cationic disorder and super-lattice structures were studied by high resolution electron microscopic (HREM) method (135-138). Twinning mainly results due to the phase transition from tetragonal to orthorhombic structure with the absorption of oxygen from the atmosphere.

1.11 SUBSTITUTION STUDIES IN YBCO

The effect of substitution on cationic and anionic sites in YBCO on the structural phase transition and the associated super-conducting properties have been studied by many groups (139-145). Substitutionl studies can shed light on how the low dimensional Cu -O networks get influenced by the dopants.

All the lanthanides fulfil the criteria for substitution for Y and their complete replacement has been possible without any significant change in the parental T_c of 90 K (146-148), exemptions are Ce, Pr, Tb. Partial replacement of Y with Bi, Ca, Sr, Tl, In etc. decreases T_c (149).

Substitutions on the Ba site by lanthanide ions lower T_c considerably (141). Small change in T_c and invariance of lattice

parameter (orthorhombic) by partial substitution of Eu and Ga for Ba has been reported. But larger ions like La, Pr etc. beyond 0.15 atoms substitutions give orthorhombic to tetragonal phase changes, but low temperature superconductivity exists in the tetragonal state (150, 151). The introduction of trivalent rare earth ions on Ba^{2+} site increases the oxygen content. Beyond the oxygen content O_7, YBCO is tetragonal and the T_c decreases (145). Many alkali and alkaline earth metals could be substituted in the Ba site of YBCO. Upto 15 mol % sodium and potassium substitutions are possible without affecting T_c (145).

As regards the substitutions at the Cu sites, there are two crystallographically distinct sites for copper, Cu(1) and Cu(2). Depending on the oxygen content Cu(1) can have 2, 4 and 6 fold coordination while the latter can exist only in the square pyramidal 5 fold coordination. The orthorhombic, superconducting YBCO compound gives a 4 fold coordination to Cu(1).

Partial replacement of Cu and its effect on oxygen stoichiometry has been studied by many groups (145, 152-154). The dopants can occupy either Cu(1) or Cu(2) site or both depending on the coordination number and ionic radii. Substitution by Fe, Co, Ni, Zn reduces T_c considerably (145). Al and Ga substitution in YBCO in place of Cu introduces orthorhombic to tetragonal transformation at about 0.05 to 0.06 atom substitution and the rate of T_c depression is very low. In the case of substitutions by Ti, Cr, Mn, Nb, W, Ag, Li, Mg and Si in place of Cu, the T_c depression is gradual and the structure is less affeccted (145).

There has been attempts (145) to replace oxygen by fluorine , chlorine and sulphur. Ovshinky et al. (155) reported high T_c in the range 200 K to 300 K in the fluorine substituted compounds, but the results are not reproducible.

1.12 FABRICATION OF YBCO FOR PRACTICAL APPLICATIONS

1.12.1 Bulk processing of YBCO

The major challenges encountered in the fabrication of the bulk superconducting ceramic compounds are (i) reproduction of the intrinsic properties of the material in the bulk components, (ii) to achieve good mechanical integrity and strength in dimensions sufficient to allow for their wide spread use. The bulk synthesised powders of YBCO with suitable additives or binders are extruded in the form of wires, tapes etc. (33, 156, 157). Ceramic-metal composites as well as ceramic-polymer composites have been fabricated for application purpose. Silver is commonly used for fabrication of ceramic-metal composites because of its non-reactivity with YBCO (158). Several techniques have been used for the fabrication of different shapes from the powder (159-163). But in bulk processed materials, the current density is extremely low compared to thin films. The reasons for low value of J_c are due to the weak coupling between grains and the absence of strong pinning centers, which results in thermally activated magnetic flux creep.

In order to enhance the current density in bulk materials melt processing with directional solidification technique are now

being widely used (164-167). Jin et al. (164) prepared highly oriented structures by melt texturing growth. In melt texturing YBCO is allowed to melt at high temperatures (1200-1250^{o} K) for a short time and cools to crystallisation temperature with specified cooling schedules. The current density in melt textured YBCO is relatively high of the order of 10^4 A/cm^2. In order to improve further the transport properties, a number of dopants have been added to enhance the processing and pinning in textured YBCO (158, 168).

1.12.2 Thick and thin films

Thick and thin films of YBCO have many technological applications. Thick films can be used for magnetic shielding devices, electrical interconnects etc. and thin films for IR sensors, for computer applications, SQUIDS etc.

Thick films can be prepared (169-171) by screen printing or plasma spraying, laser ablation or dipping a metal or substrate in a melt of YBCO. The common substrate materials for YBCO films are $SrTiO_3$, MgO, Al_2O_3, $LaAlO_3$ etc.

Thin films of YBCO have been deposited on various substrates. The common methods of deposition (172-174) are laser ablation, electron beam evaporation, molecular beam epitaxy as well as the sputtering techniques like DC, AC, RF reactive and RF magnetron sputtering. The major difficulty is the interaction between YBCO film and the substrates. The substrate effects and process constraints are discussed by Deshpanday et al. (174).

Various configurations of multilayer structures have been fabricated by different groups (175-180). Superconductor-insulator-superconductor structures made of $YBa_2Cu_3O_7/NdGdO_3/YBa_2Cu_3O_7$ have been successfully fabricated by Kobayashi et al. (175) and the reflection high energy electron diffraction (RHEED) and SEM studies showed a good interface boundary. Unit cell by unit cell grown $YBa_2Cu_3O_7/PrBa_2Cu_3O_7$ superlattice structures have been prepared by means of reactive evaporation with RHEED intensity oscillations by Kamigaki et al. (177) which can throw light on the mechanism behind high T_c superconductivity. DC superconducting quantum interference device of YBCO step-edge junctions were prepared by RF magnetron sputtering by Mitsuyoshi et al. (179) on MgO substrates and Herrmann et al. (180) on $SrTiO_3$ substrates.

REFERENCES

1. J.G. Bednorz and K.A. Muller, Z. Phys., B 64, 187 (1986).

2. M.K. Wu, J.R. Ashburn, C.J. Torng, P. H. Hor, R.L. Meng, L. Gao, Z.H. Huang, Y.Q. Wang and C.W. Chu, Phys. Rev. Lett., 58, 908 (1987).

3. C.N.R. Rao, P. Ganguly, A.K. Rayachaudhuri, R.A. Mohan Ram and K. Sreedhar, Nature, 326, 856 (1987).

4. H. Maeda, Y. Tanaka, M. Fukutomi and T. Asano, Jap. J. Appl. Phys., 27, L 209 and L 548 (1988).

5. E. Takayama-Muromachi, Y. Uchida, Y. Matsui, M. Onada and K. Kato, Jap. J. Appl. Phys. Pt. 2, 27, L 556 (1988).

6. Z.Z. Sheng, A.M. Hermann, A. Elali, C. Almasan, J. Estrada, T. Datta and R.J. Matson, Phys. Rev. Lett., 60, 937 (1988).

7. Z.Z. Sheng and A.M. Hermann, Nature, 332, 138 (1988).

8. Z.Z. Sheng, W.K. Kiehl, J. Bennett, A. Elali, D. Marsh, G.D. Mooney, F. Arammash, J. Smith, D. Viar and A.M. Hermann, Appl. Phys. Lett., 52, 1738 (1988).

9. C. Kittel, "Introduction to solid state physics", 5th edn., Wiley Eastern Ltd., New Delhi (1977).

10. G. Rickayzer, Theory of superconductivity, John Wiley, New York, 1965.

11. M. Tinkham, "Introduction to superconductivity" McGraw Hill, New York, 1979.

12. Tsuneo Nakahara, Progress in high temperature supercnductivity, Vol. 8 (Ed. C.G. Burnham and R.D. Kane) World Scientific (1988) p.88.

13. H. Kamerlingh Onnes, Akad. van Wetenschappen, 14, 818 (1911).

14. A.S. Bhalla, Rustom Roy and L.E. Cross, "Chemistry of oxide superconductors", (Ed. C.N.R. Rao), Blackwell Scientific Publications, 71 (1988).

15. R.A. Hein, J.W. Gibson, R. Mazalsky, R.C. Miller and J.K. Hulni, Phys. Rev. Lett., 12, 320 (1964).

16. Ch. J. Raub, A.R. Sweedler, M.A. Jensen, S. Broadston and B.T. Matthias, Phys. Rev. Lett., 15, 108 (1965).

16A. A.W. Wells, "Structural Inorganic chemistry", 5th Edition, 602 (1984) .
R.J. Cava, R.B. Van Dover, B. Batlogg and E.A. Rietman, Phys. Rev. Lett., 58, 408 (1987).

17. J.R. Cooper, B. Alavi, L.W. Zhou, W.P. Beyermann and G. Gruner, Phys. Rev. B., 35, 8794 (1987).

18. Ch. Laurent, S.K. Patapis, M. Laguesse, H.W. Vanderschueren, R. Rulmont, P. Tarte and M. Ausloos, Solid State Commun., 66(4), 445 (1988).

19. Y. Tokura, H. Takagi and S. Uchida, Nature, 337, 345 (1989).

20. J.T. Markert, E.A. Early, T. BjOrnholm, S. Ghamaty, B.W. Lee, J.J. Neumeier, R.D. Price, C.L. Seaman and M.B. Maple, Physica C, 158 (1&2), 178 (1989).

21. A.W. Sleight, J.L. Gillson and B.E. Bierstedt, Solid State Commun., 17, 27 (1975).

22. *R.J. Cava, B. Batlogg, J.J. Krajewski, R. Farrow, L.W. Rupp Jr.*, A.E. White, K. Short, W.F. Peek and T. Kometani, Nature, *332, 814 (1988).*

23. S. Kondoh, M. Sera, Y. Ando and M. Sato, Physica C, 157, 469 (1989).

24. R.F. Fleming, P. Marsh, R.J. Cava and J.J. Krajewski, Phys. Rev. B., 38, 7026 (1988).

25. H.W. Kroto, J.R. Heath, S.C. O'Bryan, R.F. Curl and R.E. Smally, Nature, 318, 162 (1985).

26. A.F. Hebard, M.J. Rosseinsky, R.C. Haddon, D.W. Murphy, S.H. Glamm, T.T.M. Palster, A.P. Ramirez and A.R. Kortan, Nature, 350, 600 (1991).

27. M.J. Rosseinsky, A.P. Ramirez, S.H. Glamm, D.W. Murphy, R.C. Zahurah and A.V. Makhaja, Phys. Rev. Lett., 66, 2640 (1991).

28. K. Halsczer, O. Klein, G. Gruner, J.D. Thompson, F. Dederick and R.L. Whetten, Phys. Rev. Lett., 67, 271 (1991).

29. K.G. Frase and D.R. Clarke, Adv. Ceram. Mater., 2(3 B), 295 (1987).

30. R.S. Roth, K.L. Davis and J.R. Dennis, Adv. Ceram. Mater., 2 (3 B), 303 (1987).

31. D.G. Hinks, L. Soderholm, D.W. Capone, II, J.D. Jorgensen, Ivan K. Schuller, C.U. Segre, K. Zhng and J.D. Grace, Appl. Phys. Lett., 50(23), 1688 (1987).

32. J. Karpinski, C. Beeli, E. Kaldis, E. Wisard, E. Jilek, Physica C, 153-155, 830 (1988).

33. U.V. Varadaraju and G.V. Subba Rao, "Studies of High Temperature Superconductors", 3, 229 (1989) Ed. A.V. Narlikar, Nova Science Publisher.

34. P.K. Gallagher, H.M. O'Bryan, S.A. Sunshine and D.W. Murphy, Mat. Res. Bull., 22, 995 (1987).

35. D.H.A. Blank, J. Flokstra, G.J. Gerritsma, L.J.M. Van de Klundert and G.J.M. Velders, Physica (B + C), 145(2), 222 (1987).

36. W. Desisto, N. Kamegashira, W.Y. Chung, M. Hart, J. Baglio, K. Dwight and A. Wold, Prog. High Temp. Supercond., 7, 32 (1988), (World Sci. Publ., Singapore).

37. J.M. Tarascon, P. Barboux, B.G. Bagley, L.H. Greene, W.R. Mckinnon and G.W. Hull, ACS Symp. Ser., 351, Chap. 20 (1987).

38. E.C. Behrman, Adv. Ceram. Mater., 2 (3 B), 539 (1987).

38A. D. Pandey, V.S. Tiwari and A.K. Singh, J. Phys. D. Appl. Phys., 22, 182 (1989).

39. S. Jin, T.H. Tiefel, R.C. Sherwood, G.W. Kammlott and S.M. Zahurak, Appl. Phys. Lett., 51, 943 (1987).

40. R.K. Pandey, G.R. Gilbert, W.R. Kirk, P.S. Kobiela, H. Clearfield and P.J. Squattrito, J. of Supercond., 1, 45 (1988).

41. J. Mckittrick, M.E. McHenry, C. Heramans, P. Standley, T.R.S. Prasanna, G. Kalonje and R.C. O'Mandley, Physica C, 153-155 (1988).

42. A.B. Bykov, L.N. Demyanets and I.P. Zibrov, J. Cryst. Growth, 91, 302 (1988).

42A. R. Jayavel, P. Murugakoothan, C.R. Venkateswara Rao, P. Suresh Kumar, C. Subramanian and P. Ramaswamy, Mat. Res. Bull., 26, 151 (1991).

43. Y. Hidaka, Y. Enomoto, M. Suzuki, M. Oda and T. Murakami, J. Cryst. Growth, 85, 581 (1987).

44. Z. Chen, Y. Qian, D. Sun, M. Fang, J. Xia, Z. Zhao, Y. Zhao and W.Y. Kuan, Physica C, 153-155, 409 (1988).

45. H.J. Scheel and F. Licci, J. Cryst. Growth, 85, 607 (1987).

46. A.P. Malozemoff, W.J. Gallagher and R. Schwall, ACS Symp. Series 351, Chap. 27 (1987).

47. R.J. Cava, B. Batlogg, R.B. van Dover, D.W. Murphy, S. Sunshine, T. Siegrist, J.P. Remeika, E.A. Rietman, S. Zahurak and G.P. Espinosa, Phys. Rev. Lett., 58, 1676 (1987).

48. Y. Lepage, W.R. McKinnon, J.M. Tarascon, L.H. Greene, G.W. Hull and D.M. Hwang, Phys. Rev. B., 35, 7245 (1987).

49. M.A. Beno, L. Soderholm, R.W. Capone, D.G. Hinks, J.D. Jorgensen, I.K. Schuller, C.U. Segre, K. Zhang and J.D. Grace , Appl. Phys. Lett., 51, 57 (1987).

50. F. Beech, S. Miraglia, A. Santoro and R.S. Roth, Phys. Rev. B., 35, 8778 (1987).

51. W.I.F. David, W.T.A. Harrison, J.M.F. Gum, O. Moze, A.K. Soper, P. Day, J.D. Jorgensen, D.G. Hinks, M.A. Beno, L. Soderholm, D.W. Capona, I.K. Schuller, C.U. Segre, K. Zhang and J.D. Grace, Nature, 327, 310 (1987).

52. W. Schafer, E. Jansen, G. will, J. Faber Jr. and B. Veal, Mat. Res. Bull., 23(10), 1439 (1988).

53. J.D. Jorgensen, D.G. Hinks, H. Shaked, B. Dabrowski, B.W. Veal, A.P.Paulikas, L.J. Nowicki, G.W. Crabtree, W.K. Kwok, A. Umezawa, L.H. Nunez and B.D. Dunlap, Physica B, 156-157, 877 (1989).

54. F.P. Okamura, S. Suene, I. Nakai and A. Ono, Mat. Res. Bull., 22(8), 1081 (1987).

55. T. Siegrist, S.A. Sunshine, D.W. Murphy, R.J. Cava and S.M. Zahurak, Phys. Rev. B., 35, 7137 (1987).

56. Y. Le Page, T. Siegrist, S.A. Sunshine, L.F. Schneemeyer, D.W. Murphy, S.M. Zahurak, J.V. Waszczak, W.R. McKinnon, J.M. Tarascon, G.W. Hull and L.H. Greene Phys. Rev. B., 36, 3617 (1987).

57. C.N.R. Rao, J. solid State Chem., 64, 147 (1988).

58. A. Manthiram, J. Swinnea, Z.T. Sui, H. Steinfink and J.B. Goodenough, J. Amer. Chem. Soc., 109, 6667 (1987).

59. C.N.R. Rao and B. Raveau, Acc. Chem. Res., 22, 106 (1989).

60. H.M. O'Bryan and P.K. Gallagher, Adv. Ceram. Mater., 2 (3 B), 640 (1987).

61. Kohji Kishio, Jun-ichi Shimoyama, Tetsuya Hasegawa, Koichi Kitazawa and Kazuo Fueki, Jap. J. Appl. Phys., 26(7), L1228 (1987).

62. Y. Ueda and K. Kosuge, Physica C, 156, 281 (1988).

63. R.J. Cava, B. Batlogg, C.H. Chen, E.A. Rietman, S.M. Zahurak and D. Werder, Phys. Rev. B., 36, 5719 (1987), Nature, 329, 423 (1987).

64. B.G. Bagley, L.H. Greene, J.M. Tarascon and G.W. Hull, Appl. Phys. Lett., 51, 622 (1987).

65. P. Meuffels, B. Rupp and E. Porschke, Physica C, 156, 441 (1988).

66. I. Wei Chen, S.J. Keating, C.Y. Keating, X. Wu, J. Xu, P.E. Reyes-Morel and T.Y. Tien, Solid State Commun., 63(11), 997 (1987).

67. J.D. Jorgensen, H. Shaked, D.G. Hinks, B. Dabrowski, B.W. Veal, A.P. Paulikas, L.J. Nowicki, G.W. Crabtree, W.K. Kwok, L.H . Nunez and H. Claus, Physica C, 153-155, 578 (1988).

68. Y. Hariharan, M.P. Janawadkar, V. Sankara Sastry and T.S. Radhakrishnan, Pramana-J. Phys., 31, L59 (1988).

69. H.M.O'Bryan and P.K. Gallagher, "Ceramic superconductors-II" (Ed. Man F. Yan), American Ceramic Society, (1988) p.89.

70. E. Takayama-Muromachi, Y. Uchida, M. Ishii, T. Tanaka and K. Kato, Jap. J. Appl. Phys., 26, L1156 (1987).

71. M. Tokumoto, H. Ihara, T. Matsubara, M. Hirabayashi, N. Terada, H. Oyanagi, K. Murata and Y. Kimura, Jap. J. Appl. Phys., 26, L1565 (1987).

72. P.K. Gallagher, Adv. Ceram. Mater., 2(3B), 632 (1987).

73. P.W. Anderson and Z. Zou, Phys. Rev. Lett., 60, 132 (1988).

74. S.W. Tozer, A.W. Kleinsasser, T. Penny, D. Kaiser and F. Holtzberg, Phys. Rev. Lett., 59, 1768 (1987).

75. K. Murata, K. Hayashi, Y. Honda, M. Tokumoto, H. Ihara, M. Hirabayashi, N. Terada and Y. Kimura, Jap. J. Appl. Phys., 26, L1941 (1987).

76. P. Gourieux, G. Krill, M. Maurer, M.F. Ravet, A. Menny, H. Tolentino and A. Fontaine, Phys. Rev. B., 37, 7516 (1988).

77. B. Fisher, J. Genossar, I.O. Lelong, A. Kessel and J. Ashkenazi, Physica C, 153-155, 1349 (1988).

78. Mei Yu, C. Jiang, S.M. Green, H.L. Luo and C. Politis, Z. Phys. B. Cond. Matter., 69(1), 11 (1987).

79. H.E. Horng, Physica (B+C), 148(1-3), 472 (1987).

80. V.M. Pau, V.G. Prokhorov, G.G. Kaminskij, V.S. Flis, A.G. Popov, M.G. Vasilenko Sheremetev, M.A. Kuznetsov, K.G. Tret'yachenko, V.D. Valentinov and A.A. Flis, Fiz. Nizk. Temp., 13(8), 861 (1987).

81. J. Halbritter, M.R. Dietrich, H. Kuepfer, B. Runtsch and H. Wuehl, Z. Phys. B. Cond. Matter., 71(4), 411 (1988).

82. M. Esguerra, A. Marino, G. Franco, A. Jimenez, G. Holguin and E. Posada, J. Phys. C. Solid State Phys., 21, L367 (1988).

83. R.C. Budhani, S.M.H. Tzeng and R.F. Bunshah, Phys. Rev. B., 36(16), 8873 (1987).

84. P.P. Freitas and T.S. Plaskett, Phys. Rev. B., 37, 3657 (1988).

85. N.P. Ong, "Physical Properties of High Temperature Superconductors II", Edited by Donald M. Ginsberg, 459 (1990), World Scientific, Singapore.

86. C. Uher and A.B. Kaiser and E. Gmelin, Phys. Rev. B., 36, 5680 (1987).

87. J. Genossar, B. Fisher, L.O. Lelong, J. Ashkenazi and L. Patlagan, Physica C, 157, 320 (1989).

88. H.J. Trodahl and A. Mawdsley, Phys. Rev. B., 36, 8881 (1987).

89. A.B. Kaiser and C. Uher, Aus. J. Phys., 41, 597 (1988).

90. A. Mawdsley, H.J. Trodahl, J.L. Tallon, J. Sarfati and A.B. Kaiser, Nature, 328, 233 (1987).

91. M. Ausloos, K. Durczewski, S.K. Patapis, C. Laurent and H.W. Vanderschueren, Solid State Commun., 65(5), 365 (1988).

92. W. Weber and L.F. Mattheiss, Phys. Rev. B., 37(1), 599 (1988).

93. B. Arfi, H. Bahlouli, C.J. Pethick and Pines David, Phys. Rev. Lett., 60(21), 2206 (1988).

94. J. Nowotny, M. Rekas and W. Weppner, Appl. Phys., A47(2), 205 (1988).

95. Shousheng Yan, Peixiang Lu and Qi Li, Solid State Commun., 65(5), 355 (1988).

96. I.C. Santos, E.B. Lopes, A.P. Goncalves, R.T. Henriques and M. Almeida, Physica C, 153-155, 1345 (1988).

97. S.W. Cheong, S.E. Brown, Z. Fisk, R.S. Kwo, J.D. Thompson, E. Zirngiebl, G. Gruner, D.E. Peterson, G.L. Wells, R.B. Schwarz and J.R. Cooper, Phys. rev. B., 36, 3913 (1987).

98. R. Srinivasan, V. Sankaranarayanan, N.P. Raju, S. Natarajan, U.V. Varadaraju and G.V. Subba Rao, Pramana - J. Phys., 29, L225 (1987).

99. J. Clayhold, S. Hagen, Z.Z. Wang, N.P. Ong, J.M. Tarascon and P. Barboux, Phys. Rev. B., 39, 777 (1989).

100. R. Srinivasan and V. Sankaranarayanan, Rev. Solid State Sci., 2(2-3), 277 (1988).

101. N. Sankar, V. Sankaranarayanan, L.S. Vaidhyanathan, C. Rangarajan and R. Srinivasan, Solid State Commun., 67(4), 391 (1988).

102. G. sran, W. Schiebeling, M. Lang, R. Held, U. Gottwick, F. Steglich and H. Rietschel, Physica C, 153-155, 1010 (1988).

103. C.A. Swenson, R.W. Mc Callum and K. No, Phys. Rev. B., 40, 8861 (1989).

104. S. Vieira, S. Bourgeal, R. Villar, A. Aguilo, M.A. Ramos and C. Moure, Physica C, 153-155, 1006 (1988).

105. H. Kudowaki, F.E. Kayzel and J.J.M. Franse, Physica C, 153-155, 1028 (1988).

106. S.J. Hagen, Z.Z. Wang and N.P. Ong, Phys. Rev. B., 40, 9389 (1989).

107. V. Beyot, F. Dalannay, C. Dewitte, J.P. Erauw, X. Gonze, J.P. Issi, A. Jonas, M. Kinany-Al aoui, M. Lambricht, J.P. Michenaud, J.P. Minet and L. Piraux, Solid State Commun., 63(11), 983 (1987).

108. M. Hikita and M. Suzuki, Phys. rev. B., 39, 4756 (1989).

109. K.Y. Chen and Y.J. Quian, Physica C, 159(1-2), 131 (1989).

110. M. Ausloos, C. Laurent, H.W. Vanderschueren, A. Rulmont and P. Tarte, Phys. Rev. B., 39, 2729 (1989).

111. Yasuhiro Iye, "Studies of High Temperature Superconductors", (Edited by A.V. Narlikar), Vol.2, 199 (1989), Nova Science Publishers.

112. U. Gottwick, R. Held, G. Sparn, F. Steglich, H. Rietschel, D. Evert, B. Renker, W. Bauhofer, S. von Molnar, M. Wilhelm and H.E. Hoenig, Europhys. Lett., 4, 1183 (1987).

113. L. Forro, M. Raki, C. Ayache, P.C.E. Stamp, J.Y. Henry and J. Rossat-Mignod, Physica C, 153-155, 1357 (1988).

114. Y. Iye, T. Tamegai, T. Sakakibara, T. Goto, N. Miura, H. Takeya and H. Takei, Physica C, 153-155, 26 (1988).

115A. M.D. Sastry, "Studies of High Temperature Superconductors", Edited by A.V. Narlikar , 2, 255 (1989).

115B. J.C. Gallop and W.J. Radcliffe, Supercond. Sci. Technol., 4, 568 (1991).

116. W.R. McKinnon, J.R. Morton and G. Pleizier, Solid State Commun., 65, 855 (1988).

117. M. Poirier, G. Quirion, K.R. Poeppelmeier and J.P. Thiel, J. Appl. Phys., 63, 1646 (1988).

118. H.J. Rosen, R.M. Macfarlane, E.M. Engler, V.Y. Lee and R.D. Jacowitz, Phys. Rev. B., 38, 2460 (1988).

119. Michael Stavola, D.M. Krol, W. Weber, S.A. Sunshine, A. Jayaraman, G.A. Kouroulis, R.J. Cava and E.H. Rietman, Phys. Rev. B., 36, 850 (1987).

120. M. Cardona, R. Liu, C. Thomson, M. Bauer, L. Genzel, W. Konig, A. Wittlin, U. Amador, M. Barahona, F. Fernandez, C. Otero and R. Saez, Solid State Commun., 65, 71 (1988).

121. J.R. Kirtley, R.T. Collins, Z. Schlesinger, W.J. Gallagher, R.L. Sandstrom, T.R. Dinger and D.A. Chance, Phys. Rev. B., 35, 8846 (1987).

122. D.A. Bonn, J.E. Greedan, C.V. Stager, T. Timusk, M.G. Doss, S.L. Herr, K. Kameras and D.B. Tanner, Phys. Rev. Lett., 58, 2249 (1987).

123. M.K. Crawford, W.E. Farnet, M.C. McCarron III and R.K. Bordia, Phys. Rev. B., 38, 11382 (1988).

124. Rudolf Feile, Physica C, 159 (1 & 2), 1 (1989).

125. R. Vijaraghavan, A.K. Rajarajan and L.C. Gupta, "Studies of High Temperature Superconducgors", Edited by A.V. Narlikar, Vol. 2, 79 (1989)., Nova Science Publishers.

126. J.M. Traquada, D.E. Cox, W. Kunnman, G. Shirane, M. Suenaga, P. Zolliker, D. Vaknin, S.K. Sinha, M.S. Alvarez, A.J. Jacobson and D.N. Johnston, Phys. Rev. Lett., 60, 156 (1988).

127. F. Mila and T.M. Rice, Phys. Rev. B., 40(16), 11382 (1989).

128. A.J. Vega, M.K. Crawford, E. McCarron and W.E. Farneth, Phys. Rev. B., 40, 8878 (1989).

129. M. Itoh, K. Karashima, M. Kyogoku and I. Aoki, Physica C, 160(2), 177 (1989).

130. D.D. Sarma, K. Sreedhar, P. Ganguly and C.N.R. Rao, Phys. Rev. B., 36, 2371 (1987).

131. A. Bianconi, Appl. Surf. Sci., 6, 392 (1980).

132. K.B. Garg, A. Bianconi, S. Della Longa, A. Clozza, M. De Santis and A. Marcelli, Phys. Rev. B., 38, 244 (1988).

133. A. Bianconi, J. Budnick, G. Demazeau, A.M. Flank, A. Fontaine, P. Lagarde, J. Jego Duez, A. Recolevski, A. Marcelli and M. Verdaguer, Physica C, 153-155, 117 (1988).

134. K.B. Garg, R.K. Singhal, K.V.R. Rao, U. Chandra, H.S. Chauhan, J. Singh, K.S. Ferath and I C. Jain, Phys. Stat. Sol. (b), 147, 343 (1988).

135. M. Hervieu, B. Domenges, C. Michel, J. Provost and B. Raveau, J. Solid State Chem., 71, 263 (1987).

136. M. Hervieu, C. Michel and B. Raveau, "Studies of High Temperature Superconductor", Edited by A.V. Narlikar, Nova Science Publishers, Vol. 3, 50 (1989).

137. E.A. Hewat, M. Dupuy, A. Bourret, J.J. Capponi and M. Marezio, Nature, 327, 400 (1987).

138. N.P. Huxford, D.J. Eaglesham and C.J. Humphreys, Nature, 329, 812 (1987).

139. P.H. Hor, R.L. Meng, Y.Q. Wang, L. Gao, Z.J. Huang, J. Bechtold, K. Forster and C.W. Chu, Phys. Rev. Lett., 58, 1891 (1987).

140. J.M. Tarascon, W.R. McKinnon, L.H. Greene, G.W. Hull and E.M. Vogel, Phys. Rev. B., 36, 226 (1987).

141. A. Suzuki, E.V. Sampathkumaran, K. Kohn, T. Shibuya, A. Tohdake and M. Ishikawa, Jap. J. Appl. Phys., 27, L792 (1988).

142. S. Li, E.A. Hayri, K.V. Ramanujachary and M. Greenblatt, Phys. Rev. B., 38, 2450 (1988).

143. J.P. Franck, J. Jung and M.A.K. Mohamed, Phys. Rev. B., 36(4), 2308 (1987).

144. Y. Maeno, M. Kato, Y. Aoki and T. Fujita, Jap. J. Appl. Phys., 26, L1982 (1987).

145. A.V. Narlikar, C.V. Narasimha Rao and S.K. Agarwal, "Studies of High Temperature Superconductors I", Edited by A.V. Narlikar, Vol. 1, 341 (1989) and the references in it.

146. G.V. Subbarao, in "Chemistry of Oxide Superconductors", Ed. C.N.R. Rao, Blackwell Scientific Publications, 65 (1988).

147. T. Kaneko, H. Toyodo, H. Fujita, Y. Oda, T. Kohara, K. Ueda, Y. Yamada, I. Nakada and K. Asayama, Jap. J. Appl. Phys., 26, L1956 (1987).

148. L.F. Schneemmeyer, J.V. Waszezak, S.M. Zahorak, R.B. van Dover and T. Siegrist, Mat. Res. Bull., 22, 1467 (1987).

149. G. Svensson, Z. Hegedus, L. Wang and D. Rapp, Physica C, 153-155, 864 (1988).

150. M. R. Harrison, I.C.S.T. Hegedus, W.G. Freeman, R. Jones, P.P. Edwards, W.I.F. David and C.C. Wilson, in "Chemistry of Oxide Superconductors", Ed. C.N.R. Rao, Blackwell Scientific Publications, 137 (1988).

151. A. Tokiwa, Y. Syono, M. Kikuchi, R. Suzuki, T. Kajitani, N. Kobayashi, T. Sasaki, O. Nakatsu and Y. Muto, Jap. J. Appl. Phys., 27, L1009 (1988).

152. G. Xiao, F.H. Streitz, A. Garvin, Y.W. Du and C.L. Chein, Phys. Rev. B., 35, 8782 (1987).

153. E. Takayama-Muromachi, Y. Uchida and K. Kato, Jap. J. Appl. Phys., 26, L2087 (1987).

154. M. Hiratani, Y. Ito, K. Miyauchi and T. Kudo, Jap. J. Appl. Phys., 26, L1997 (1987).

155. S.R. Ovshinky, R.T. Young, D.D. Allred, G. DeMaggio and G.A. Van der Leeden, Phys. Rev. Lett., 58, 2579 (1987).

156. F.H. Streitz, M.Z. Cieplak, Gang Xiao, A. Gavrin, A. Bakshai and C.L. Chien, Appl. Phys. Lett., 52(11), 927 (1988).

157. D.W. Johnson, Jr., E.M. Gyorgy, W.W. Rhodes, R.J. Cava, L.C. Feldman and R.B. van Dover, Adv. Ceram. Mater., 2(3 B), 364 (1987).

158. A. Goyal, P.D. Furkenbusch, D.M. Kroeger and S.J. Burns, Physica C, 182, 203 (1991).

159. L.E. Murr, A.W. Hare and N.G. Eror, Nature, 329, 6134 (1987).

160. T.J. Richardson and L.C. Dejonghe, Appl. Phys. Lett., 53, 2342 (1988).

161. G. Arcangel, R. Fava, A. Masci, A. Nardi, R. Vattaroni and C. Zondini, World Congress on Superconductivity, Prog. in High Temp. Superconductivity, Series 8, 433 (1988).

162. B.C. Hendrix, J.C. Borofka, T. Abe, J.K. Tien, T. Caulfield and S.M. Reichman, Proc. of the North East Regional Meet., Processing and Application of High Tc supercond. Status and Prospects, May 9-11, Pitscaway, USA, 1988.

163. Quentin Robinson, P. Georgopoulos, D. Lynn Johnson, Henry O. Marcy, Carl R. Kannewurf, S.J. Hwu, Tobin J. Marks, K.R. Poeppelmeier, S.N. Song and J.B. Ketterson, Adv. Ceram. Mater., 2(3 B), 380 (1987).

164. S. Jin, T. Tiefel, R. Sherwood, M. Davis, R. van Dover, G. Kammlott, R. Fastnacht and K. Keith, Appl. Phys. Lett., 52, 2074 (1988).

165. K. Salama, V. Selvamanickam, L. Gao and K. Sun, Appl. Phys. Lett., 54, 2352 (1989).

166. M. Murakami, S. Gotoh, N. Koshizuka, S. Tanaka, T. Matsuhita, S. Kambe and K. Kitazawa, Cryogenics, 30, 57 (1990).

167. R.L. Meng, C. Kinalidis, Y. Sun, L. Gao, Y. Tao, P. Horr and C.W. Chu, Nature, 345, 326 (1990).

168. P. McGinn, W. Chen, N. Zhu, C. Varanasi, L. Tan and D. Balkin, Physica C, 183, 51 (1991).

168B. M. Murakami, Supercond. Sci. Technol., 5, 185 (1992).

169. E. Beyne, C. Deneffe, J. Roggen, J. Fransaer, O. Arkens and O. Vanderbiest, Physica C, 153-155, 808 (1988).

170. N.P. Bansal, R.N. Simon and D.E. Farrell, Proc. 90th Annual Meeting of the Am. Ceram. Soc., Cincinnati, May 1988.
U.V. Varadaraju, G.V. Subba Rao, K.D. Chandrasekaran and A. Baradarajan, Thin Solid Films, 164, 119 (1988).

171. J.J. Cuomo, C. Richa d Guarnieri, S.A. Shivashankar, R.A. Roy, D.S. Yee and R. Rosenberg, Adv. Ceram. Mater., 2, 422 (1987).

172. S. Mohan, "High Temperature Superconductor", Edited by S.V. Subramanyam and E.S. Raja Gopal, Wiley Eastern Ltd., 234 (1989).

173. S.B. Ogale, "High Temperature Superconductors", (Ed. S.V. Subramanyam and E.S.R. Gopal), Wiley Eastern Ltd., New Delhi, 100 (1989).

174. C. Deshpandey and R.F. Bunshah, "Studies of High Tc Superconductors", Vol. 3 (Ed. A.V. Narlikar), Nova Scientific Publishers, 75 (1989).

175. J. Kobayashi, Y. Tazoh, M. Mukida and S. Miyazawa, Physica C, 185-189, 2029 (1991).

176. M.A.M. Gijs, J.B. Giesbers, F.C.M.J.M. Van Delft, C.E. Timmering, A.M. Gerrits and A. Slob, Appl. Phys. Lett., 59, 1233 (1991).

177. K. Kamigaki, T. Terashima, K. Shimura, Y. Bando and H. Torauchi, Physica C, 183, 252 (1991).

178. Hisao Hayakawa and Akira Fujimaki, International Conference on Superconductivity, Bangalore, (1990) p.363
(Ed. S.K. Joshi, C.N.R. Rao and S.V. Subramaniyam), World Scientific, Singapore.

179. Mitsuyoshi Yoshi, Jun-ichi Kita, Osamu Nakatsu and Yasuhara Yamada, Jap. J. Appl. Phys., 30, L587 (1991).

180. K. Herrmann, Y. Zhang, H.M. Much, J. Schubert, W. Zander and A.I. Braginski, Supercond. Sci. technol., 4, 583 (1991).

CHAPTER 2

EXPERIMENTAL METHODS

This chapter describes the method of preparation as well as the instrumental techniques used in the characterisation of different materials.

2.1 PREPARATION OF CERAMIC SAMPLES

The ceramic samples were prepared by solid state reaction method. In the solid state reaction method of preparation of compounds, appropriate amount of constituent oxides, carbonates or nitrates are weighed, mixed thoroughly in an agate mortar. Mixing can be carried out in dry or wet conditions. The mixed powder was dried at 100^{o} C to dry away the moisture and other organic solvents. It was then allowed to react at high temperatures by heating in high temperature furnaces. The particulars of heating temperatures, rate of heating, time of heating etc. vary from material to material and are described in respective sections of each material. The calcined powders were then ground well and pressed in the form of pellets and sintered at high temperatures. Again the sintering temperature, time of sintering and the atmosphere and rate of heating and cooling are described under specific topics of preparation. The samples prepared by solid state reaction method were characterised by XRD, SEM and other techniques.

2.2 RESISTIVITY MEASUREMENTS

Resistivity measurements on samples in the form of pellets were done by the dc four probe method in Vander Pauw geometry (1) which is a common method of measuring the resistivity of thin films and sheets of irregular shape but have uniform thickness.

Consider a flat lamella of any shape as shown in Fig. 2.1. Make four point contacts M, N, O and P at arbitrary places. Current I_{MN} is applied to contact M and taken off at contact N. The potential difference $V_P - V_O$ measured between P and O is given by

$$R_{MN,OP} = \frac{V_P - V_O}{I_{MN}}$$

Similarly

$$R_{NO,PM} = \frac{V_M - V_P}{I_{NO}}$$

This method is based on the theorem that between $R_{MN,OP}$ and $R_{NO,PM}$, there exists the simple relation

$$\exp\left(\frac{\pi d}{\rho} R_{MN,OP}\right) + \exp\left(-\frac{\pi d}{\rho} R_{NO,PM}\right) = 1 \qquad (1)$$

where d is the thickness of the sample and ρ the resistivity of the material. In the general case it is not possible to express ρ explicitly in known functions. The solution can be however written in the form

$$\rho = f \frac{\pi d}{\ln 2} \quad \frac{R_{MN,OP} + R_{NO,PM}}{2} \qquad (2)$$

where f is a factor which is a function of the ratio $R_{MN,OP}/R_{NO,PM}$ as plotted in Fig. 2.2. Thus to determine ρ, first calculate $R_{MN,OP}/R_{NO,PM}$ and obtain the corresponding value of f from Fig. 2.2 and then find ρ using equation (2).

The sample holder used in the present study is shown in Fig. 2.3. The specimen is mounted on a copper plate at the end of a copper tube isolated from it by a thin layer of insulating varnish. Four contacts were given on the periphery of the sample using conducting silver paste (curing at $100^{o}C$). Four copper leads were attached to these contacts. A calibrated platinum resistance thermometer (Lakeshore Pt 103 RTD) was fixed to the copper strip very close to the sample. The leads from the contacts as well as the Pt RTD elements were anchored to the larger copper tube and taken out at the other end of the tube. The sample holder set up was introduced into a cylindrical brass vessel. The sample holder was fixed firmly at the top of the brass vessel in such a way that (i) the sample holder did not touch the sides or bottom of the brass vessel, (ii) closure at the top was air tight. The brass vessel was evacuated and a small amount of nitrogen gas was introduced. The whole set up was then introduced into a liquid nitrogen Dewar. The experiment was conducted by cooling the sample continuously at a very low rate and taking the reading at

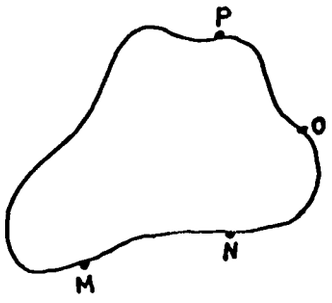

Fig. 2.1: A flat lamella of arbitrary shape with four contacts M, N, O and P on the periphery as used in the van der Pauw's method

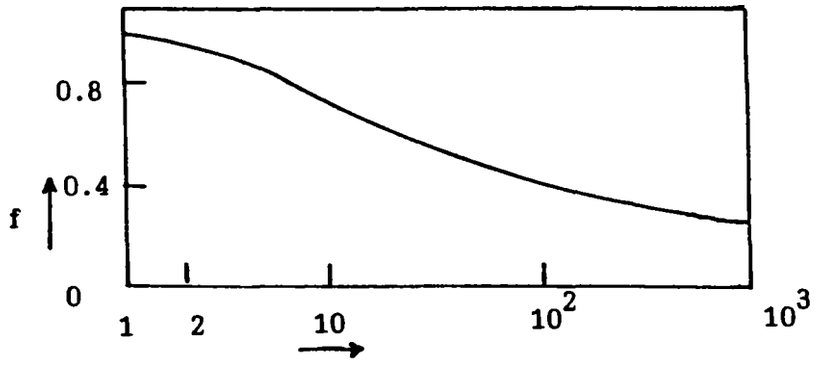

Fig. 2.2: f vs $R_{MN,OP}/R_{NO,PM}$ there exists the relation

$$\text{Cosh}\ \frac{(R_{MN,OP}/R_{NO,PM}) - 1}{(R_{MN,OP}/R_{NO,PM}) + 1}\ \frac{\ln 2}{f} = 1/2 \exp \frac{\ln 2}{f}$$

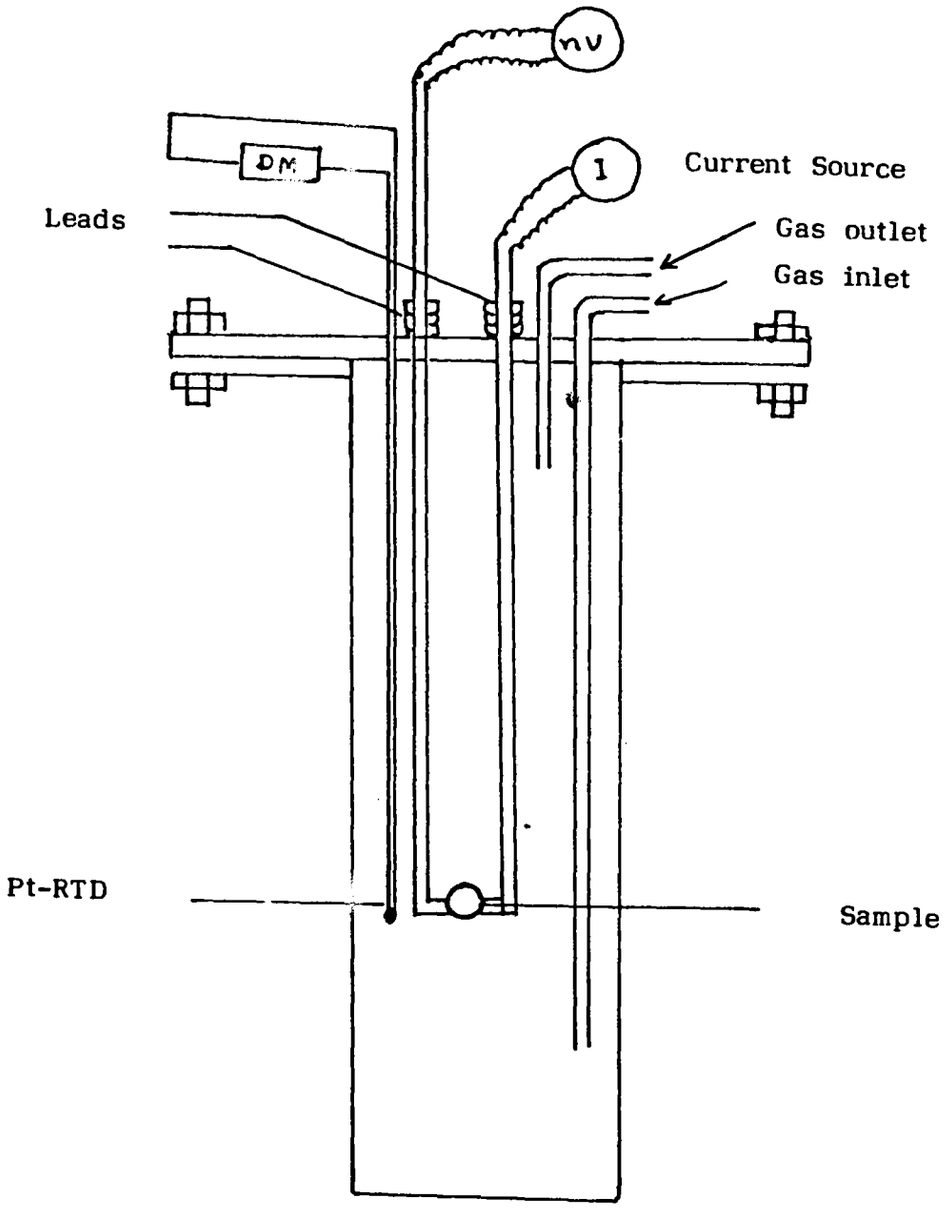

Fig. 2.3: Sample holder to measure the electrical resistivity of samples in the form of pellets

close intervals. The rate of cooling was controlled by introducing appropriate amount of carrier gas (nitrogen) into the brass vessel as well as by rising the dewar smoothly and slowly by means of a lab jack.

To measure the resistivity, a constant current (in the range 1-10 mA) was passed through the sample (between contacts M and N) from a constant current source (Keithley source 220). The voltage drop was measured between O and P with a nanovoltmeter (Keithley model 181). The current was reversed between M and N and again the reading was taken to check the accuracy. The same current was then sent through the sample between the contacts N and O and voltage measured between M and P.

At the superconducting transition temperature T_c, the voltmeter reading suddenly dropped to zero while a current was passed through the sample.

2.3 CURRENT DENSITY MEASUREMENTS

The current density of superconducting samples were measured from 92 K to 77 K in zero magnetic field by direct method.

For current density measurements, samples in the form of sintered bars about 2.5 cm length, 3 mm breadth and 1 to 1.5 mm thickness were used. Four contacts were given linearly as shown in Fig. 2.4, two at the ends of the bar to pass the current from a dc current source and two contacts 1.5 cm apart in the middle for measuring the voltage 'V' developed across the samples due

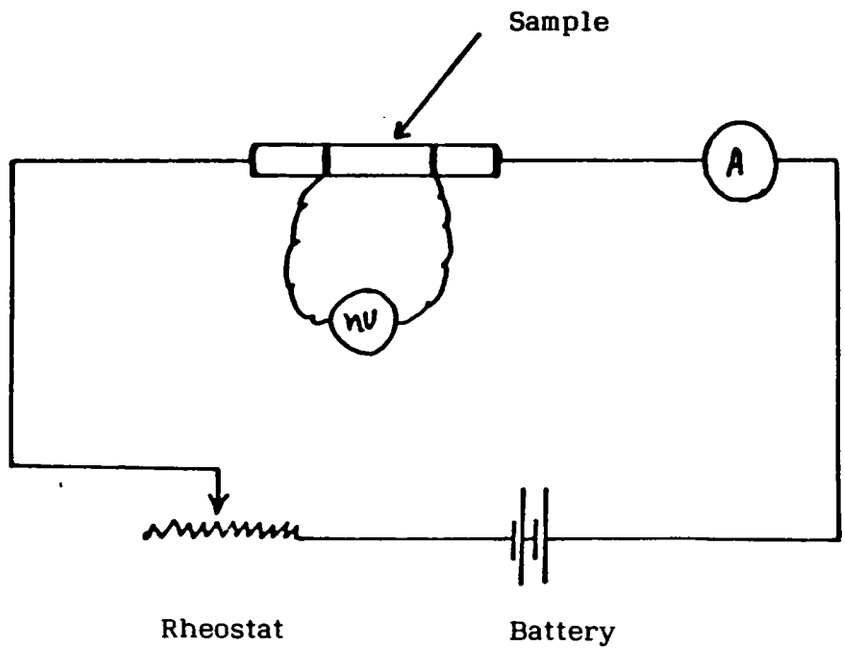

Fig. 2.4: Schematic diagram for current density measurements.

to a current 'I' along the length of the bar. A lead acid battery connected in series to the sample along with an ammeter to read the current and a rheostat to vary the current is used as current source in this measurement. The contacts for current leads were made with indium contacts with negligible contact resistance, so that extremely high values of current passes through the bar without much self heating at the contacts. All other experimental set up for current density measurements are same as that employed for resistivity measurements except the current source and the linear contacts.

For measuring the current density, a current of 10 mA from the battery was passed through the sample. The amount of current can be controlled by a rheostat connected in series with battery as shown in Fig. 2.4. In the superconducting state (at 92 K), the voltmeter shows zero voltage. As the current increases, the voltmeter starts showing some voltage and the current density is taken such that the voltmeter shows a maximum of 50 nV. The sample is cooled below 92 K, again the current density is measured as before. The current density was measured in close intervals of temperature down to 77 K. For calculating the actual current density, the cross sectional area of the bar is taken into account.

2.4 THERMOELECTRIC POWER MEASUREMENTS (TEP)

If there exists a temperature gradient ΔT across a sample (Fig. 2.5), then an emf ΔE is developed across the sample called

the thermo-emf. The magnitude of the emf is proportional to the temperature gradient if this difference ΔT is small. The ratio $\frac{\Delta E}{\Delta T}$ is the thermoelectric power of the solid or the Seebeck coefficient (s). If the face at higher temperature shows a positive polarity relative to the face at lower temperature, then S has a positive sign. The absolute thermoelectric power of the samples is determined by subtracting from the measured value of the thermopower, the absolute thermopower of copper, if copper plates were used as the contact material at the two faces of the sample. To obtain the thermopower of the copper plates used, one determines the thermopower of a standard substance relative to the copper specimen and thus deduces the absolute thermopower of the copper plate used. The standard substance used in this study is pure lead for which absolute thermopower data for each temperature is available in the literature (2).

The sample holder is shown schematically in Fig. 2.6. The sample holder contains a base plate MI and a top plate M2 of stainless steel. Between M1 and M2 there are two copper plates P1 and P2. P1 and P2 are insulated from M1 and M2 by means of teflon sheets TF1 and TF2 respectively. By turning the nut on the screws the plate P1 can be pressed against plate P2. The sample X is placed in between P1 and P2. Two chromel-alumel thermocouples whose junctions are electrically insulated but thermally bonded (by a thin layer of epoxy resin) to the copper plates P1 and P2 to measure the temperature difference between the two plates. Two copper leads are connected to the plates P1 and P2 to measure the

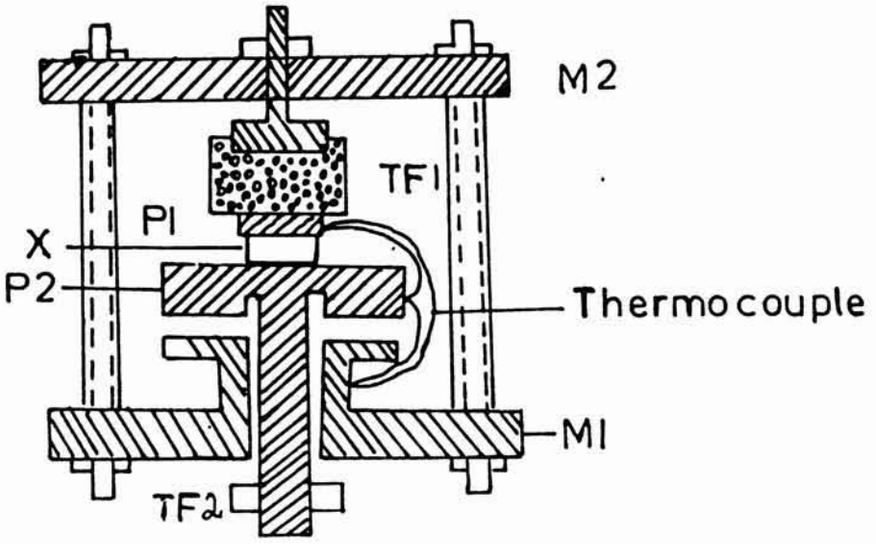

Fig. 2.6: Schematic diagram of the sample holder used in thermopower measurement

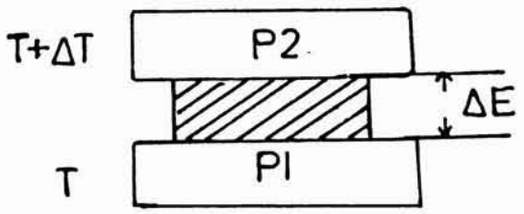

Fig. 2.5: Principle of thermo emf measurement

thermo emf ΔE. The absolute temperature is measured by platinum resistance thermometer (Lakeshore Pt 103 RTD) which is placed very close to P2. The thermocouple wires and the electrical leads are anchored from the top of plate P2 (Fig. 2.6).

The differential thermo emf across the sample was measured by a Keithley 181 nanovoltmeter. The temperature difference across the samples were measured in terms of millivolts. If required, the temperature of the plate P1 can be varied and maintained at a given temperature with a small heater (A standard resistor was used for this purpose).

In the experiment the sample was mounted between the copper plates which were tightened by screws. The sample holder was then introduced into a brass tube which could be evacuated through a side tube. The brass tube with the sample holder was introduced into a Dewar flask containing liquid nitrogen. The brass tube was kept much above the liquid nitrogen vessel to begin with. It was then evacuated to about 10 torr and then partially filled with Ar which acts as a carrier gas to control the rate of cooling. A convenient rate of slow cooling which would give steady temperatures for a sufficient length of time for taking readings was achieved by reducing the distance between the level of liquid nitrogen in the Dewar flask and the brass tube by raising the Dewar flask. The temperature difference can be measured to an accuracy of 2% and the thermo-emf can be measured to an accuracy of 50 nanovolts. This procedure gives reproducible results.

2.5 X-RAY POWDER DIFFRACTION STUDIES

X-ray powder diffraction technique was used for identification of phases, determination of lattice parameters and to study the phase transitions in $YBa_2Cu_3O_{7-\delta}$ and Ba_2YAO_6 compounds. In the powder method, the incident mono-chromatic radiation strikes a finely powdered sample. X-rays get diffracted from the crystallites in the sample and the diffracted rays from individual crystallites that happened to be oriented with planes making an incident angle θ with the beam satisfy the Bragg equation $n\lambda = 2\ d\ \sin\theta$ where λ is the wavelength of the incident radiation and d the interplanar spacing. These Bragg angles (θ) and the set of interplanar spacings are related to the unit cell parameters and Miller indices are assigned to the individual reflections. The methodology of the calculations involved is discussed in literature (3).

For the present study the x-ray diffractograms are recorded with a vertical Phillips 1710 goniometer. The X-ray diffractometer is operated using CuK_α radiation with a nickel filter. When perfect lattice parameter measurements are to be made, high angle ($2\theta \simeq 80$) reflections are chosen. The reflection peaks are recorded with slow scanning speed ($1/4^o$/min) with a chart speed of (1 mm/min). Silicon is used as the internal standard. The lattice parameters were determined using the least square method (4).

2.6 SCANNING ELECTRON MICROSCOPY

The microstructure (grain size and distribution) and

densification etc. for YBCO, BYAO and composites were studied using scanning electron microscopy. Scanning electron microscope JEOL JSM 35C was used for this investigation.

In scanning electron microscopy, a focussed electron beam is impinged on the sample. The reflected beam is analysed by suitable devices to get well defined pictures of sample surfaces.

Sample preparation for SEM studies involves polishing the sample surface and giving a conductive coating to avoid sparking. The surfaces for SEM study were prepared as follows. The surface of the ceramic that has to be examined was initially abraded with metallographic abrasive papers. Then the samples were fixed on a block of thermosetting plastic. The sample was polished on the pad cloth using fine abrasives like diamond paste of 6, 3, 1, 1/4 micron size. The samples were cleaned using an ultrasonic cleaner in acetone. Etching was done in dilute HNO_3 for about 30 seconds and washed in acetone immediately. The surface is again cleaned with ultrasonic cleaner in acetone. The polished sample surface was primarily examined under an optical microscope for the microstructure study.

The polished surfaces of the ceramic was then coated with gold by sputtering technique. The thickness of the gold coating was about $100^{o}A$.

Samples were then mounted in the chamber of the electron microscope and the system was evacuated to 10^{-6} torr pressure.

The electron beam was directed on selected areas according to the requirement. In this study the samples were photographed at a magnification of 1000-2000.

2.7 MEASUREMENT OF DIELECTRIC PROPERTIES

The dielectric properties of the ceramic compounds Ba_2YAO_6 have been measured using an impedence analyser (Hewlet Packard model 4192) in the frequency range from 30 Hz to 13 MHz at room temperature. The samples in the form of circular discs of diameter 10 to 12 mm and thickness 1 to 1.50 mm were used for the measurements. Both surfaces of the pellets were made flat by polishing and cleaned the surface with acetone. Room temperature curing silver paint was applied to both the surfaces and was dried at $200^{o}C$ for 2 hours. Copper leads were taken from the silver electroded surfaces. The capacitance and dissipation factor were directly measured from the impedence analyser as a function of frequency.

The dielectric constant calculated from the capacitance by the formula (5)

$$C = \frac{\varepsilon \varepsilon_o A}{d}$$

where ε the dielectric constant, ε_o the permittivity of free space, d thickness of the sample and A the area of the disc. The permittivity of free space is $\varepsilon_o = 8.854 \times 10^{-12}$ F/m.

REFERENCES

1. L.J. Van der Pauw, Phillips Res. Rep., 13, 1 (1958).

2. Cusack and P. Kendell, Proc. Phys. Soc., 72, 898 (1959).
R. Srinivasan, "High Temperature Superconductors" (Ed. S.V. Subramanyam and E.S.R. Gopal), Wiley Eastern Ltd., 86 (1980).

3. R.W.M. D'Eye and E. Wait, "X-ray powder photography in inorganic chemistry", Butterworths Scientific Publ., 70 (1960).

4. H.P. Klug and L.E. Alexander, "X-ray diffraction procedures", 2nd Edition, Wiley-Interscience Publication, 597 (1974).

5. W.D. Kingery, H.K. Bowen and D.R. Uhlmann, Introduction to ceramics, Wiley, New York, 1976.

CHAPTER 3

EFFECT OF VARIOUS ADDITIVES ON HIGH TEMPERATURE SUPERCONDUCTOR $YBa_2Cu_3O_{7-\delta}$ (ADDITIVES: Nb_2O_5, Sb_2O_3, SnO_2, ZrO_2 OR BeO)

3.1 INTRODUCTION

The discovery of high temperature superconductivity in copper oxide based materials has generated enormous amount of activities on these materials because of their high scientific and technological potential. One of the immediate approaches towards the search for new and better materials is made through doping studies. Doping studies can provide information about the fundamental mechanism behind the observed properties, improve the properties of existing materials, provide new materials and compounds with superior properties and tailor the properties of existing materials for specific technological applications. During doping, the dopants can go into the lattice of the host material, or can react with the host material to form a second phase or can remain as an impurity. In conventional superconductors, additives and second phases along with the parent phase have a prominent role in enhancing the current densities to several times especially in an applied magnetic field through a phenomena called flux pinning (1). The presence of minor quantities of suitable additives and impurities acts as flux trapping centers, so that extremely high values of current passes through the superconductor in presence of applied magnetic field. This chapter describes the effect of additives on high temperature

superconductor $YBa_2Cu_3O_{7-\delta}$, its superconducting properties, crystal structure, current densities etc.

During doping the dopants can go into the lattice sites of the host material or can remain as an impurity in the host material or can react with the host material forming a second phase which depends on the host material, its crystal structure and the nature of the dopants. The effects of dopants which substitute for various cationic and anionic sites of YBCO have been studied extensively by many researchers and have been described briefly in chapter 1. The variations in the superconducting properties and other physical and structural properties due to substitution have been established by now (2-6). The studies have shown that various rare earth substitutions for yttrium have the same effect on superconducting properties except in the case of Ce, Pr and Tb which destroy the high T_c properties. The role of Y and other rare earths in YBCO is to provide the characteristic crystal structure possessing the CuO net-works. Substitutions for Ba affect slightly, but there are remarkable changes in superconducting properties in the case of dopants which directly or indirectly interfere the CuO net-works. The cation and anion substitutions at these net-work sites, in general, lead to lowering of T_c through a host of reasons like localization of carriers, reduction in effective carrier concentration, obstruction of hopping process etc., and the effect is more prominent when the average spacing between dopants in the net-work matches with the range of coherence in the a-b plane.

Though there are several reports (2-6) on the effect of dopants which substitute for various lattice sites of YBCO, there are very few reports on the effect of dopants which do not substitute for different lattice sites of YBCO.

In the present investigation certain inert oxides such as Nb_2O_5, Sb_2O_3, SnO_2, ZrO_2 and BeO have been selected as additives because of certain special features of these oxides when added to YBCO superconductor. A survey of literature shows that these dopants do not reduce the superconducting transition temperature of YBCO upto a higher level of dopant concentration (7-15). Secondly it is found that these dopants react with YBCO forming a second phase except BeO. There are controversies about the nature of the dopant substitutions. Some authors claim that these dopants go into the lattice of YBCO for smaller concentrations (16 - 23). Even though the above oxides react with YBCO, the superconducting properties are not deteriorated at all, but in certain cases it enhances the superconducting properties. For example, addition of SnO_2 to YBCO enhances the current density by three times through modified microstructure and flux pinning action (10). Mössbauer spectroscopic studies on SnO_2 doped YBCO have been carried out for some basic understanding of the compound YBCO (18,24). Addition of Nb_2O_5 enhances the sintered density as well as current density of YBCO (14). Zirconia addition enhances the mechanical properties of high T_c superconductors (7). It has been reported by many researchers that good quality films can be grown on

zirconia substrates (25-27). The interfacial reaction is least for the films of YBCO deposited on yttria stabilized zirconia. Considerable amount of work has been done on the use of zirconia as a buffer layer in between various substrates such as Si, SiO_2, Al_2O_3 and high T_c films (28,29). But a comprehensive study on the reaction kinetics of YBCO-ZrO_2 system is lacking. Doping effects of Sb_2O_3 on YBCO are not available in literature (12). Thick films of YBCO have been fabricated on BeO substrates by Dabrowski et al. (15) since it is non-reactive. Because of these important characteristics of the above additives, a detailed study on the effect of these oxides on the superconducting properties of high T_c superconductors would be highly appropriate or adequate at present.

3.2 STUDIES ON Nb_2O_5 ADDED YBCO

3.2.1 Preparation of Nb_2O_5 added YBCO

Pure YBCO has been prepared from its constituent oxides and carbonates by solid state reaction method. Stoichiometric amount of pure and dried (99.9%) oxides and carbonates are weighed, mixed thoroughly in an agate mortar with acetone as wetting media. It was dried thoroughly, and calcined in an alumina crucible at 950^{o}C for 24 hours with one intermediate grinding. The phase purity of the compound YBCO has been confirmed by x-ray powder diffraction method. The pure YBCO prepared by this method was used for further investigations on additive effects.

For the preparation of Nb_2O_5 added YBCO, high purity Nb_2O_5

was added to the pure YBCO in the weight percentages 0.2, 0.5, 1.0, 1.5 and 2.0. The Nb_2O_5 added YBCO powder was mixed thoroughly in an agate mortar. Special care was taken to see that the dopants added to YBCO has mixed thoroughly to YBCO without any loss. It was then pressed in the form of pellets of diameter 12 mm and thickness 2 to 2.5 mm in a stainless steel die by uniaxial pressing with a pressure of 5 metric tonnes. The pellets were then kept on an alumina plate and sintered at 950^{o}C in air for 15 hours. The sintered pellets were then cooled slowly to room temperature in oxygen atmosphere (1^{o} C/min). Also samples were quenched to room temperature from 950^{o}C in air, in nitrogen atmosphere and into liquid nitrogen.

3.2.2 Nb_2O_5 added YBCO cooled slowly to room temperature

3.2.2.1 Resistivity of slow cooled samples

The resistivity of Nb_2O_5 added YBCO cooled slowly to room temperature in oxygen atmosphere was measured by Van der Pauw method described in chapter 2, as a function of temperature. The temperature-resistance curves for different amounts of Nb_2O_5 added YBCO are shown in Fig. 3.1. All the samples showed a metallic character with normal state resistivity almost in the same range as that of pure YBCO. Also the samples showed a superconducting transitition at 92 K, same as that of pure YBCO. There was no reduction in the T_c value due to Nb_2O_5 addition upto 2.0 wt% of Nb_2O_5. In the present investigation we have added Nb_2O_5 to YBCO upto

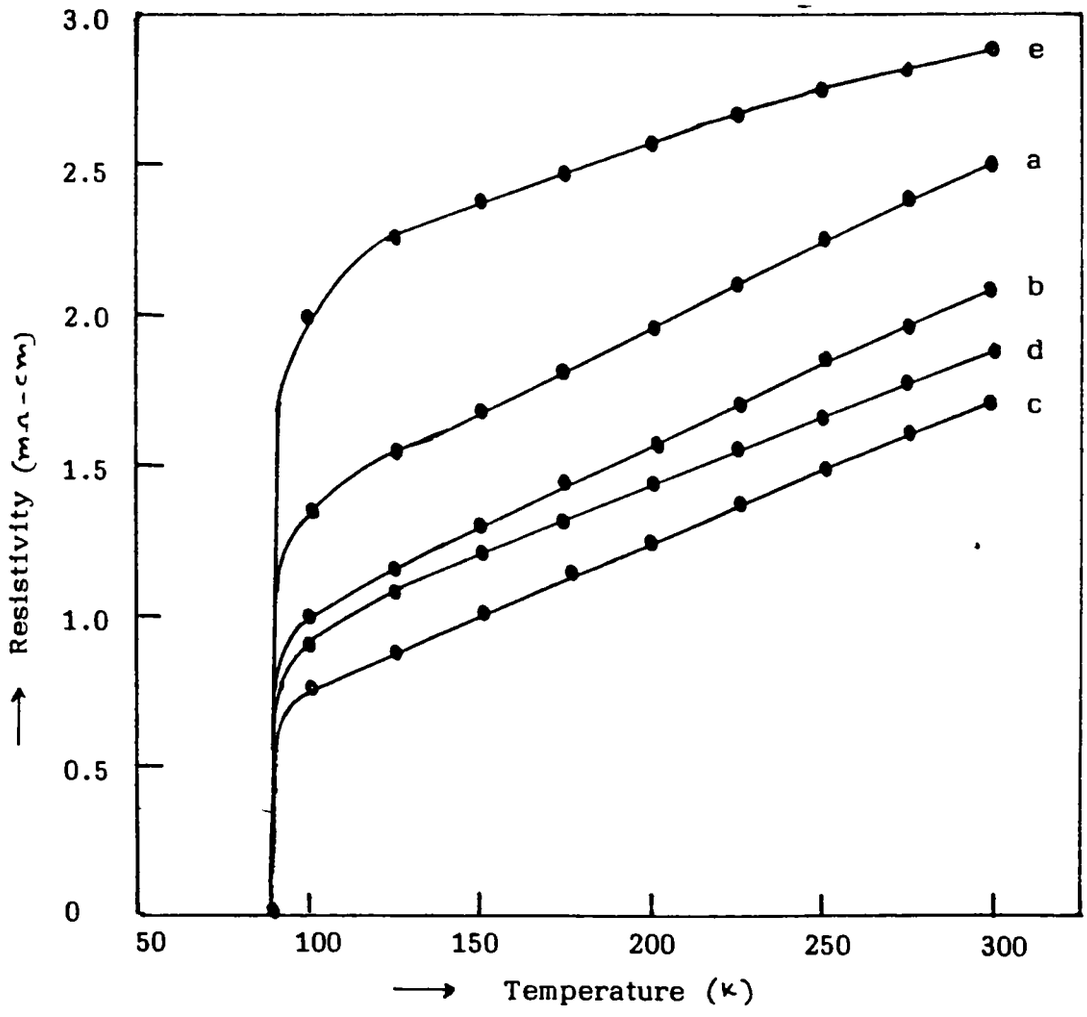

Fig. 3.1: Temperature-resistacne curve of different wt % of Nb_2O_5 added YBCO cooled slowly to room temperature in oxygen atmosphere

(a) 0 ; (b) 0.5 ; (c) 1.0; (d) 1.5; (e) 2.0

All the samples showed superconducting transition at 92 K, same as that of pure YBCO

2.0 wt %. Further addition of Nb_2O_5 increases the sintering temperature. For example, 5.0 wt % of Nb_2O_5 added YBCO sinteres only above 970°C which showed superconducting transition at a temperature same as that of pure YBCO. The temperature-resistance measurements show that the superconducting transition temperature is not affected with the addition of Nb_2O_5. The effect of addition of large amounts of the dopant is described in chapter 5.

3.2.2.2 X-ray powder diffraction studies on slow cooled samples

X-ray powder diffraction studies were carried out on Nb_2O_5 added YBCO sintered at 950°C and cooled slowly to room temperature in oxygen atmosphere to see its crystal structure variations due to Nb_2O_5 addition. Fig. 3.2 shows the powder diffraction pattern for various amounts of Nb_2O_5 added YBCO. All the doped samples show an orthorhombic structure as expected for a superconducting YBCO sample. No appreciable variation in lattice parameters has been observed due to Nb_2O_5 addition. But a few additional peaks at $2\theta = 30.1^o$, 42.8^o and 53^o apart from those of pure YBCO can be seen in the diffraction pattern. The presence of additional peaks indicate that Nb_2O_5 reacts with YBCO forming a second phase. The positions of the additional peaks and the intensity ratios exactly matches with that of Ba_2YNbO_6 compound (JCPDS file 24-1042) a cubic perovskite material. Further in the present investigation we have shown that the secondary phase formed in YBCO-Nb_2O_5 system is the compound Ba_2YNbO_6 by synthesising the compound and studying the phase compatibility between YBCO and Ba_2YNbO_6. A detailed study on

Fig. 3.2: XRD pattern of different wt % of Nb_2O_5 added YBCO cooled slowly to room temperature in oxygen atmosphere

(a) 0 ; (b) 0.5 ; (c) 1.0 ; (d) 2.0

All the smamples showed orthorhombic structure with no appreciable variations in lattice parameters.

the synthesis of Ba_2YNbO_6 and its coexistence with YBCO are described in chapters 4 and 5.

The x-ray powder diffraction studies show no appreciable variation in lattice parameters due to Nb_2O_5 addition. It also shows that a secondary phase is forming due to Nb_2O_5 addition. Since there is no lattice parameter variation, it indicates that probably niobium is not going appreciably into the lattice of YBCO and the presence of secondary phase in XRD confirms this conclusion. But some researchers have reported (19) that small percentage of niobium is going into the lattice of YBCO. The superconducting properties of YBCO are highly dependent on its crystal structure. The crystal structure in turn depends on its oxygen stoichiometry and the nature of dopants. In the present study it is found that Nb_2O_5 is not going into the lattice of YBCO and is not affecting its crystal structure and superconducting properties. As a result there is no reduction in superconducting transition temperature due to Nb_2O_5 addition as observed by resistivity measurements.

3.2.2.3 Density measurements

Measurement of density of any polycrystalline material is essential to evaluate its various measured properties. The current densities and various other electrical and magnetic properties of superconductors are dependent on its density. The oxygen absorption or oxygenation process in highly dense YBCO and single crystal YBCO are very slow compared to porous material or those materials which are in the powder form (30).

The bulk densities of pure and Nb_2O_5 added YBCO cooled slowly to room temperature are measured by Archimedes method and are given in Table 3.1. The density of YBCO varies with Nb_2O_5 addition and becomes maximum for about 1.0 wt % of Nb_2O_5. The increase in density of Nb_2O_5 added YBCO is reported by Matsubara et al. (14) as due to the modified microstructure by the formation of secondary phases.

Table 3.1: Density of Nb_2O_5 added YBCO cooled slowly to room temperature in oxygen atmosphere

Wt % of Nb_2O_5	Sintering temperature (^oC)	Density (gm/cm^3)
0	950	5.78
0.5	950	5.86
1.0	950	5.99
1.5	960	5.97
2.0	960	5.79

3.2.2.4 Current density of slow cooled samples

The temperature-resistance measurements have shown that there is no variation in superconducting transition temperature due to Nb_2O_5 addition. Hence it is important to study other superconducting properties especially the current density due to doping. The current densities of pure and Nb_2O_5 added YBCO cooled slowly

in oxygen atmosphere were measured as a function of temperature in zero magnetic field by the method described in chapter 2. Fig. 3.3 shows the current density of Nb_2O_5 added YBCO as a function of temperature. The current density of Nb_2O_5 added YBCO is found to have increased by three times as compared to that of pure YBCO. The enhanced current density can be attributed to the flux pinning action of the secondary phases formed due to Nb_2O_5 addition or due to the increased density or due to their combined effect. It has already been reported by Matsubara et al. (14) that the enhancement in current density in Nb_2O_5 doped YBCO is due to the formation of fine microstructure and the flux pinning action of secondary phases.

Scanning electron microscopic studies were carried out on polished surfaces of Nb_2O_5-added YBCO to observe the microstructural features. Fig. 3.4 shows the SEM picture of pure and doped YBCO which were cooled slowly to room temperature in oxygen atmosphere. The micrograph shows a fine and reduced grain size due to doping. The formation of secondary phases can be observed in the microstructure and is distributed throughout the bulk of the material. From the figure it is evident that the samples are non-porous or in another words the Nb_2O_5-added samples are highly dense. The increase in current density is due to the increased density and modified microstructure as observed by SEM micrographs.

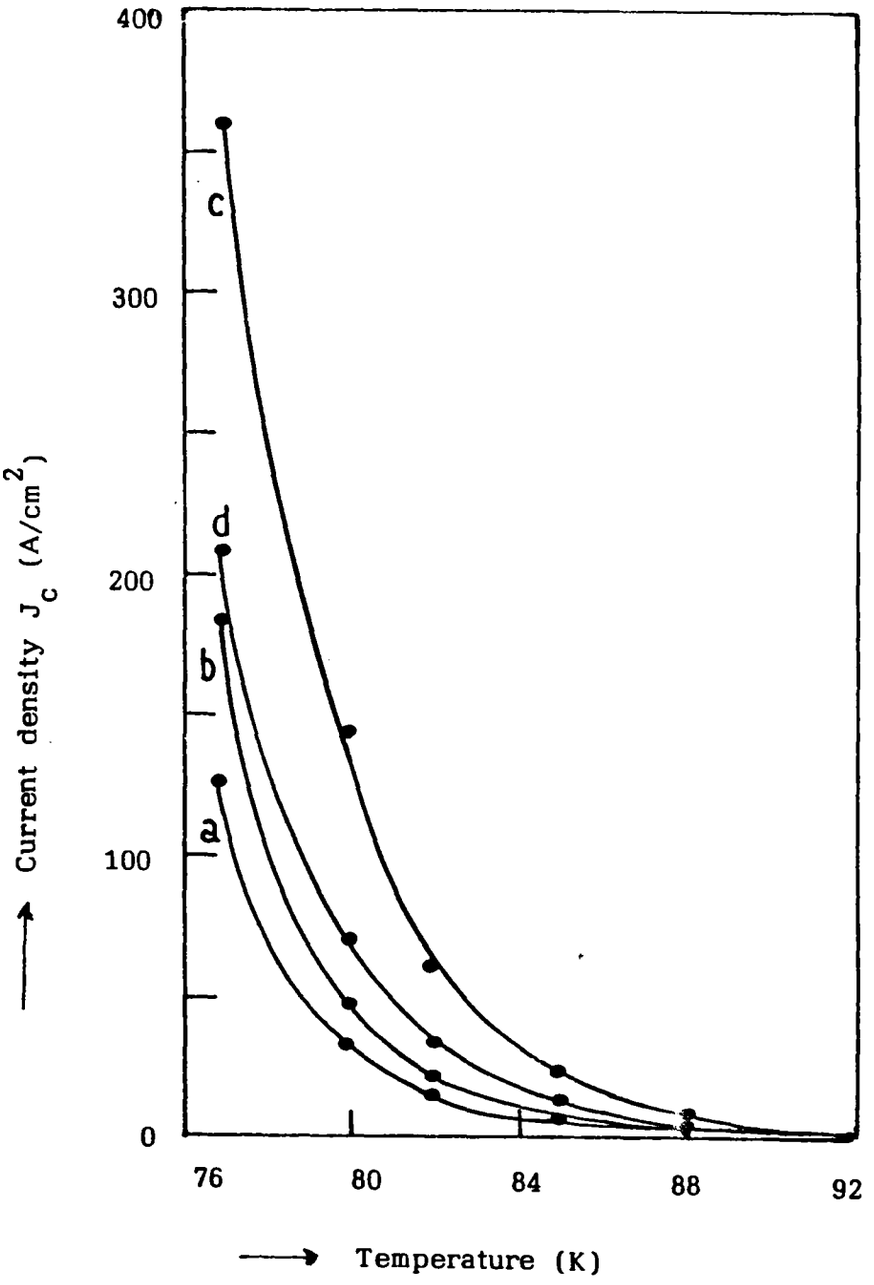

Fig. 3.3: Variation of current density (J_c) as a function of temperature for different wt % of Nb_2O_5 added YBCO cooled slowly to room temperature in oxygen atmosphere

(a) 0; (b) 0.5 ; (c) 1.0 ; (d) 1.5

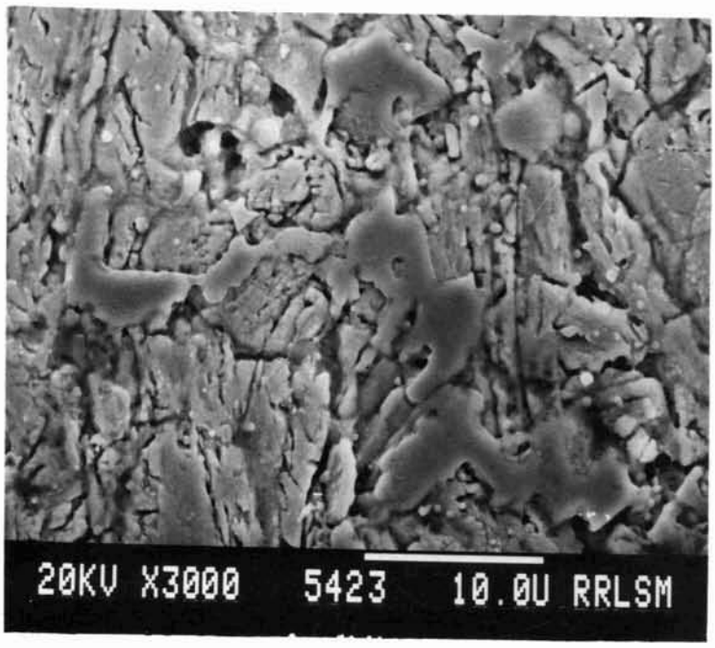

(a)

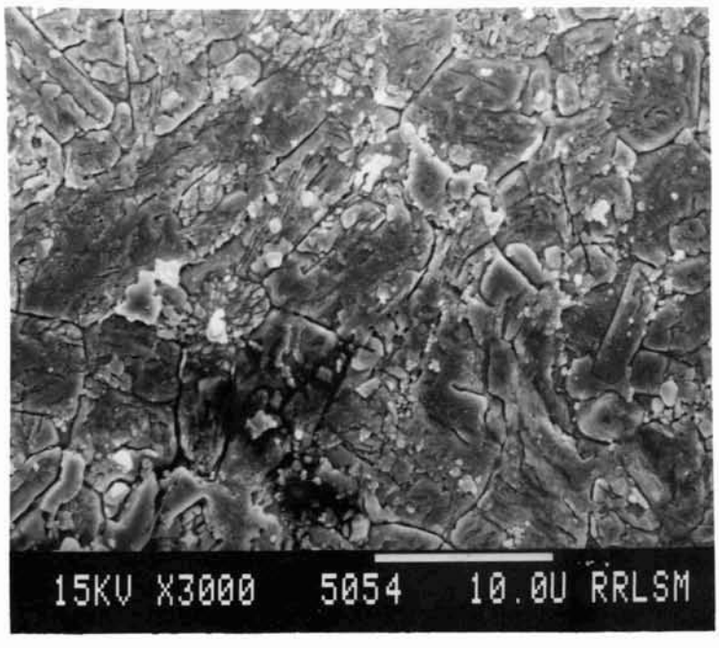

(b)

Fig. 3.4: Scanning electron micrographs of Nb_2O_5 added YBCO along with pure YBCO
(a) pure YBCO ; (b) 1.0 wt % Nb_2O_5 added YBCO

3.2.3 Nb_2O_5 added YBCO quenched from 950°C to room temperature

The studies on Nb_2O_5 added YBCO have shown that there is no variation in its physical as well as superconducting properties due to doping, but enhanced the current density by two to three times. The superconducting properties of YBCO are highly dependent on its crystal structure and oxygen stoichiometry. The crystal structure and oxygen stoichiometry again depend on the processing parameters. For obtaining an orthorhombic superconducting phase, slow cooling of processed YBCO in an oxygen atmosphere is essential. The samples quenched from higher temperatures normally show a semiconducting or an insulating behaviour. In the following we describe the studies on doped YBCO quenched to room temperature and into liquid nitrogen temperature.

3.2.3.1 Resistivity of Nb_2O_5 added YBCO quenched to room temperature

The resistivity of Nb_2O_5 added YBCO quenched from 950° C to room temperature in oxygen atmosphere are shown in Fig. 3.5 as a function of temperature. From the figure it is clear that all the doped samples show metallic behaviour with superconducting transition around 92 K. The undoped YBCO quenched to room temperature shows semiconducting behaviour with no superconducting transition upto liquid nitrogen temperature as expected. Even a small amount of (0.2 wt %) Nb_2O_5 is enough to get a superconducting sample on quenching to room temperature. There is no variation in the superconducting transition temperature of the quenched samples

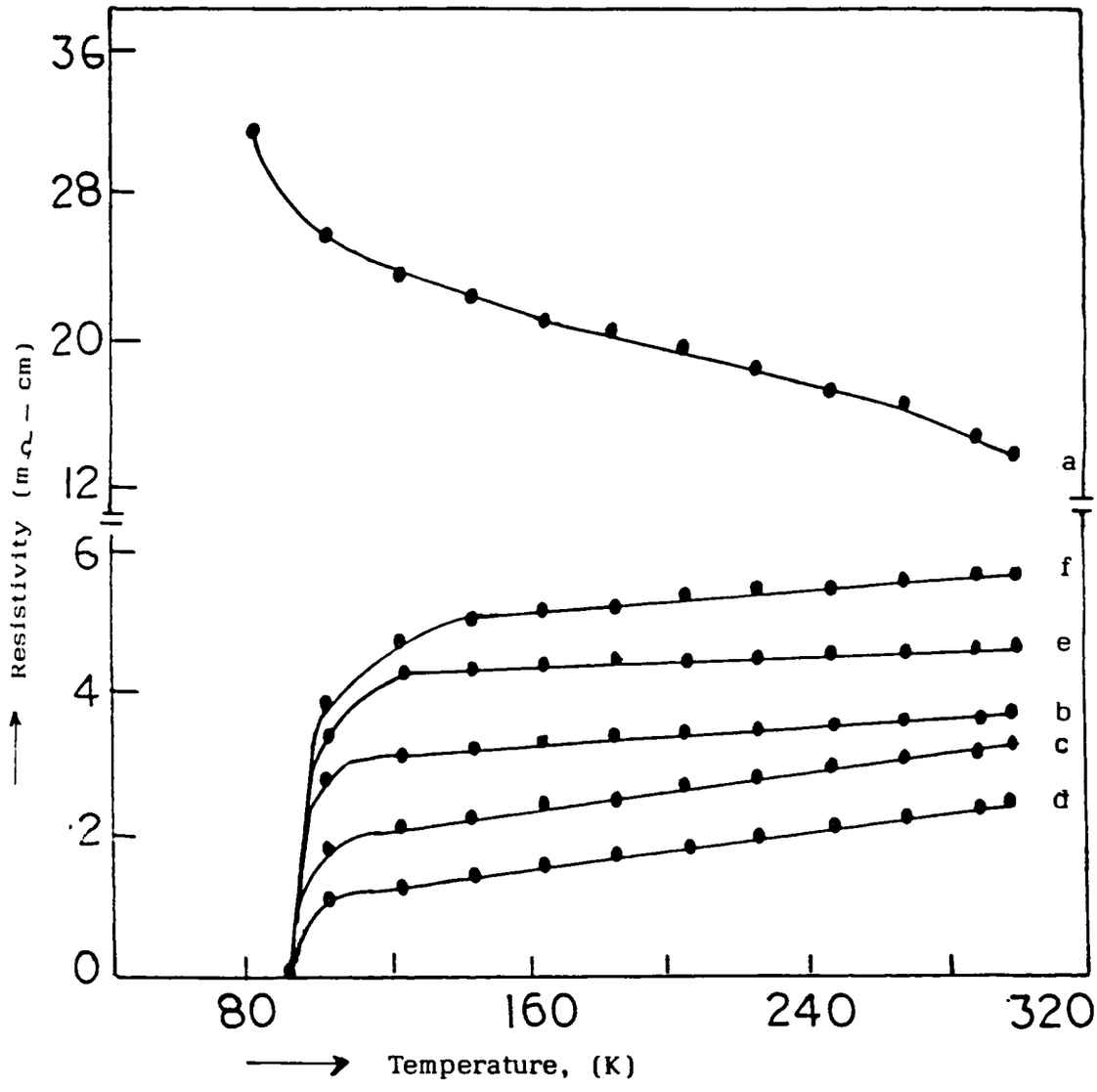

Fig. 3.5: Temperature-resistance curve of different wt % of Nb_2O_5 added YBCO quenched from 950°C to room temperature in oxygen atmosphere

(a) 0 ; (b) 0.2 ; (c) 0.5 ; (d) 1.0 ; (e) 1.5 ; (f) 2.0

All the samples showed superconducting transition at 92 K except the undped YBCO

with various concentration of the dopant as in the case of slow cooled samples.

The samples which were quenched to room temperature in nitrogen atmosphere and to liquid nitrogen showed a semiconducting behaviour in their R-T curve. Fig. 3.6 shows the R-T curve for samples quenched to different atmospheres. Thus it is evident from the figure that even in the case of doped YBCO, the superconductivity depends on the atmosphere in which the quenching process was carried out. This means that the superconducting properties of doped YBCO are also highly dependent on the processing conditions and atmosphere.

3.2.3.2 XRD studies on quenched YBCO

The crystal structure of pure and doped YBCO which are quenched to room temperature was studied by XRD method. The undoped YBCO showed a tetragonal structure (see Fig. 3.7) as expected. But in the case of Nb_2O_5 added YBCO it is found that the samples which are quenched to room temperature in oxygen atmosphere show an orthorhombic structure. Usually the tetragonal to orthorhombic transformation takes place as the sample cools below $700^{o}C$ with absorption of oxygen from atmosphere and this transformation is a time dependent process, and hence slow cooling of processed YBCO in an oxygen atmosphere is an essential pre-requisite for superconductivity. But in the case of doped YBCO, the fast cooling process (quenching to room temperature from sintering temperature) yields an orthorhombic phase instead of tetragonal phase.

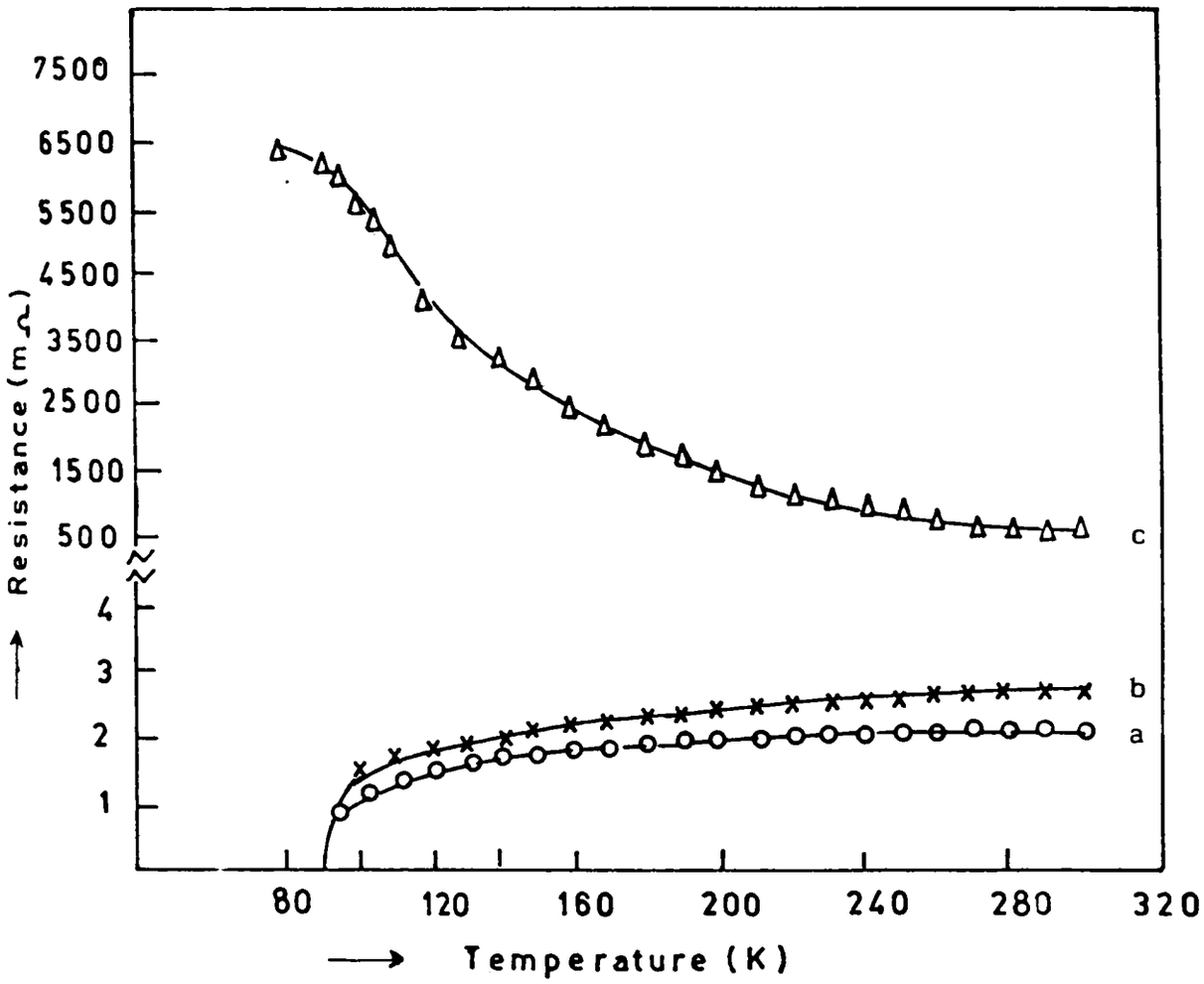

Fig. 3.6: Temperature-resistance curve of 1.0 wt % Nb_2O_5 added YBCO quenched to different atmospheres

(a) oxygen; (b) air; (c) nitrogen

The samples quenched in oxygen and air showed superconductivity whereas the samples quenched in nitrogen show semiconductivity

Fig. 3.7: XRD pattern of different wt % of Nb_2O_5 added YBCO quenched from 950°C to room temperature in oxygen atmosphere

(a) 0 ; (b) 0.5 ; (c) 1.0 ; (d) 1.5 ; (e) 2.0.

Thus no slow cooling or oxygen annealing process is required in the case of YBCO added with Nb_2O_5 sintered at 950^oC for obtaining a superconducting orthorhombic phase.

One possible reason for obtaining orthorhombic phase in quenched YBCO may be due to the shift in the thermodynamic phase transition temperature to 950^oC by Nb_2O_5 addition. High temperature x-ray diffraction studies can reveal the shift in the thermodynamic transition temperature. But indirect experiments have been carried out to verify it. The doped samples sintered at 950^oC for 15 hours are quenched to room temperature in gaseous nitrogen atmosphere at room temperature. The XRD pattern for the sample quenched in nitrogen atmosphere is shown in Fig. 3.8. The sample shows a tetragonal structure. In case the doped YBCO retains orthorhombic structure at higher temperatures of 950^oC etc., then the samples quenched to nitrogen atmosphere also should have shown orthorhombic structure; instead it showed a tetragonal structure. It confirms that there is no shift in the thermodynamic transformation temperature of YBCO due to Nb_2O_5 addition.

3.2.3.3 Oxygen content of quenched YBCO

The oxygen content in the doped samples which were quenched to room temperature in oxygen atmosphere is determined by iodometric titration method (31) neglecting the amount of secondary phase formed. It is found that the oxygen content in doped samples lies in the range 6.74 to 6.85 for 0.5 wt % to 2.0 wt %

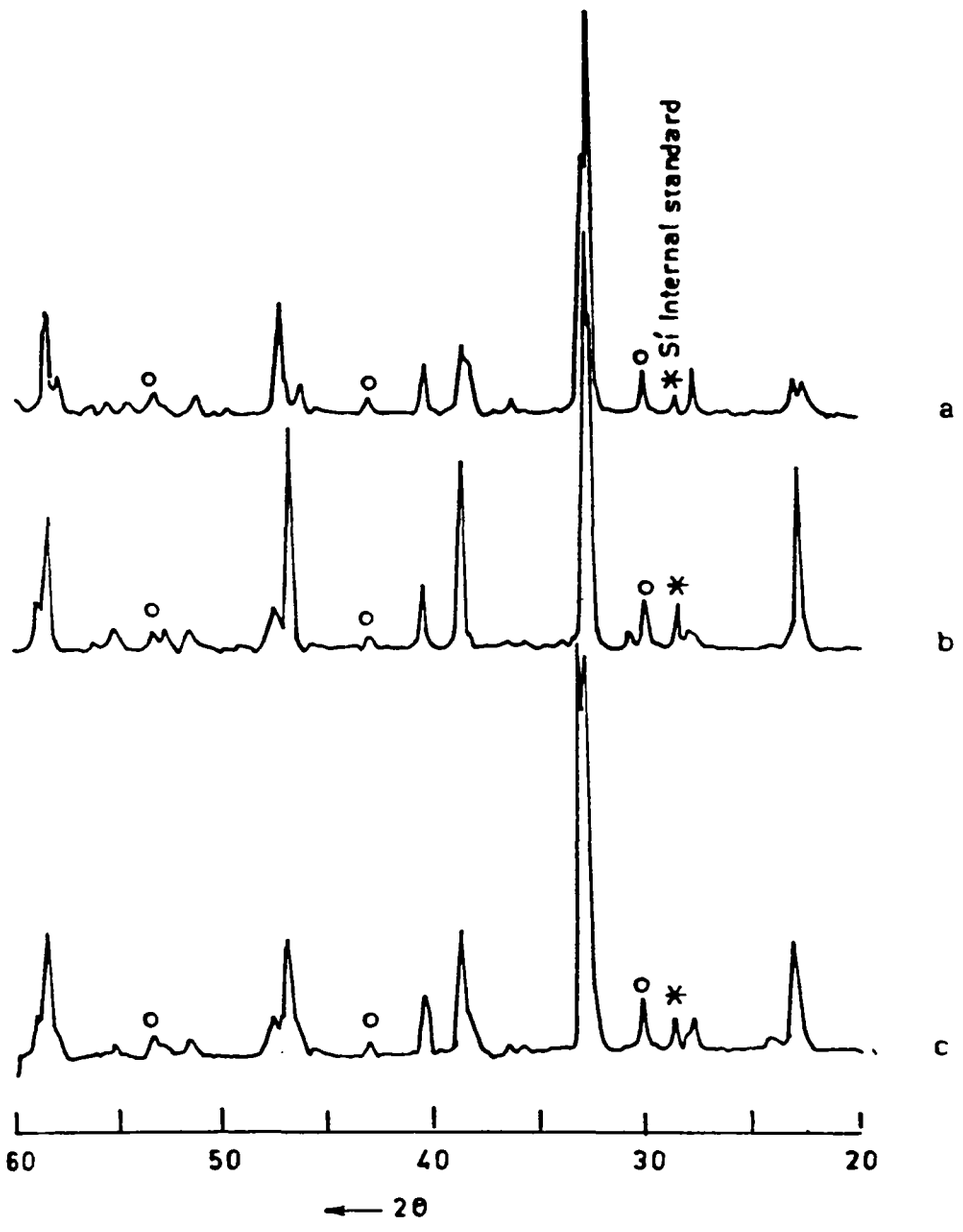

Fig. 3.8: XRD pattern of 1.0 wt % Nb_2O_5 added YBCO quenched into (a) nitrogen, (b) oxygen, and (c) air atmosphere

of Nb_2O_5 addition. There will be slight error in the determination of oxygen content because of the presence of secondary phase. Table 3.2 shows the oxygen stoichiometry of Nb_2O_5 added YBCO quenched to room temperature in oxygen atmosphere.

Table 3.2: The oxygen content of Nb_2O_5 added YBCO quenched from 950^oC to room temperature in oxygen atmosphere

Wt % of Nb_2O_5	Sintering temperature (^oC)	Oxygen content 'X' ($YBa_2Cu_3O_x$)
0	950	-
0.5	950	6.74
1.0	950	6.78
1.5	950	6.80
2.0	950	6.85

3.3 STUDIES ON Sb_2O_3 ADDED YBCO

3.3.1 Preparation of Sb_2O_3 added YBCO

High purity (99.9%) Sb_2O_3 was added to pure YBCO compound in the weight percentages 0.2, 0.5, 1.0, 1.5, 2.0 and mixed thoroughly in an agate mortar. It was then pressed in the form of pellets and sintered as in the case of Nb_2O_5 added YBCO discussed in section 3.2. The samples which are sintered at 950^oC for 15 hours are either cooled slowly in oxygen atmosphere or quenched

to room temperature in air, oxygen and nitrogen atmosphere and also into liquid nitrogen. The superconducting and other physical properties of Sb_2O_3 added YBCO processed as above were studied to see the effect of Sb_2O_3 addition in YBCO.

3.3.2 Sb_2O_3 added YBCO cooled slowly in oxygen atmosphere

3.3.2.1 Resistivity of slow cooled samples

The resistivity of Sb_2O_3 added YBCO cooled slowly to room temperature in oxygen atmosphere was measured by Van der Pauw method. Fig. 3.9 shows the temperature-resistance curve of Sb_2O_3 added YBCO for different amounts of Sb_2O_3. All the samples showed a metallic behaviour with superconducting transition at 92 K, same as that of pure YBCO. Thus Sb_2O_3 addition has no effect on the superconducting transition temperature of YBCO as in the case of Nb_2O_5 added YBCO. The room temperature resistivity of Sb_2O_3 doped YBCO lies almost in the same range as that of pure YBCO upto 2.0 wt % of Sb_2O_3 addition. The sintering temperature increases as the amount of Sb_2O_3 addition increases further.

3.3.2.2 XRD studies on slow cooled samples

The crystal structure of Sb_2O_3 added YBCO were studied by XRD method. Fig. 3.10 shows the powder diffraction pattern for different wt % of Sb_2O_3 added YBCO cooled slowly in oxygen atmosphere. All the samples show orthorhombic structure as expected for a superconducting YBCO. The lattice parameters of pure and Sb_2O_3 added YBCO were calculated and found to be same.

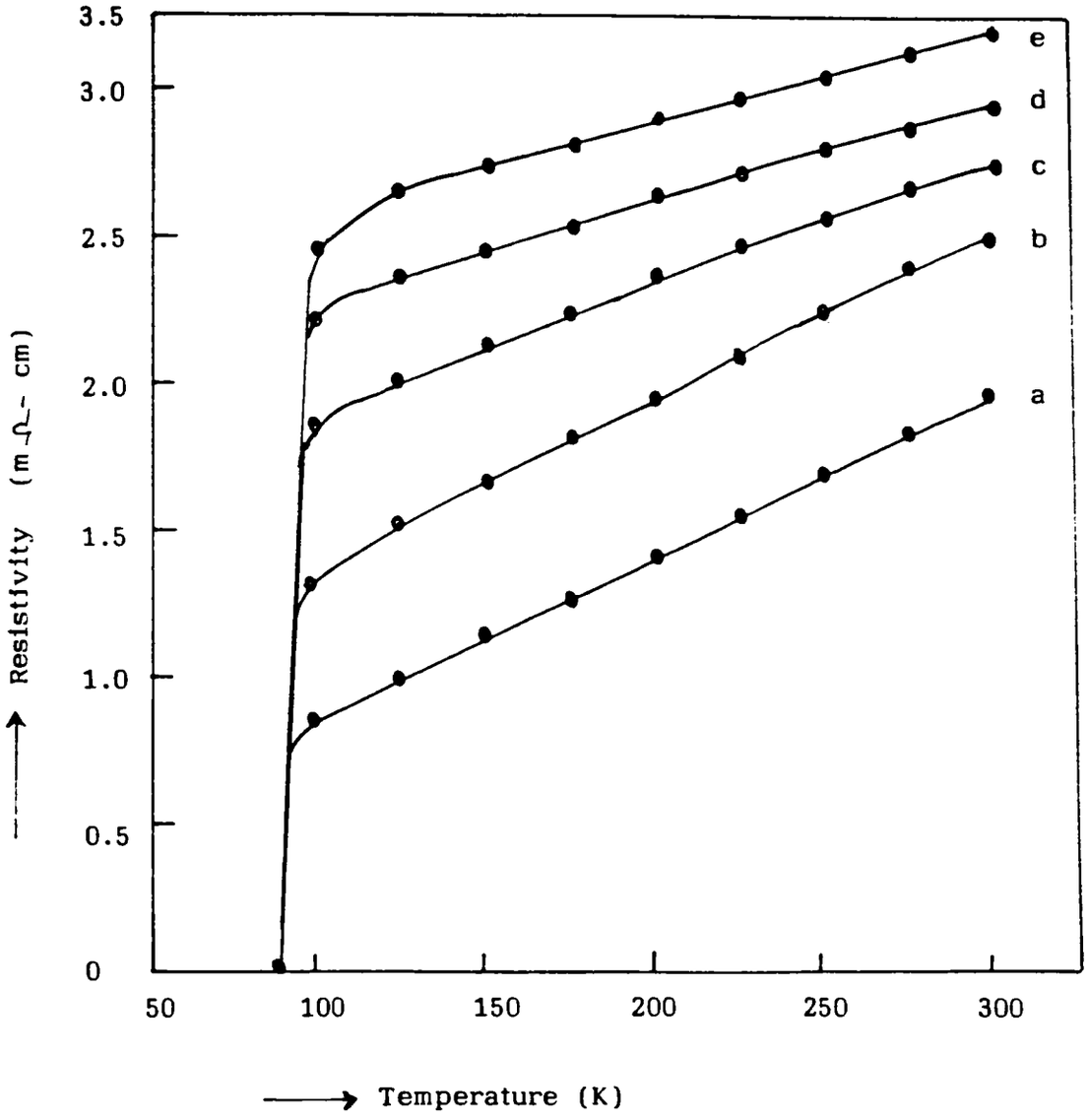

Fig. 3.9: Temperature-resistance curve of different wt % of Sb_2O_3 added YBCO coolwed slowly to room temperature in oxygen atmosphere

(a) 0 ; (b) 0.5 ; (c) 1.0 ; (d) 1.5 ; (e) 2.0

All the samples showed superconducting transition at 92 K

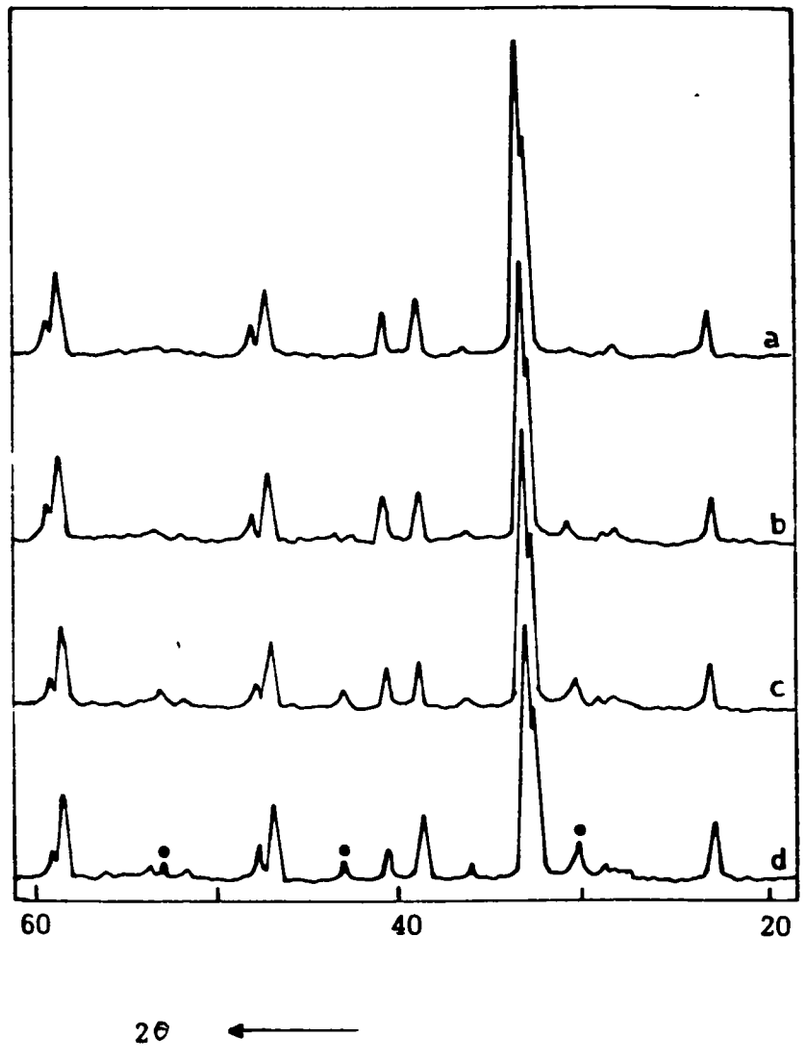

Fig. 3.10: XRD pattern of different wt % of Sb_2O_3 added YBCO cooled slowly to room temperature in oxygen atmosphere

(a) 0 ; (b) 0.5 ; (c) 1.0 ; (d) 2.0

All the samples showed orthorhombic structure with no appreciable variation in lattice parameter.

In Fig. 3.10 we can see some additional peaks apart from those of pure YBCO. The presence of additional peaks indicates that there are secondary phases in doped YBCO due to the reaction between YBCO and Sb_2O_3 on sintering at 950^oC. The positions of the additional peaks are at $2\theta = 30.1^o$, 42.8^o and 53^o and are exactly at the same positions of the impurity peaks in Nb_2O_5 doped YBCO with identical lattice spacing and intensity ratio. Due to the isostructural nature, the impurity phase in Sb_2O_3 doped YBCO has been assumed as due to structurally similar compound Ba_2YSbO_6. The formation of Ba_2YSbO_6 has been confirmed by preparing Ba_2YSbO_6 as a single phase material from its constituent oxides and the details of preparation and characterisation are described in chapter 4.

The Sb_2O_3 added YBCO shows no appreciable variation in lattice parameters, but forms a secondary phase by reacting with YBCO. It means that Sb_2O_3 is not going appreciably into the lattice of YBCO and does not affect its crystal structure and hence the superconducting properties. The superconducting transition temperature of YBCO is highly dependent on its crystal structure and oxygen stoichiometry. Since antimony is not going into the lattice site of YBCO and is not affecting the crystal structure and oxygen stoichiometry, the superconducting transition temperature keeps same as that of pure YBCO.

3.3.2.3 Density of slow cooled samples

The bulk density of pure and Sb_2O_3 added YBCO was measured and is given in Table 3.3. The density of YBCO increased slightly due to Sb_2O_3 addition. The increase in density may be

due to the liquid phase formation on adding Sb_2O_3 to YBCO and the liquid phase modifies the grains and grain boundaries.

Table 3.3: The bulk density and current density of Sb_2O_3 added YBCO cooled slowly to room temperature in oxygen atmosphere

Wt % of Sb_2O_3	Sintering temperature (^oC)	Density (gm/cm^3)	Current density (A/cm^2)
0	950	5.78	135
0.5	950	5.88	102
1.0	950	5.89	130
1.5	960	5.84	30
2.0	960	5.82	20

As in the case of Nb_2O_5 added YBCO, the current density of Sb_2O_3 added YBCO was measured to study the effect of Sb_2O_3 on the current carrying capacity of YBCO. The current density measurements show (Table 3.3) that there is no increase in current density due to Sb_2O_3 addition even though the transition temperature remains same as that of pure YBCO. The secondary phase formed due to Sb_2O_3 addition is very similar to the secondary phase formed in Nb_2O_5 added YBCO. The slight decrease in current density may be due to the weak link produced by the secondary phase Ba_2YSbO_6 between the superconducting grains. The secanning electron microscopic studies did not show any appreciable reduction in grain size

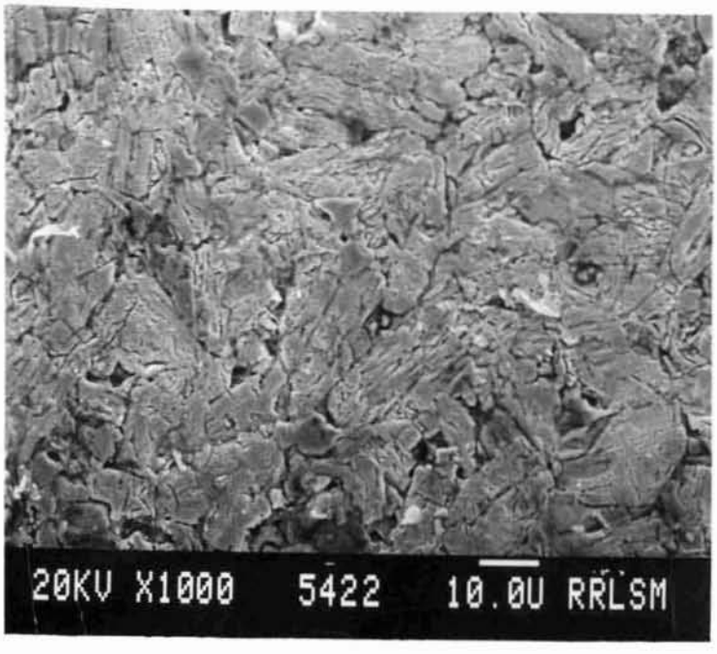

Fig. 3.11: Scanning electron micrograph of 1.0 wt % Sb_2O_3 added YBCO cooled slowly to room temperature in oxygen atmosphere

due to Sb_2O_3 addition (Fig. 3.11).

3.3.3 Sb_2O_3 added YBCO quenched to room temperature

The studies on Sb_2O_3 added YBCO have shown that the superconducting transition temperature and crystal structure are not affected with the addition of Sb_2O_3. Since the crystal structure, oxygen stoichiometry and the superconducting transition temperature of YBCO are highly dependent on its processing parameters such as cooling rate, atmosphere, sintering temperature etc., it will be interesting to study the crystal structure and superconducting properties of doped YBCO which are cooled fast or quenched in different atmospheres. In the following we discuss the effect of quenching of Sb_2O_3 added YBCO in different atmospheres.

3.3.3.1 Superconductivity in Sb_2O_3 added YBCO quenched to room temperature

The temperature-resistance curves for Sb_2O_3 added YBCO quenched from 950^{o}C to room temperature in an oxygen atmosphere are shown in Fig. 3.12. All the doped samples show a metallic behaviour with superconducting transition at 92 K. The undoped YBCO shows a semiconducting behaviour. Even a small amount of (0.2 wt %) of Sb_2O_3 is enough to get a superconducting YBCO by quenching to room temperature. The samples which are quenched to room temperature in gaseous nitrogen atmosphere and into liquid nitrogen did not show any superconducting transition. They showed semiconducting behaviour in the R-T curve as expected.

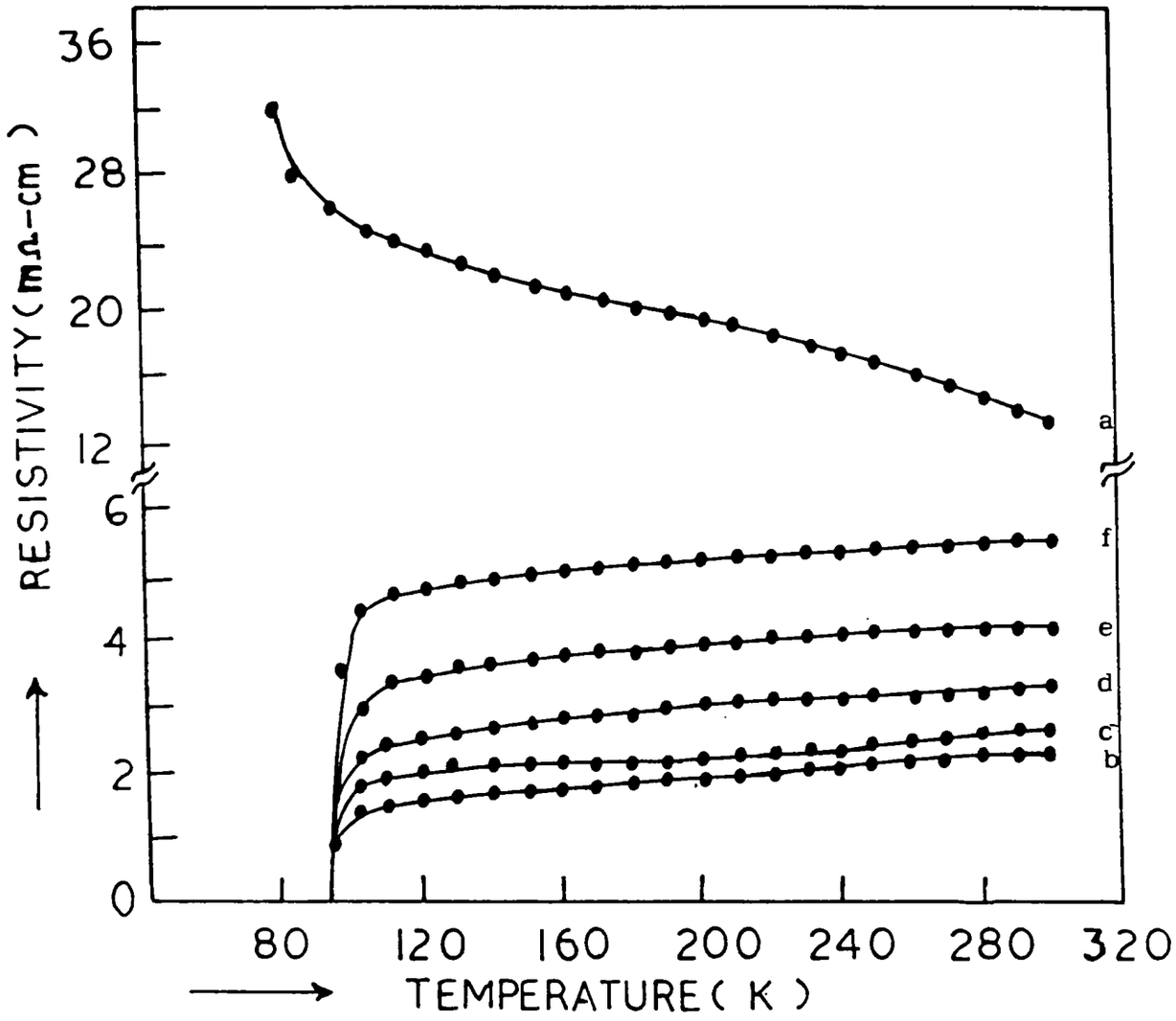

Fig. 3.12: Temperature-resistance curve of different wt % of Sb_2O_3 added YBCO quenched from 950°C to room temperature in an oxygen atmosphere

(a) 0 ; (b) 0.2 ; (c) 0.5 ; (d) 1.0 ; (e) 1.5 ; (f) 2.0

All the samples showed superconducting transition at 92 K except the undoped YBCO (a)

The DC susceptibility of Sb_2O_3 added YBCO quenched to room temperature in oxygen atmosphere was measured as a function of temperature in a magnetic field of 50 Gauss using a SQUID magnetometer. The undoped YBCO quenched to room temperature did not show a diamagnetic transition whereas all the Sb_2O_3 doped YBCO showed diamagnetic transition at about 92 K. The DC susceptibility curve (Fig. 3.13) shows that the volume fraction of superconducting phase increases as the amount of Sb_2O_3 addition increases. Further the DC susceptibility measurements also proves that the superconductivity in doped YBCO quenched to room temperature is not a surface phenomena. In case it is a surface phenomena, the field cooled susceptibility curve should not show any diamagnetic transition as observed in the present investigation.

3.3.3.2 XRD studies on Sb_2O_3 added YBCO quenched to room temperature

The crystal structure of pure and doped YBCO which were quenched to room temperature in oxygen atmosphere is studied by x-ray diffraction method. All the doped samples show an orthorhombic structure as in the case of Nb_2O_5 added YBCO. But the Sb_2O_3 doped YBCO quenched to room temperature in nitrogen atmospheres showed tetragonal structures and are not superconducting. The experimental results indicate that the doped samples absorb oxygen from the surroundings and transform to orthorhombic form within a few minutes, whereas in the case of samples which are quenched to nitrogen atmosphere, there is no oxygen to absorb from

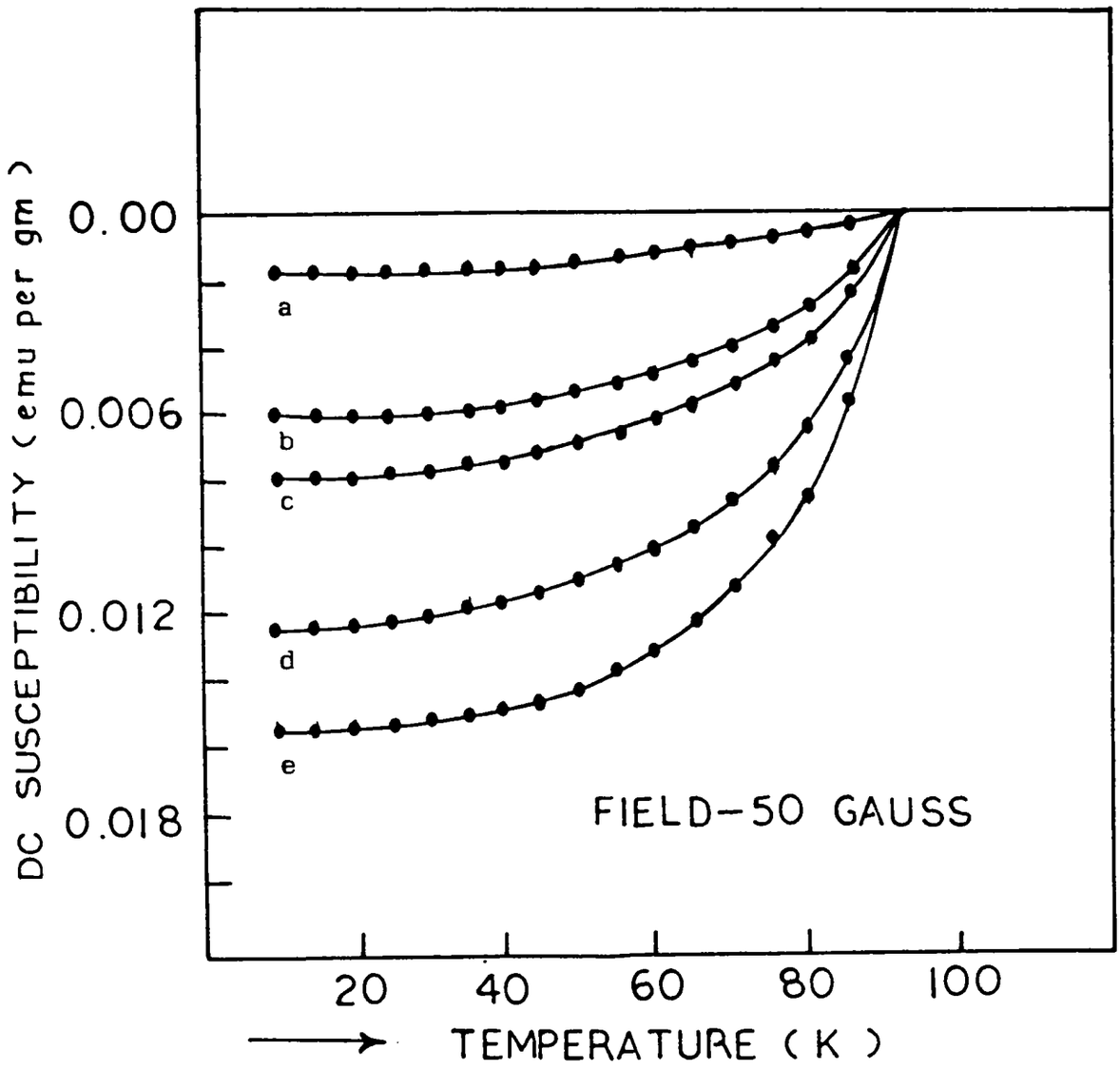

Fig. 3.13: Field cooled DC susceptibility curve of different wt % of Sb_2O_3 added YBCO quenched from 950°C to room temperature in an oxygen atmosphere
(a) 0 ; (b) 0.5 ; (c) 1.0 ; (d) 1.5 ; (e) 2.0

the surroundings to transform to orthorhombic structure and as a result it shows tetragonal structure.

3.3.3.3 Determination of oxygen content

The oxygen content in Sb_2O_3 added samples quenched to room temperature in oxygen atmosphere was determined by iodometric titration method (31) neglecting the amount of secondary phase formed due to Sb_2O_3 addition. Table 3.4 gives the values of oxygen content for different amounts of Sb_2O_3 addition. The oxygen content varies from 6.72 to 6.87. Since the percentage of Sb_2O_3 added to YBCO is small the percentage of secondary phase formed in the system will also be very small and the error in the determination of oxygen content in doped YBCO by the above method will be negligible. The oxygen content determination indicates that the Sb_2O_3 added YBCO quenched to room temperature absorbed enough oxygen required for transforming to superconducting orthorhombic phase.

Table 3.4: The oxygen content of Sb_2O_3 added YBCO quenched to room temperature in oxygen atmosphere from the sintering temperature

Wt % of Sb_2O_3	Sintering temperature, (^oC)	Oxygen content 'X' ($YBa_2Cu_3O_x$)
0	950	-
0.5	945	6.72
1.0	950	6.78
1.5	950	6.82
2.0	950	6.87

3.4 STUDIES ON SnO_2 ADDED YBCO

3.4.1 Superconductivity in SnO_2 added YBCO

The SnO_2 added YBCO was prepared in a similar way as that of Nb_2O_5 added YBCO. The superconducting transition temperature of SnO_2 added samples was studied by temperature-resistance measurements. All the slow cooled samples showed superconducting transition at 92 K, same as that of pure YBCO (Fig. 3.14). The superconducting transition temperature has not been affected with the addition of SnO_2 as in the case of Nb_2O_5 or Sb_2O_3. The room temperature resistivity of SnO_2 added samples are found to be in the same range as that of undoped YBCO cooled slowly to room temperature. The R-T curve shows metallic behaviour with sharp superconducting transition at 92 K.

The temperature-resistance measurements of SnO_2 added YBCO quenched from 950^oC to room temperature in oxygen atmosphere also showed metallic behaviour with superconducting transition at 92 K as in the case of Nb_2O_5 or Sb_2O_3 added YBCO. The superconducting transition temperature is same irrespective of the amount of SnO_2 addition (Fig. 3.15). The samples which are quenched to room temperature in nitrogen atmosphere show semiconducting behaviour with no superconducting transition down to 77 K. The samples which are quenched into liquid nitrogen are nonsuperconducting as in the case of Nb_2O_5 added YBCO.

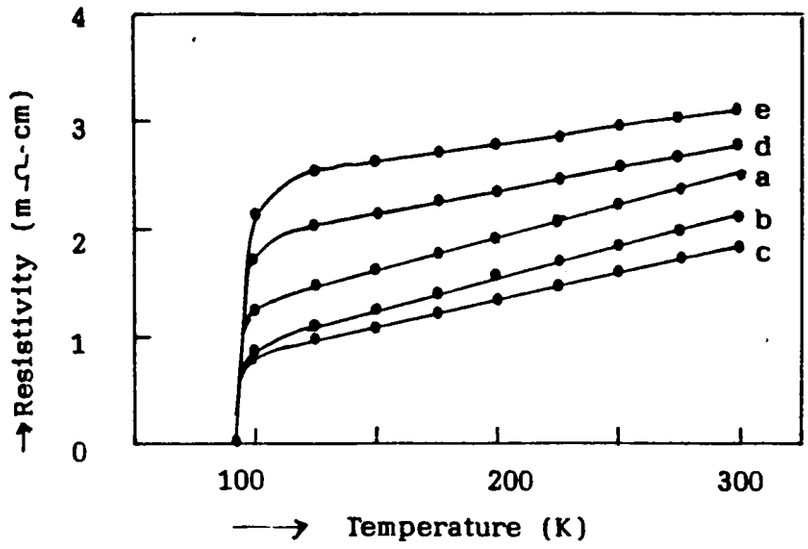

Fig. 3.14: Temperature-resistance curve of different wt % of SnO_2 added YBCO cooled slowly to room temperature in oxygen temperature
(a) 0; (b) 0.5 ; (c) 1.0 ; (d) 1.5 ; (e) 2.0
All the samples showed superconducting transition at 92 K

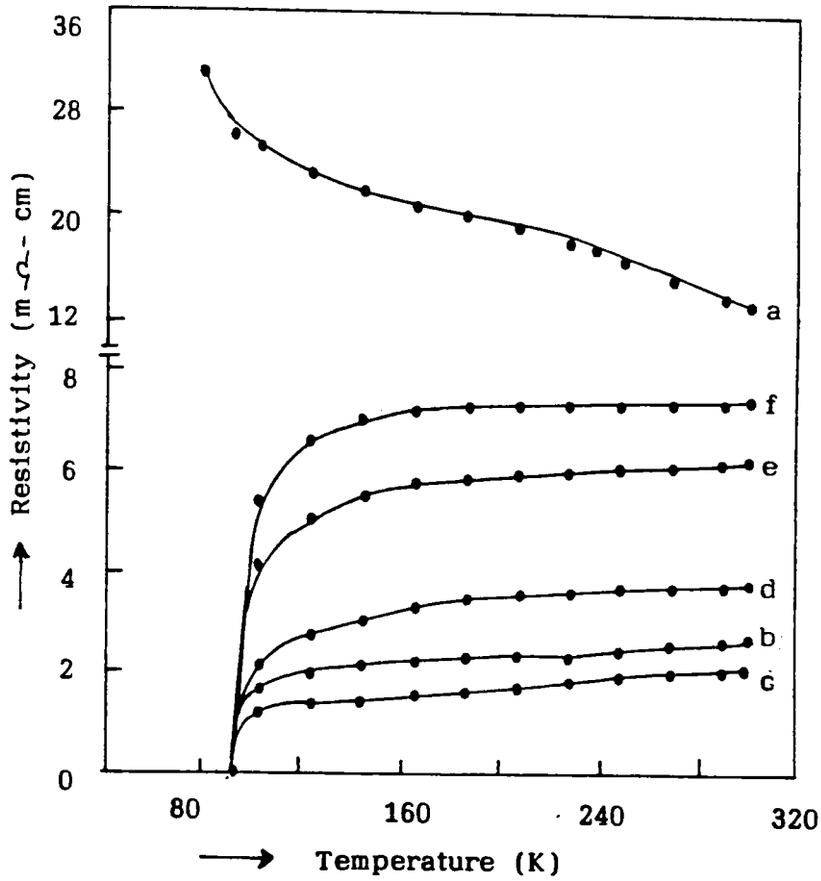

Fig. 3.15: Temperature-resistance curve of different wt % of SnO_2 added YBCO quenched from 950°C to room temperature in oxygen atmosphere
(a) 0; (b) 0.2 ; (c) 0.5 ; (d) 1.0 ; (e) 1.5 ; (f) 2.0
All the samples showed superconducting transition at 92 K except the undoped YBCO (a).

3.4.2 Crystal structure of SnO_2 added YBCO

The crystal structure of SnO_2 added YBCO was studied by XRD method. All the slow cooled samples showed superconducting orthorhombic structure with no appreciable variation in lattice parameters. Fig. 3.16 shows the powder diffraction pattern of SnO_2 added YBCO cooled slowly to room temperature in oxygen atmosphere. From the figure it is evident that there are a few additional peaks at $2\theta = 30.1^{o}, 42.8^{o}, 53^{o}$ apart from those of pure YBCO. From the figure it is also evident that there is no measurable variation in lattice parameters and at the same time presence of additional peaks indicate that SnO_2 has not gone into the lattice of YBCO, but forms a secondary phase by reacting with YBCO at higher temperatures of sintering. In literature it has been reported (10) that the second phase formed in YBCO due to SnO_2 doping is the compound $BaSnO_3$, a cubic perovskite material. But in the present investigation it is found that the second phase formed during high temperature sintering of YBCO-SnO_2 system is a new compound Ba_2YSnO_6 isostructural with the compound Ba_2YNbO_6. Details of preparation of the compound Ba_2YSnO_6 and its characterisation are described in chapter 4 and further confirmed that the second phase in the system is the new compound Ba_2YSnO_6 and not $BaSnO_3$ by studying the reactivity between the two compounds YBCO and Ba_2YSnO_6.

X-ray powder diffraction patterns were recorded for SnO_2 added YBCO quenched to room temperature in oxygen atmosphere. All the SnO_2 added YBCO which were quenched to room temperature

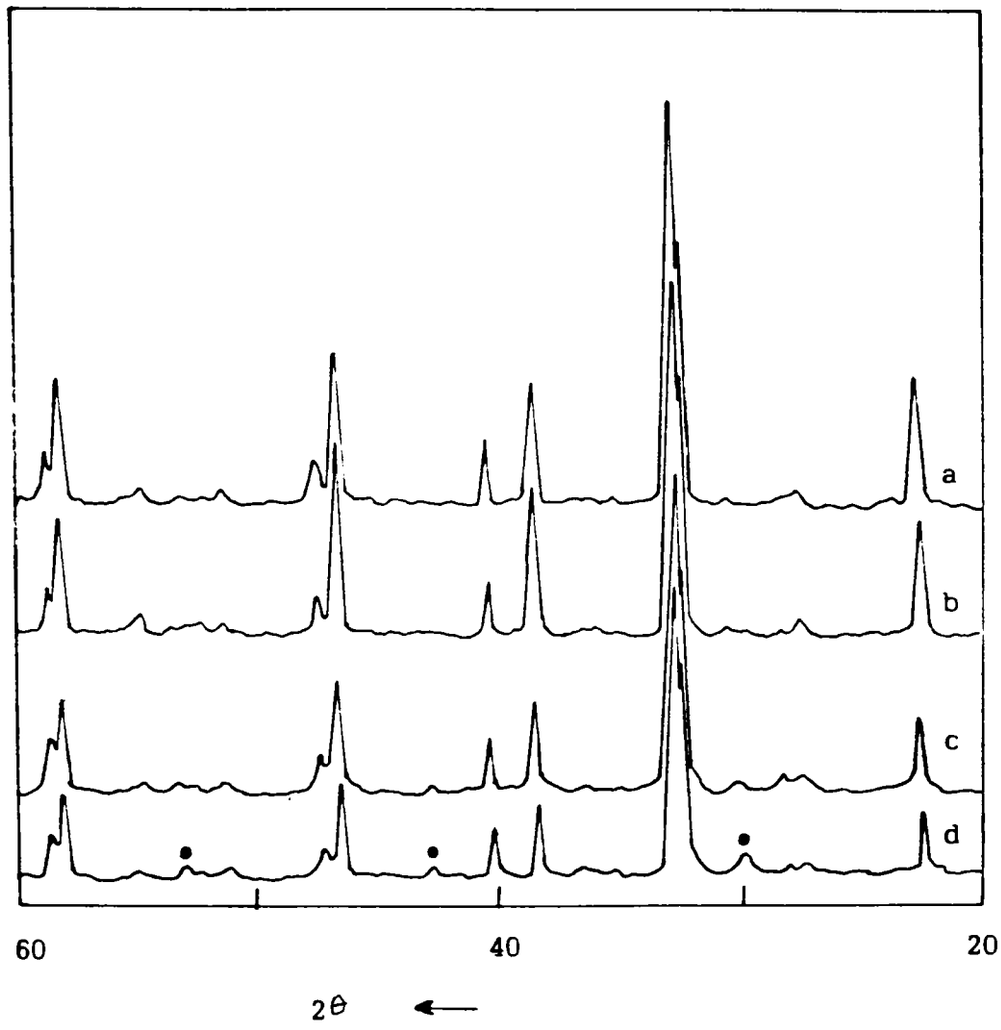

Fig. 3.16: XRD pattern of different wt % of SnO_2 added YBCO cooled slowly to room temperature in oxygen atmosphere

(a) 0 ; (b) 0.5 ; (c) 1.0 ; (d) 2.0

All the samples showed orthorhombic structure with no appreciable variation in lattice parameters

showed orthorhombic structure instead of tetragonal structure as in the case of Nb_2O_5 added YBCO. In order to see any shift in thermodynamic transformation temperature of YBCO due to SnO_2 addition, samples were quenched to room temperature in nitrogen atmosphere which resulted in tetragonal structure indicating that there is no real shift in the thermodynamic transformation temperature due to SnO_2 addition. The samples which were quenched into liquid nitrogen always showed a tetragonal structure.

3.4.3 Determination of oxygen content

The oxygen content in SnO_2 added YBCO which are quenched from 950^oC to room temperature in oxygen atmosphere has been determined by iodometric titration method (31) neglecting the small amount of secondary phase formed due to SnO_2 addition. Table 3.5 gives the oxygen content in SnO_2 added YBCO. All the doped samples which are quenched in oxygen atmosphere have shown oxygen content above 6.70. Thus the oxygen content determination shows that the samples have absorbed enough oxygen to transform from tetragonal to the orthorhombic structure during the short period of quenching.

3.4.4 The current density of SnO_2 added YBCO cooled slowly to room temperature in oxygen atmosphere

The current densities of SnO_2 added YBCO cooled slowly to room temperature in oxygen atmosphere were measured by the method described in chapter 2. The current density increased by three times as that of pure YBCO. Fig. 3.17 shows the variation

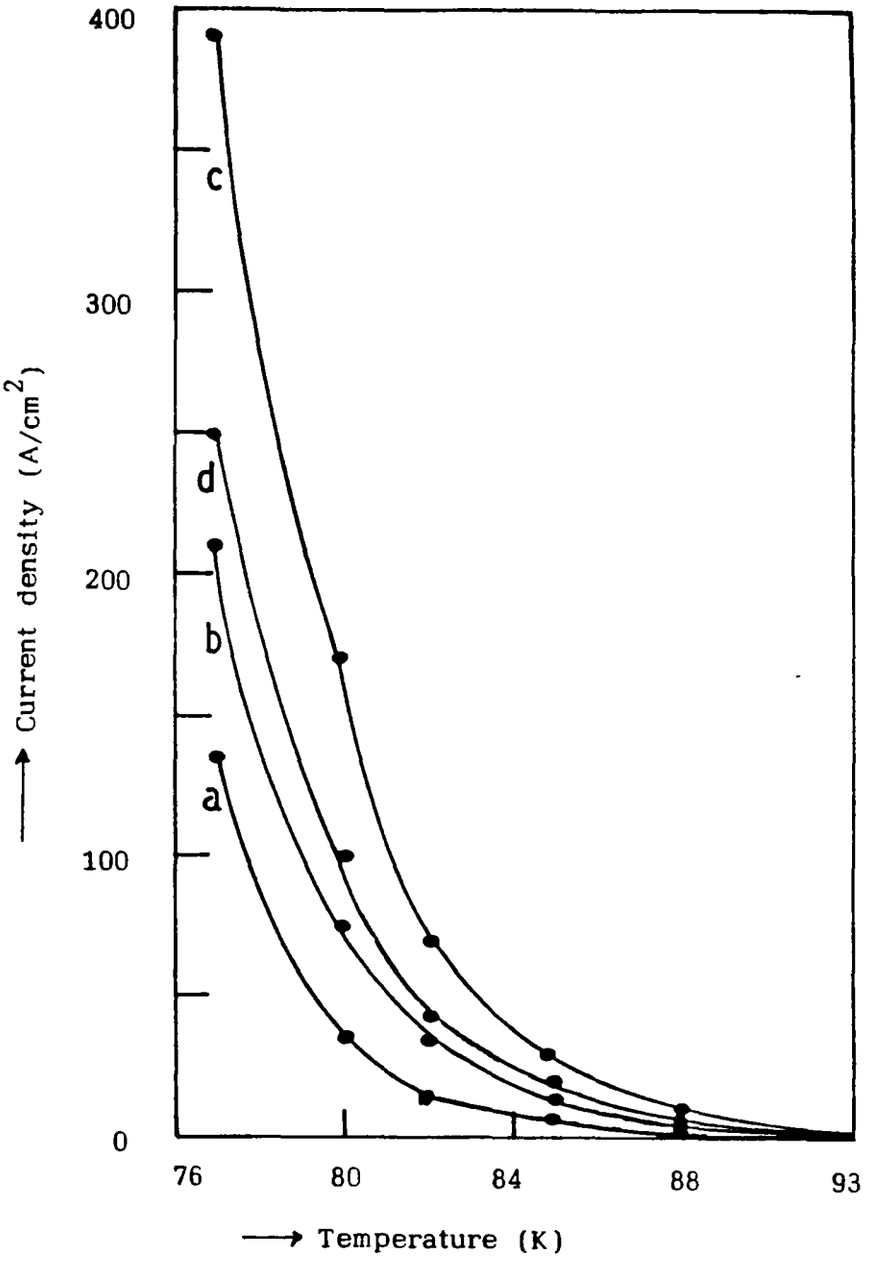

Fig. 3.17: variation of current density (J_c) as a function of temperature for different wt % of SnO_2 added YBCO cooled slowly to room temperautre in oxygen atmosphere

(a) 0 ; (b) 0.5 ; (c) 1.0 ; (d) 1.5

of current density as a function of temperature for different weight percentages of SnO_2 addition. The enhancement in current density in SnO_2 doped YBCO has been attributed to the flux pinning action of the secondary phase formed in the system.

Table 3.5: The oxygen content of SnO_2 added YBCO quenched from 950^oC to room temperature in an oxygen atmosphere

Wt % of SnO_2	Sintering temperature, (^oC)	Oxygen content 'X' ($YBa_2Cu_3O_x$)
0	950	-
0.5	950	6.70
1.0	950	6.76
1.5	950	6.78
2.0	950	6.82

The bulk densities of SnO_2 added YBCO have been measured and are given in Table 3.6. The density of SnO_2 added YBCO is found to have increased compared to pure YBCO. The scanning electron micrograph (Fig. 3.18) shows a uniform microstructure with a little porous area.

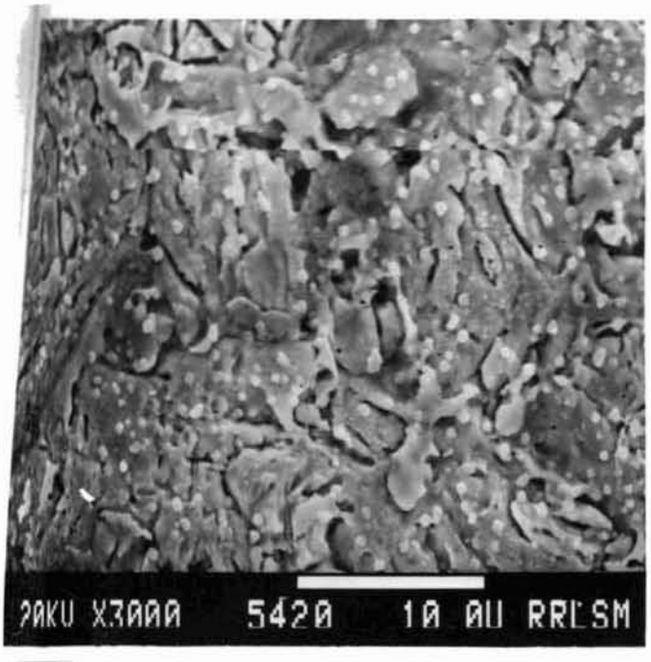

Fig. 3.18: Scanning electron micrograph of 1.0 wt % of SnO_2 added YBCO cooled slowly to room temperature in oxygen atmosphere

Table 3.6: Density of SnO_2 added YBCO cooled slowly to room temperature in oxygen atmosphere

Wt % of SnO_2	Sintering temperature, (^oC)	Density (gm/cm^3)
0	950	5.78
0.5	950	5.88
1.0	950	6.04
1.5	950	5.98
2.0	960	5.84

3.5 STUDIES ON ZrO_2 ADDED YBCO

ZrO_2 added YBCO was prepared by adding different wt % of pure (99.9%) ZrO_2 to YBCO compound. It was then thoroughly mixed and sintered at 950^oC as before. The sintered pellets were either quenched to room temperature in air, oxygen and nitrogen atmospheres or into liquid nitrogen. Samples were also cooled slowly to room temperature in oxygen atmosphere. The superconducting and other physical properties of ZrO_2 added YBCO processed as above were studied.

3.5.1 Superconductivity in ZrO_2 added YBCO

The resistivity of ZrO_2 added YBCO was measured from room temperature to liquid nitrogen temperature. Fig. 3.19 shows the temperature-resistance curve for ZrO_2 added YBCO cooled slowly

to room temperature in oxygen atmospheere. All the doped samples showed metallic behaviour with superconducting transition at 92 K. The room temperature resistivity of doped sample lies almost in the same range as that of pure YBCO. Thus the superconducting transition temperature of YBCO and its normal state resistivity have not been affected with the addition of ZrO_2 into YBCO.

The temperature-resistance curves for ZrO_2 added YBCO which are quenched from 950^{o}C to room temperature in oxygen atmosphere are shown in Fig. 3.20. In this case also all the samples showed metallic behaviour with superconducting transition at 92 K as in the case of other dopants. The R-T measurements on samples which are quenched in nitrogen atmosphere and into liquid nitrogen showed semiconducting behaviour. Thus the superconductivity in ZrO_2 doped YBCO depends on its processing atmosphere.

3.5.2 Crystal structure of ZrO_2 added YBCO

The crystal structure of ZrO_2 added YBCO was studied by XRD method. Fig. 3.21 shows the powder diffraction pattern for different wt % of ZrO_2 added YBCO cooled slowly to room temperature in oxygen atmosphere. All the doped samples showed orthorhombic structure. There is no appreciable variation in lattiice parameters due to ZrO_2 addition. But a few additional peaks appeared at positions 2θ = 30.1^{o}, 42.8^{o} and 53^{o} which are not present in the pattern recorded for pure YBCO. The lattice spacing and intensity ratios of the impurity peaks match with that of Nb_2O_5 added YBCO. In analogy with the secondary phase Ba_2YNbO_6 in YBCO-Nb_2O_5 system,

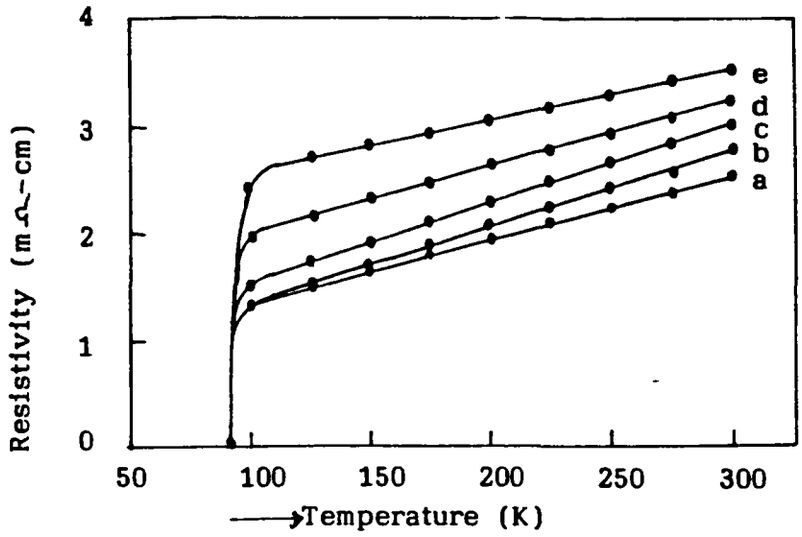

Fig.3.19: Temperature-resistance curve of different wt % of ZrO_2 added YBCO cooled slowly to room temperature in oxygen atmosphere
(a) 0 ; (b) 0.5 ; (c) 1.0 ; (d) 1.5 ; (e) 2.0

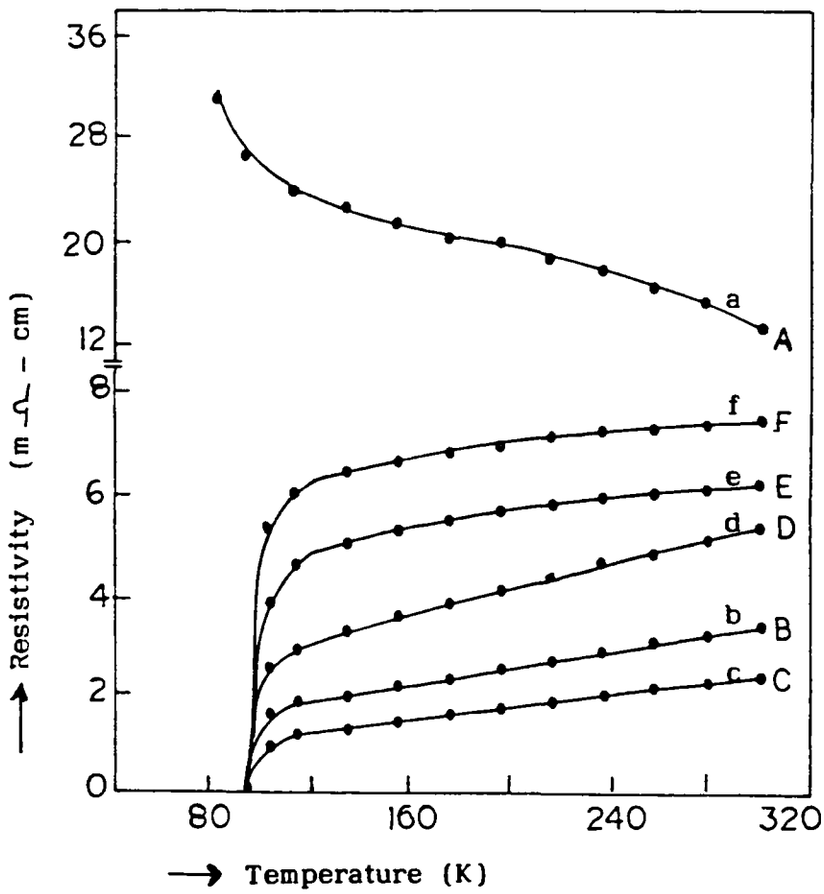

Fig. 3.20: Temperature-resistance curve of different wt % of ZrO_2 added YBCO quenched from 950°C to room temperature in oxygen atmosphere
(a) 0 ; (b) 0.2 ; (c) 0.5 ; (d) 1.0 ; (e) 1.5 ; (f) 2.0

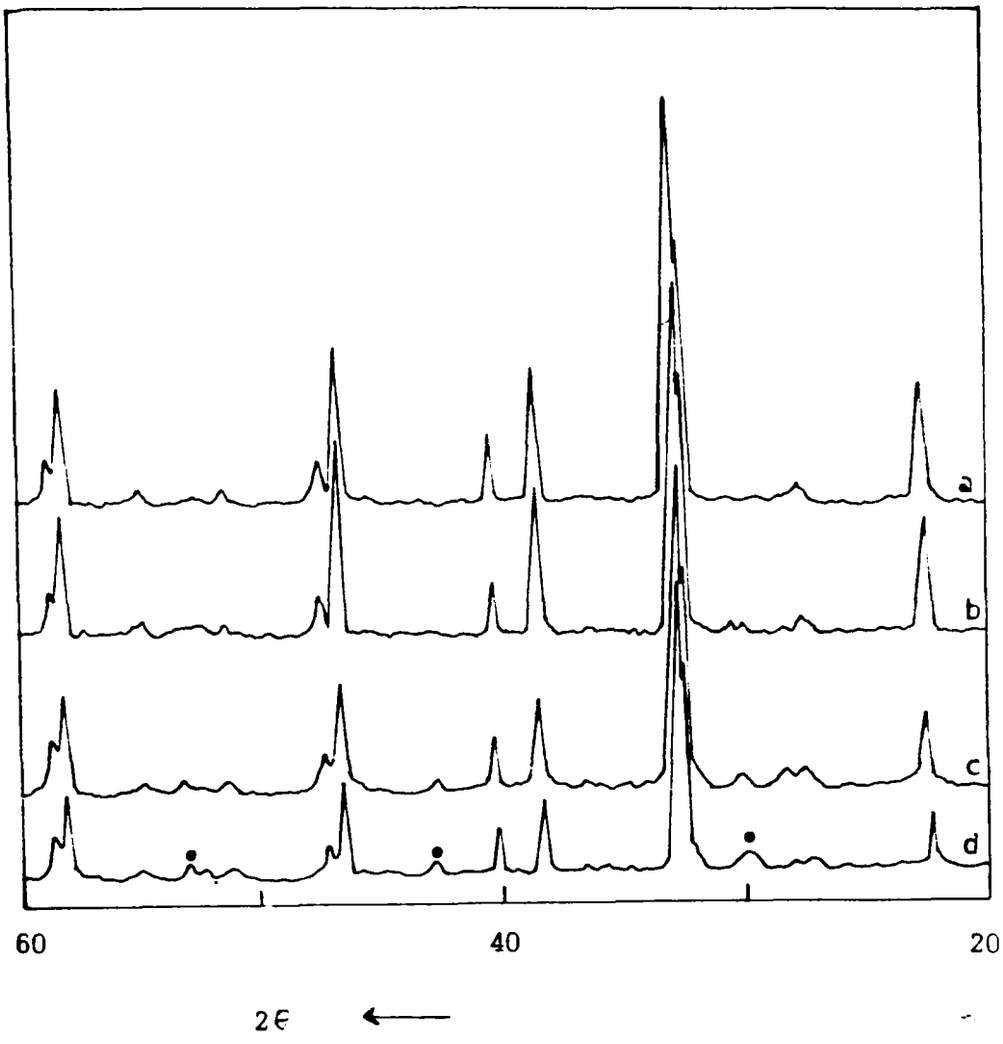

Fig. 3.21: XRD pattern of different wt % of ZrO_2 added YBCO cooled slowly to room temperature in oxygen atmosphere
(a) 0 ; (b) 0.5 ; (c) 1.0 ; (d) 2.0
All the samples showed orthorhombic structure with no appreciable variation in lattice parameter

it has been assumed that in the present case the secondary phase formed is a new compound having the chemical formula Ba_2YZrO_6 , a cubic perovskite compound. It has been reported by earlier researchers (26) that the secondary phase in YBCO-ZrO_2 system is the compound $BaZrO_3$ and its derivatives. But in the present investigation, we found the existence of the compound Ba_2YZrO_6 and have synthesised the compound as a single phase material (see chapter 4).

Since there is no lattice parameter variation due to ZrO_2 addition and a secondary phase is forming by reacting with YBCO, it has been concluded that zirconia is not going into the lattice of YBCO to an appreciable extent. As a result there is no reduction in the superconducting transition temperature due to ZrO_2 addition.

The XRD studies on ZrO_2 added YBCO quenched to room temperature also showed orthorhombic structure instead of tetragonal structure as in the case of previous dopants Nb_2O_5, Sb_2O_3, SnO_2 . The samples which are quenched to nitrogen atmosphere and into liquid nitrogen showed tetragonal structure. Thus as in the case of Nb_2O_5 addition, the superconducting properties of ZrO_2 added YBCO depends on the processing conditions and atmospheres.

3.5.3 Current density of ZrO_2 added YBCO cooled slowly to room temperature

The superconducting transition temperature of YBCO is not affected with the addition of ZrO_2 into YBCO. It will be interesting to study other superconducting properties such as critical current density etc. The current density of ZrO_2 added YBCO cooled slowly

to room temperature in oxygen atmosphere was measured at 77 K in zero field and are given in Table 3.7 along with the sintering temperature and bulk density. The current density is found to be decreasing with the addition of ZrO_2 . The decrease in current density may be due to the weak link between superconducting grains because of the presence of secondary phase Ba_2YZrO_6 at the grain boundaries. Scanning electron micrograph (Fig. 3.22) shows a uniform microstructure with relatively low porosity.

Table 3.7: Current density of ZrO_2 added YBCO cooled slowly to room temperature in oxygen atmosphere along with sintering temperature and bulk density

Wt % of ZrO_2	Sintering temperature, (^oC)	Bulk density (gm/cm^3)	Current density (A/cm^2)
0	950	5.78	130
0.5	950	5.80	130
1.0	950	5.88	118
1.5	960	5.89	100
2.0	960	5.87	78

3.5.4 Determination of oxygen content of ZrO_2 added YBCO

The oxygen content of ZrO_2 added YBCO processed at 950^oC and quenched to room temperature in oxygen atmosphere are given in Table 3.8. The oxygen content lies between 6.70 to 6.83, so that

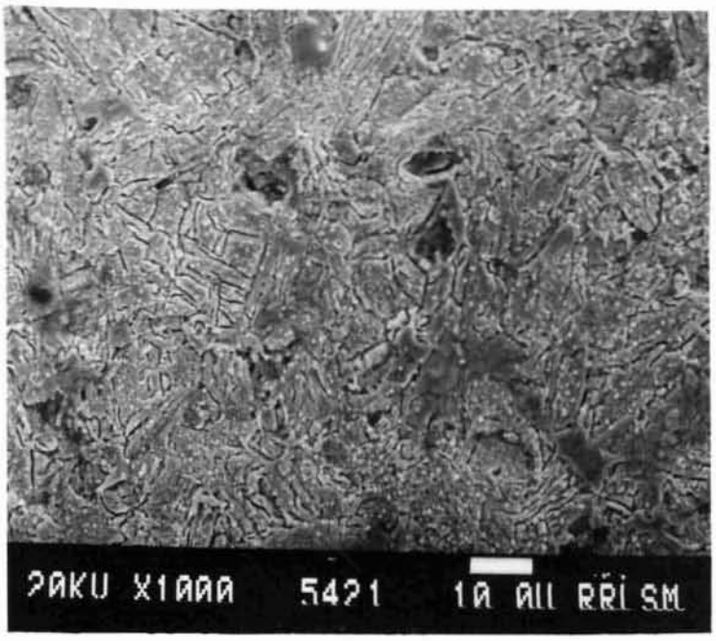

Fig. 3.22: Scanning electron micrograph of 1.0 wt % of ZrO_2 added YBCO cooled slowly to room temperature in oxygen atmosphere

it retains orthorhombicity and superconductivity even by quenching from 950^{o}C to room temperature. In the case of tetragonal YBCO the oxygen content is below 6.5. The doped samples have absorbed considerable amount of oxygen from the surrounding atmosphere during the short period of cooling to make its oxygen content normal.

Table 3.8: Oxygen content of ZrO_2 added YBCO quenched from 950^{o}C to room temperature in oxygen atmosphere

Wt % of ZrO_2	Sintering temperature, (^{o}C)	Oxygen content 'X' ($YBa_2Cu_3O_x$)
0	950	-
0.5	950	6.70
1.0	950	6.74
1.5	950	6.79
2.0	950	6.83

3.6 STUDIES ON BeO ADDED YBCO

The previous sections of this chapter deal with the effect of dopants which do not substitute appreciably for any lattice sites of YBCO, but reacts with YBCO during processing forming secondary phases and the associated variations in the structural and superconducting properties. The present section describes the attempt to substitute BeO into YBCO. Taking the atomic valency and ionic size into consideration, beryllium can substitute for Cu in YBCO

compound. But the substitution studies have shown that BeO neither goes into the lattice of YBCO nor reacts with YBCO if the processing temperatures are limited at 950^{o} C. Almost all the known elements either substitute for different lattice sites of YBCO affecting its superconducting and physical properties or react with YBCO and form secondary phase apart from variations in superconducting properties. Beryllia has been suggested as a suitable substrate for the deposition of superconducting thin films, because of its non-reactive nature with YBCO and good thermal conductivity.

In order to study whether beryllia goes into the lattice of YBCO, samples were prepared by mixing stoichiometric amounts of Y_2O_3, $BaCO_3$, CuO and BeO in the required proportion to get the composition $Y_{1-x}Be_xBa_2Cu_3O_{7-\delta}$ where x = 0 to 0.4. The mixture was then calcined at 930^{o}C for 24 hours with one intermediate grinding. The calcined material then powdered thoroughly and pressed in the form of pellets. It was then sintered at 950^{o}C for 15 hours in oxygen atmosphere and cooled slowly to room temperature. The resistivity of the above samples were measured as a function of temperature by four probe method (see Fig. 3.23). The resistivity measurements show metallic behaviour with superconducting transition at 92 K. For low amount of BeO ($x < 0.3$), T_c remains almost constant at 92 K whereas for higher levels of BeO T_c reduces slightly. Thus BeO has no effect on the superconducting transition temperature of YBCO. The samples which were quenched to room temperature in oxygen atmosphere showed a semiconducting behaviour with no superconducting transition even at liquid nitrogen

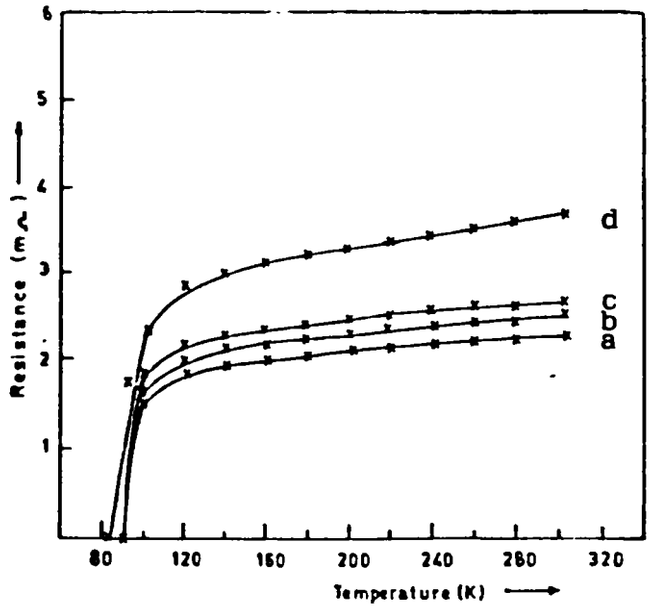

Fig. 3.23: Temperature-resistance curve of $Y_{1-x}Be_xBa_2Cu_3O_{7-\delta}$ for different values of x

(a) 0.05 ; (b) 0.10 ; (c) 0.20 ; (d) 0.30

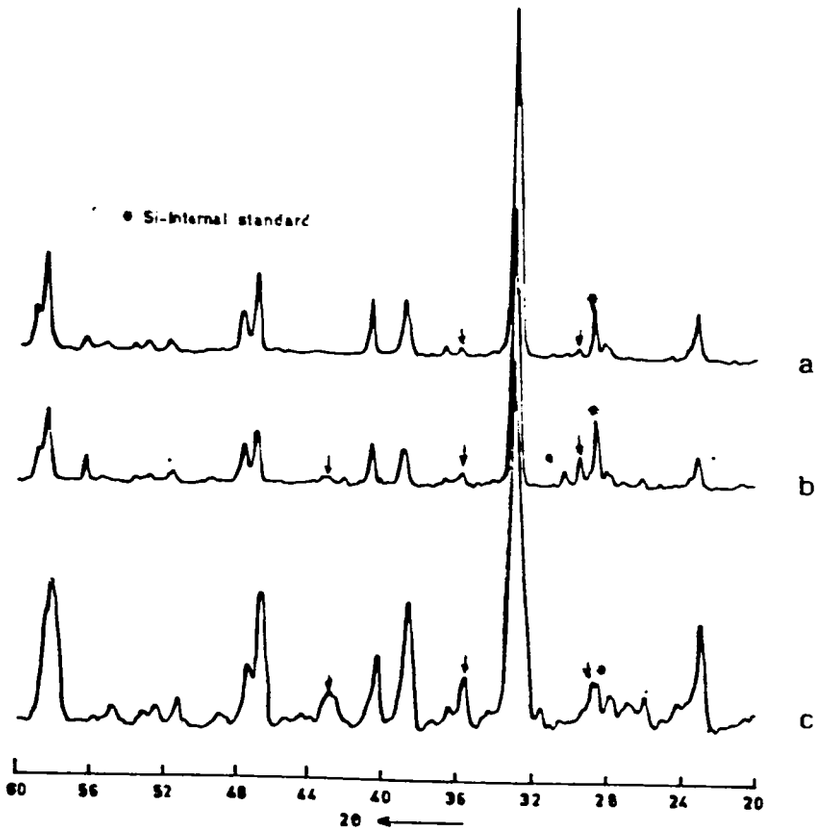

Fig. 3.24: XRD pattern of $Y_{1-x}Be_xBa_2Cu_3O_{7-\delta}$ for different values of x

(a) 0.05 ; (b) 0.20 ; (c) 0.30

Impurity peaks are indicated as ↓

temperature. The crystal structure of the samples has been studied by XRD method. Fig. 3.24 shows the powder diffraction pattern for different percentages of BeO substitution. The pattern does not show any measurable change in the lattice constants which indicates that BeO has not gone into the lattice sites of YBCO. The impurity peaks in the figure are due to the nonstoichiometry in the YBCO compound by BeO substituion ($Y_{1-x}Be_xBa_2Cu_3O_7$). The observed slight reduction in T_c for the higher level of BeO can be attributed to the presence of impurities due to yttrium defficiency in the compound. Thus the substitution studies show that BeO is not going appreciably into the lattice of YBCO and hence no reduction in T_c.

To study the effect of addition of BeO into YBCO high purity BeO was added to YBCO in the mole ratio 1:0.1, 1:0.2, 1:0.5, 1:1 and mixed thoroughly and sintered in the form of pellets at 950^oC for 15 hours and cooled slowly to room temperature in oxygen atmosphere. The structural and superconducting properties were studied. The resistivity of BeO added YBCO was measured as a function of temperature. Fig. 3.25 shows the R-T curve for different amount of BeO added YBCO sintered at 950^oC. All the samples show metallic behaviour with superconducting transition at 92 K. For higher mole percentages of BeO (in equimolar ratio of YBCO and BeO), T_c slightly reduces to 89 K. The resistivity studies show that even equal mole ratio of YBCO and BeO gives superconducting transition around 90 K which means that practically there is no interaction between YBCO and BeO even if the processing temperatures are 950^oC and above. X-ray powder diffraction studies were

carried out on BeO added YBCO to see the structural variations due to BeO addition. Fig. 3.26 shows the powder diffraction pattern for BeO added YBCO sintered at 950^{o}C. From the figure it is very clear that there is no reaction between YBCO and BeO at processing temperatures of 950 ^{o}C. If there were reaction between YBCO and BeO, additional peaks apart from those of YBCO and BeO would have observed in the diffraction pattern. The absence of BeO peaks in the x-ray diffraction pattern may be due to the low scattering of x-rays from BeO, as compared to YBCO. This is confirmed by taking XRD pattern from samples containing equimolar ratio of YBCO and BeO before and after sintering. The XRD pattern thus obtained are exactly identical. The pattern taken before sintering did not show any peaks corresponding to BeO and there is no indication for any beryllate formation during sintering.

Non-reactivity of BeO with YBCO

The present investigation on YBCO-BeO system has shown that there is practically no reaction between YBCO and BeO below 950^{o}C. Also the studies have shown that BeO does not go into the lattice sites of YBCO and as a result, the superconducting transition temperature is not affected. Almost all the known elements either go into the lattice of YBCO and deteriorate its superconducting properties or react with YBCO and form secondary phases. Since BeO is inert towards YBCO, it has been suggested as a suitable substrate for YBCO thin films. The only disadvantage with BeO is the lattice mismatch between BeO and YBCO for the epitaxial growth of thin films.

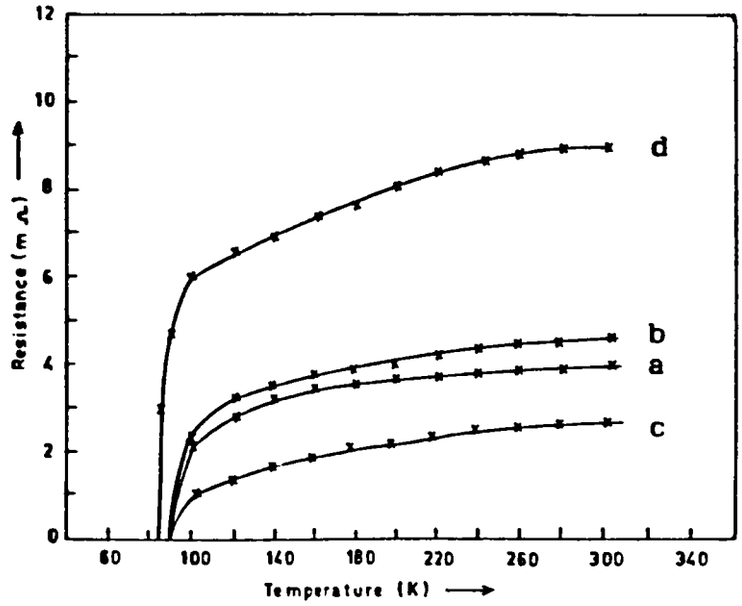

Fig. 3.25: Temperature-resistance curve of different mole ratio of YBCO and BeO
(a) 1 : 0.1 ; (b) 1 : 0.2 ; (c) 1 : 0.5
(d) 1 : 1

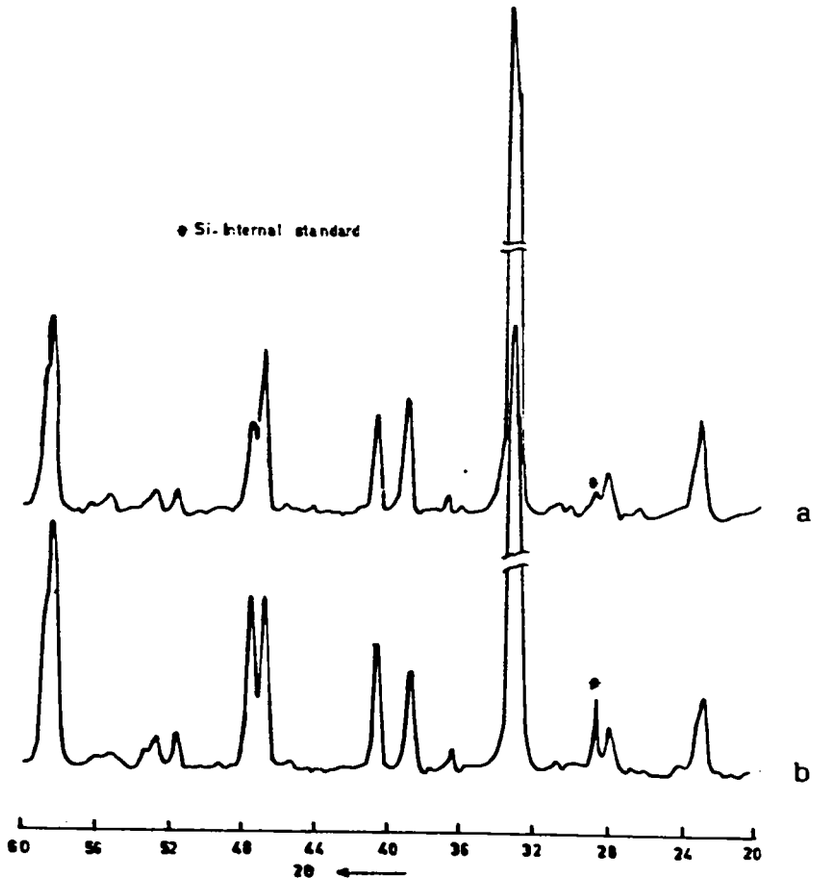

Fig. 3.26: XRD pattern of different mole ratios of YBCO and BeO
(a) 1 : 0.5 ; (b) 1 : 1

3.7 DISCUSSION

3.7.1 Effect of additives on YBCO

The present investigation describes the effect of certain additives on high temperature superconductor $YBa_2Cu_3O_{7-\delta}$. The temperatue-resistance measurements on dopant (Nb_2O_5, Sb_2O_3, SnO_2 and ZrO_2, BeO) added YBCO shows a metallic behaviour with superconducting transition at about 92 K in all the cases for small amount ($<$ 2.0 wt %) of addition. The studies show that the superconducting transition temperature is not affected by the addition of these oxides. The x-ray powder diffraction studies on dopant added YBCO show that there is no measurable change in lattice parameters due to the above dopants. But a few additional peaks were observed in the XRD pattern for Nb_2O_5, Sb_2O_3, SnO_2 and ZrO_2 added YBCO. In the case of BeO added YBCO no additional peaks were observed. The additional peaks are obviously due to the secondary phases formed by the reaction between YBCO and the oxides Nb_2O_5, Sb_2O_3, SnO_2 and ZrO_2 when processed at 950^{o}C. Since there is no lattice parameter variation due to the above additives and at the same time presence of secondary phases have been observed in the XRD pattern of dopant added-YBCO, it indicates that probably the above dopants are not going appreciably into the lattice sites of YBCO. A few investigators have reported(16,20,23) that Nb_2O_5, SnO_2 and ZrO_2 etc. go into the lattice sites of YBCO, affecting the crystal structure and the superconducting transition temperature. But at the same time there are reports (8,10,14) claiming that they

do not go into the lattice of YBCO and do not deteriorate the superconducting properties such as T_c, J_c etc. Studies on Sb_2O_3 and BeO doped YBCO are very scarce to see (12,15).

By taking into account of the ionic radii of the above dopants along with valency, there are chances for these oxides to go into various lattice positions in YBCO. In the present investigation, since there is no measurable change in lattice parameters due to dopant addition, we conclude that the above dopants are not going into the lattice sites of YBCO (some trace amount of dopants may be going into the lattice sites which is not revealed by x-ray) and are not affecting the crystal structure of YBCO or the CuO_2 plane or the local environment of CuO_2 planes (the supercurrents are supposed to be carried through CuO_2 planes). Since the crystal structure and the CuO_2 planes are not affected by the above dopants, the superconducting properties of YBCO are not affected with the addition of the above oxides and the superconducting transition temperature remains same as that of pure YBCO (92 K) which have been confirmed by resistivity measurements.

The high temperature ceramic superconductors exhibit granular properties and the current densities depend on the processing parameters. The anisotropy also influences the current density of YBCO. The current density can increase or decrease (32) according to the intergrain contacts as well as orientation of grains in bulk sintered samples. The intergrain contacts again depend on the grain size and its distribution. In inhomogeneous superconductors the intergrain

contacts get influenced by the inhomogeneties present in the compound. In the present investigation, it is found that the current densities of Nb_2O_5 and SnO_2 doped YBCO increase by two to three times whereas the current densities of Sb_2O_3 and ZrO_2 doped YBCO found to be more or less same as that of pure YBCO. The enhancement in current density of Nb_2O_5 and SnO_2 doped YBCO can be attributed either to the improved intergrain contact or to the flux pinning action of the secondary phase formed or to both. It has been reported by Matsubara et al. (14) that in Nb_2O_5 doped YBCO, the enhancement in current density is due to the increased density and the fine grain size because of doping. In SnO_2 doped YBCO it has been reported (10) that the enhanced current density is due to the modified microstructue as well as due to the flux pinning effect of secondary phases. In the case of Sb_2O_3 and ZrO_2 additions, the secondary phases must have deteriorated the intergrain contacts which results in low current densities.

X-ray powder diffraction studies on doped YBCO show additional peaks at $2\theta = 30.1^o$, 42.8^o, 53^o other than those for pure YBCO. The additional peaks indicate that the above oxides react with YBCO forming a second phase. The secondary phase formed in YBCO-Nb_2O_5 system has been identified as Ba_2YNbO_6, a perovskite material from the data available in the JCPDS file. The positions of the impurity peaks in the case of SnO_2, Sb_2O_3 and ZrO_2 added YBCO coincide with that of Nb_2O_5 added YBCO. Due to the isostructural nature of the secondary phases in the case of other dopants, we have presumed that the secondary phases formed by

the above oxides are Ba_2YSnO_6, Ba_2YSbO_6 and Ba_2YZrO_6 respectively. The preparation of these compounds is described in chapter 4 and their phase compatibility with YBCO has been discussed in chapter 5 and the studies confirmed our conclusions about the nature of the secondary phases formed due to the additives. In literature, the secondary phases have been reported as $BaSnO_3$ and $BaZrO_3$ and Sb_2O_5 in the case of SnO_2, ZrO_2 and Sb_2O_3 added YBCO. But our studies show that it is not so, but a new series of compounds Ba_2YNbO_6, Ba_2YSnO_6, Ba_2YZrO_6 and Ba_2YSbO_6 respectively.

The studies on BeO added YBCO have shown that BeO does not go into the lattice of YBCO. Also it does not react with YBCO. As a result the superconducting transition temperature of YBCO is not affected with BeO. Almost all the known elements either go into the lattice of YBCO and deteriorate its superconducting properties or react with YBCO and form secondary phases. Since BeO is inert towards YBCO, it can be used as a suitable substrate for YBCO thin films. The only disadvantage with BeO is the lattice mismatch with the superconductor YBCO for the epitaxial growth of thin films.

3.7.2 Enhanced oxygen absorption in doped YBCO

The high temperature superconductor YBCO is processed by heating at $950^{o}C$ for several hours followed by slow cooling to room temperatue in oxygen atmosphere where YBCO absorbs oxygen and transforms to superconducting orthorhombic phase. If we quench the processed YBCO from high temperatures to room temperature or to

liquid nitrogen temperature, we will get a non-superconducting tetragonal phase. In order to make it orthorhombic and superconducting, annealing at a temperature between 300-600^{o} C in an oxygen atmosphere is essential.

In the present investigation, we have quenched YBCO doped with Nb_2O_5, Sb_2O_3, SnO_2 and ZrO_2 into different atmospheres. The temperature-resistance measurements on doped YBCO which are quenched to room temperature in air or oxygen atmosphere showed superconducting transition at 92 K same as that of slow cooled samples. The undoped samples showed a semiconducting behaviour with no superconducting transition till 77 K. The XRD studies show that the dopant added samples which are quenched to room temperature are having orthorhombic structure whereas the undoped samples show a tetragonal structure. The possible reasons for obtaining superconductivity and orthorhombic structure in dopant added YBCO are (1) enhanced oxygen absorption due to dopant addition, (2) a rise in thermodynamic phase transition temperature, and (3) internal oxidation mechanism of the dopants.

The oxygen content determination shows that the doped YBCO have absorbed enough oxygen required for orthorhombicity and superconductivity in $YBa_2Cu_3O_{7-\delta}$ compound. The possibility of shifting the thermodynamic phase transition temperature to higher temperatures of 950^{o}C has been studied and ruled out. In case the thermodynamic phase transformation temperature has increased to higher temperature of 950^{o}C, then the samples quenched from 950^{o}C to room temperature in nitrogen atmosphere or to liquid nitrogen also should

have shown orthorhombic structure, instead it has shown a tetragonal structure.

If the superconductivity in quenched YBCO is due to the internal oxidation mechanism by the addition of the above oxides, it should show orthorhombic structure for those samples which are quenched in nitrogen atmosphere. Even though the amount of dopant is very small (0.2 wt % of oxides), it gives an orthorhombic structure, but with internal oxidation mechanism, such a small quantity of the oxides cannot provide enough oxygen for its transformation to orthorhombic structure on quenching. Also it is to be noted that the above oxides added to YBCO are not remaining as it is or as reduced oxides, but forms a secondary phase Ba_2YAO_6 (A = Nb, Sb, Sn, Zr). Hence in the present experimental investigation, the possibility of internal oxidation mechanism has been ruled out. The only viable process is the fast oxygen absorption of dopant added YBCO compared to undoped YBCO. The density measurements on pure and doped YBCO show that the enhanced oxygen absorption is not due to the increased porosity in dopant added YBCO but can be attributed to the modified microstructure of YBCO and fine grain size due to the addition of the oxides as observed by SEM micrographs.

3.8 CONCLUSION

The following conclusions have been drawn by the studies on the effect of additives on YBCO.

1. All the dopants presently investigated do not go appreciably into the lattice of YBCO.

2. The crystal structure of YBCO is not affected with the addition of the oxides and no measurable variations in lattice parameters have been observed.

3. The superconducting tranition temperature remains same as that of undoped YBCO.

4. The dopants Nb_2O_5, Sb_2O_3, SnO_2 and ZrO_2 react with YBCO forming secondary phases which are distributed in the bulk of YBCO.

5. The secondary phases formed due to the above dopants are a new class of compounds having the chemical formula Ba_2YAO_6 (A = Nb, Sb, Sn and Zr), a cubic perovskite material. In literature it has been reported as $BaSnO_3$, $BaZrO_3$ etc. and the present investigation shows that it is not $BaAO_3$, but a new compound Ba_2YAO_6.

6. Addition of Nb_2O_5, SnO_2, Sb_2O_3 and ZrO_2 enhances the oxygen absorption capability of YBCO considerably due to the modified microstructure. Due to the enhanced oxygen absorption, the doped YBCO gives superconducting

orthorhombic phase even by quenching from 950 ^{o}C to room temperature in oxygen atmosphere.

7. Addition of small amounts of Nb_2O_5 and SnO_2 increase the current density of YBCO whereas Sb_2O_3 and ZrO_2 do not show any increase in current density.

8. BeO neither goes into the lattice of YBCO nor reacts with YBCO. It does not enhance the current density or oxygen absorption capability of YBCO.

REFERENCES

1. A.V. Narlikar and S.N. Ekbote, "Superconductivity and superconducting materials", South Asian Publishers, New Delhi (1983).

2. J.T. Markert, Y. Dalichaouch and M.B. Maple, "Physical properties of high temperature superconductors-I", (Ed. Donald M. Ginsberg), World Scientific, Singapore, 265 (1988).

3. A.V. Narlikar, C.V. Narasimha Rao and S.K. Agarwal, "Studies of high temperature superconductors-I", (Ed. A.V. Narlikar), 341 (1989).

4. B.W. Lee, J.M. Ferreira, Y. Dalichaouch, M.S. Torikachvili, K.N. Yang and M.B. Maples, Phys. Rev., B 37, 2368 (1988).

5. J.M. Tarascon, P. Barboux, P.F. Miceli, L.H. Greene, G.W. Hull, M. Eibschutz and S.A. Sunshine, Phys. Rev., B 37, 7458 (1988).

6. A. Suzuki, E.V. Sampathkumaran, K. Kohn, T. Shibuya, A. Tohdake and M. Ishikawa, Jap. J. Appl. Phys., 27, L 584 (1988).

7. K.C. Goretta, O.D. Lacy, U. Balachandran, D. Shi and J.L. Routbort, J. Mater. Sci. Lett., 9, 380 (1990).

8. Takashi Asaka, Yoshiyuki Okazawa, Yasukishiomi and Kyoji Tachikawa, Jap. J. Appl. Phys., 30, L 1264 (1991).

9. S.B. Qadri, L.E. Toth, M. Osofski, S. Lawrence, D.V. Gubsen and S.A. Wolf, Phys. Rev., B 37, 7235 (1987).

10. Hozo Osamura, Norikazu Matsukura, Yukhide Kusumoto, Shojira Ochiai, Baorong Ni and Teruo Matsushita, Jap. J. Appl. Phys., 29, L 1621 (1990).

11. D.Y. Zhang, G.M. Wang, Y.X. Wang, Z.H. Wang and Y.H. Zheng, Solid State Commun., 75, 629 (1990).

12. Kiejin Lee, B.K. Jeon, Gwangseo Park, Pansupsong and Seung Pyungchoi, Solid State Commun., 79, 237 (1991).

13. Makote Kuwabara and Narutoshi Kusaka, Jap. J. Appl. Phys., 27, L 1504 (1988).

14. G. Matsubara and Y. Okabe, Jap. J. appl. Phys., 29, L 785 (1990).

15. B. Dabrowski and D.G. Hinks, Mod. Phys. Lett., B 3, 509 (1989).

16. P. Boelchand, R.N. Enzweiler, I. Zitkovsky, J. wells, W. Bresser, D. Mac Daniel, R.L. Mang, P.H. Hor, C.W. Chu and C.Y. Huang, Phy. rev., B 37, 3766 (1988).

17. T. Nishida, M. Katada and Y. Matsumoto, Jap. J. Appl. Phys., 29, 259 (1990).

18. M. Pasternak and R.D. Taylor, Solid State Commun., 69, 1161 (1989).

19. Y. Matsumoto, T. Abe, M. Tanaka, T. Tazawa and E. Sato, Mat. Res. Bull., 23, 1241 (1988).

20. A.S. Bhalla, R. Ray and L.E. Cross, "Chemistry of oxide superconductors", (Ed. C.N.R. Rao), Blackwell Sci. Pub., 76 (1988).

21. P.K. Metha, R.D. Tadalia, O.M. Prakash, D.T. Adroja, P.D. Prabhawalkar, N. Venkataramani, S.K. Malik and A.V. Narlikar, Bull. Mater. Sci., 14, 871 (1991).

22. M.F. Yan, W.W. Rhodes, P.K. Gallagher, J. Appl. Phys., 63, 821 (1988).

23. H. Hojaji, A. Barkatt, S. Hu and K.A. Michael, Mat. Res. Bull., 25, 765 (1990).

24. Y. Yuen, C.L. Lin, J.E. Crow, G.N. Myer, R.E. Salomon, P. Schlottmann, N. Bykovetz and W.N. Herman, Phys. Rev., B 37, 3770 (1988).

25. S.W. Filipczuk, R. Driver and G.B. Smith, Physica C, 170, 457 (1990).

26. M.J. Cima, J.S. Schneider, S.C. Peterson and W. Coblenz, Appl. Phys. Lett., 53, 710 (1988).

27. A. Bailey, G. Alvarez, T. Puzzer, D.N. Mathews, K. Sealey, G.J. Russel and K.N.R. Taylor, Aust. J. Phys., 347 (1990).

28. O. Eible, K. Hradil and H. Schmidt, Physica C, 177, 89 (1991).

29. G. Ockenfub, F. Baudenbacher, W. Prusseit-Elffroth, H. Hirata, P. Berberich and H. Kinder, Physica C, 180, 30 (1991).

30. H.M.O'Bryan and P.K. Gallagher, "Ceramic superconductors - II" (Ed. Man F. Yan), American Ceramic Society, Ohio, 89 (1988).

31. D.C. Harris and T.A. Hewsten, J. Solid State Chem., 69, 182 (1987).

32. M. Murakami, Supercond. Sci. Technol., 5, 185 (1992).

CHAPTER 4

SYNTHESIS OF Ba_2YAO_6: A NEW CLASS OF CERAMIC COMPOUNDS FORMED IN $YBa_2Cu_3O_7$-A_xO_y SYSTEMS (A = Nb,Sb,Sn or Zr)

We have seen in chapter 3 that the superconducting transition temperature of YBCO is not affected by the addition of the oxides Nb_2O_5, Sb_2O_3, SnO_2 or ZrO_2. It is also observed that the above oxides react with YBCO during sintering, forming secondary phases Ba_2YNbO_6, Ba_2YSbO_6, Ba_2YSnO_6 and Ba_2YZrO_6. All the compounds are isostructural and can be represented by the formula Ba_2YAO_6 (A = Nb,Sb,Sn or Zr). Even though the crystal structure of the compound Ba_2YNbO_6 has been reported in JCPDS file, very little is known about this compound (1). In literature there are no reports on compounds Ba_2YSbO_6, Ba_2YSnO_6 or Ba_2YZrO_6. In the present investigation the compounds have been prepared as single phase materials and the crystal structure has been indexed as cubic perovskite.

4.1 SYNTHESIS AND CHARACTERISATION OF Ba_2YNbO_6 (BYNO)

4.1.1 Preparation of BYNO

The compound BYNO has been prepared as a single phase material from its constituent oxides. Stoichiometric amount of high purity Y_2O_3, $BaCO_3$ and Nb_2O_5 were weighed, mixed thoroughly in an agate mortar with acetone as mixing media. It was dried and calcined at 1300^oC for 10 hours in an alumina crucible. The

calcined material was powdered thoroughly and pressed in the form of pellets by uniaxial pressing at a pressure of 5 tonnes. It was then sintered at temperatures between 1350^{o} C to 1450 ^{o}C for 10 hours. The material was found to be highly porous. In order to enhance the compound formation and sinterability, small amount of CuO was added to the mixture and sintered between 1350 to 1450^{o} C for 10 hours. Highly dense and sintered pellets were obtained in the case of Ba_2YNbO_6 doped with CuO and sintered at 1400^{o}C.

4.1.2 Crystal structure of BYNO

The crystal structure of Ba_2YNbO_6 has been reported as cubic perovskite with lattice parameter a = 8.436 A in the JCPDS file (24-1042). Even though the compound has been reported, very little is known about the preparation, characterisation and properties of the material. In the present investigation the crystal structure of BYNO has been studied by x-ray powder diffraction method. Fig. 4.1 a shows the powder diffraction pattern of BYNO prepared by heating at 1400^{o}C for 10 hours in air and furnace cooled to room temperature. From the figure it is clear that the diffraction pattern is not of a single phase compound, but it contains other phases also. Even though there is compound formation the reaction is not complete; it is a multiphase compound. In order to obtain a single phase compound the reaction temperature has been increased to higher temperatures of 1500^{o} C and more. The elevated reaction temperature and the prolonged sintering time do not give a single phase compound, instead the compound melts and reacts with the

alumina crucible. The samples pressed in the form of pellets and kept for sintering did not get sintered. On cooling, the samples became powder after some time. It appears that some phase transformation takes place on Ba_2YNbO_6 compound sintered without any additives. Originally we observed the compound formation in YBCO-Nb_2O_5 system and it was assumed that presence of some impurities could enhance the compound formation. Since YBCO contains CuO, which has a low melting point compared to Y_2O_3 and $BaCO_3$; CuO was added to Ba_2YNbO_6 to enhance the compound formation and sinterability. The CuO added BYNO when sintered at 1350^oC for 10 hours, gave almost a single phase compound with no observable impurity peaks in the XRD. The quantity of CuO required to give a single phase compound is of the order of 0.5 to 1.0 wt % of CuO in the stoichiometric compound Ba_2YNbO_6 . The samples pressed in the form of pellets sintered very well on heat treatment without cracking or crumbling into powder.

Fig. 4.1b shows the powder diffraction pattern of 0.5 wt% CuO added BYNO sintered at 1350^oC for 10 hours. The XRD pattern is indexed as a cubic perovskite with lattice parameter a = 8.436 A. The above value matches with the data given in the JCPDS file (24-1042). Thus the XRD studies show that a small amount of CuO is essential to enhance the compound formation as well as to get a stable single phase compound. The exact role of CuO is not very well understood at present. At higher temperatures of processing, either CuO must have melted and ran out of the sample or got doped with Ba_2YNbO_6 . The amount of CuO required to stabilise the phase

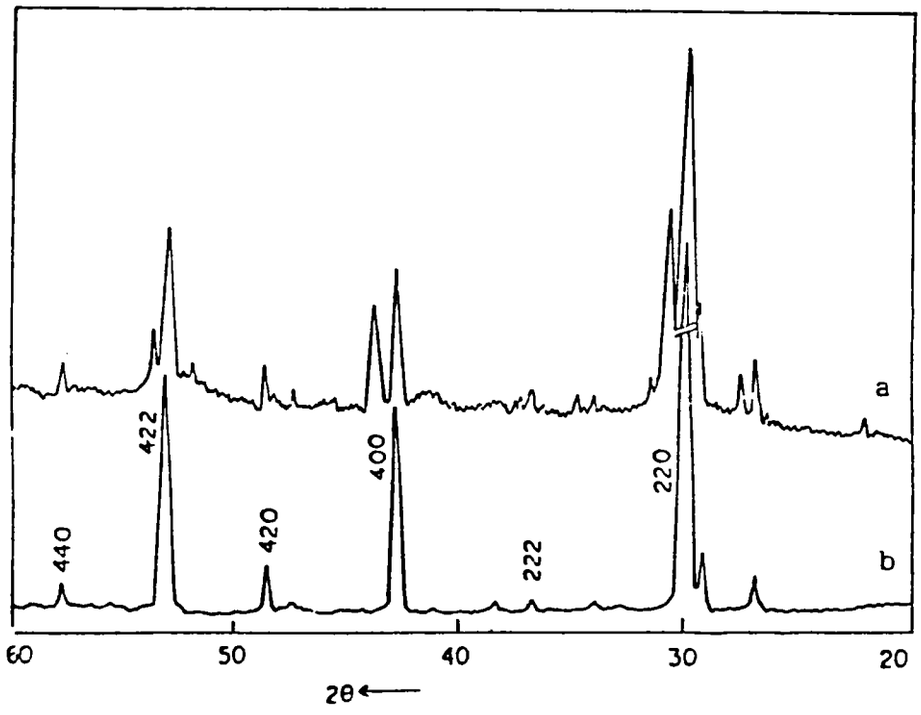

Fig. 4.1: XRD pattern of (a) BYNO prepared without CuO; (b) BYNO prepared with 0.5 wt % CuO.

is small and is of the order of 0.5 wt %. Attempts have been made to prepare Ba_2YNbO_6 as a single phase compound by adding other impurities viz. PbO, Bi_2O_3, ZnO, Li_2CO_3, Na_2CO_3, K_2CO_3, MgO etc., instead of CuO. But it is found that none of the above additives can give a single phase compound as given by CuO.

4.1.3 Density measurements

The theoretical density of the compound Ba_2YNbO_6 has been calculated from its atomic mass and crystal structure. The cubic perovskite cell of BYNO contains four unit formulae of atoms. The density was calculated based on the number of atoms per unit cell. The theoretical density calculated as 6.109 gm/cm^3. The measured densities without any CuO are about 4.9 to 5.0 gm/cm^3 and is very low, about 78% of theoretical density. The samples sintered at 1350^oC with 0.5 wt % of CuO are found to have a density of 5.80 gm/cm^3 which is about 95% of the theoretical density. Table 4.1 shows the densities of BYNO for various amounts of CuO addition with their respective sintering temperatures. Thus CuO not only enhance the compound formation but also the sintered density of the compound through liquid phase sintering. The properties of a polycrystalline material are highly dependent on its bulk density. To study the properties of any material, the density of the specimen tested should be as near as possible to the theoretical density. At the same time presence of liquid phase and other impurities should be eliminated. In the case of Ba_2YNbO_6 formation and densification, CuO has been used as an additive to its constituent oxides.

The effect of CuO impurity will get reflected in the measured properties of the compound. For obtaining intrinsic parameters studies on single crystals are required.

4.1.4 Resistivity of BYNO

The dc resistivity of BYNO was measured using a dc electrometer (Keithley model 602). The resistivity was found to be of the order of 10^9 Ω-cm. For small amount of CuO addition, there was no variation in the resistivity values of BYNO. But as the amount of CuO increases, the resistivity decreases and is given in Table 4.1. Since the dc resistivity of 0.5 wt % CuO added BYNO is extremely high, BYNO can be considered as an insulator. From the table it is evident that for low percentages of CuO, the resistivity remains more or less the same. It means that CuO is not affecting the electronic structure of BYNO appreciably if the additions are small. It only enhances the compound formation and densification. For higher percentages, the resistivity suddenly drops to a very low value and affects its electronic structure.

4.1.5 Dielectric properties of BYNO

Dielectric properties are an important class of material properties. They give the response of the material media to various electric fields passing through the material. Dielectric properties are highly dependent on crystal structure and polarisability of the material. In polycrystalline material, the dielectric properties again depend on grain size, grain boundaries, their distribution

and the nature of the impurity phases present or it is a bulk property. That is, the dielectric properties measured on polycrystalline material with inhomogeneities and other impurities, are not the true dielectric properties of the material, it is a modulated picture of all the effects. Measurements on single crystals can give more accurate values.

Table 4.1: The density and resistivity of BYNO for various amount of CuO addition with respective sintering temperatures

Amount of CuO (wt %)	Sintering temperature (^{o}C)	Density (gm/cm^3)	Resistivity (Ω- cm)
0	1400	4.5	-
0.5	1400	5.80	5×10^9
1.0	1400	5.83	3.8×10^9
2.0	1350	5.85	3×10^9
3.0	1300	5.84	5×10^8
5.0	1250	5.81	7×10^5
10.0	1100	5.80	3×10^3

The dielectric properties of BYNO, sintered with 0.5 wt % of CuO, were measured using an impedence analyser as a function of frequency at room temperature, by the method described in chapter 2. Fig. 4.2 gives the variations of dielectric constant and dissipation factor of BYNO, as a function of log frequency. The dielectric constant found to be constant from KHz to MHz region. The dissipation

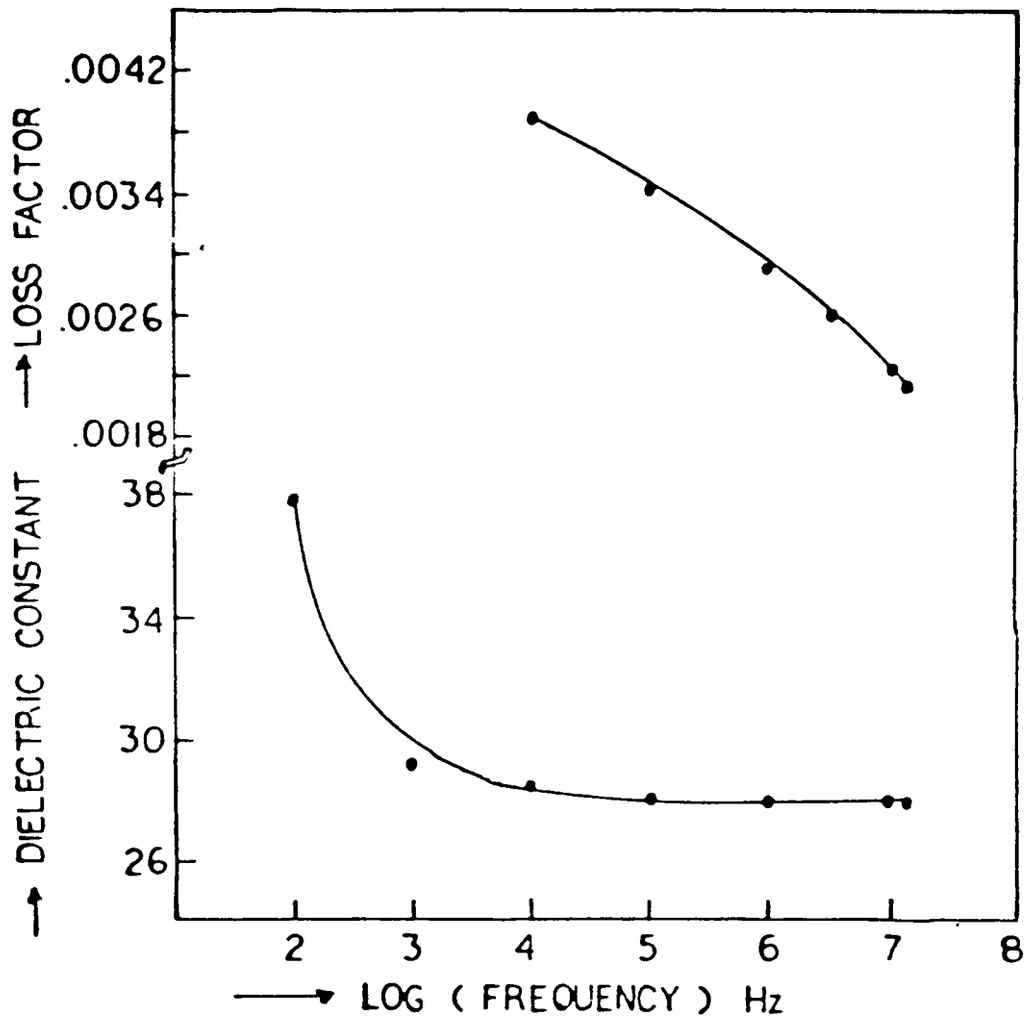

Fig. 4.2: Variation of dielectric constant and dissipation factor as a function of frequency of the compound BYNO

factor is also very low in the frequency range studied presently. But the value of dielectric constant is high in the Hz to KHz region and decreases fast as the frequency increases to KHz region. This high value of dielectric constant at low frequencies can be attributed to the space charge polarisations taking place while a time varying electric field passes through it and, this space charge polarisation becomes inoperative as the frequency increases and hence the dielectric constant decreases at a faster rate. Since the value of dielectric constant keeps a steady value from KHz to MHz region, the magnitude of orientation polarisation and ionisation polarisation are very low. At frequencies of MHz and higher region, only electronic polarisation mechanism is operative and its magnitude is relatively large. The dissipation factor is a measure of loss of electrical energy in the dielectric medium. The compound BYNO shows a low dissipation factor and can be used as a good dielectric material. Since the superconducting properties of YBCO are not deteriorated by the presence of BYNO, it can be used as a substrate for the deposition of YBCO thin and thick films.

4.1.6 Microstructure of BYNO

Microstructural characterisation of polycrystalline materials are very important to assess the measured properties. Fig. 4.3 shows the Scanning Electron Micrograph on polished surfaces of BYNO sintered at $1350^{o}C$ with 0.5 wt % of CuO. The micrograph clearly shows a uniform pattern with practically no secondary phase. The location of CuO is not clear from the micrograph. Also in the

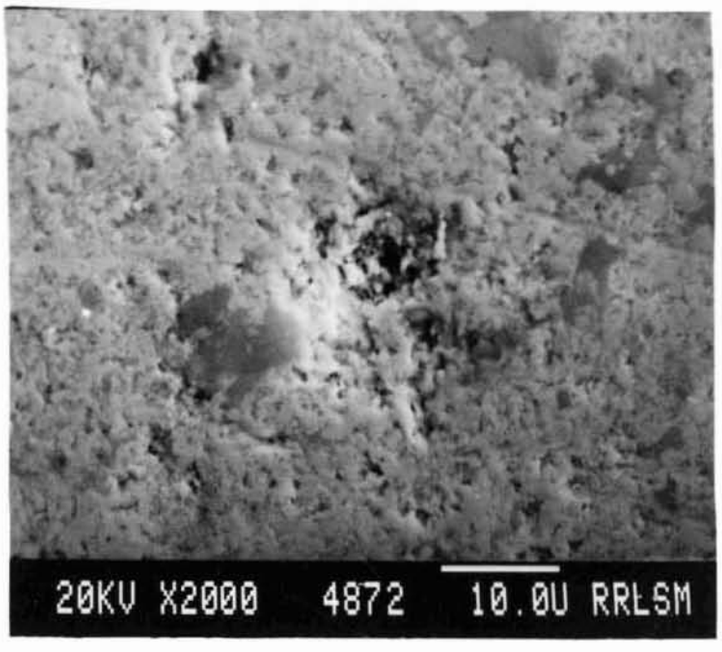

Fig. 4.3: Scanning electron micrograph of EYNO

figure, a few pores can be seen which agrees with the density measurement (95% of theoretical density). Absence of pores and secondary phase gives a rough estimate that the properties measured are approximately equal to their true values (almost equal to that of single crystals) even though grain boundary effects still exist. Thus the microstructural studies on polished surface of the compound give a rough idea about the properties measured.

4.1.7 Reactivity of YBCO with BYNO

The reactivity of YBCO with BYNO has been carried out primarily to study the existence of the two compounds at 950^{o}C and to prove that, the secondary phase formed in YBCO-Nb_2O_5 system (described in chapter 3) heat treated at 950^{o}C, is the compound Ba_2YNbO_6. Equimolar ratio of YBCO and BYNO are mixed thoroughly in agate mortar. It was then pressed in the form of pellets and sintered at 950^{o}C for 10 hours. The sintered samples were cooled slowly to room temperature in air. The x-ray powder diffraction pattern of the mixture prepared as above, is shown in Fig.4.4. For comparison the powder pattern of pure YBCO and pure BYNO are also provided in the figure. From the figure it is clear that practically there is no reaction between YBCO and BYNO at 950^{o}C. In case there were any reactions between YBCO and BYNO, then the XRD pattern (Fig. 4c) should have shown additional peaks apart from those of pure YBCO and pure BYNO. The non-reactivity of YBCO with BYNO confirmed our finding about the identification of the secondary phase in YBCO-Nb_2O_5 system.

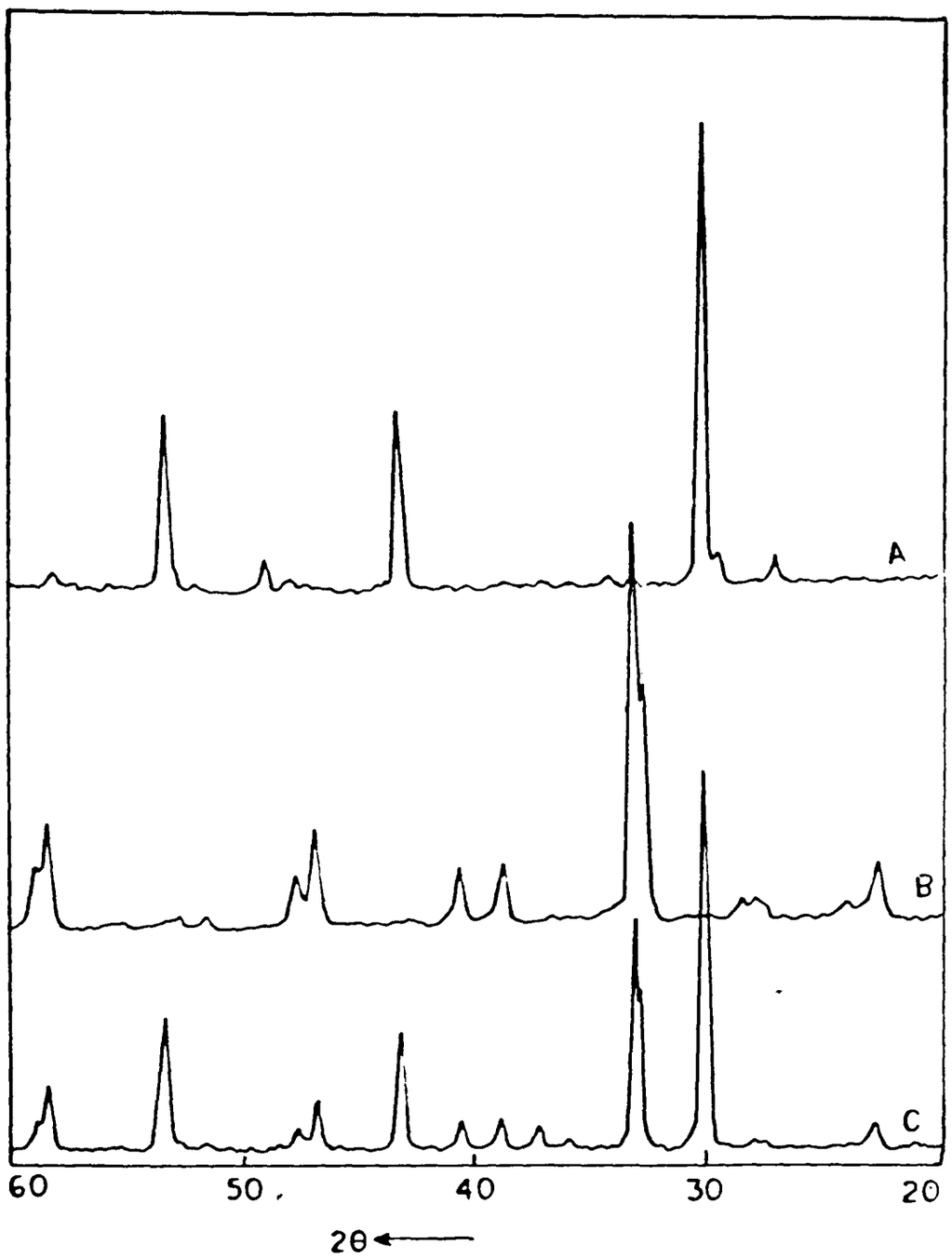

Fig. 4.4: XRD patterns of (A) pure YBCO; (B) pure BYNO; (C) 1:1 mole mixture of YBCO and BYNO heated at 950°C to study the phase compatibility at 950°C.

The non-reactivity of BYNO with YBCO is of considerable importance. Almost all the known insulating materials react with YBCO and destroy its superconducting properties. As a result there is no ideal substrate material for the deposition of YBCO thin and thick films. It is possible to make use of BYNO as an ideal non-reactive substrate material for the deposition of YBCO thin films. Moreover, it is possible to prepare superconductor-insulator (YBCO-BYNO) composites (discussed in chapter 5) and the percolation studies can provide information about the fundamental understandings of superconductivity.

4.2 SYNTHESIS AND CHARACTERISATION OF Ba_2YSnO_6 (BYSnO)

4.2.1 Preparation of BYSnO

The doping studies on YBCO with Nb_2O_5 have shown that the secondary phase formed in the system is the compound Ba_2YNbO_6 and has been proved by synthesising the compound and studying the reactivity between them. In a similar analogy, we came to the conclusion that the secondary phase in YBCO-SnO_2 system is the compound Ba_2YSnO_6. In Fig. 4.5, x-ray powder diffraction pattern of 5.0 wt % SnO_2 doped YBCO is provided along with the powder pattern of 5.0 wt % Nb_2O_5 doped YBCO for comparison. From the figure it is evident that the positions of the impurity peaks are almost in the same positions as that of BYNO and the intensity ratios are also the same. Due to the isostructural nature of the impurity peaks in both the cases, we assumed that the secondary phase in SnO_2 doped YBCO is a new compound Ba_2YSnO_6 and

Fig. 4.5: A comparison of XRD pattern of 5 wt % of dopant added YBCO to verify the isostructural nature of the secondary phases formed in YBCO due to dopants

(a) Nb_2O_5 ; (b) Sb_2O_3 ; (c) SnO_2 ; (d) ZrO_2

not the compound $BaSnO_3$ as reported by many other researchers (2,3). By taking valency into consideration, the chemical formula of the compound can be written as $Ba_2YSnO_{5.5}$. It is a new compound and has not been reported earlier in literature. The compound has been synthesised as a single phase material and the details of preparation are described below. In the text we represent the compound Ba_2YSnO_6 as BYSnO.

Stoichiometric amounts of high purity Y_2O_3, $BaCO_3$ and SnO_2 are weighed, mixed thoroughly and calcined at 1300^oC for 10 hours. It was then powdered thoroughly and pressed in the form of pellets and sintered at 1350^oC to 1450^oC for 10 hours in air and furnace cooled to room temperature. As in the case of Ba_2YNbO_6 , the samples obtained are not single phase compounds and are not sintered properly. In order to enhance the compound formation and sinterability, small amount (about 0.5 wt %) of CuO was added to the mixture of BYSnO and sintered at 1350^oC for 10 hours and cooled slowly.

4.2.2 Crystal structure of BYSnO

The crystal structure of BYSnO has been studied by x-ray powder diffraction technique. Fig. 4.6 shows the powder diffraction pattern of BYSnO sintered at 1400^oC for 10 hours and furnace cooled to room temperature. From the powder diffraction pattern, it is evident that the compound BYSnO has formed along with other unknown phases. Increasing the sintering temperature and time, did not yield a single phase compound, rather the compound starts

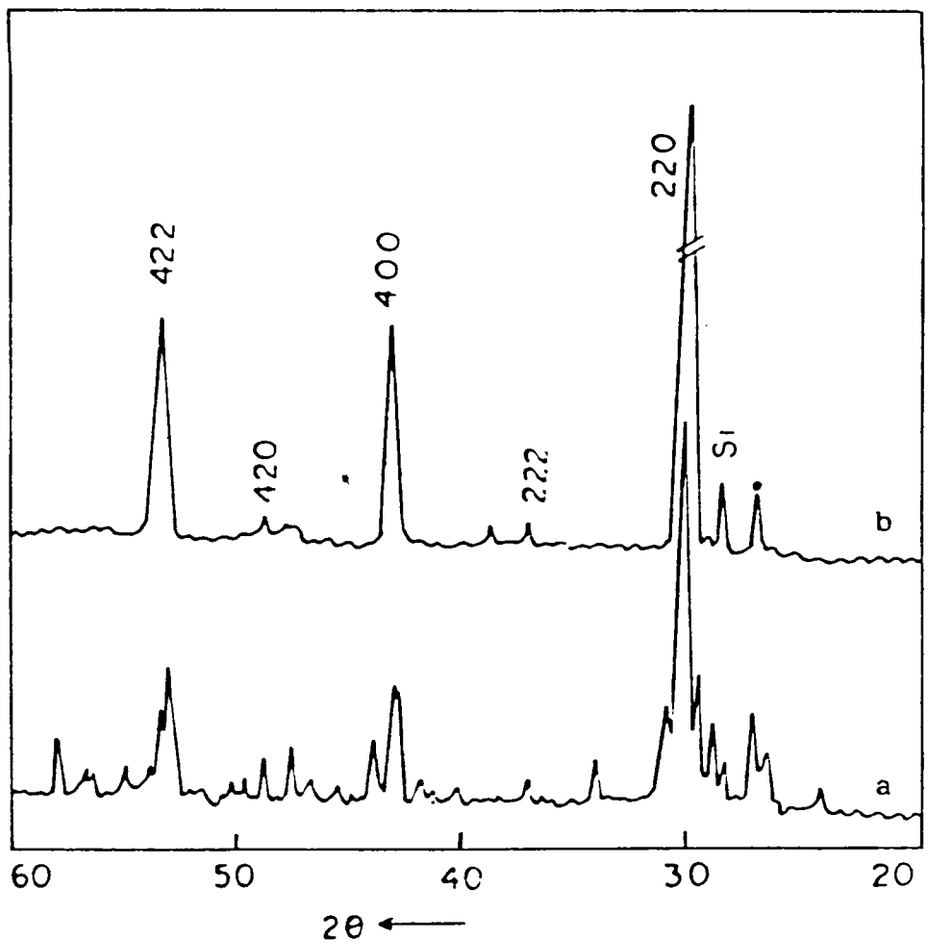

Fig. 4.6: XRD pattern of (a) BYSnO prepared without CuO, (b) BYSnO prepared with 0.5 wt % CuO

melting and reacting with the alumina crucible at temperatures above 1500^{o} C. Attempts have been made to prepare the compound BYSnO by starting from nitrate mixtures of constituent elements instead of oxides and carbonates. The compound BYSnO starts forming even at a lower temperature of 900^{o}C, but it did not yield a single phase compound even when prepared at temperatures of 1400^{o} C. Always there is considerable amount of impurity phases along with the compound BYSnO. As in the case of BYNO preparation, CuO has been used as an additive for compound formation and sintering and found that CuO enhances the compound formation and sintering. Fig. 4.6b shows the powder diffraction pattern of 0.5 wt % CuO added BYSnO sintered at 1350^{o} C for 10 hours and furnace cooled to room temperature. The pattern was indexed for a cubic material with lattice parameter a = 8.420 A.

4.2.3 Density of BYSnO

The theoretical density of BYSnO has been calculated as in the case of Ba_2YNbO_6 taking into account of its crystal structure and the number of atoms in one unit cell. The theoretical density calculated is found to be 6.32 gm/cm^3. The compound BYSnO when sintered without any sintering aid was found to be highly porous with no mechanical strength and crumbled into powder. The density is measured and found to be about 4.8 gm/cm^3. Since the density is very low, any measurements on such samples are meaningless and have not been carried out. But the density achieved by the addition of 0.5 wt % CuO to BYSnO is found to be about 6.12 gm/cm^3

when sinterd at 1350^{o}C for 10 hours. The density is about 95% of the theoretical density. Addition of CuO not only resulted in single phase compound but also improved the density to a considerable extent. Table 4.2 shows the density of BYSnO with sintering temperature for different amount of CuO addition. The mechanical strength of the sintered pellets also increased. Various properties of the compound BYSnO were studied with these dense samples.

Table 4.2: Table showing the density and resistivity of BYSnO for various amount of CuO addition with corresponding sintering temperature

Amount of CuO (wt %)	Sintering temperature (^{o}C)	Density (gm/cm^{3})	Resistivity (Ω-cm)
0	1400	4.8	-
0.5	1350	6.12	1.6×10^{7}
1.0	1350	6.16	1.4×10^{7}
2.0	1300	6.18	1.35×10^{7}
3.0	1300	6.10	4×10^{6}
5.0	1200	6.08	9×10^{5}

4.2.4 Resistivity of BYSnO

The dc resistivity of polycrystalline compound BYSnO prepared with 0.5 wt % of CuO was measured using a solid state electrometer. The resistivity was found to be of the order of 10^{7} Ω-cm.

Table 4.2 gives the resistivity of different amounts of CuO added BYSnO with respective sintering temperatures. The resistivity decreases drastically as the amount of CuO increases. As in the case of BYNO, in order to prepare a single phase and sintered body, CuO was added to the compound BYSnO and as a result the bulk resistivity measured is not the true resistivity of the compound, rather it is a combined effect of all the impurities and defects.

4.2.5 Dielectric properties of BYSnO

The dielectric properties of the compound BYSnO were measured using an impedance analyser in the frequency range 30 Hz to 13 MHz at room temperature. Fig. 4.7 shows the plot of dielectric constant and dissipation factor as a function of frequency. In the low frequency region, the dielectric constant is very high and decreases rapidly as the frequency increases. The high value of dielectric constant in the low frequency region is due to the large values of space charge and orientation polarisations occurring in the material, when a time varying electric field passes through it. Correspondingly, the dissipation factor is also very high. From the figure it is also evident that BYSnO shows ionisation polarisation and it decreases as the frequency increases. At higher frequencies, in the MHz region, the dielectric constant is about 10 and is slightly higher than that of Al_2O_3, but much less than that of $SrTiO_3$ (ε = 250) and $LaAlO_3$ (ε = 23). In this case also, the values of dielectric constant and dissipation

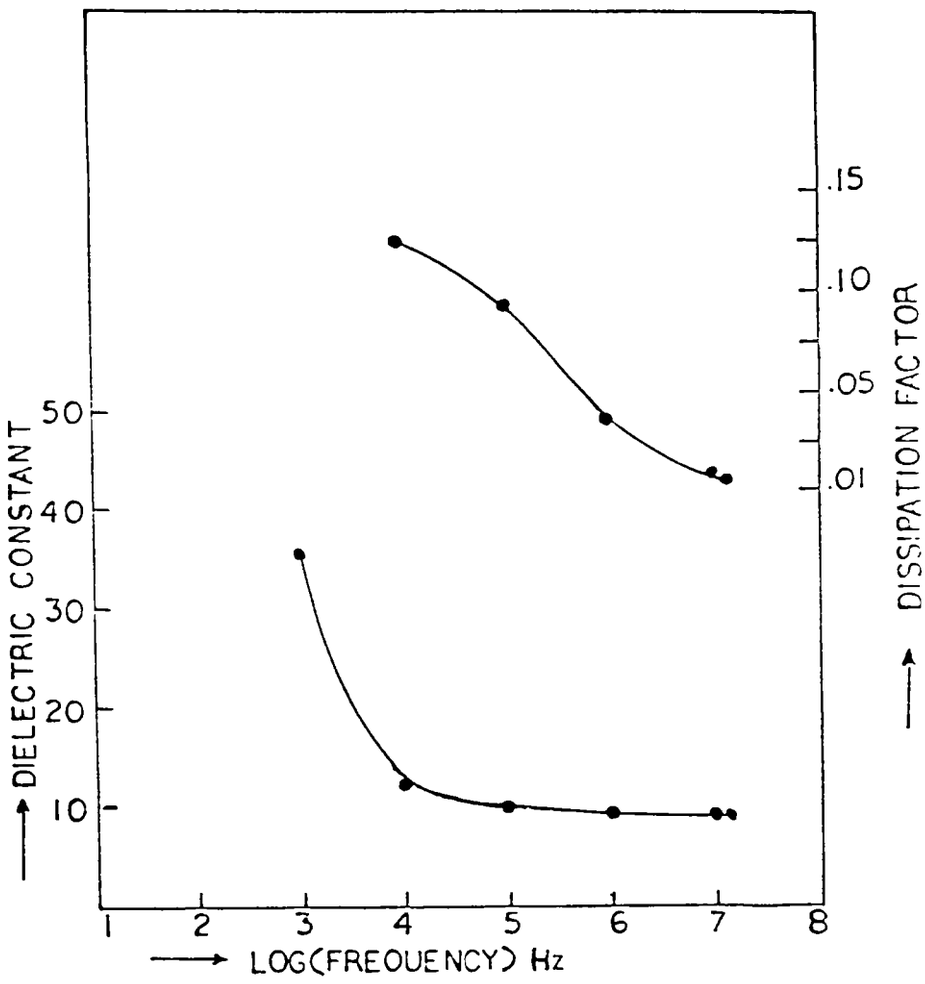

Fig. 4.7: Variation of dielectric constant and dissipation factor as a function of frequency of BYSnO

factor measured are not its true values (since it is not a single crystal), rather it gives the bulk properties of the compound. The space charge and orientation polarisations arise mainly from the CuO impurity added to BYSnO in order to enhance the compound formation as well as sintering.

Scanning electron microscopic studies on polished surfaces of BYSnO were carried out to see the surface morphology and microstructural behaviour. Fig. 4.8 shows the SEM micrograph for 0.5 wt% CuO added BYSnO sintered at 1350^{o}C and cooled slowly to room temperature. The micrograph shows fine and uniform grains with a few porous areas. The SEM picture does not show presence of any additional phases. Also the presence of CuO which was added to BYSnO cannot be seen from the micrograph. Since there are very few pores in BYSnO combined with uniform distribution of grains, as observed by SEM, gives approximately the true values of the material properties measured on BYSnO.

4.2.6 Reactivity of YBCO with BYSnO

The reactivity of the new compound BYSnO with the superconductor YBCO has been studied by XRD method. Equimolar ratio of YBCO and BYSnO were mixed thoroughly and pressed in the form of pellets. The pellets were then sintered at 950^{o}C for 10 hours and cooled slowly to room temperature in air. Fig. 4.9 shows the powder diffraction pattern of a pure YBCO, pure BYSnO and a mixture of YBCO and BYSnO heated at 950^{o}C for 10 hours. From

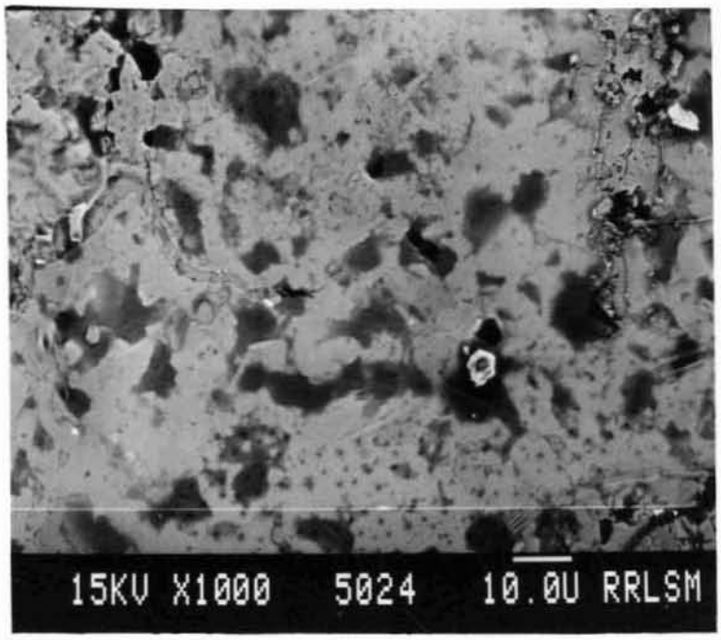

Fig. 4.8: Scanning electron micrograph of BYSnO

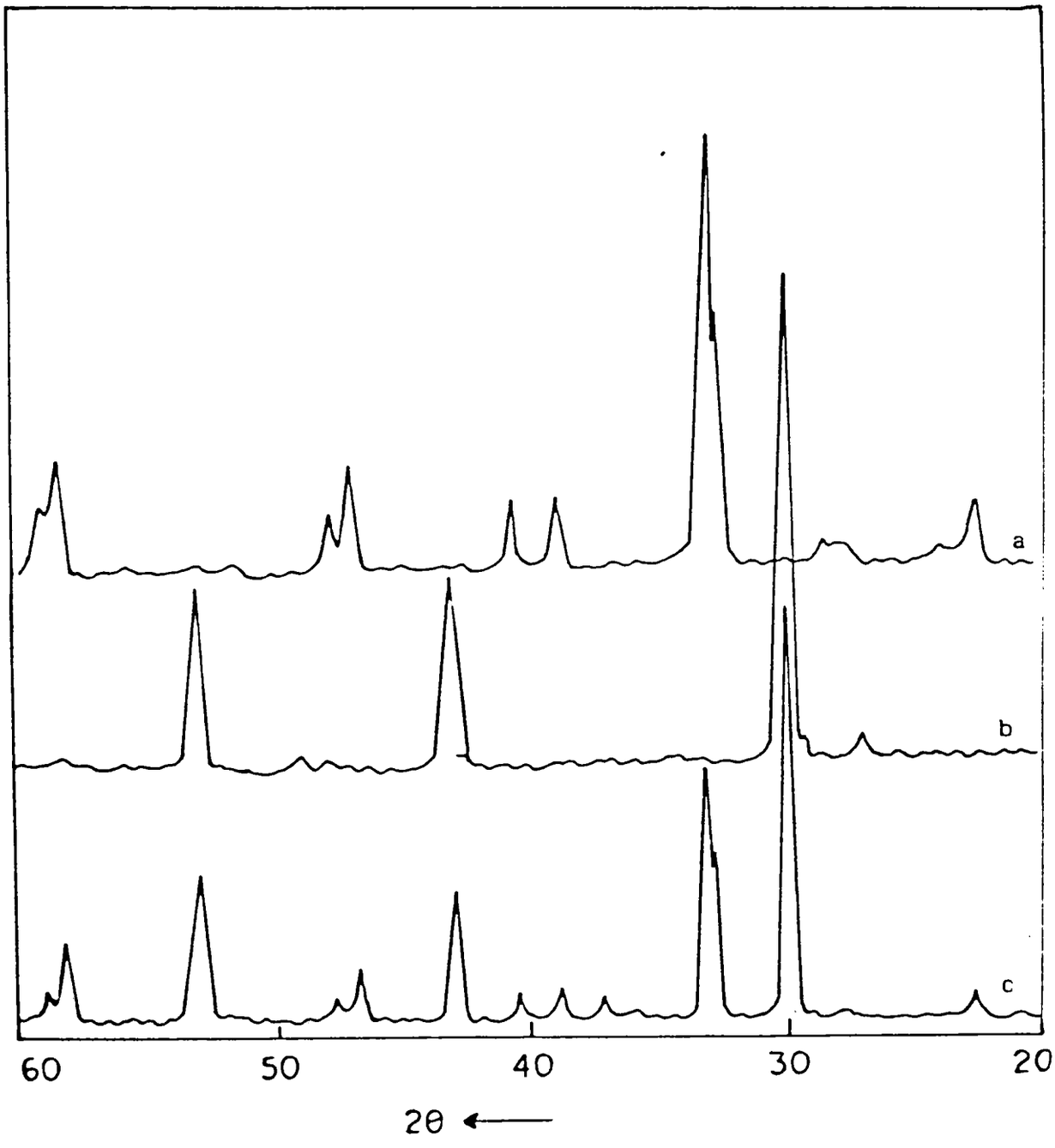

Fig. 4.9: XRD pattern of (a) pure YBCO, (b) pure BYSnO, (c) 1:1 mole mixture of YBCO : BYSnO

the figure it is clear that there is practically no reaction between YBCO and BYSnO. If there was reaction between the two compounds, then in the powder diffraction pattern, some additional peaks other than those of pure YBCO and BYSnO would have appeared. Absence of reaction between the two compounds shows that the two phases co-exist at $950^{o}C$ without any interaction and thus proves our observation. Since there is no reaction between YBCO and BYSnO, it can be used as a good substrate for the deposition of YBCO thin and thick films.

4.3 SYNTHESIS AND CHARACTERISATION OF Ba_2YZrO_6 (BYZO)

4.3.1 Preparation of BYZO

Stoichiometric amount of pure Y_2O_3, $BaCO_3$ and ZrO_2 were weighed, mixed thoroughly in an agate mortar with acetone as grinding media. It was dried, calcined at $1300^{o}C$ in an alumina crucible for 10 hours and furnace cooled. It was then ground thoroughly and pressed in the form of pellets, sintered at $1350^{o}C$ to $1450^{o}C$ for 10 hours and furnace cooled to room temperature. Physical inspection of the samples shows that the material is highly porous having no mechanical strength and gets powdered after some time as in the case of Ba_2YNbO_6 or Ba_2YSnO_6. In order to obtain a highly dense and sintered body, slight amount of CuO was added (0.5-1.0 wt%) to the material and sintered at $1400^{o}C$ for 10 hours and cooled slowly. The CuO added BYZO showed high density with good mechanical strength. Apart from CuO, other impurities such as Bi_2O_3,

PbO, TiO_2, ZnO etc. were also tried, but did not have any effect on the sintering characteristics of the compound BYZO. The samples as prepared above, were studied for their crystal structure, dielectric and microstructural properties.

The crystal structure of the compound BYZO has been studied by x-ray powder diffraction method. Fig. 4.10 a shows the powder diffraction pattern of BYZO prepared as described earlier by heating at 1400 ^{o}C for 10 hours. The XRD pattern obtained is not of a single phase compound, rather it contains other impurities as in the case of BYSnO and BYNO. Fig. 4.10b shows the XRD pattern of 0.5 wt % CuO added BYZO sintered at 1400^{o}C for 10 hours in air and furnace cooled to room temperature. The pattern clearly indicates the formation of a single phase compound with practically no impurities. The pattern was indexed as a cubic perovskite structure with lattice parameter a = 8.44 A. It is a new compound and has not been reported earlier. As in the case of other compounds discussed in the previous sections, a small amount of CuO is found to be essential for obtaining a single phase compound and a sintered body of BYZO.

4.3.2 The density and resistivity of BYZO

The theoretical density of BYZO has been calculated as 6.0 gm/cm^3 based on its structural formula and lattice parameter. The bulk density of BYZO sintered at 1400^{o} C for 10 hours with 0.5 wt % of CuO was found to be 5.45 gm/cm^3 which is about 90% of the theoretical density. The samples which were sintered at

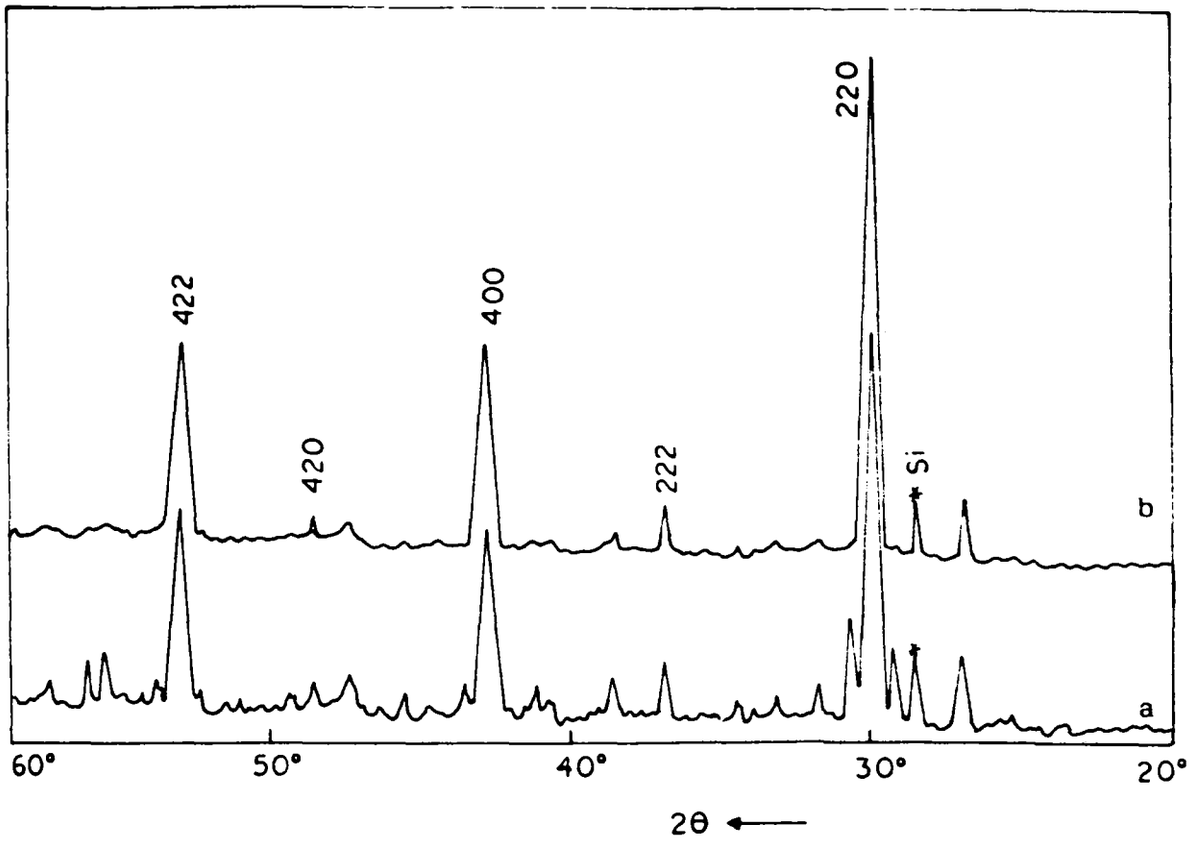

Fig. 4.10: XRD pattern of (a) BYZO prepared without CuO;
(b) BYZO prepared with 0.5 wt % CuO

1450^{o}C without any CuO were found to be highly porous and mechanically very weak and were not suitable for any measurements. If we add more amount of CuO, the sintered density increases through liquid phase sintering which is not advisable for studying the properties of a compound (see Table 4.3). All the measurements were carried out on 0.5 wt % CuO added BYZO sintered at 1400^{o}C and furnace cooled to room temperature in air.

Table 4.3: The density and resistivity of BYZO for different amounts of CuO addition with corresponding sintering temperatures

Amount of CuO (wt %)	Sintering temperature (^{o}C)	Density (gm/cm^{3})	Resistivity (Ω-cm)
0	1450	-	-
0.5	1400	5.45	3×10^{9}
1.0	1400	5.51	3×10^{8}
2.0	1350	5.55	5×10^{8}
3.0	1300	5.55	6×10^{7}
5.0	1200	5.62	4×10^{5}

The dc resistivity of the compound BYZO were measured by two-probe method after giving silver electrode at the two faces of the pellets. A dc solid state electrometer was used for the measurement. The resistivity was found to be of the order of $10^{8}\ \Omega$cm for 0.5 wt % CuO added BYZO sintered at 1400^{o}C. For higher amount of CuO addition the resistivity is slightly less, but for a

5 wt % CuO added BYZO, the resistivity comes down to 10^5 Ω cm. In BYZO the resistivity decreases at a faster rate compared to that of Ba_2YNbO_6 as the amount of CuO increases. Table 4.3 gives the resistivity value of different amounts of CuO added BYZO with respective sintering temperature and density. Since the compound has been prepared by adding CuO, the bulk resistivity obtained should not be taken as its true resistivity, rather it is a combined effect of all. Fig. 4.11 shows the SEM micrograph of BYZO sintered at 1400^{o}C for 10 hours with 0.5 wt % of CuO. The compound BYZO has a fine grain size with practically uniform grain distribution. Presence of secondary phases cannot be observed in the micrograph. In the micrograph a few porous area can be observed which is in accordance with the density measurements.

4.3.3 Dielectric properties

The dielectric properties of the new compound BYZO have been measured as a function of frequency at room temperature using an impedence analyser. Fig. 4.12 shows the variation of dielectric constant and dissipation factor as a function of frequency for samples sintered at 1400 ^{o}C with 0.5 wt % of CuO. Even though the dielectric constant is low, the loss factor is very high. From the figure it is clear that as the frequency increases from Hz region to KHz region, the dielectric constant drastically reduces to a low value which is expected for a material having free space charges. As the time varying electric field passes through the material medium, space charge polarisation and orientation polarisation take place which give rise to high values of dielectric constant at low

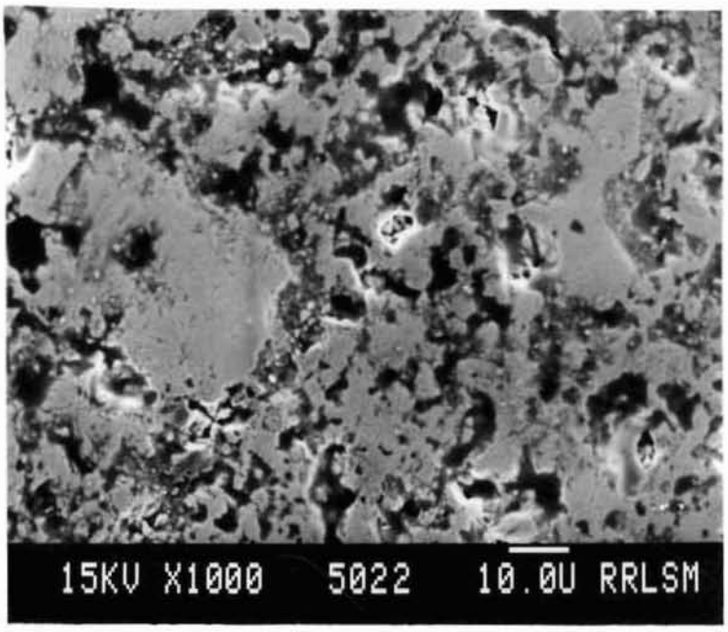

Fig. 4.11: Scanning electron micrograph of BYZO

frequencies. As the frequency increases, these polarisation mechanisms become inoperative and the dielectric constant reduces drastically. The values of ionisation and electronic polarisations are low for BYZO because at MHz region, the dielectric constant is low ($\simeq$ 10).

4.3.4 Elastic properties of BYZO

Measurements of elastic properties are very important from materials science point of view. It gives the resultant strain in the material due to the stress experienced. The elastic modulii of the compound BYZO has been measured as a function of temperature from room temperature to liquid nitrogen temperature. In order to understand the variation in the elastic properties of BYZO, we have measured the longitudinal ultrasonic velocity at 10 MHz, as a function of temperature. The measurements have been carried out using a MATEC ultrasonic pulse echo overlap system. The samples used for the measurements are in the form of circular discs of diameter 10 mm and thickness 2.5 mm. The opposite faces are finally polished so that they are plane and parallel to each other.

The quartz transducer with resonance frequency 10 MHz is bonded to the sample with silicone grease which is found as a suitable bonding material for a wide range of temperatures for longitudinal as well as transverse waves. The sample with the transducer is held in a suitable sample holder in a cryostat. Using liquid nitrogen as the cryogen, the temperature of the sample is lowered to 90 K. A temperature controller is used to control the

temperature of the sample. In order to avoid thermal gradients and errors in temperature readings due to the thermal inertia of the sample holder, the cooling rate is kept relatively small of the order of 0.5 K/mim. For measuring ultrasound velocity, we have used the pulse echo overlap technique (4). Echoes due to multiple reflections at sample faces have been selected and overlaped on the oscilloscope screen and by measuring the frequency and travel time at which the oscilloscope is triggered, the velocity has been calculated. By varying the temperature of the sample, the velocity measurements have been carried out from 90 K to 300 K. The elastic constant is calculated using the equation

$$C = \rho V^2$$

where V is the appropriate velocity and ρ is the density of the sample which is found to be $\simeq 5260$ kg/m^3. The variations of the longitudinal elastic modulus C_{11} as a function of temperature is shown in Fig. 4.13. As the temperature decreases, the elastic constant increases which is the normal behaviour of any solid. A small change in slope is observed at temperatures $\simeq$ 225 K. Below this temperature, the rate of increase decreases on cooling. No significant hysterisis in the variation of C_{11} has been found between cooling and heating cycles.

4.3.5 Thermal properties of BYZO

Thermal properties of any solid material are important, because they give information about the response of the material

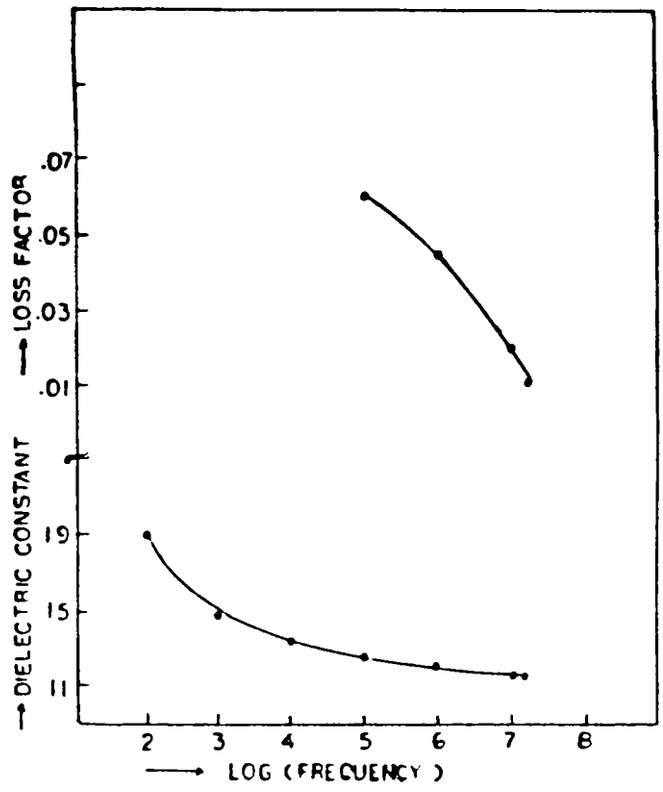

Fig. 4.12: Variation of dielectric constant and dissipation factor as a function of frequency of BYZO

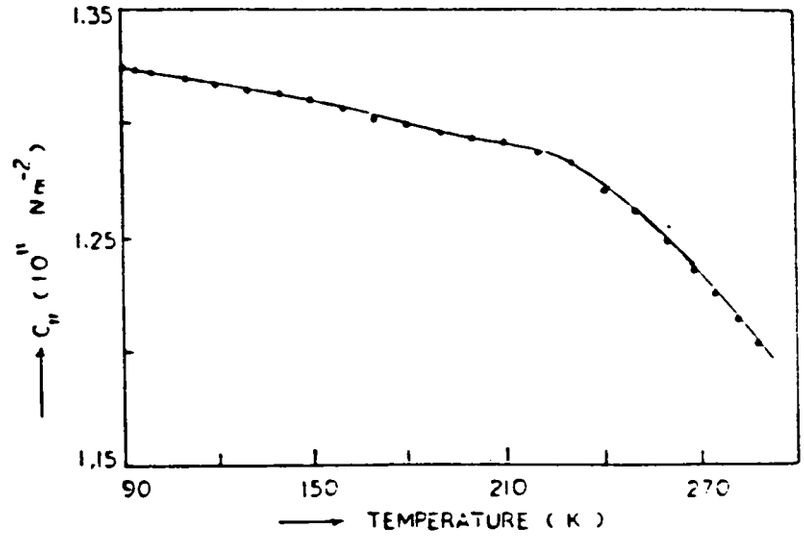

Fig. 4.13: Variation of longitudinal elastic modulus C_{11} as a function of temperature of BYZO

to different thermal atmospheres. The thermal properties such as specific heat and thermal conductivity of BYZO have been measured as a function of temperature. The specific heat of the sample is measured using a differential scanning calorimeter (Perkin Elmer DSC-7) by the ratio method (5) with sapphire as the specific heat standard. Known mass of powdered sample is taken in an aluminium pan and sealed. The pan is then placed in the calorimeter and the heat flow into the sample is plotted along with sapphire which is the reference sample. From these two plots the specific heat calculated by the equation

$$C_{ps} = \frac{H_S \cdot M_R \cdot C_{PR}}{H_R \cdot M_S}$$

where C_p, H and M are the specific heat, heat flow and mass respectively with subscripts S and R referring to the sample and the reference respectively. Specific heat at various temperatures have been determined by doing the above calculation at the desired temperatures. The variation of specific heat with temperature for the sample is shown in Fig. 4.14. The specific heat follows the normal behaviour till 450 K on heating and then increases gradually. In the region between 90 K and 450 K the specific heat of the material shows no anomalous change.

The thermal diffusivity is measured as a function of temperature using the photo accoustic (PA) method (6). A PA spectrometer in which, the cell has provision to change the backing material

of the sample, has been used for this purpose. A powerful Xe lamp, a monochromator, a mechanical light chopper and a lock-in amplifier are the other modules of the experimental set up (7). Sample for this measurement has been prepared by hand lapping and polishing the bulk material. The sample is thinned down to approximately 80 um. The PA amplitude as well as the phase has been measured as a function of chopping frequency F. The thickness of the sample is so chosen that it is thermally thin for $f < f_c$, the characteristic frequency and thermally thick for $f > f_c$. The PA amplitude versus the chopping frequency has been plotted. The slope of the plot sharply changes at f_c at which the sample undergoes a change from a thermally thin regime to thermally thick regime and the thermal diffusivity α is given by $f_c t^2$, where t is the thickness of the samples. The measurements have been carried out at a large number of fixed temperatures between 90 K and 300 K.

The thermal conductivity K is defined by combining the specific heat data and thermal diffusivity data making use of the relation

$$k = \alpha \rho C_p$$

The variation of thermal conductivity with temperature is shown in Fig. 4.15. On heating K increases at first and then slowly saturates at about 225 K.

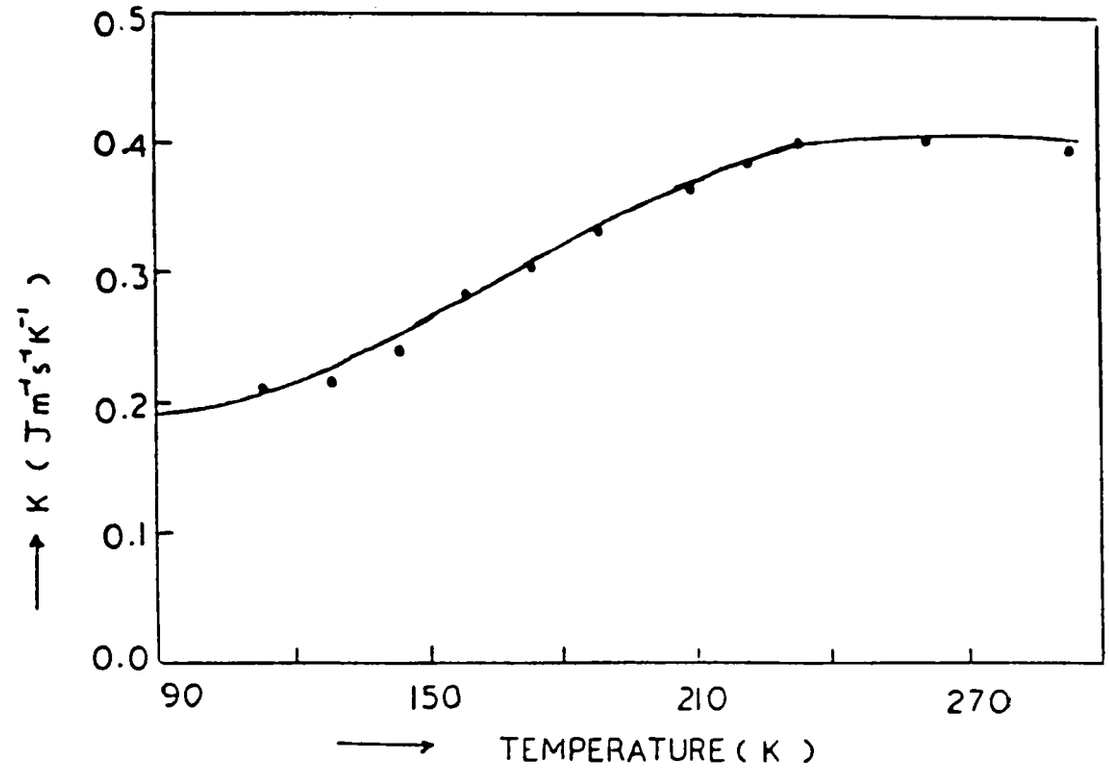

Fig. 4.15: Variation of thermal conductivity as a function of temperature of BYZO

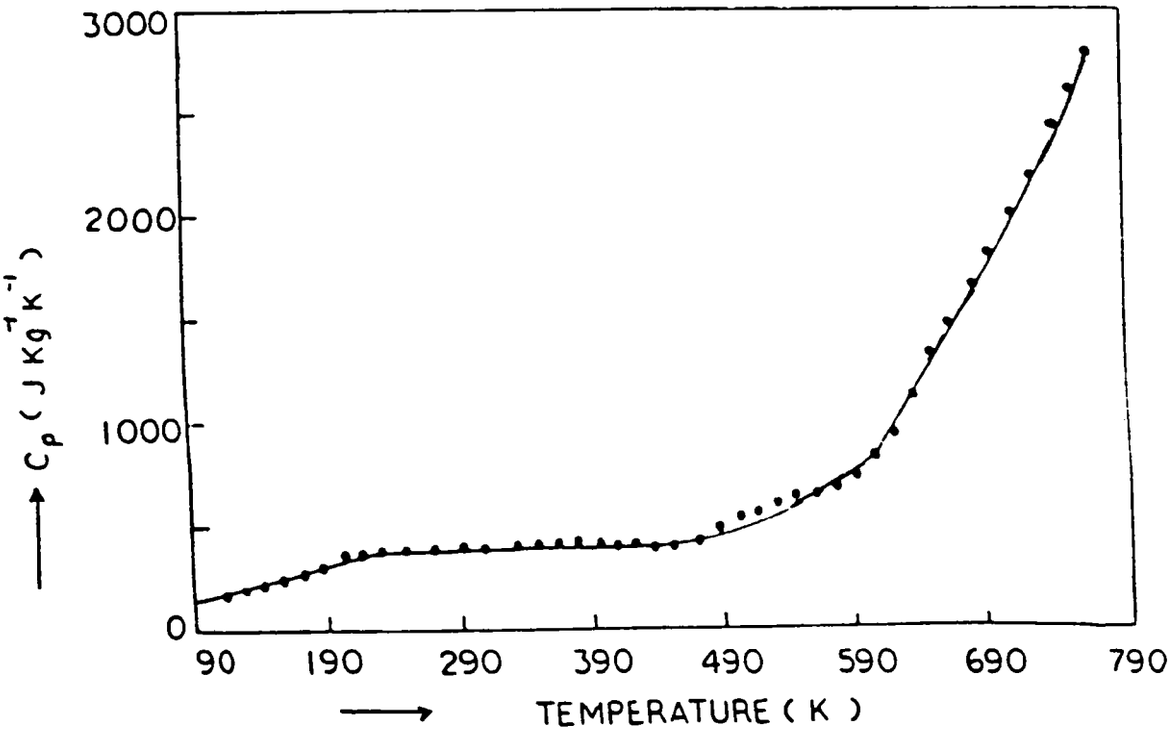

Fig. 4.14: Variation fo specific heat with temperature of BYZO

4.3.6 Reaction between BYZO and YBCO

Since the compound BYZO first appeared as a second phase in YBCO-ZrO_2 system and the superconducting transition temperature is not affected, it was assumed that there will not be any reaction between YBCO and BYZO. The reactivity of YBCO with BYZO was further studied in order to prove their co-existence at temperatures of 950^{o}C. The usual sintering temperature of YBCO is around 950^{o} C and in the system YBCO-ZrO_2 heated at 950^{o}C, the secondary phase formed was reported (8,9) as $BaZrO_3$ by various researchers. In order to confirm the secondary phase in the system YBCO-ZrO_2 as the compound BYZO, the reactivity between YBCO and BYZO was studied. Equimolar ratio of two were mixed thoroughly and pressed in the form of pellets and sintered at 950^{o}C for 10 hours. Fig.4.16 shows the powder diffraction pattern of the mixture of YBCO and BYZO heated at 950^{o}C. From the XRD pattern it is evident that practically there is no reaction between YBCO and BYZO. If there is any reaction between the two compounds, then it should have reflected in the XRD pattern. Absence of additional peaks and structural transformations confirmed that there is not much interaction between the two compounds at this temperature of processing. Due to the non-reactivity of YBCO with the new compound BYZO, it can be used as a substrate material for the deposition of YBCO thin and thick films.

Fig. 4.16: XRD pattern of (a) pure YBCO, (b) pure BYZO, (c) 1:1 mole mixture of YBCO : BYZO heated at 950°C for 10 hrs.

4.4 SYNTHESIS AND CHARACTERISATION OF Ba_2YSbO_6 (BYSbO)

4.4.1 Preparation of BYSbO

High purity Y_2O_3, $BaCO_3$, Sb_2O_3 are weighed in the required ratio, mixed thoroughly in an agate mortar with acetone as mixing media. It was then calcined at 1300^oC for 10 hours and furnace cooled to room temperature. The calcined material was ground thoroughly and pressed in the form of pellets as before. The pellets were then sintered at temperatures between 1350 to 1450^oC for 10 hours and furnace cooled. In order to enhance the compound formation and sintering, small amount of CuO was adde to the mixture and sintered at 1400^oC for 10 hours. These samples were used to study their crystal structure, electric and dielectric properties and microstructural properties.

The crystal structure of the compound BYSbO was studied by x-ray powder diffraction method. Figure 4.17 shows the powder diffraction pattern for pure BYSbO heated at 1400^oC for 10 hours. Even though the major peaks are due to the compound BYSbO, considerable amount of secondary phase is also present in the above prepared material as revealed by x-ray diffraction pattern. As in the case of other compounds discussed earlier, elevated heating temperature or prolonged time of heating do not result in single phase material, rather than melting the compound. Figure 4.17b shows the powder diffraction pattern for BYSbO prepared with 1 wt% of CuO sintered at 1400^oC for 10 hours. The x-ray pattern thus

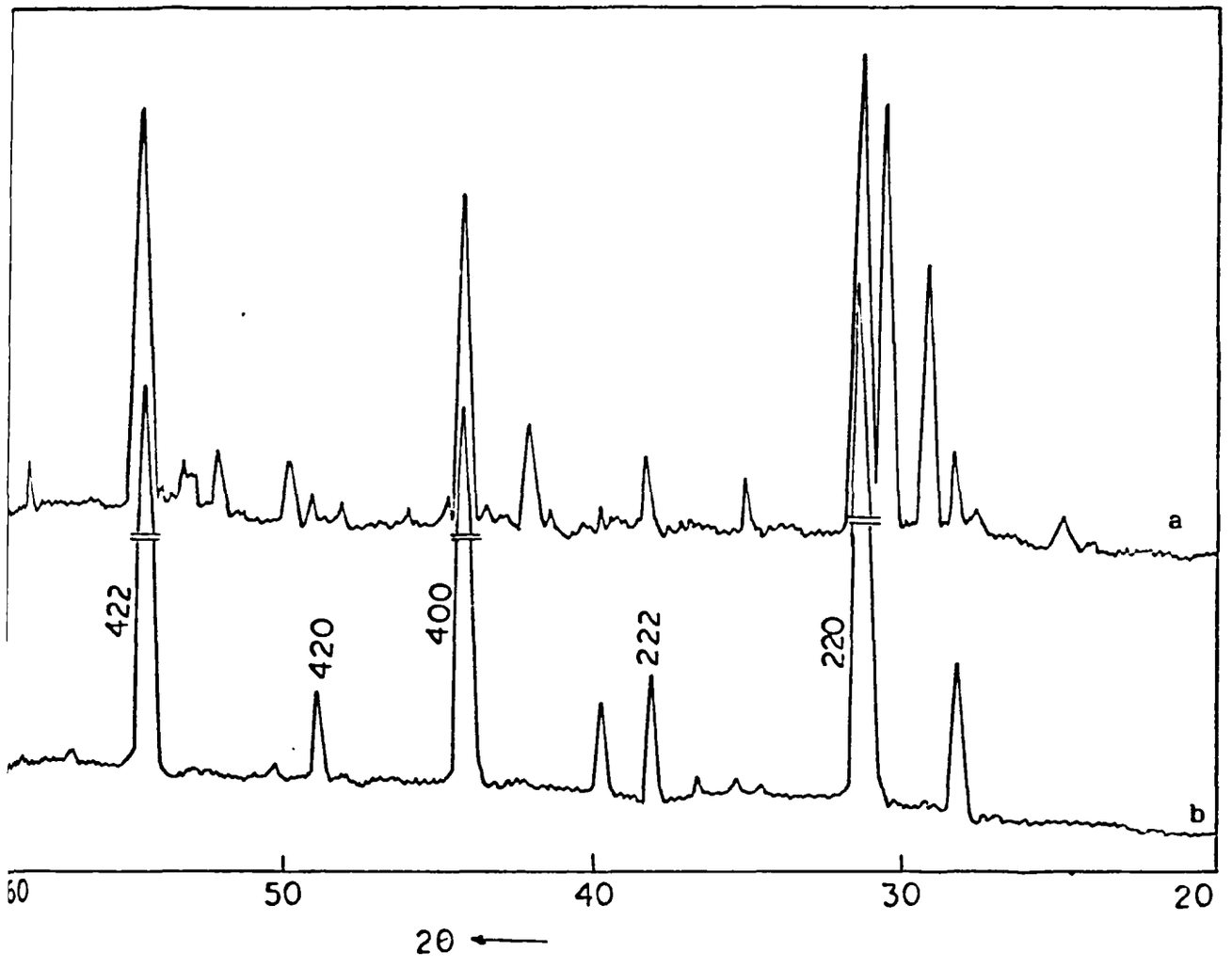

Fig. 4.17: XRD pattern of (a) BYSbO prepared without CuO,
(b) BYSbO prepared with 0.5 wt % CuO

obtained is for a single phase compound with practically no impurities. The pattern was indexed for a cubic perovskite structure and the lattice parameter calculated as a = 8.40 A.

4.4.2 Density and resistivity of BYSbO compound

The theoretical density of BYSbO compound has been calculated based on its crystal structure and cell volume. The theoretical density calculated found to be 6.45 gm./cm^3 . The bulk density of BYSbO without any CuO addition was found to be very low, but the density measured for 1.0 wt % CuO added BYSbO was found to be 5.91 gm/cm^3 which is about 90% of theoretical density. When we add CuO a liquid phase is formed, which enhances the compound formation as well as sintering of the material. The optimum amount of CuO required to get a well sintered body is about 1.0 wt % of CuO compared to 0.5 wt % of CuO in other compounds discussed earlier.

The dc resistivity of the BYSbO samples sintered with CuO were measured by two-probe method using an electrometer. For 1.0 wt % CuO added BYSbO, the resistivity was found to be about 10^8 Ω- cm in the same range as that of other compounds. As we add more CuO, the resistivity remains same as that of BYSbO upto 3 wt % of CuO addition. But for a 5 wt % CuO added BYSbO, the resistivity decreases. The sintering temperature and resistivity values of different amounts of CuO added BYSbO are given in Table 4.4.

Table 4.4: The density and resistivity of BYSbO for various amounts of CuO addition with respective sintering temperatures

Amount of CuO (wt %)	Sintering temperature (^{o}C)	Density (gm/cm^3)	Resistivity (Ω cm)
0	1450	-	-
1	1400	5.91	1.7×10^8
2	1400	5.98	1.6×10^8
3	1350	5.99	1.4×10^8
5	1300	6.00	8×10^6
10	1200	6.08	5×10^3

Scanning electron microscopic studies were carried out on polished surfaces of the material in order to study the microstructural properties such as porosity, grain size and its distribution, surface morphology and secondary phases etc. From Fig. 4.18 it is clear that the compound with 1.0 wt % of CuO sintered at 1400^{o} C has very fine grain size and their distribution is almost uniform. There is no detectable amount of secondary phases as evident from the figure. Presence of pores can be observed, but the percentage is very low in accordance with the density measurements. The presence of CuO is not observable from the SEM micrographs.

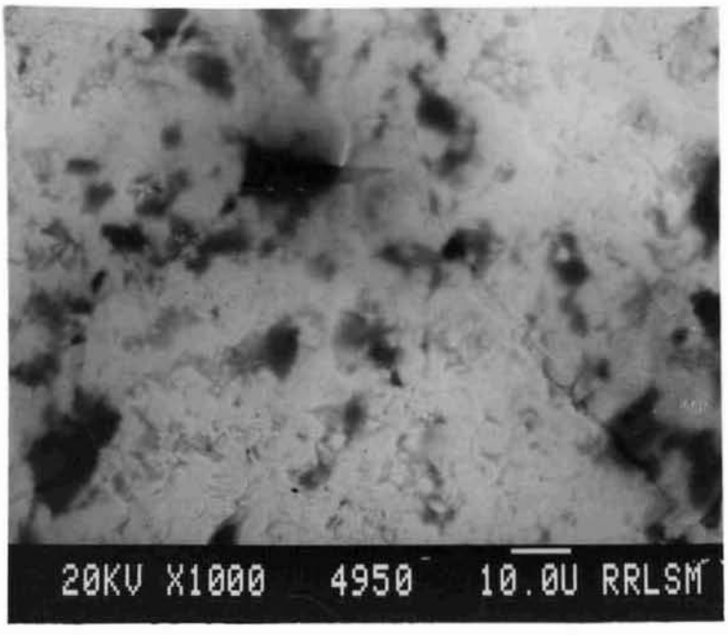

Fig. 4.18: Scanning electron micrograph of BYSbO

4.4.3 Dielectric properties of the compound BYSbO

The dielectric properties of the compound prepared as above with 1.0 wt % CuO were studied using an impedence analyser. The variations of dielectric constant and dissipation factor are plotted in Fig. 4.19 as a function of frequency. From the figure it is evident that the dielectric constant decreases considerably as the frequency increases. The reduction in the value of dielectric constant can be attributed to the large values of space charge polarisation and orientation polarisations occurring during the application of electric field. Space charge polarisations and orientational polarisation are undesirable in a dielectric material for its use as substrates. Also high loss factor is not good for a substrate material. One probable reason for high loss factor may be due to the presence of CuO which has been added to BYSbO for compound formation and sintering.

4.4.4 Reactivity of YBCO with BYSbO

The compound BYSbO first appeared as a second phase in YBCO-Sb_2O_3 system, and it is expected that there will not be any reaction between YBCO and BYSbO. Also from a technological point of view, Ba_2YSbO_6 can be used as a substrate for YBCO thin films, if the reactivity is less or there is no reaction at all. With this point of view, equimolar ratio of two compounds were mixed thoroughly and pressed in the form of pellets. It was then sintered at 950^{o}C for 10 hours. X-ray powder diffraction pattern for (a) pure

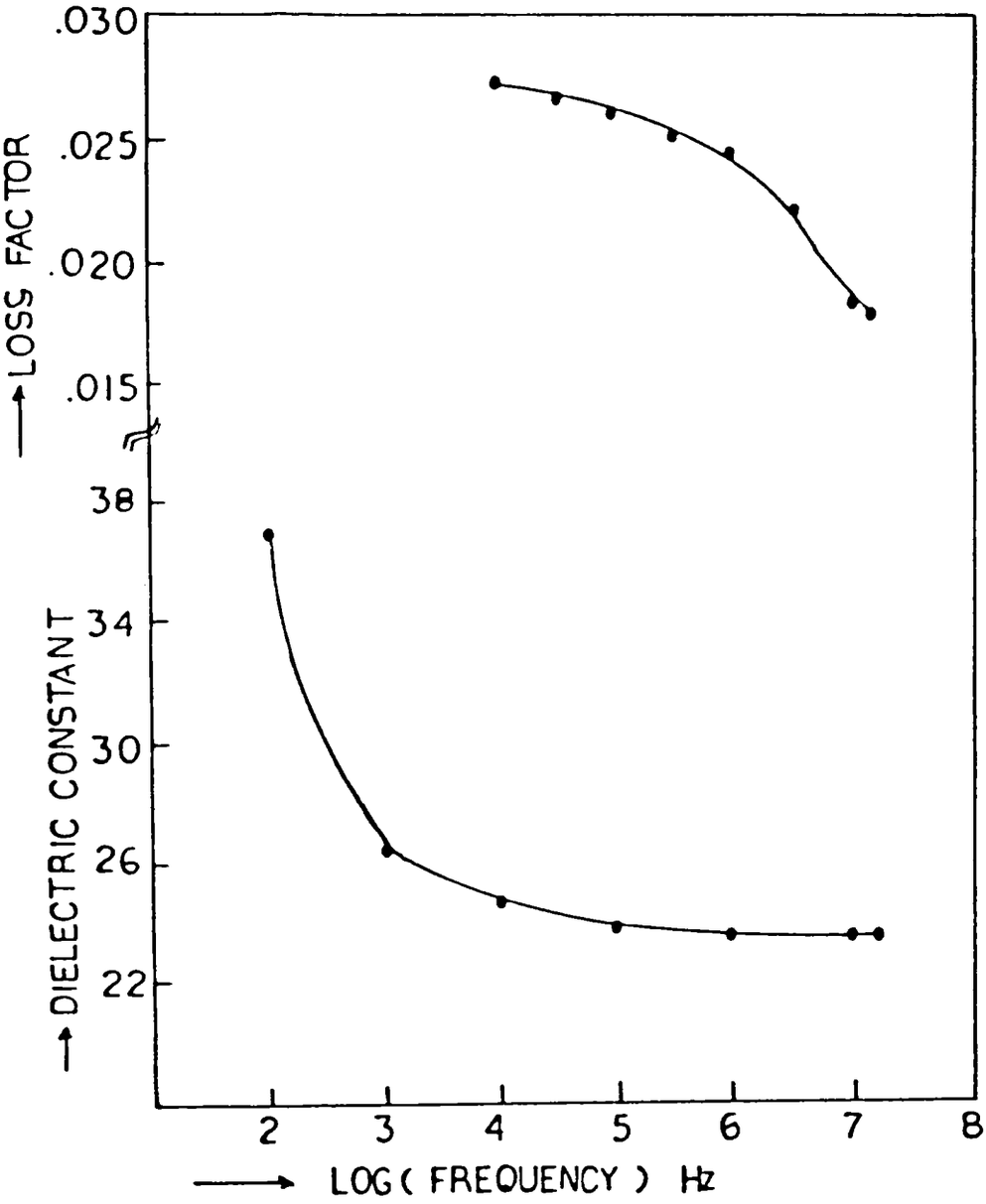

Fig. 4.19: Variation of dielectric constant and dissipation factor as a function of frequency for BYSbO

Fig. 4.20: XRD pattern of (a) pure YBCO, (b) pure BYSbO, (c) 1:1 mole mixture of YBCO:BYSbO heated at 950°C for 10 hrs.

YBCO, (b) pure BYSbO, (c) 1:1 mole mixture of YBCO and BYSbO heated at 950^{o}C are shown in Fig. 4.20. From the figure it is clear that practically there is no reaction between the two compounds at 950^{o}C. If there is reaction between the two compounds, then in the x-ray pattern it should be reflected. The x-ray diffraction pattern did not show any additional peaks apart from those for pure YBCO and BYSbO. Due to the non-reactivity of BYSbO with YBCO, it is inferred again that the secondary phase formed in YBCO-Sb_2O_3 system is the compound Ba_2YSbO_6 and has been suggested as a promising substrate for the deposition of YBCO thin and thick films.

4.5 DISCUSSION

The present investigation gives a detailed description of the preparation of a new class of ceramic compounds all having the same crystal structure and chemical formula. The preparation methods are also the same. In all the four compounds presence of CuO was found essential for obtaining a single phase material and for getting a highly dense and sintered body. Absence of CuO results in impurity phases (as evident from XRD studies) and shattering of the sintered product into powder during cooling (in the absence of CuO the mechanical strength is very poor). The exact role of CuO is not understood at present. Also whether CuO goes into the lattice of YBCO has not been investigated. The amount of CuO required for the purpose of obtaining a single phase compound is very small and is of the order of 0.5 wt %. Since

CuO melts above 950^{o}C, either it must have melted and ran out of the body or formed some liquid phase by reacting with the constituent materials and the small amount of liquid phase formed may be enhancing the compound formation and sintering.

Even though the compound Ba_2YNbO_6 has been reported earlier (1) very few studies can be seen on this compound. Recently Mitsuhira Takata et al. (10) studied the dielectric properties of a similar rare earth compound Ba_2YbNbO_6 for its possible use as a dielectric resonator material. But the compound Ba_2YbNbO_6 prepared by them is not a single phase compound, rather it contains other phases also. Since it is very difficult to get a single phase compound of Ba_2YNbO_6, in literature we cannot see a detailed study of this compound and its characterisation. The present investigation gives the preparation method of a single phase compound BYNO. The compounds viz. Ba_2YSnO_6 and Ba_2YZrO_6 are new compounds and have not been reported earlier.

The general structural formula for the series of compounds can be represented by Ba_2YAO_6 (where A = Nb, Sb, Sn and Zr). Since all the compounds are isostructural, their preparative conditions are also similar. The properties of the compounds are also more or less same with no remarkable difference in electrical and dielectric properties.

The compounds Ba_2YAO_6 appeared as a secondary phase YBCO-A_xO_y system (where A = Nb, Sb, Sn or Zr). In literature we can see considerable number of works on SnO_2 and ZrO_2 doped

YBCO (2,3,8,9). The secondary phase formed in YBCO-SnO_2 system has been reported as $BaSnO_3$ (2,3) and the effect of addition of $BaSnO_3$ in YBCO on the enhancement of current density has been studied by McGinn et al. (11). Few groups have claimed that Sn goes into the lattice sites of YBCO (12,13), but the transition temperature remains same as that of pure YBCO. They also carried out the Mossbauer spectroscopic studies on SnO_2 doped YBCO. But in the present investigation we identified the secondary phase as Ba_2YSnO_6 and synthesised the compound as a single phase material and proved the co-existence of YBCO and Ba_2YSnO_6 without any reaction or interaction between the two to show that the secondary phase is Ba_2YSnO_6 and not $BaSnO_3$. In the case of ZrO_2 doped YBCO the secondary phase has been reported as $BaZrO_3$ (8,9). Since ZrO_2 is being widely used as a good buffer layer in between various substrates and YBCO thin films, a detailed study on the secondary phase in YBCO-ZrO_2 system is very important. In the present investigation we identified the secondary phase as Ba_2YZrO_6 and not as $BaZrO_3$. The compound has been prepared as a single phase material and indexed the crystal structure. The co-existence of YBCO with Ba_2YZrO_6 has been studied and found that there is no reaction between the two at 950^oC and thus proved that the secondary phase is Ba_2YZrO_6. In the case of Nb_2O_5 and Sb_2O_3 the nature of the secondary phases has not been reported. But we identified the secondary phases as Ba_2YNbO_6 and Ba_2YSbO_6 and proved by studying their co-existence with YBCO at 950^oC.

Table 4.5: Various properties of the new compounds

Compound	BYNO	BYSnO	BYSbO	BYZO
Crystal system	cubic a = 8.436 A	cubic a = 8.420	cubic a = 8.40	cubic a = 8.44
Theoretical density gm/cm^3	6.109	6.320	6.45	6.00
DC resistivity Ω-cm	5×10^9	1.6×10^7	1.7×10^8	3×10^9
Dielectric constant at 1 M Hz	28	10	20	15
Loss factor at 1 M Hz	10^{-3}	10^{-2}	10^{-2}	10^{-2}

The studies have shown that the newly developed ceramic compounds do not react with the superconductor YBCO. The measurements on electrical resistivity show that these compounds are insulators. Table 4.5 gives the different properties of the new compounds. The values of dielectric constant found to be for Ba_2YNbO_6 = 28, Ba_2YSbO_6 = 20, Ba_2YSnO_6 = 10, Ba_2YZrO_6 = 15 which are higher than that of alumina but much less than that of $SrTiO_3$ ($\varepsilon \simeq$ 250), a usual substrate for YBCO thin films. Due to the nonreactivity of the above compounds with YBCO, the new compounds can be used as good substrates for the deposition of YBCO thin and thick films. The only difficulty with the new compounds

is that there is lattice mismatch between YBCO and the new compounds and epitaxial film growth is difficult. But at the same time it should be noted that the lattice parameters of the new compounds are almost double to that of MgO (a = 4.21 A), a common substrate for the deposition of YBCO thin films.

Now consider the compound Ba_2YSnO_6. The compound can be considered as a rare earth doped perovskite compound $BaSnO_3$. The doping mechanism can be schematically represented as below:

$$2\ BaSnO_3 \xrightarrow{\text{Y doping for Sn}} 2\ Ba\ Y_x\ Sn_{1-x}\ O_3$$

$$\xrightarrow{\text{When } x = 0.5} 2\ Ba\ Y_{0.5}\ Sn_{0.5}\ O_3$$

$$\longrightarrow Ba_2\ Y\ SnO_6$$

In a similar way we can consider the other compounds as rare earth doped perovskite compounds. In general the doping mechanism can be represented as

$$2\ Ba\ A\ O_3 \xrightarrow{\text{Y doping for A}} 2\ Ba\ Y_x\ A_{1-x}\ O_3$$

(Cubic perovskite)

$$\xrightarrow{\text{When } x = 0.5} 2\ Ba\ Y_{.5}\ A_{.5}\ O_3$$

$$\longrightarrow Ba_2\ YAO_6$$

(cubic perovskite)

where A = Nb,Sb,Sn or Zr

Thus all the four compounds show identical doping mechanism and have same structural properties.

The compounds belong to $(NH_4)_3$ Fe F_4 class of compounds with space group Fm3m. The crystal structure is schematically shown in Fig. 4.21. It is very similar to the compound Ba Pb_{1-x} Bi_xO_3 a non-copper oxide superconductor discovered by Sleight et al. (14) with a transition temperature of 13 K approximately.

4.6 SCOPE FOR FUTURE INVESTIGATIONS ON NEW COMPOUNDS Ba_2YAO_6

Since the compounds Ba_2YAO_6 do not react with the superconductor YBCO, thin film deposition on substrates made of Ba_2YAO_6 can be carried out. Since almost all the known ceramic insulators react with YBCO and deteriorate the superconducting properties, good quality films of YBCO are not met with success. However, with sophisticated instruments and innovative techniques of deposition, fairly good quality films are being made on various substrates. But the quality of the films are not so good to make use of it into technological devices where the salient features of superconductors are being made use of for more efficiency compared to conventional materials. Due to the non-reactivity, excellent quality films are expected on substrates made of Ba_2YAO_6 where the salient features of high temperature superconductors can be exploited into technological devices. But it is needed to have a suitable deposition technique.

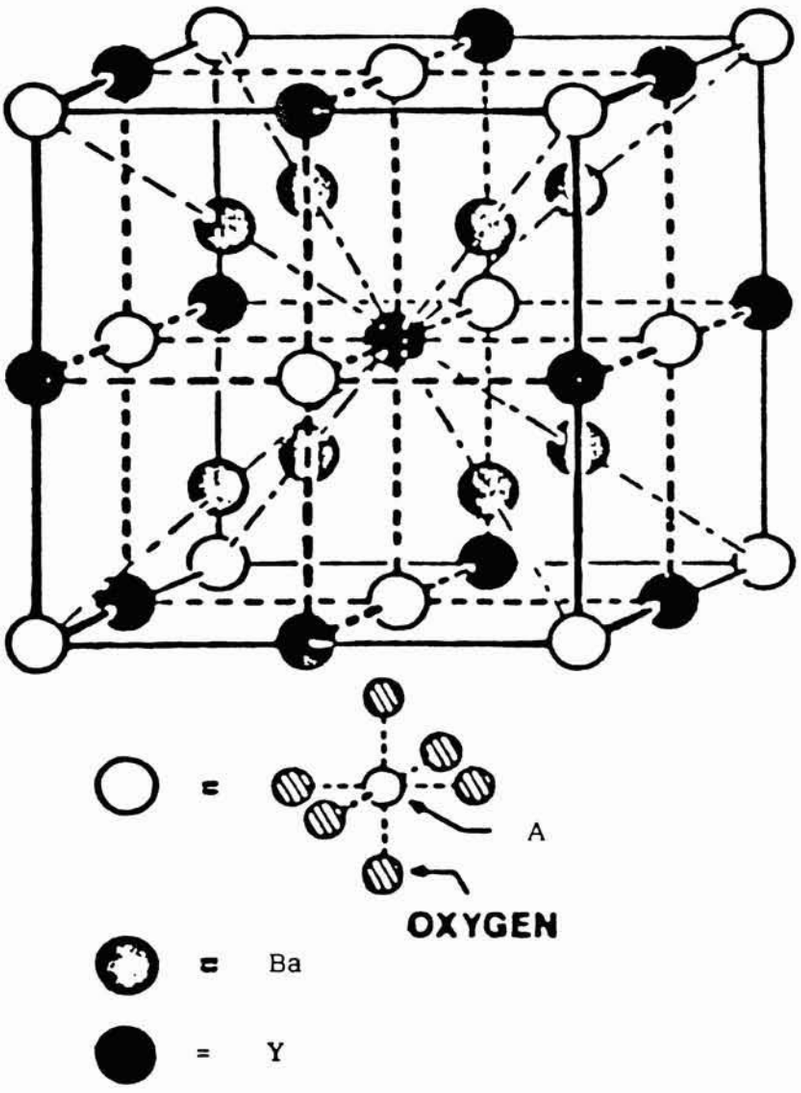

Fig. 4.21: Crystal structure of $Ba_2^{2+}\ Y^{3+}A^{5+}O_6$ ordered perovskite structure

Another aspect of studies is the substitution for various lattice sites of the compound Ba_2YAO_6 and the resultant variations in crystal structure, electric and dielectric properties and various other physical properties. It is possible to replace Y completely by other rare earth elements. The general formula can be written as Ba_2LnAO_6 where Ln = rare earth elements, A = Nb, Sb, Sn and Zr. Similarly it is possible to substitute the divalent cation Ba^{2+} by Ca and Sr. It will be interesting to study these aspects and the associated property changes.

Another interesting aspect is the effect of CuO addition in the formation of the compounds Ba_2YAO_6 and its sinterability. It is found that extremely small amount of CuO is required for obtaining a single phase as well as sintered body. As we add more and more amount of CuO, the electrical conductivity of YBCO increases considerably (see Tables 1-4). The insulator to metal transition due to CuO doping is also interested to study and the associated density of electronic states. Since the compounds are structurally identical to the non-copper oxide superconductor $Ba\ Pb_{1-x}\ Bi_xO_3$ a search for superconductivity in Ba_2YSbO_6 with suitable doping may be interesting.

Finally in the compounds Ba_2YSnO_6 and Ba_2YZrO_6 if we take the valency into consideration, the chemical formula can be written as $Ba_2YSnO_{5.5}$ and $Ba_2YZrO_{5.5}$. But its structure can accommodate oxygen content upto 6.0. Hence it will be interesting to study the oxygen ion conductivity of these two compounds. The compound

$YBa_2Cu_3O_{7-\delta}$ is found to be a good oxygen ion conductor due to the excess oxygen in the structure. In a similar analogy it is expected that Ba_2YZrO_6 and Ba_2YSnO_6 can be good oxygen ion conductors and one can exploit this property of the material into practical devices. Already ZrO_2 and SnO_2 are known (15) as good oxygen ion conductors. Good ionic conductivity is expected in the above two compounds and further studies are needed in this direction.

REFERENCES

1. McIlvried and McCarthly, Penn state University (1972).

2. Hoge Osamura, Norkazu Matsukura, Yukihide Kusumoto, Shojira Ochiai, Baorong Ni and Tesue Matsushita, Jap. J. Appl. Phys., 29 L 1621 (1990).

3. M. Pasternak and R.D. Taylor, solid state Commun., 69, 1161 (1989).

4. E.A. Papadikis, Physical Accoustics, Vol. 12 (Ed. W.P. Mason and R.V. Thurstin), academic Press, New York (1976).

5. N.J. O'Neill, J. Analytical Chemistry, 38, 1331 (1966).

6. P. Charpentier, F. Lapoutre and L. Bestrand, J. Appl. Phys., 53, 608 (1982).

7. K.N. Madhusoodanan, J. Phillip, G. Parthasarathy, S. Ashokan and E.S.R. Gopal, Philosophical Magazine, B 58, 123 (1988).

8. S.W. Filipczuk, Physica C, 173, 1 (1991).

9. M.J. Cima, J.S. Schneider, S.C. Peterson and W. Coblenz, Appl. Phys. Lett., 53, 710 (1988).

10. Mitsuhiro Takata and Keisuke Kageyama, J. Am. Ceram. Soc., 72, 1955 (1989).

11. P. McGinn, W. Chen, N. Zhu, C. Varanasi, L. Tan and D. Balkin, Physica C, 183, 51 (1991).

12. Y. Yuen, C.L. Lin, J.E. Crow, G.N. Myer, R.E. Solomon, P. Schlottmann, N. Bykovetz and W. N. Harman, Phys. Rev., B 37, 3770 (1988).

13. T. Nishida, M. Katada and Y. Matsumoto, Jap. J. Appl. Phys., 29, 1259 (1990).

14. A.W. Sleight, J.L. Gillson and B.E. Bierstedt, Solid State Commun., 17, 27 (1975).

15. Paul Hagen Muller and W. Vangool, Solid Electrolytes, Academic Press, New York (1978).

CHAPTER 5

TRANSPORT PROPERTIES OF CERAMIC INSULATOR-SUPERCONDUCTOR COMPOSITES: A PERCOLATION STUDY

5.1 INTRODUCTION

In the previous chapter we have described the synthesis of a new class of ceramic compounds Ba_2YAO_6 which appeared as a secondary phase in YBCO due to the dopants Nb_2O_5, Sb_2O_3, SnO_2 and ZrO_2. The real existence of the compounds have been proved by synthesising the compounds and have further determined the crystal structure and their electric, dielectric, thermal and elastic properties. Also it was found that there was no reaction between YBCO and Ba_2YAO_6 at normal processing temperatures. This chapter describes the preparation of ceramic insulator-superconductor composite for the first time, even though considerable amount of work have been carried out (1-5) on superconductor-noble metal composites where the reactivity is least. Previously there was no study on a ceramic insulator-superconductor composite system, primarily because almost all the known ceramic insulators react with YBCO at elevated temperatures of processing and destroy the superconducting properties. The new compounds developed by us are found to be non-reactive with YBCO and it is the first attempt to prepare a real ceramic insulator-superconductor composite which contains the high temperature superconductor $YBa_2Cu_3O_{7-\delta}$.

The high temperature ceramic superconductors exhibit granular properties. The study of superconducting small aggregates, clusters or particles are very important from both fundamental and technological stand point. Due to the short coherence length and large penetration depth along with the granular nature of high T_c superconductors, it will be interesting to study the percolation and fractual properties, quantum size effects, thermal fluctuations and size effects on superconductivity.

A ceramic insulator-superconductor composite system provides superconducting small aggregates along with insulating phase without deteriorating its properties. Preparation of such a composite system provides considerable information from both fundamental and technological point of view. Recently there were a few attempts to study the percolation behaviour of superconductor-noble metal composites based on electrical transport and magnetisation properties (2,3). It was found that noble metals such as gold and silver form composites with YBCO without deteriorating the properties of YBCO. The percolation model equations cannot be strictly applied to such a system due to the low resistivity ratio of the two at room temperature. Recently Lin (6) proposed a scaling factor to explain the observed deviations in the critical exponents describing the transport properties of Ag-YBCO composites. They studied a model system Ag-$PrBa_2Cu_3O_7$ and showed that the deviations of critical exponents are due to the low resistivity ratio of superconductor to metal compared with that of insulator to metal and not due to any other interactions. In this chapter the normal state percolation

and superconducting state percolation behaviour of insulator-superconductor composite systems have been studied based on transport properties and the implications of the results obtained have been discussed from both fundamental and technological point of view.

The ceramic insulator-superconductor composite systems presently investigated are:

i. Ba_2YNbO_6 - $YBa_2Cu_3O_{7-\delta}$

ii. Ba_2YSnO_6 - $YBa_2Cu_3O_{7-\delta}$

iii. Ba_2YSbO_6 - $YBa_2Cu_3O_{7-\delta}$

iv. Ba_2YZrO_6 - $YBa_2Cu_3O_{7-\delta}$

The above four composite systems can be represented for convenience as Ba_2YAO_6 - $YBa_2Cu_3O_{7-\delta}$ (BYAO-YBCO) where A = Nb, Sb, Sn or Zr. The above systems have been selected for investigation primarily because almost all the known ceramic insulators react with YBCO and destroy superconductivity. But the above systems form composite without any degradation in the superconducting properties of YBCO.

5.2 WHAT IS A PERCOLATION MODEL

The percolation model was originally proposed (7) to describe how fluid spreads through porous media, branching polymers form a gel, electron migration in a solid, disease infects a community and other similar phenomena. Because of its generality and relative simplicity it has found many applications ranging

from the physics of quarks to the extraction of oil from sand stones.

Consider a regular lattice where lattice sites can have two states; either black or white (7). A cluster is defined as a group of black sites connected by nearest neighbour distances. There is a critical point $V = V_c$ below which only finite clusters exist, but for $V \geq V_c$ a fraction of the black sites belong to an infinite cluster and a percolation is possible. Below the percolation threshold, $V < V_c$, there is no infinite cluster of black sites. From V_c the fraction of sites belonging to the infinite cluster grows drastically, it has a non-analytic point at V_c. This non-analycity is characteristic for the percolation threshold, and is usually described by a power law asymptotically close to V_c.

Consider the case of a metal-insulator composite system. The resistivity of insulator is very high. If we add metal to insulator, the resistivity of the composite remains more or less same as that of insulator upto a critical volume fraction of metal in the composite. If the volume fraction of metal increases beyond the critical volume, the resistivity reduces drastically to that of pure metal. The critical volume fraction of metal required to have a continuous net work or to become an infinite cluster is called the percolation threshold value. The transport properties can be described by a set of exponential equations below and above the threshold volume. The relations are (2,7,8)

$$\rho = \rho_0 (V_m - V_c)^{-t} \qquad \text{for } V_m > V_c \qquad (1)$$

$$\rho' = \rho_0' (V_c - V_m)^{u} \qquad \text{for } V_m < V_c \qquad (2)$$

where ρ and ρ' are the resistivities of the composites, ρ_0 , ρ_0' are constants, V_m volume fraction of metal in the system and V_c the threshold volume. 't' and 'u' are critical exponents describing the transport properties. The values of V_c, t and u obtained for different systems of composites vary due to many factors. 't' and 'u' are a measure of order of interaction between normal metal and insulator. The value obtained for percolation threshold is around 17 vol % of metal in the system for a perfect metal-insulator composite without any interaction or reaction between the two. The expected values of critical exponents are $t \simeq 1.7$ and $u \simeq 0.7$ approximately. The values obtained by experimental methods vary slightly around this value. An appreciable variation of critical exponents from the above values indicates that the system is not forming a perfect composite.

5.3 STUDIES ON Ba_2YNbO_6 - $YBa_2Cu_3O_{7-\delta}$ (BYNO-YBCO) COMPOSITES

5.3.1 Preparation of BYNO-YBCO composites

Pure YBCO has been prepared from its constituent oxides and carbonates by solid state reaction method as described in chapter 3. The ceramic insulator Ba_2YNbO_6 (BYNO) is prepared by the method described in chapter 4. The composite BYNO-YBCO have been prepared by mixing the two compounds in different

volume percentages taking into account of their theoretical densities. Table 5.1 shows the different volume ratios of composites prepared from zero vol % to 100 vol % of BYNO. The compounds were thoroughly mixed, then pressed in the form of pellets 12 mm diameter and 2 to 2.5 mm thickness by uniaxial pressing.

Table 5.1: Different volume percentages of BYNO-YBCO composites and their corresponding sintering temperature and densities

Vol % of YBCO	Vol % of BYNO	Sintering temperature (^{o}C)	Density (gm/cm^3)
100	0	950	5.80
90	10	950	5.83
80	20	950	5.89
70	30	965	5.91
60	40	980	5.80
50	50	990	5.80
40	60	1010	5.68
30	70	1030	5.50
20	80	1050	5.44
15	85	1080	5.46
10	90	1100	5.40
5	95	1200	5.52
0	100	1350	5.58

It was then sintered at temperatures from 950^{o} C to 1350^{o} C for 12 hours. The sintered samples were then cooled slowly to room temperature in oxygen atmosphere. The sintering temperature for different composite ratios are also given in table 5.1. The composite prepared as above has been used to study the superconducting properties and percolation properties at normal state and superconducting state by resistivity, XRD and scanning electron microscopic techniques. The densities of the composites were measured by Archimedes method and are given in Table 5.1. It should be noted that the sintering temperature of BYNO-YBCO composites increases as the vol % of BYNO in the system increases. The sintering temperatures are optimised in order to get a continuous grain to grain net work of YBCO without loosing the superconducting properties. The densities of the composites remain more or less same for low vol % of BYNO, but for higher vol % of BYNO, the density decreases as shown in Table 5.1.

5.3.2 Temperature-resistance studies on BYNO-YBCO composites

The resistivities of the composites BYNO-YBCO were measured as a function of temperature by four probe method as described in chapter 2. Fig. 5.1 shows the temperature-resistance curve for different volume percentages of BYNO in the composite. For clarity and readability the normalised resistivity ρ/ρ_r is plotted against temperature where ρ is the resistivity and ρ_r the resistivity at room temperature. All the composite samples showed a metallic behaviour in their resistivity curves and are

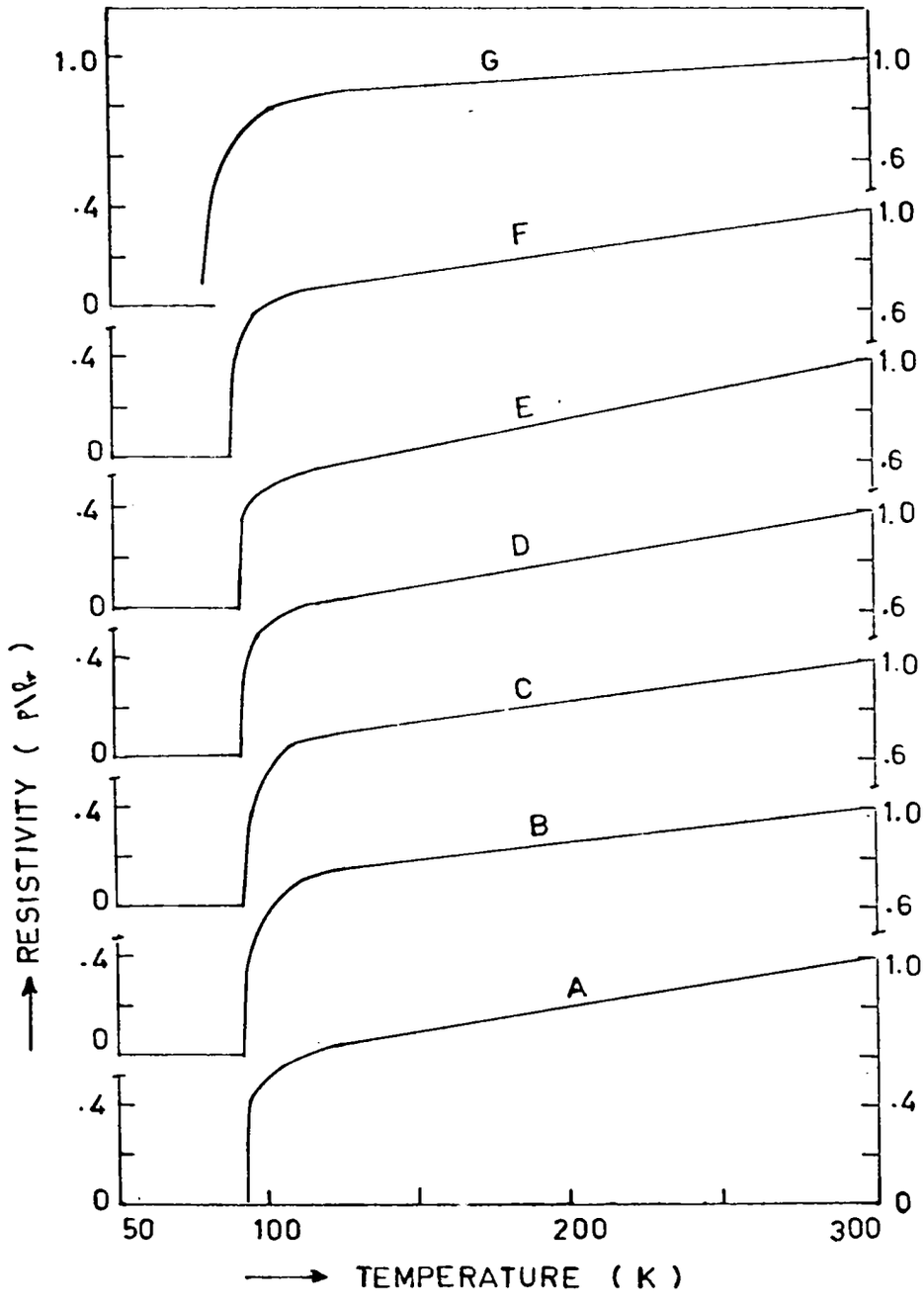

Fig. 5.1: Temperature-resistance curve of BYNO-YBCO composites with different vol % of BYNO (A) 0, (B) 10, (C) 20, (D) 30, (E) 50, (F) 70, (G) 80

For simplicity and clarity, the normalised resistivity ρ/ρ_r is plotted against temperature where ρ_r the room temperature resistivity

superconducting above liquid nitrogen temperature upto 80 vol % of BYNO in the system. For a composite with 50 vol % of BYNO, the superconducting transition temperature is same as that of pure YBCO. But for the composite with 80 vol % of BYNO, its resistance does not become zero even at liquid nitrogen temperature. The resistivity does not become zero due to the absence of enough superconducting net-works through the bulk of the samples. For still higher vol % of BYNO, its normal state resistivity becomes too high and by four probe method it was found very difficult to measure the resistivity. The resistivity in the higher resistance side of the composites were measured by two probe method using a Keithley solid state electrometer. The resistivity was found to be of the order of 10^{8} Ω-cm. The resistance-temperature measurements show that the superconducting percolation threshold value is around 20 vol % of YBCO in the composite. That is if the vol % of YBCO is more than 20 vol %, the system shows superconductivity. At the percolation threshold, i.e. for 20 vol % of YBCO the superconducting grain to grain net work becomes infinite and shows superconductivity.

The variation of normal state resistivity at room temperature for different vol % of BYNO is plotted in Fig. 5.2a. The normal state resistivity showed a drastic variation in its value around 80 vol % of BYNO in the system. For low vol % of BYNO, the normal state resistivity is almost same as that of pure YBCO as evident from the figure. For higher vol % of BYNO above 80%, the resistivity of the composite is nearly equal to that of pure insulator BYNO .

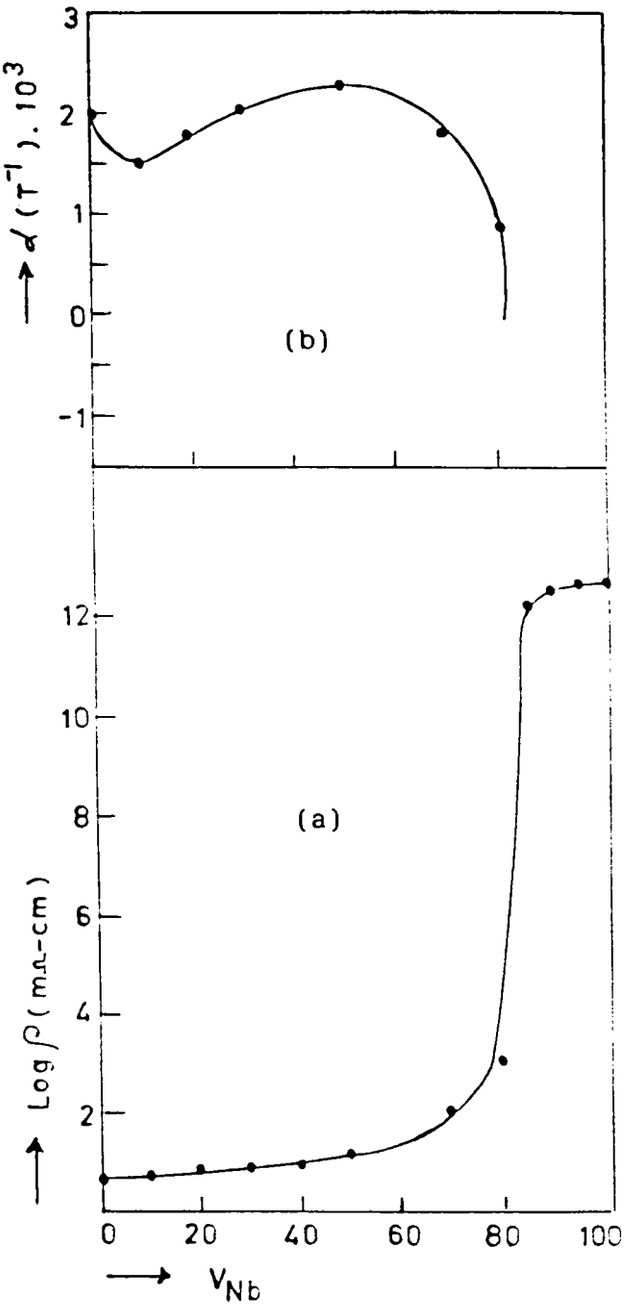

Fig. 5.2: Variation of (a) normal state resistivity ρ, and (b) temperature coefficient of resistivity $\alpha = \frac{1}{\rho}\frac{d\rho}{dT}$, at room temperature as a function of vol % (V_{Nb}) of BYNO in the composite

The temperature coefficient of resistivity at room temperature ($\alpha = \frac{1}{\rho}\frac{d\rho}{dT}$) is also given in Fig. 5.2b, as a function of vol % of BYNO. The temperature coefficient of resistivity also showed a sharp variation around 80 vol % of BYNO. Thus from Fig. 5.2, we can infer that the normal state percolation threshold value of the ceramic insulator-superconductor composite BYNO-YBCO is around 80 vol % of BYNO or the percolation threshold is around 20 vol % of YBCO. That is when the volume percent of YBCO in the composite is around 20 vol %, the composite system shows its resistivity nearly equal to that of pure YBCO. The exact value of percolation threshold is found from the percolation model equations by considering the superconductor YBCO as a metal and the ceramic BYNO as an insulator.

The transport properties of an insulator-superconductor composite in the normal state can be represented by the percolation equations.

$$\rho = \rho_0 \, (V_s - V_c)^{-t} \qquad \text{for} \quad V_s > V_c \tag{3}$$

$$\rho' = \rho_0' \, (V_c - V_s)^{u} \qquad \text{for} \quad V_s < V_c \tag{4}$$

where ρ and ρ' are respectively the resistivities of the composites for V_s vol % of superconductor above and below the percolation threshold volume V_c and 't' and 'u' are the critical exponents describing the transport properties. The values of t, u, ρ_0, ρ_0' are calculated from the log-log plot of ρ versus $(V_s - V_c)$ and ρ' versus $(V_c - V_s)$ which gives a straight line. The exact value of V_c is taken such that the log-log plot of ρ versus $(V_s - V_c)$

and ρ' versus $(V_c - V_s)$ both give exactly a straight line. The log-log plot of equations (3) and (4) is shown in Fig. 5.3 and the values of V_c, t, u, ρ_o, ρ_o' obtained as

V_c = 17 vol %

t = 1.675

u = 0.375

ρ_o = 6.309×10^{3} mΩ-cm

ρ_o' = 2.51×10^{12} mΩ-cm

The values obtained for the ceramic insulator-superconductor composite (BYNO-YBCO) matches very well with that calculated for an ideal insulator-conductor composite system. The value of critical exponent 't' describing the transport properties in the metallic side of the system agrees with the theoretically expected value. But the value of the critical exponent 'u' which explains the transport properties in the insulating side of the composite deviates from the theoretically expected value. Since the value of critical exponent 't' matches with the predicted value, it implies that the system forms a composite in the lower volume side of BYNO (upto 83 vol % of BYNO) without much interaction or reaction between the two compounds. The deviation in the critical exponent 'u' can be explained in the following way.

The usual sintering temperature of YBCO is around 950^{o}C followed by slow cooling in order to absorb oxygen from the atmosphere and the associated structural transformation and

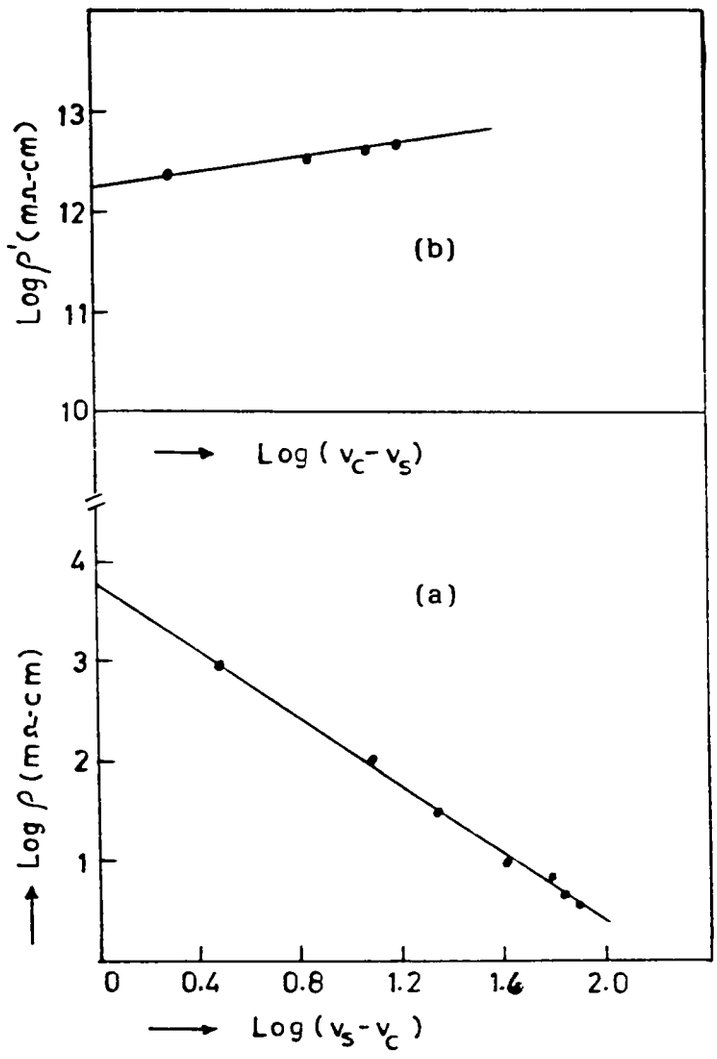

Fig. 5.3: Log-lot plot of (a) ρ versus (V_s - V_c), and (b) ρ' versus (V_c - V_s) of BYNO-YBCO composites where V_c the threshold volume and ρ and ρ' are the resistivities of the composites for vol % of superconductor (v_s) above and below the threshold volume V_c.

superconductivity. If we process YBCO by heating above 950^{o}C, it starts melting and decomposes into Y_2BaCuO_5, $BaCuO_2$ and CuO. In the BYNO-YBCO composite, as the vol % of BYNO increases the sintering temperature of the composite also increases as given in Table 5.1. For example a composite with 50-50 volume ratio sinters at temperatures around 990^{o}C and a composite with 70 vol % of BYNO sinters only above 1000^{o}C. At these elevated temperatures of sintering there is every possibility for YBCO in the composite to melt and decompose and react with BYNO in the system. But upto a moderate temperature of 1000^{o}C and slightly above, the reaction and decomposition of YBCO is not appreciable in the composite BYNO-YBCO. As the vol % of BYNO increases further, the sintering temperature also increases and accelerated decomposition and reactions are expected and the system no more forms a real composite. Thus the deviation in the critical exponent 'u' can be attributed to the possible reactions and decompositions taking place in the system due to the elevated temperatures required for processing of the composite at higher volume ratio of BYNO.

5.3.3 X-ray diffraction studies on BYNO-YBCO composites

X-ray powder diffraction studies were carried out on composite samples prepared as described in section 5.3.1 to monitor the reaction between the compounds BYNO-YBCO. Fig. 5.4 shows the powder diffraction pattern for different volume ratios of composites. For low vol % of BYNO, there is no appreciable reaction between the two compounds. The x-ray pattern shows (Fig. 5.4 b&c) only

Fig. 5.4: XRD pattern of BYNO-YBCO composites with different vol % of BYNO in the system (A) 0, (B) 30, (C) 50, (D) 70, (E) 100

peaks corresponding to the phases BYNO and YBCO. No additional peaks can be observed in the diffraction patttern upto 50 vol % of BYNO even though the processing temperatures are about 990^{o}C. It means that the thermal stability of YBCO has increased upto higher temperature in the composite system BYNO-YBCO. The temperature-resistance studies on 50-50 ratio of composite showed a superconducting transition at 92 K same as that of pure YBCO. Thus from both x-ray diffraction studies and temperature-resistance studies, it can be seen that there is no reaction or deterioration of superconducting properties for a 50:50 volume ratio of BYNO-YBCO processed at 990^{o}C.

For higher vol % of BYNO, we can observe some additional peaks due to impurity phases apart from the phases YBCO and BYNO, which indicates the possible reaction between the two compounds during processing. But it should be noted that the amount of impurity phases formed are very small and the extent of reaction is very less even though the processing temperatures are above 1000^{o} C. (Fig. 5.4 d). Hence at this processing temperatures, the superconducting properties are not drastically affected. In the R-T curve we can observe a slight reduction in T_c value (for 70 vol % T_c = 85 K and for 80 vol % T_c $<$ 77 K) which is in accordance with the slight amount of reaction taking place in the system. Thus both x-ray powder diffraction studies and resistivity studies give complimentary results.

5.3.4 Microstructure of BYNO-YBCO composites

Scanning electron microscopic studies on polished surfaces of BYNO-YBCO composites were carried out to see its microstructural features. Fig. 5.5 shows the scanning electron micrograph of the composites with different vol % of BYNO. The figure clearly shows the presence of two distinct phases (as evidenced by the difference in contrast) corresponding to BYNO and YBCO with sharp boundary between the two. As the volume % of BYNO increases we can observe an increase in the corrresponding phase in the micrograph. The figure clearly shows that there is no diffusion or reaction at the interface between the two phase, rather an extremely sharp phase boundary is observed (Fig. 5.5 a&b). It has a sharp boundary between the two phases which again confirms that there is no reaction between the two compounds, but forms a real composite. Also it is evident from the figure that there is continuous grain to grain net work of YBCO in the composite which gives rise to superconducting transition as observed by resistivity measurements. Thus x-ray, SEM and resistivity measurements complementarily prove that practically there is no reaction between YBCO and BYNO if the processing temperatures are controlled properly.

5.4 STUDIES ON Ba_2YSnO_6-$YBa_2Cu_3O_{7-\delta}$ (BYSnO-YBCO) COMPOSITES

5.4.1 Preparation of BYSnO-YBCO composites

Pure YBCO was prepared as described earlier. Pure ceramic insulator BYSnO was prepared as described in chapter 4 by solid

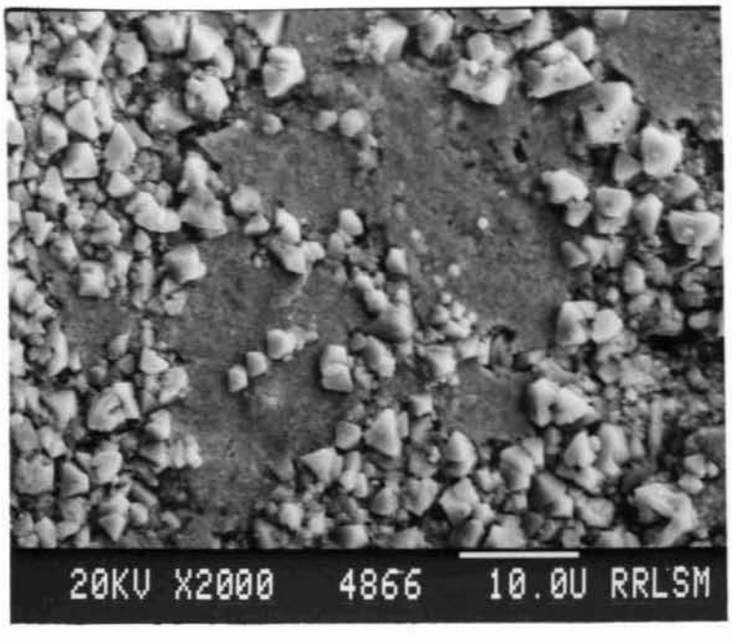

(a)

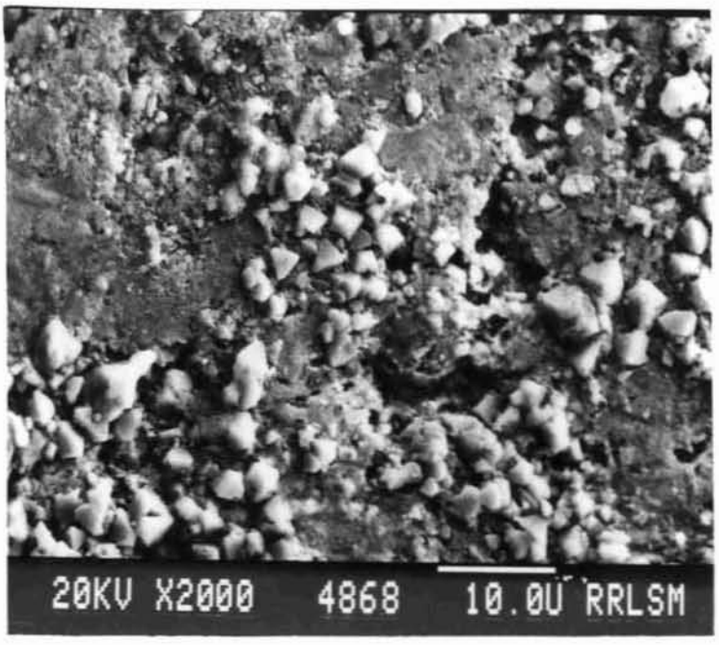

(b)

Fig. 5.5: Scanning electron micrograph for different volume ratio of BYNO : YBCO composites
(a) 30 : 70 ; (b) 50 : 50

state reaction method. Ceramic insulator-supercnductor composites were prepared for different volume percentages of BYSnO by mixing BYSnO and YBCO in the required volume ratio by taking into account of their theoretical densities. The thoroughly mixed samples were pressed in the form of pellets of 12 mm diameter and 2 to 2.5 mm thickness by uniaxial pressing and sintered at temperatures ranging from 950 ^{o}C to 1350 ^{o}C depending upon the composition. Table 5.2 gives the composition of composites along with their sintering temperature.

Table 5.2: Composition of BYSnO-YBCO compposites and their sintering temperature and densities

Vol % of YBCO	Vol % of BYSnO	Sintering temperature (^{o}C)	Density (gm/cm^{3})
100	0	950	5.80
90	10	950	5.85
80	20	950	5.90
70	30	965	5.92
60	40	980	5.88
50	50	990	5.85
40	60	1010	5.75
30	70	1030	5.68
20	80	1050	5.60
15	85	1070	5.58
10	90	1100	5.65
5	95	1150	5.68
0	100	1350	5.75

The samples sintered for 12 hours were furnace cooled to room temperature in oxygen atmosphere. The composite samples prepared as above were used for measuring the superconducting transition temperature, XRD studies, microstructural characterisation and for percolation model studies. The densities of the composites were measured by Archimedes method and the values are given in Table 5.2.

5.4.2 Resistivity studies on BYSnO-YBCO composites

The resistivities of the composites were measured by four probe method from room temperature to liquid nitrogen temperature. All the samples prepared upto 80 vol % of BYSnO showed a metallic behaviour with superconducting transition above liquid nitrogen temperature. Even though the composite with 80 vol % of BYSnO showed superconducting transition above liquid nitrogen temperature, its resistance did not become exactly zero even down to a temperature of 77 K. Also it showed semiconductor character in its R-T curve till its transition temperature with a sharp transition to superconducting state above liquid nitrogen temperature. All the other samples showed a metallic behaviour in their R-T curve as shown in Fig. 5.6. In the figure, the normalised resistivity ρ/ρ_r is plotted against temperature for different volume ratios of composites, where ρ_Y is the room temperature resistivity. For samples with higher vol % of insulator (BYSnO vol % $>$ 80) their resistance becomes too high, and a two probe method was used to measure the resistivity. The BYSnO-YBCO composite showed a superconducting percolation threshold around 20 vol % of YBCO. It means that

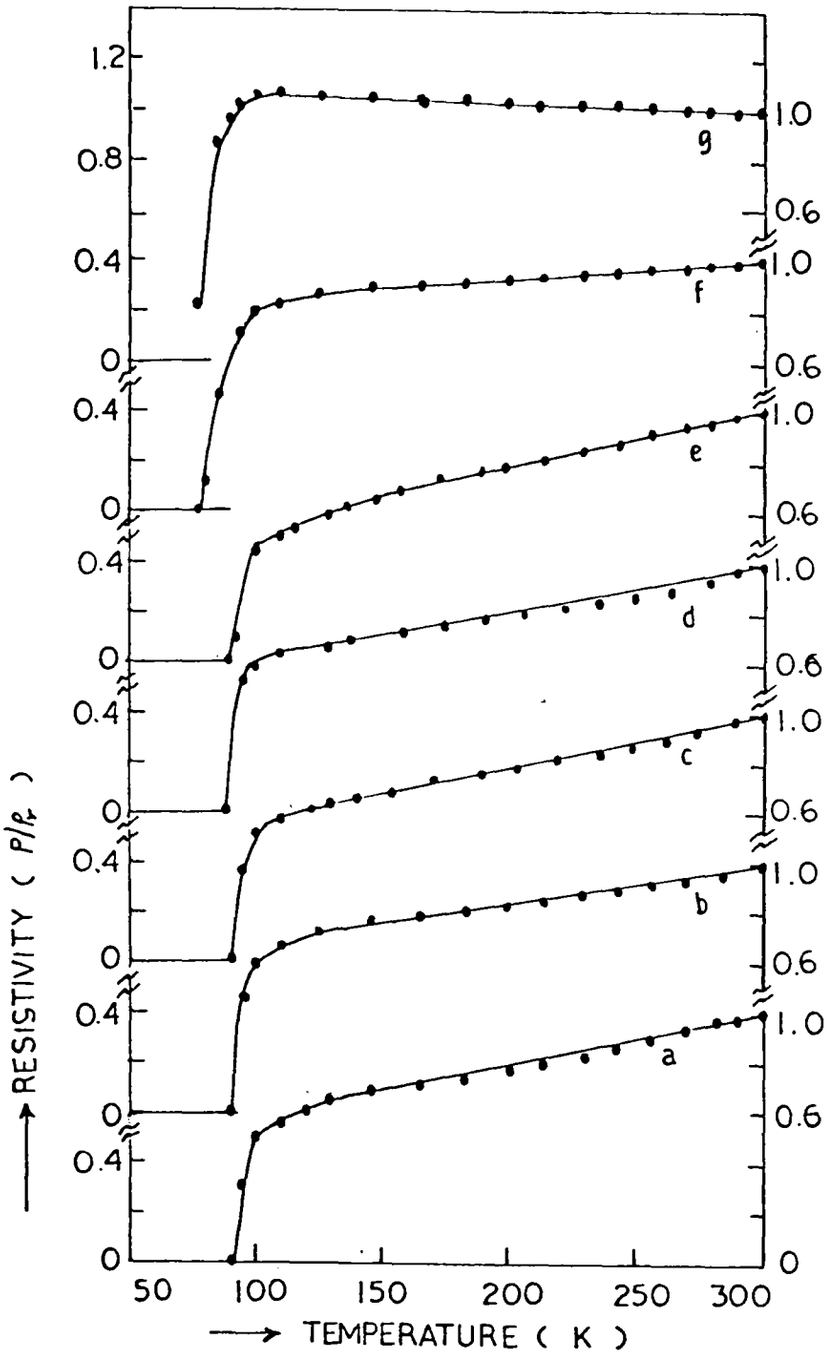

Fig. 5.6: Temperature-resistance curve of BYSnO-YBCO composites with different vol % of BYSnO (a) 0, (b) 10, (c) 20, (d) 30, (e) 50, (f) 70, (g) 80.
All the samples showed a metallic behaviour with superconducting transition around 92 K. The composite with 80 vol % of BYSnO showed semiconducting behaviour with sharp transition into superconducting state above 77 K, but its resistance does not become zero even at 77 K.

when the volume percent of YBCO is 20 or above, there are interconnected net works of superconducting grains for the supercurrent to pass through the material. But for lower vol % of YBCO ($< 20\%$) the continuous net work of superconducting grains breaks away, and its resistance becomes nearly equal to that for pure insulator BYSnO.

The variation of normal state resistivity for different vol % of BYSnO in the composite is plotted in Fig. 5.7. The variation of temperature coefficient of resistivity $\left(\alpha = \frac{1}{\rho}\frac{d\rho}{dT}\right)$ is also given in figure 5.7. Both the normal state resistivity and the temperature coefficient of resistivity showed a sharp deviation in their values at about 80 vol % of BYSnO in the composite. Thus the normal state percolation threshold value for the insulator-superconductor composite BYSnO-YBCO lies around 20 vol % of YBCO. The actual value of percolation threshold volume can be calculated from the equations governing the transport properties of the composites (equations (3) and (4)) by considering BYSnO as insulator and YBCO at room temperature as metal. The percolation threshold value V_c is taken such that log-log plot gives a straight line. The log-log plot of equations (3) and (4) for the BYSnO-YBCO composites are shown in Fig. 5.8. The critical values obtained from Fig. 5.8 are

$V_c = 20$

$t = 1.80$

$u = 1.23$

$\rho_0 = 9.77 \times 10^3$ m Ω -cm

$\rho_0' = 5.62 \times 10^8$ m Ω -cm

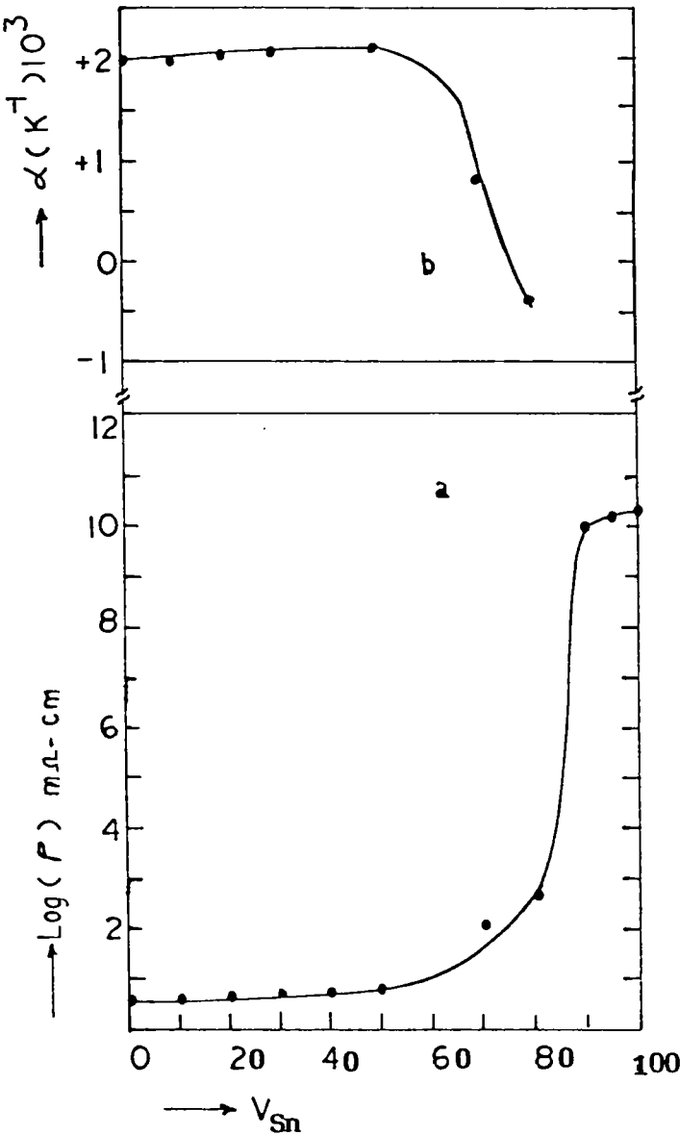

Fig. 5.7: Variation of (a) normal state resistivity ρ, and (b) temperature coefficient of resistivity $\alpha = \frac{1}{\rho}\frac{d\rho}{dT}$ at room temperature as a function of vol % (V_{Sn}) of BYSnO

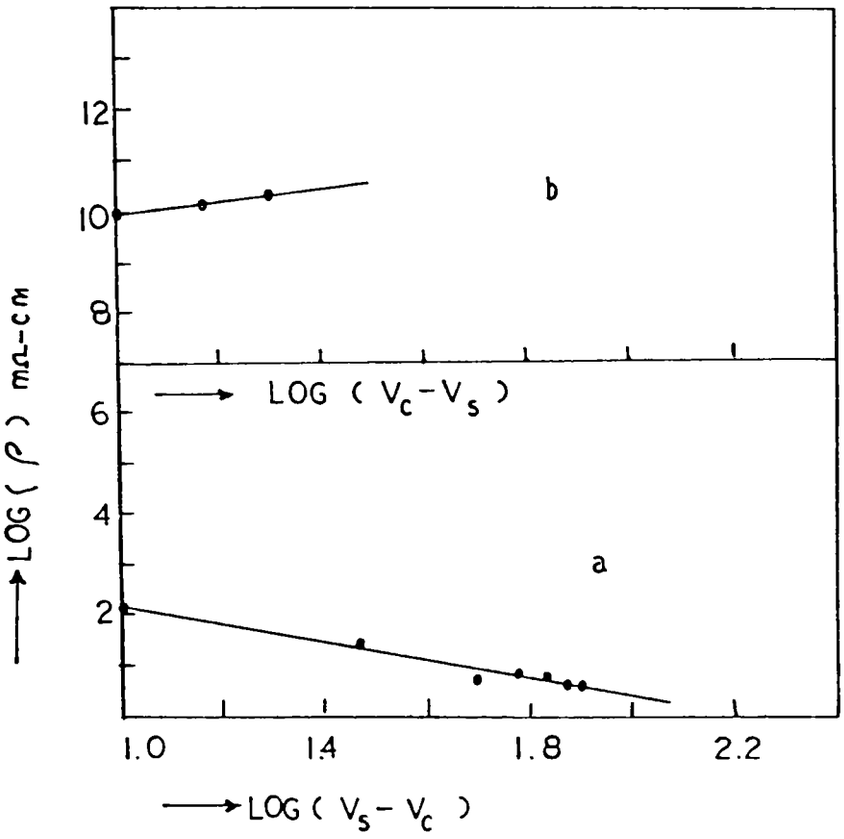

Fig. 5.8: Log-log plot of (a) ρ versus ($V_s - V_c$) and (b) ρ' versus ($V_c - V_s$) of BYSnO-YBCO composites where V_c the threshold volume and ρ and ρ' are the resistivities of the composites for V_s vol % of superconductor above and below the percolation threshold volume V_c.

The percolation threshold value V_c is nearly equal to that for ideal insulator-conductor composite system. Also the values of critical exponents 't' and 'u' agree with those values expected theoretically. Thus the percolation model studies for the normal state transport properties show that BYSnO-YBCO forms a real composite without much reaction or interaction between the two. Also it should be remembered that the processing temperature for composites with higher vol % BYSnO is higher than that for pure YBCO. At this elevated temperatures, there are chances for decomposition of YBCO and also for reaction with BYSnO. Still the percolation studies show that the system forms a composite without much reaction or decomposition between the two compounds or in other words, it is not at all affecting the transport properties at normal temperatures. Both the normal state percolation threshold value and superconducting percolation threshold value found to be in the same range for the above system i.e. about 20 vol % of YBCO.

5.4.3 XRD Studies on BYSnO-YBCO composites

X-ray powder diffraction studies were carried out to identify different phases existing in the composite BYSnO-YBCO system and to see the extent of reaction between the two compounds. Fig. 5.9 shows the powder diffraction pattern for different vol % of BYSnO in the composite. The XRD patterns for 30 vol % and 50 vol % of BYSnO do not show any additional peaks other than those of pure YBCO and BYSnO. It indicates that BYSnO-YBCO system forms perfect composite upto 50 vol % of BYSnO without any reaction or interaction

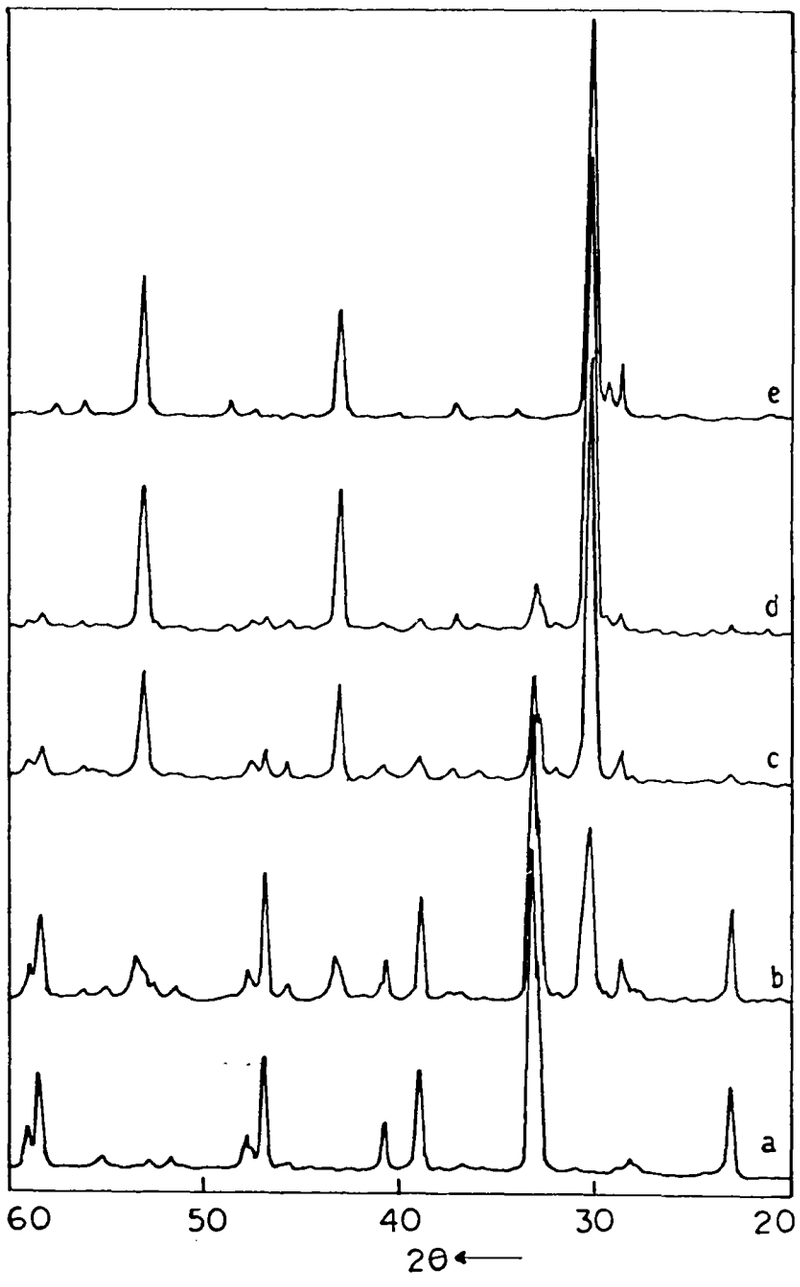

Fig. 5.9: XRD pattern of BYSnO-YBCO composites for different vol % of BYSnO

(a) 0, (b) 30, (c) 50, (d) 70, (e) 100

or decomposition. The processing temperature for 50 vol % of BYSnO is around 990^{o}C, still it does not show any reaction or degradation in its superconducting properties. The powder diffraction pattern for 70 vol % of BYSnO shows orthorhombic YBCO phase along with the major phase BYSnO. Also a few impurity peaks can be observed in Fig. 5.9 d which may be due to some decomposition product of YBCO or due to some minor reaction between YBCO and BYSnO. The processing temperatures are above 1000^{o}C and at this elevated temperature naturally one expects decomposition of YBCO along with some reaction. But in the composite system, the rate of decomposition is reduced due to the presence of BYSnO, retaining the orthorhombic structure of YBCO and its superconductivity. The resistivity measurements clearly shows the superconducting transition upto 80 vol % of BYSnO. Thus in the composite, YBCO does not loses its structure and superconducting properties even by processing above 1000^{o}C as evidenced from x-ray diffraction studies and by resistivity measurements. But in the case of almost all the known ceramic insulators, the superconducting properties of YBCO is lost when it is processed along with the insulator above 950^{o}C.

5.4.4 Microstructure of BYSnO-YBCO composites

SEM pictures of BYSnO-YBCO composites are shown in Fig. 5.10. From the micrograph it is evident that there are two distinct phases corresponding to YBCO and BYSnO. There is no indication of any reaction between YBCO and BYSnO. Also the grain size becomes smaller and smaller as the amount of BYSnO in the

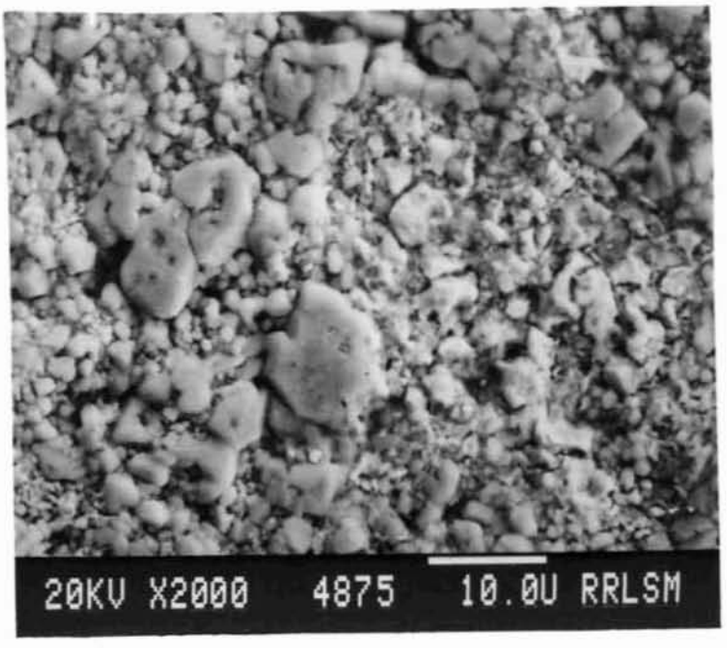

(a)

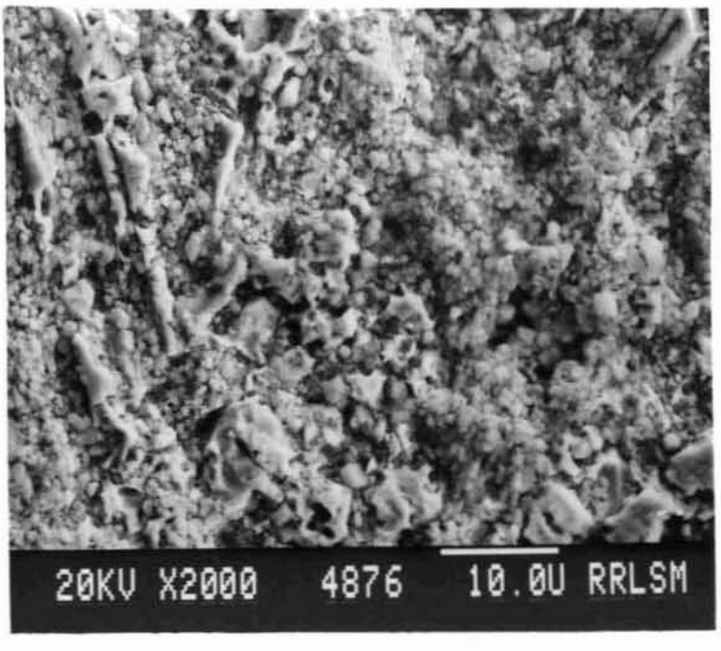

(b)

Fig. 5.10: Scanning electron micrographs for diffferent volume ratios of BYSnO : YBCO composites
(a) 30 : 70 ; (b) 50 : 50

system increases (see Fig. 5.10a and b corresponding to 30 and 50 vol % of BYSnO). (In the present system, it forms a uniform and fine mixture of two phases. There are no sharp grain boundaries between BYNO and YBCO grains. Thus the SEM pictures of BYSnO and BYNO composites differ in their microstructural properties, even though the x-ray and resistivity measurements showed identical properties).

5.5 STUDIES ON Ba_2YSbO_6-$YBa_2Cu_3O_{7-\delta}$ (BYSbO-YBCO) COMPOSITES

5.5.1 Preparation of BYSbO-YBCO composites

Pure YBCO has been prepared as described in chapter 3. The ceramic insulator BYSbO was prepared from its constituent oxides by solid state reaction method as described in the previous chapter. YBCO and BYSbO were mixed into different volume ratios taking into account of their theoretical densities. It was then thoroughly mixed and pressed in the form of pellets. The pellets were sintered in oxygen atmosphere for 12 hours in the temperature range $950^{o}C$ to $1350^{o}C$ depending on the vol % of BYSbO and cooled slowly to room temperature. The details of different volume ratios of composites, their corresponding sintering temperatures and densities are given in Table 5.3. It was found that the densities of composites are more or less the same as that of YBCO.

Table 5.3: Compositions of BYSbO-YBCO composites and corresponding sintering temperature and densities

Vol % of YBCO	Vol % of BYSbO	Sintering temperature (^{o}C)	Density (gm/cm^3)
100	0	950	5.80
90	10	950	5.82
85	15	960	5.81
80	20	960	5.85
70	30	970	5.84
60	40	980	5.80
50	50	1000	5.63
40	60	1020	5.55
30	70	1040	5.56
20	80	1070	5.58
10	90	1150	5.58
0	1000	1350	5.68

5.5.2 Resistivity studies on BYSbO-YBCO composites

The normal state transport properties and superconducting properties of ceramic insulator-superconductor composite BYSbO-YBCO were studied by measuring the resistivities of the composites as a function of temperature. Fig. 5.11 shows the temperature-resistance curve for different volume ratios of BYSbO in the composite. The R-T curve shows a metallic behaviour and are superconducting

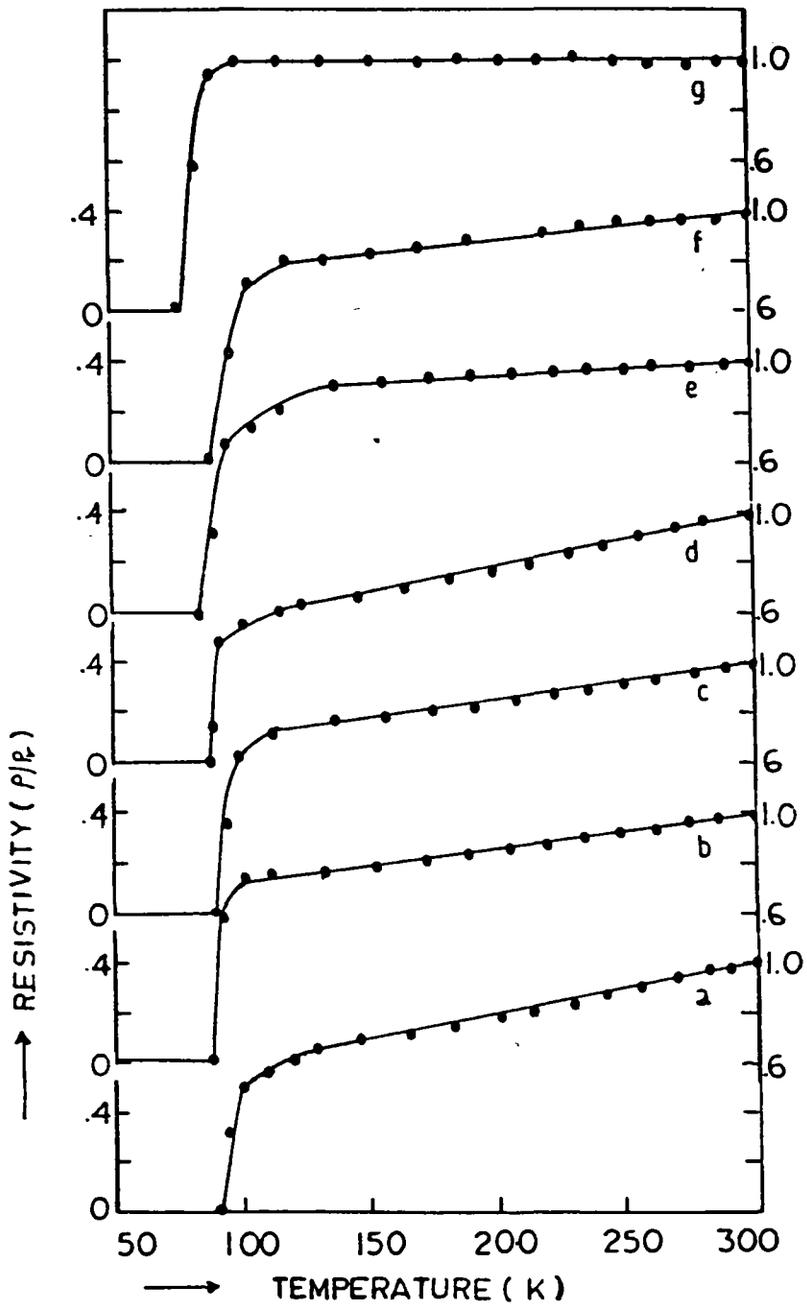

Fig. 5.11: Temperature-resistance curve of BYSbO-YBCO composites for different vol % of BYSbO

(a) 0, (b) 10, (c) 20, (d) 30, (e) 40, (f) 40, (g) 60.

All the samples showed metallic behaviour with superconducting transition above liquid nitrogen temperature upto 60 vol % of BYSbO in the system

at 92 K for low vol % of BYSbO. As the vol % of BYSbO increases the transition temperature decreases slightly. The composite with 60 vol % of BYSbO is superconducting above liquid nitrogen temperature, but for higher vol %, the resistivity increases to a higher value and there is no superconducting transition till 77 K. In the case of BYNO and BYSnO, there was superconducting transition upto 80 vol % of insulating phase in the composite system. But in BYSbO-YBCO composite, the system no more shows superconductivity if the volume fraction of insulating phase is more than 60%, or it is not forming a composite with a continuous net work of YBCO. This may be due to the reaction between YBCO and BYSbO during processing or due to the decomposition of YBCO at elevated processing temperatures. In the case of BYNO-YBCO and BYSnO-YBCO composites, even elevated temperatures of processing do not result in any reaction or decomposition or do not deteriorate the superconducting properties upto 80 vol % of insulator. The superconducting percolation threshold value of BYSbO-YBCO composite lies around 60% of BYSbO or 40% of YBCO. That is if the volume percent of YBCO is less than 40% the system BYSbO-YBCO do not show any superconducting transition by resistivity measurements.

In Fig. 5.12, the variation of normal state resistivity at room temperature is plotted as a function of volume fraction of insulating phase BYSbO. The normal state resistivity showed a sharp variation in its value for about 65 vol % of BYSbO. The variation in the resistivity is not as sharp as that in the case of BYNO and BYSnO composites. The temperature coefficient of

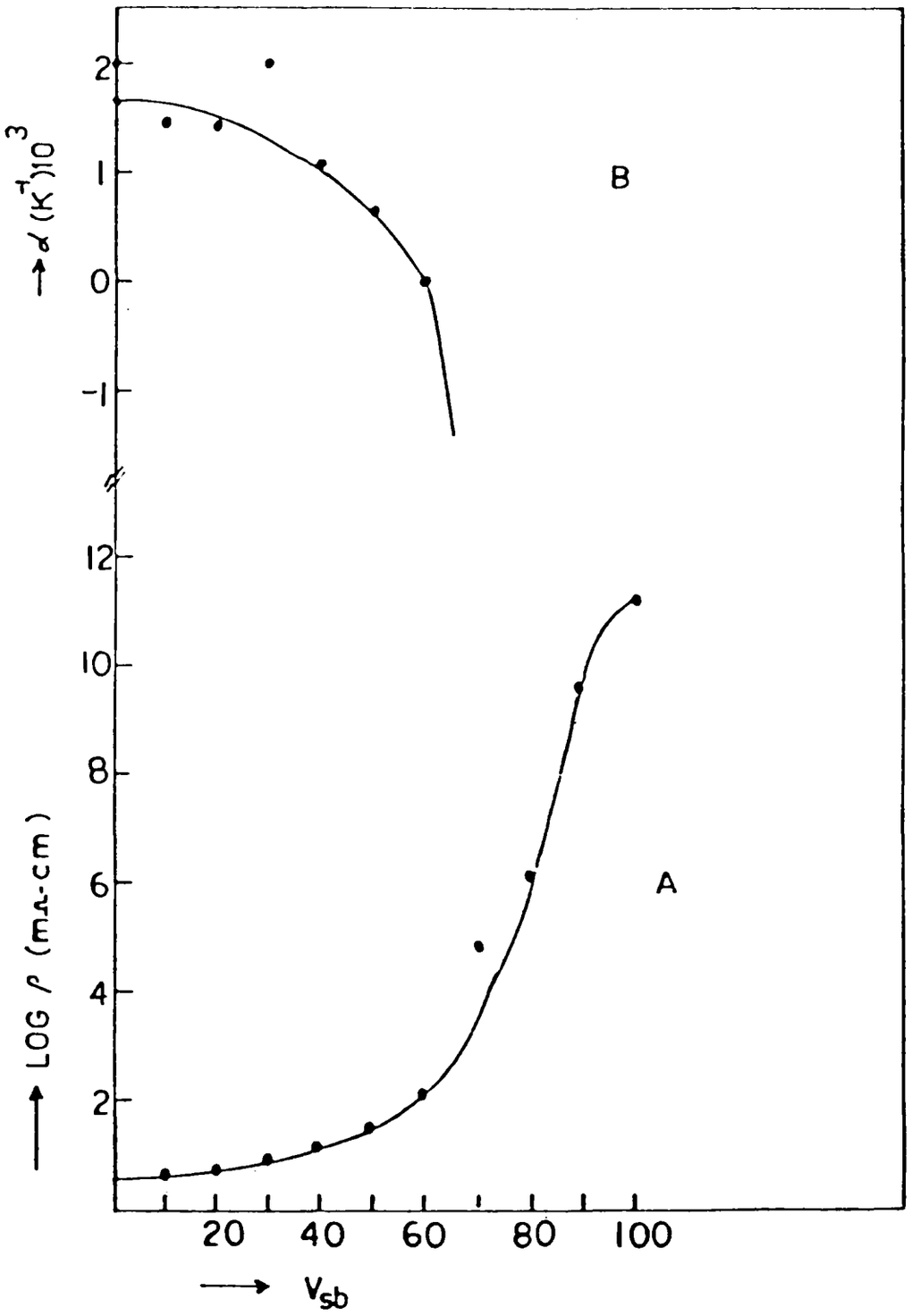

Fig. 5.12: Variation of (a) normal state resistivity ρ , and (b) temperature-coefficient of resistivity $\alpha = \frac{1}{\rho}\frac{d\rho}{dT}$ at room temperature as a function of vol % (V_{Sb}) of BYSbO in the composite

resistivity (2) is also plotted in figure. Both the normal state resistivity and temperature coefficient of resistivity showed a drastic variation around 65 vol % of BYSbO (or 35 vol % of YBCO).

The normal state transport properties of the composites can be explained by the equations (3) and (4) given in section 5.3.2 by considering YBCO as a metal and BYSbO as an insulator. The log-log plot of equations (3) and (4) for BYSbO-YBCO composites are shown in Fig. 5.13 with the threshold volume V_c = 30%. (The log-log plot gives a straight line when the value of V_c is 30%). The values of critical exponents describing the transport properties of the composite systems are calculated from Fig. 5.13. The values obtained from the figure are

V_c = 30

t = 1.80

u = 10.56

ρ_o = 7.05 Ω-cm

ρ_o' = 5×10^{-6} Ω-cm

The percolation threshold volume V_c is much higher than that expected for an ideal insulator-normal metal composite system. It means that the system does not form a perfect insulator-superconductor composite for higher volume fractions of BYSbO. The probable reason is the reaction between the two compounds at elevated temperatures or the decomposition of YBCO at higher temperatures of 1000^{o} C and above. It is well known from the phase

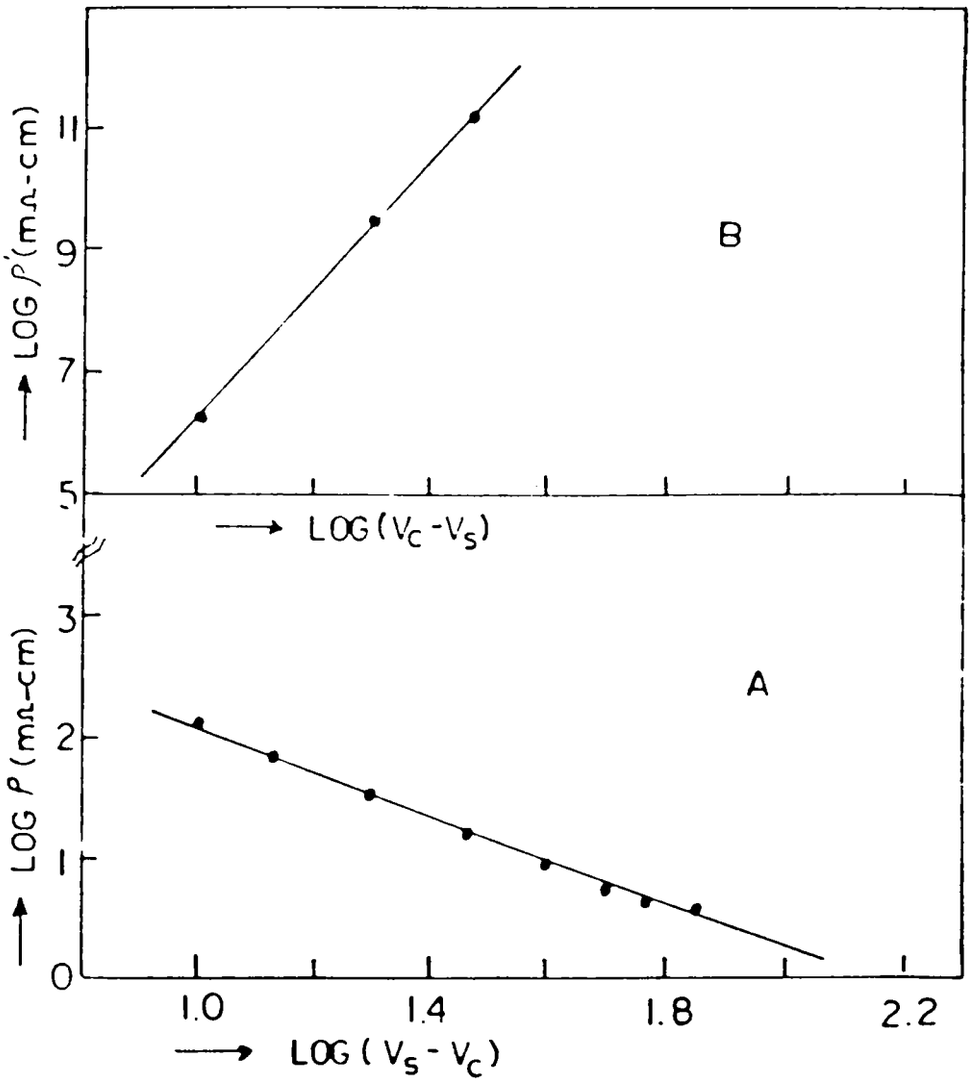

Fig. 5.13: Log-log plot of (a) ρ versus $(V_s - V_c)$ and (b) ρ' versus $(V_c - V_s)$ for the composites where ρ and ρ' are the resistivities of the composites for V_s vol % of superconductor above and below the percolation threshold volume V_c.

diagram studies (13) of YBCO that it decomposes into Y_2BaCuO_5 and BaCuO at 970^{o}C and bove, and the rate of decomposition increases as the temperature increases which explains the observed deviation in the percolation threshold value from theoretically expected value for a composite. The value of critical exponent 't' lies in the same range as that for ideal system whereas the value of 'u' deviates considerably from the expected value. Since the value of 't' obtained matches with the theoretical value, we can infer that the system forms a composite for low volume percentages of BYSbO where the processing temperatures are below 1000^{o}C.

The critical exponent 'u' explains the transport properties of the composite system for higher volume percentages of insulating phase. In the present system the large deviation in the value of 'u' indicates that YBCO does not for composite with BYSbO for volume fraction of BYSbO above 70%. If we prepare the composite at a temperature of about 950-1000^{o}C, there will not be any reaction . In order to have superconducting grain to grain bonding, it is necessary to process the composite with higher vol % of BYSbO at higher temperatures. If there is no grain to grain bonding, then there will not be any interconnected superconducting paths for the supercurrent to flow and the resistivity measurements will not give proper values. Magnetic measurements can give the superconducting transition temperature. In the present study we have sintered the composite at higher temperatures to have proper sintering so that there will be grain to grain bonding. The processing temperature for higher vol % of insulator BYSbO is above 1000^{o}C (see Table 5.3)

and naturally one expects decomposition or reaction which explains the observed deviations of the percolation threshold value as well as the deviation in the critical exponent 'u'.

5.5.3 XRD studies on BYSbO-YBCO composites

The different phases present in the ceramic composite BYSbO-YBCO systems are identified by x-ray powder diffraction method. Fig. 5.14 shows the powder diffraction pattern for different volume ratios of the composite prepared as above in section 5.5.1. Fig. 5.14a shows the pattern of pure YBCO, (b) that of 30 vol % of BYSbO (c) and (d) are that of 50% and 70% of BYSbO. In (b) and (c) we can clearly observe the presence of two phases viz., YBCO and BYSbO without much reaction between the two compounds. But for a 70 vol % of BYSbO in the composite, we can observe some additional peaks other than those of YBCO and BYSbO. The impurity phases may be due to the decomposition or reaction taking place at higher sintering temperatures. Also the temperature-resistance measurements show that the composites are no more superconducting. The intensity of YBCO peaks are extremely small for 70 vol % of BYSbO. Thus the x-ray diffraction studies and resistivity measurements give complementary results.

5.5.4 Scanning electron microscopy of BYSbO-YBCO composites

Scanning electron microscopic studies were carried out on polished surfaces of the ceramic insulator-superconductor composite BYSbO-YBCO to see the microstructural features such as distribution

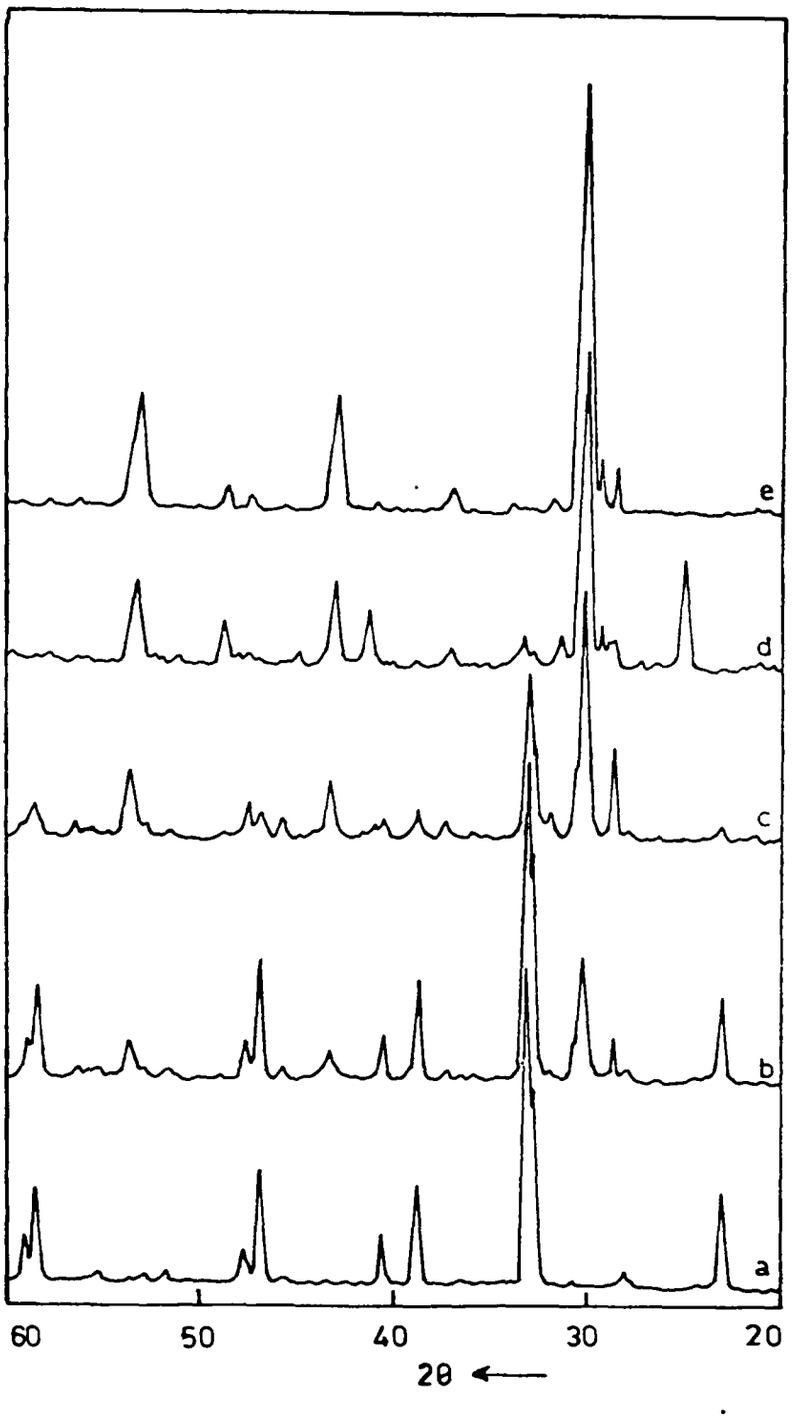

Fig. 5.14: XRD pattern of BYSbO-YBCO composites for different vol % of BYSbO

(a) 0, (b) 30, (c) 50, (d) 70, (e) 100

of different phases, their morphology, and the extent of additional phases formed due to reaction. Fig. 5.15 shows the SEM pictures of BYSbO-YBCO composites processed as above for different vol % of BYSbO. Fig. 5.15a shows a 40 vol % and b shows a 60 vol % of BYSbO in the composite. In (a) we can clearly observe only two phases corresponding to YBCO and BYSbO whereas in (b) we can see the presence of additional phase other than BYSbO and YBCO due to the reaction between YBCO and BYSbO. Since YBCO strongly reacts with BYSbO for higher ($>$ 60%) vol % of BYSbO, the amount of YBCO is very small as evident from Fig. b which is in agreement with resistivity and XRD studies. Thus SEM studies give a complementary proof for resistivity and XRD studies of BYSbO-YBCO composites.

5.6 STUDIES ON Ba_2YZrO_6-$YBa_2Cu_3O_{7-\delta}$ (BYZO-YBCO) COMPOSITES

5.6.1 Preparation of BYZO-YBCO composites

Pure YBCO and BYZO are prepared by solid state react method as explained in previous chapters. The ceramic insulato superconductor composites have been prepared by mixing different volume percentages of YBCO and BYZO taking into account of their theoretical densities. The powder was mixed thoroughly in an agate mortar and pressed in the form of pellets of 12 mm diameter and 2 to 2.5 mm thickness by uniaxial pressing. The pellets were then sintered for 12 hours at temperatures between 950^{o}C to 1350^{o}C depending on the vol % of BYZO. The details of various compositions and the corresponding sintering temperatures are provided in Table 5.4.

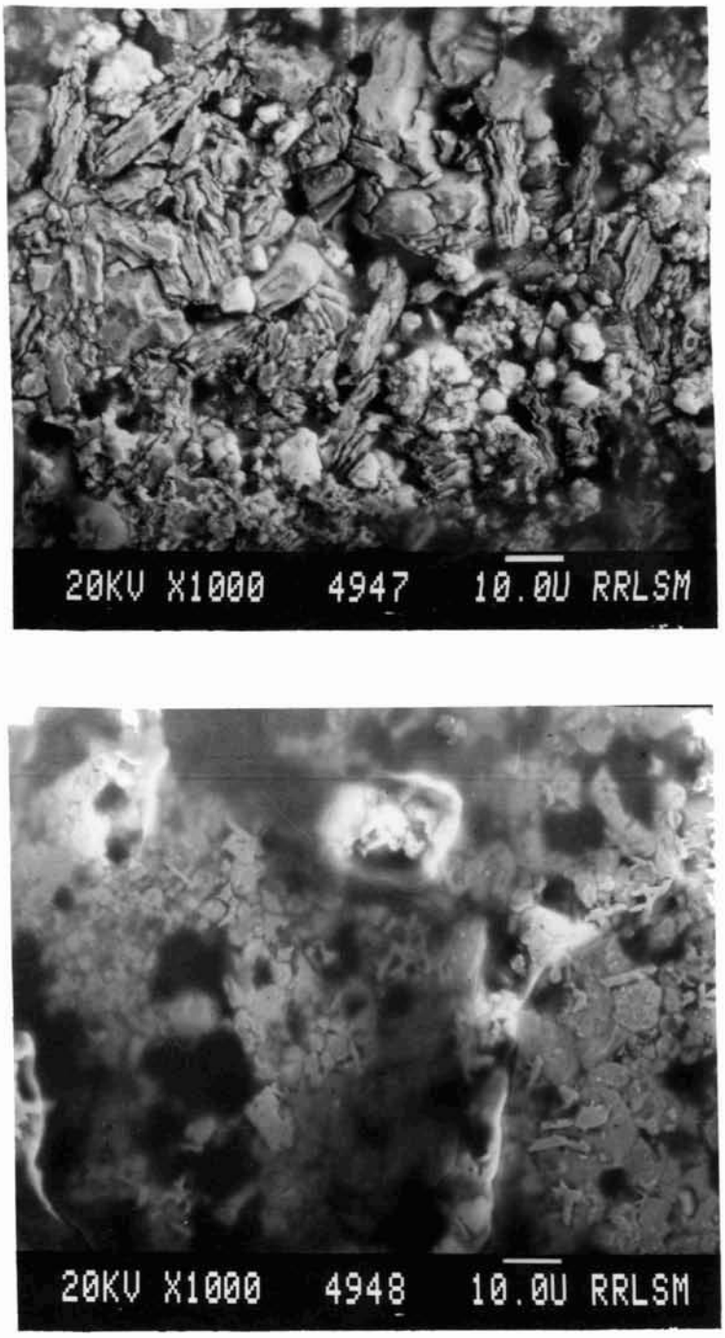

(a)

(b)

Fig. 5.15: Scanning electron micrographs for different volume ratios of BYSbO : YBCO composites
(a) 40 : 60 ; (b) 60 : 40

The samples prepared as above were used to study their normal state and superconducting properties. The densities of the composites were measured by Archimedes method and are given in Table 5.4. The densities in the higher volume side of BYZO found to be less than that of pure YBCO.

Table 5.4: Compositions of BYZO-YBCO composites with corresponding sintering temperature and densities

Vol % of YBCO	Vol % of BYZO	Sintering temperature (^{o}C)	Density (gm/cm^3)
100	0	950	5.80
90	10	950	5.85
80	20	960	5.88
70	30	970	5.90
60	40	980	5.85
50	50	990	5.75
40	60	1020	5.60
30	70	1050	5.52
20	80	1100	5.50
10	90	1150	5.52
0	100	1350	5.54

5.6.2 Resistivity of BYZO-YBCO composites

The resistivity of BYZO-YBCO composites has been measured as a function of temperature and is plotted in Fig. 5.16 for different volume ratios of composites. The composites show a metallic behaviour in their R-T curve from room temperature to the superconducting transition temperature. The composite with 60 vol % of insulator showed a superconducting transition with zero resistance at liquid nitrogen temperature whereas with 50 vol % and 30 vol % of insulating phases show superconducting transition at 92 K. Thus the superconducting percolation threshold value for BYZO-YBCO composite is around 60 vol % of BYZO in the composite (the superconducting percolation threshold is around 40 vol % of YBCO in the composite). The resistivities of composite samples with higher volume percentages of BYZO are very high and have been measured by two probe method using a Keithley electrometer.

The variation of normal state resistivity at room temperature as a function of vol % of insulating phase BYZO is plotted in Fig. 5.17. The temperature coefficient of resistance $\alpha = \frac{1}{\rho}\frac{d\rho}{dT}$ is also shown in Fig. 5.17. Both the normal state resistivity and temperature coefficient of resistivity show a variation in their magnitude at about 65 vol % of insulating phase. Thus the percolation threshold value for normal state resistivity lies around 35 vol % of YBCO below which the composite shows a higher resistance which is close to the resistivity of the insulator. The actual value of percolation threshold volume can be calculated from the percolation

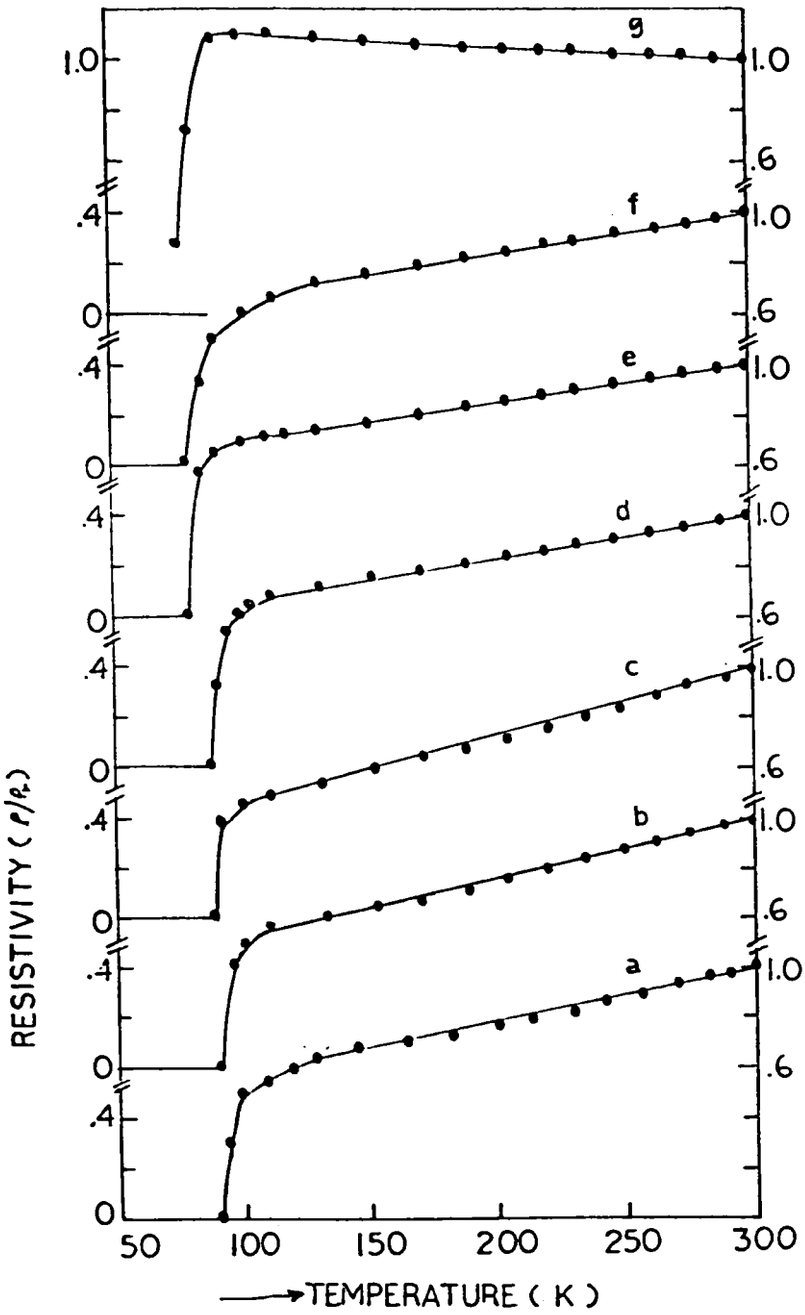

Fig. 5.16: Temperature-resistance curve of BYZO-YBCO composites for different vol % of BYZO in the system

(a) 0, (b) 10, (c) 20, (d) 30, (e) 40, (f) 50, (g) 60

All the samples showed metallic behaviour with superconducting transition above liquid nitrogen temperature upto 50 vol % of BYZO in the system. The samples with 60 vol% of BYZO showed semiconducting behaviour with superconducting transition above 77 K, but its resistance does not become zero.

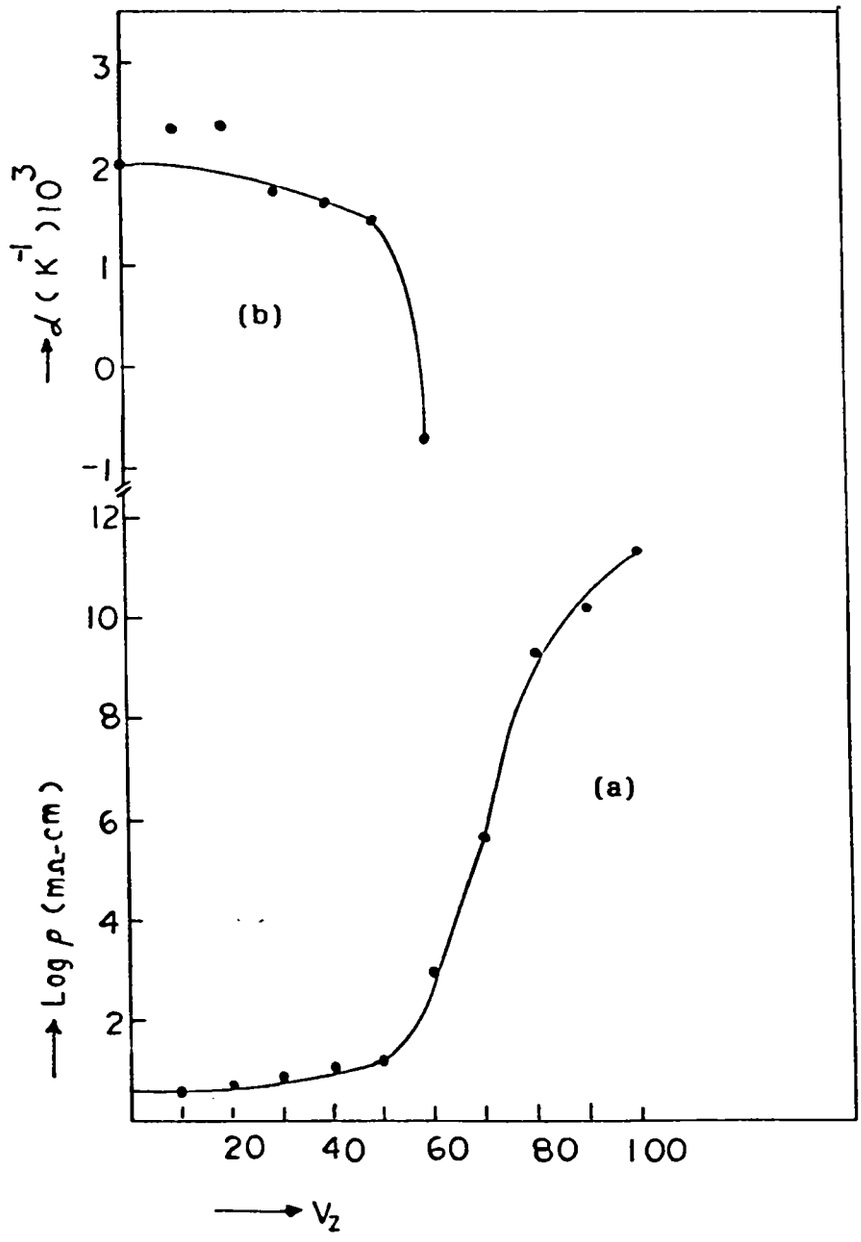

Fig. 5.17: Variation of (a) normal state resistivity , and (b) temperature coefficient of resistivity $\alpha = \frac{1}{\rho}\frac{d\rho}{dT}$ at room temperature as a function of vol % (V_z) of BYZO in the composite

model equations governing the transport properties of the composite system (refer equations 3 & 4). The percolation threshold value V_c calculated from the log-log plot of equations 3 and 4 for the BYZO-YBCO composite is 35 vol % of YBCO. The critical exponents calculated from Fig. 5.18 are

$$t = 1.70$$

$$u = 5.25$$

and the values of constants are

$$\rho_o = 3.981 \text{ ohm-cm}$$

$$\rho_o' = 1.995 \text{ ohm-cm}$$

The value obtained for the critical exponent 't' matches with that for an ideal insulator-conductor composite system whereas the value of 'u' deviates considerably. It means that for low vol % of BYZO, the processing temperatures are around 950^{o}C to 1000^{o}C and forms a good composite without losing the superconducting properties. For higher vol % of BYZO, the processing temperatures are above 1000^{o} C and at these temperatures enhanced decomposition or reaction occurs. As a result YBCO no more forms good composite with BYZO above 65 vol % of the insulating phase. Hence the deviation in the critical exponent 'u' which describes the transport properties of the composite in the higher resistivity side is justified.

5.6.3 XRD studies of BYZO-YBCO composites

The phase analysis and reactivity studies on BYZO-YBCO

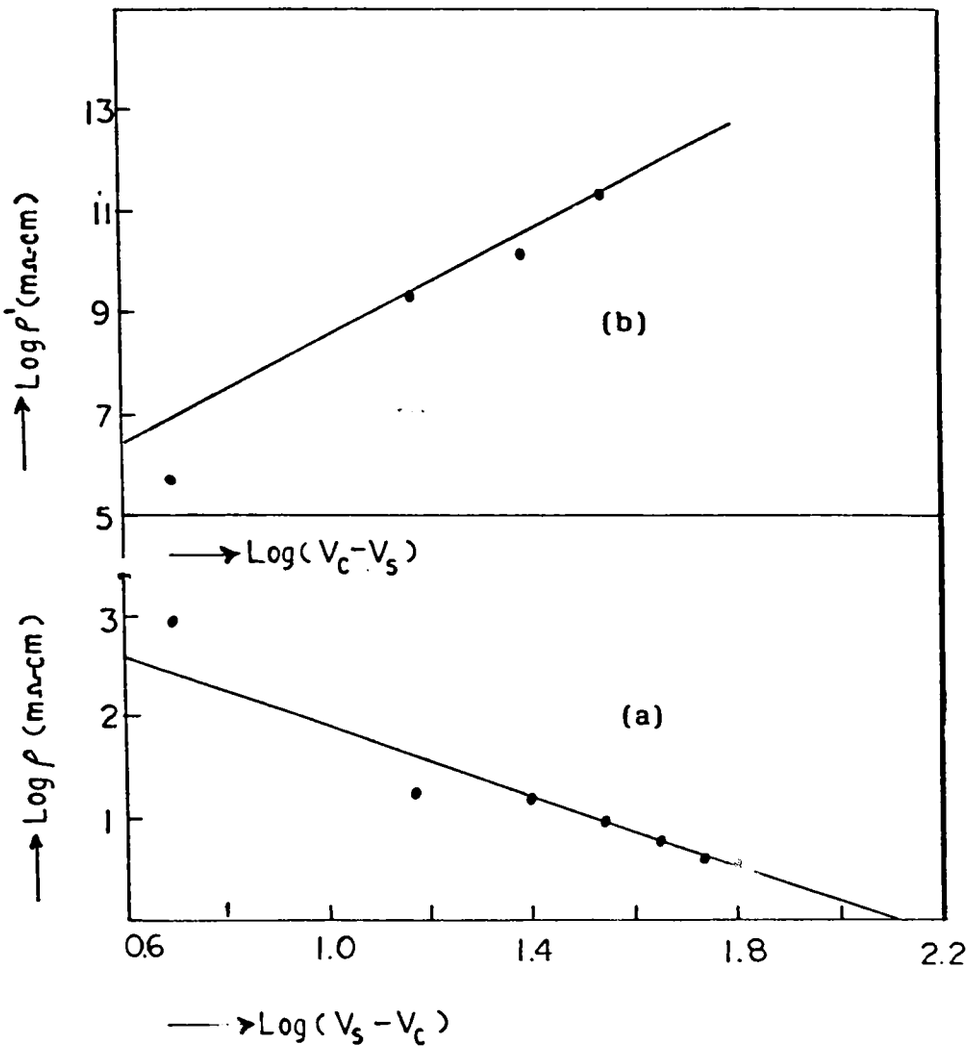

Fig. 5.18: Log-log plot of (a) ρ versus $(V_s - V_c)$ and (b) ρ' versus $(V_c - V_s)$ for BYZO-YBCO composites where ρ and ρ' are the resistivities of the composites for V_s vol % of supercnductor above and below the threshold volume V_c.

composites were carried out by x-ray diffraction technique. Figure 5.19 shows the powder diffraction pattern for different volume percentages of the composite processed as described in section 5.6.1. From the XRD patterns it is evident that for low volume fraction of BYZO, the processing temperatures are around 950-1000^{o} C and practically there is no reaction between YBCO and BYZO (see Fig. 5.19 b and c). For higher volume percentages, there is appreciable reaction between the compounds and additional peaks apart from YBCO and BYZO appear in the diffraction pattern. The additional peaks due to decomposition or reaction are primarily because of the elevated processing temperatures ($>1000^{o}$ C). Thus the x-ray diffraction studies give explanation for the R-T measurements of the BYZO-YBCO composites.

5.6.4 SEM studies on BYZO-YBCO composites

The microstructural charactors of BYZO-YBCO composites were studied by scanning electron microscopic technique. Fig. 5.20 shows the SEM pictures of BYZO-YBCO composites for different volume percentages of BYZO. The figure shows only two phases (BYZO and YBCO) for low vol % of BYZO (Fig. 5.20a) but for higher volume percentages it clearly shows additional phases (Fig. 5.20b) apart from those of YBCO and BYZO. The amount of YBCO phase seen in Fig. 5.20 b is negligible which indicates that YBCO has reacted with BYZO and destroyed its superconducting properties in agreement with the resistivity and XRD studies. Since all the YBCO has reacted with BYZO at elevated temperatures of processing ($>1000^{o}$C),

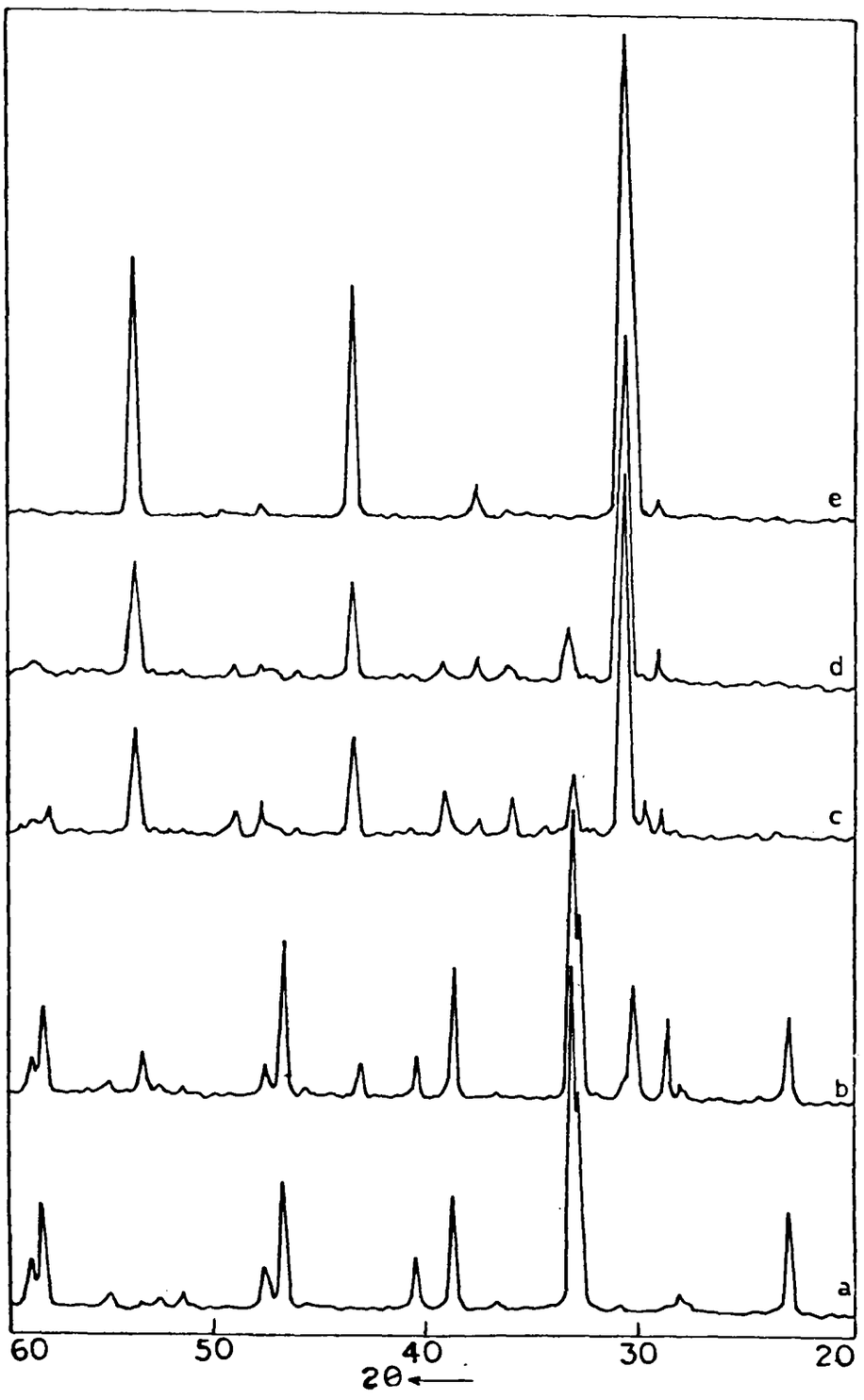

Fig. 5.19: XRD pattern of BYZO-YBCO composites for different vol % of BYZO

(a) 0, (b) 30, (c) 50, (d) 70, (e) 100.

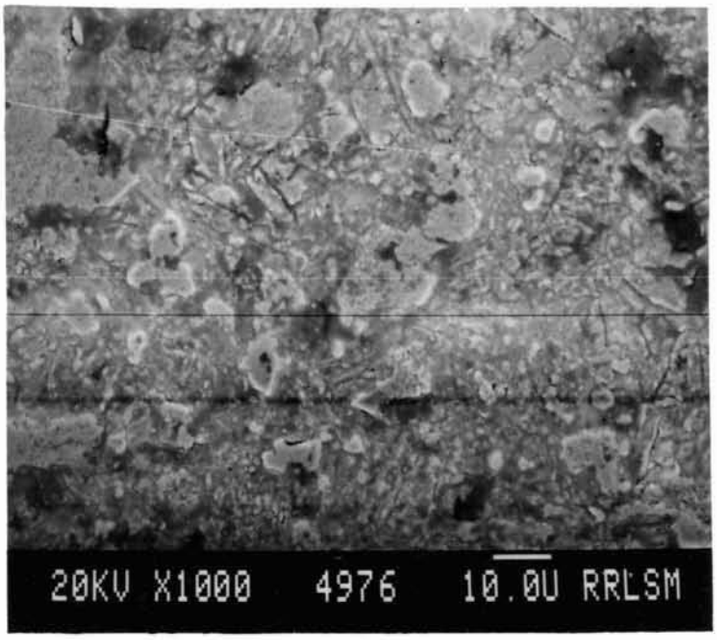

(a)

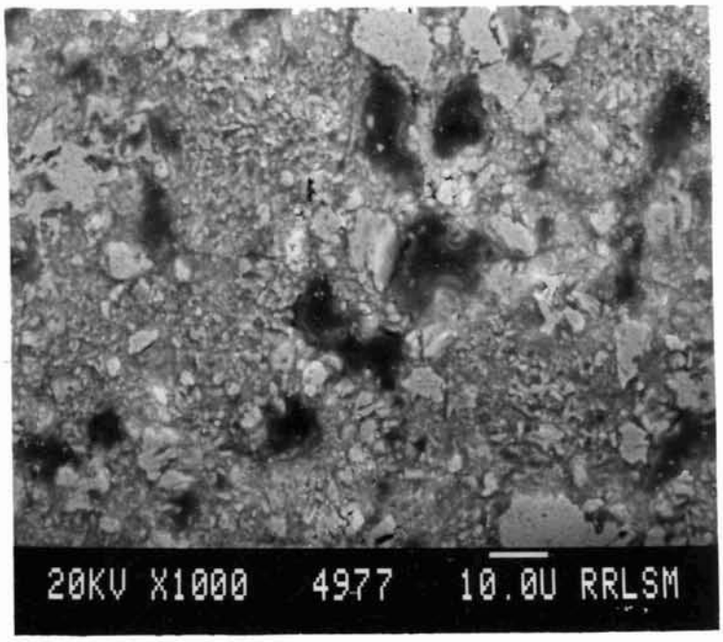

(b)

Fig. 5.20: Scanning electron micrographs for different volume ratios of BYZO : YBCO composites
(a) 40 : 60 ; (b) 60 : 40

YBCO no more forms composite with BYZO for higher vol % of BYZO in the system.

5.7 DISCUSSION

In this chapter the preparation of a new series of ceramic insulator-superconductor composites has been described. The present investigation is the first work on a ceramic insulator-superconductor composite system, prepared successfully without deteriorating the superconducting properties of YBCO. Almost all the known ceramic insulators react with the high temperature superconductor YBCO and destroy its superconducting properties. As a result there was no successful attempt to prepare a ceramic insulator-superconductor composite. There were (1-5) attempts to prepare normal metal-superconductor composites due to the non-reactivity of silver and gold with YBCO. Also there are reports (9,10) about the preparation of superlattice structures with Ag and with structurally similar compounds $PrBa_2 Cu_3 O_7$ which is a non-superconductor and has explained its implications on fundamental understanding of high T_c superconductivity through proximity effect studies (9,10). The present investigation shows a new series of compounds which forms composite with the superconductor YBCO.

The studies on BYNO-YBCO system have shown that there is no reaction between YBCO and BYNO at normal temperatures (950 ^{o}C) of processing. Even at elevated temperatures of 1000^{o} C, YBCO retains its superconducting properties without any reaction with BYNO or any decomposition by itself as in pure YBCO. The percolation

theory has been applied to the composite system to explain its transport properties by considering YBCO as a normal metal and BYNO as an insulator. The model obeys very well as in the case of a normal metal-insulator composite system. The superconducting and normal state percolation threshold values found to be in the same range which is about 17 vol % of YBCO (see Table 5.5).

Table 5.5: Comparison of critical parameters of Ba_2YAO_6-$YBa_2Cu_3O_{7-\delta}$ composite percolation systems

System	Percolation threshold volume		t	u
	Superconducting	Normal state		
BYNO-YBCO	20	17	1.675	0.375
BYSnO-YBCO	20	20	1 80	1.23
BYSbO-YBCO	40	30	1.80	10.56
BYZO-YBCO	40	35	1 70	5.25

The critical exponent 't' which describes the transport properties in the metallic side of the composite system agrees with that expected for an ideal composite system. It means that the system forms a good composite upto the threshold volume that is about 83 vol % of BYNO. However, the critical exponent 'u' which describes the transport properties in the insulating sides of the composites deviates from that of expected value and has been explained as due to the possible reaction between BYNO and YBCO at elevated

processing temperatures of 1050^{o}C and above. It means that beyond the threshold value i.e. for more than 83 vol % of BYNO, the system reacts and does not form a perfect composite.

In the case of BYSnO-YBCO composite, the percolation threshold volume is about 20% of YBCO in the system which is approximately equal to the theoretically expected value for a perfect composite system. Also the critical exponents agree with the theoretically expected value but the exponent 'u' deviates slightly and can be explained as in the case of BYNO-YBCO system. But in the case of BYSbO-YBCO and BYZO-YBCO composites, the threshold values obtained are around 35 vol % of YBCO, below which there is no superconducting grain to grain net work or in other words the composite does not show any superconductivity if the volume percent of YBCO is less than 35%. The threshold value is much higher than the expected value (17%) for a perfect composite system. Also for the composites BYSbO-YBCO and BYZO-YBCO, the percolation model has been applied to describe the transport properties. The value of the critical exponent 't' agrees with the predicted value, but the value of critical exponent 'u' deviates considerably in both the cases. The large deviation in the value of critical exponent 'u' implies that the two systems BYSbO-YBCO and BYZO-YBCO are not forming a good composite for higher volume ratios of BYSbO and BYZO, but they react and interact with YBCO and destroy the superconducting properties. But the systems form composites upto 65 vol % of BYSbO (or BYZO) where the processing temperatures are below 1000^{o}C. For higher volume percentages, the

processing temperature increases above 1000^{o} C and destroys the superconducting properties.

X-ray powder diffraction studies on the above composite systems have shown that practically there is no reaction between YBCO and BYNO or BYSnO throughout the entire volume range. Also when YBCO is processed with BYNO or BYSnO, there is no drastic decomposition of YBCO even at elevated temperatures of processing above 1000^{o} C. But in the case of BYSbO-YBCO and BYZO-YBCO, the composite systems show reaction between the two at higher volume side of insulators where the processing temperatures are about 1000^{o} C and above. However, in all the cases, there is no reaction between YBCO and the insulators for low volume sides of insulator as evident from x-ray and SEM studies where the processing temperatures are less than 1000^{o}C.

Almost all the known ceramic substrate materials react with YBCO and hence successful fabrication of thin films and patterns are difficult, even though thin films of YBCO are grown on single crystals of MgO, $SrTiO_3$ and $LaAlO_3$ with advanced and sophisticated instrumentation. Due to the non-reactivity of YBCO with the above insulating materials, it is expected that good quality films of YBCO can be deposited on substrates made of these insulators. By making use of the insulators developed in the present investigation it is possible to grow good quality films on substrate made of these ceramics. The only undesirable parameter for growing good quality films is the lattice mismatch between these compounds and YBCO.

Another possibility is the fabrication of superconducting superlattice structures of insulator/superconductor/insulator configuration made use of BYNO/YBCO/BYNO/YBCO and BYSnO/YBCO/BYSnO/YBCO structures. There were attempts to study (9, 10) the proximity effect on PrBCO/Ag/PrBCO/Ag systems and PrBCO/YBCO/PrBCO/YBCO configurations with varying modulation wavelengths (where PrBCO = $PrBa_2Cu_3O_7$) Since both Ag and YBCO as well as PrBCO and Ag are having resistivity in the metallic order, such studies will not lead to a definite conclusion, although it will give some idea about the nature of superconducting mechanism in high T_c superconductors. But studies on S/I/S/I (S = superconductor, I = insulator) configuration with suitable modulation wavelengths can provide definite conclusion about the nature of superconducting mechanism. The high reactivity of all the known insulators limits the fabrication of such superlattice structures. The present investigation suggests that such superlattice structure fabrication is possible if we utilize Ba_2YAO_6 as insulator along with the superconductor YBCO in the structure S/I/S/I.

REFERENCES

1. L. Ganapathi, A. Kumar and J. Narayanan, J. Appl. Phys., 66, 5935 (1989).

2. G. Xiao, F.H. Streitz, M.Z. Cieplak, A. Bakhshai, A. Garvin and C.L. Chien, Phys. Rev. B 38, 776 (1988).

3. B. Ropers, R. Cannet, F. Carmona and S. Flandrois, Solid State Commun., 75, 791 (1990).

4. T. Nishio, Y. Itoh, F. Ogasawa, M. Suganuma, Y. Yamada and V. Mizutani, J. Mater. Sci., 24, 3228 (1989).

5. A. Goyal, S.J. Burns and P.D. Funkenbusch, Physica C, 168, 405 (1990).

6. J.,J. Lin, Phys. Rev., B 44, 789 (1991).

7. J. Kerteszi and T. Vicsek, 53 (1982), "Sintering Theory and Practice" (Ed. D. Kolar, S. Pejovnik and M.M. Ristic) Elsevier Scientific, Amsterdam.

8. D. Stauffer, Phys. Rep., 54, 1 (1979).

9. K. Kamigaki, T. Tarashima, K. Shimura, Y. Bando and H. Terauchi, Physica C, 183, 252 (1991).

10. M.A.M. Gijs, J.B. Giesbers, F.C.M.J.M. Van Delft, C.E. Timmering, A.M. Gerrits and A. Slob, Appl. Phys. Lett., 59, 1233 (1991).

CHAPTER 6

STUDIES ON NOBLE METAL-SUPERCONDUCTOR COMPOSITE Ag-YBCO

6.1 INTRODUCTION

The discovery of high temperature superconducting transition in CuO based materials has opened new vistas for both theoreticians and experimentalists because of its high scientific and technological potential. Experimentally it is now possible to fabricate CuO based superconductors into different forms and shapes such as wires, tapes, discs, sheets, coils etc. and thin film and junction devices. The chief impediment to fabricate these materials into useful shapes is its brittleness. Commercially useful high temperature superconductors will require improvement of mechanical and electrical properties as well as thermal and environmental stabilization during service. One of the methods to toughen the ceramic is to make composite with metals. In order to improve the mechanical properties as well as to provide thermal and environmental stabilization, composites with both non-noble and noble metals have been investigated (1-5). It was found that both Au and Ag does not destroy the superconducting properties of YBCO whereas most of the other metals deteriorate the properties. Among the attempts YBCO-Ag composites seem to be promising. Silver additions enhance the environmental stability, drastically lower the normal state resistivity, and significantly enhance the J_c. The composite superconductor is easy to form and shape due to increased malleability

Preparation of superconducting wires and tapes by powder in tube method is now well established. Metal superconductor composites have the advantages of self protection from thermal run aways.

In the present investigation Ag-YBCO composites have been prepared and studied the superconducting properties as well as normal state transport properties. Percolation theory was applied to describe the transport properties of the composite in the normal state and superconducting state. Percolation theory has widely been used to explain the transport properties of normal metal-insulator composites having very high resistivity ratio of insulator to metal. In chapter 5 it has been explained the transport properties of ceramic insulator-superconductor composites having high resistivity ratio in the normal state as well as superconducting state by percolation theory. In the present case the superconductor $YBa_2Cu_3O_{7-\delta}$ and the normal metal Ag are having a low resistivity ratio at normal temperatures. Recently Lin (6) suggested a scaling factor to explain the observed deviation in the critical exponents by studying a model composite system $PrBa_2Cu_3O_7$-Ag where $PrBa_2Cu_3O_7$ is structurally similar to YBCO, but at the same time not a superconductor. In Ag-YBCO composites, both Ag and YBCO are having metallic conductivity and the resistivity ratio at room temperature is of the order of 10^3 only (6).

6.2 PREPARATION

Pure YBCO was prepared from its constituent oxides by solid

state reaction method as explained in previous chapters. The composite Ag-YBCO prepared with different vol % of Ag in the system by taking into account of the theoretical densities of Ag and YBCO. Silver nitrate was used as the source for Ag which gives better dispersion and distribution of Ag in YBCO compared to metallic Ag powder. The sample was heated to temperatures above 600^{o} C for 15 hours to decompose the silver nitrate. It was powdered again and pressed in the form of pellets by uniaxial pressing. The pellets were then sintered between temperatures from 950^{o} C to 800^{o}C for 15 hours depending upon the vol % Ag in the composite. Table 6.1 gives different volume ratios of Ag-YBCO composites with corresponding sintering temperature and density. The samples were then cooled slowly to room temperature in an oxygen atmosphere. The Ag-YBCO composites prepared as described above were studied for their superconducting properties, normal state properties and structural and microstructural properties.

Table 6.1: Different volume ratios of Ag-YBCO composites with corresponding sintering temperature and densities

Vol % of Ag	Vol % of YBCO	Sintering temperature (^{o}C)	Density (gm/cm^{3})
0	100	950	5.80
10	90	930	5.88
20	80	920	6.15
30	70	900	7.12
50	50	890	9.00
70	30	850	9.80
100	0	830	10.35

6.3 RESISTIVITY STUDIES

The superconducting transition temperature of Ag-YBCO composites was determined by resistivity measurements. Figure 6.1 shows the temperature-resistance curves for the composite with different vol % of Ag. For clarity, the normalised resistivity ρ/ρ_r is plotted against temperature in the figure where ρ_r is the room temperature resistivity. The composite samples showed a superconducting transition upto 70 vol % of Ag in the system. For higher vol % of Ag, the samples showed a metallic behaviour in their R-T curve, but there was no superconducting transition down to liquid nitrogen temperature. It means that there exists continuous net work of YBCO through the matrix of Ag if the volume fraction of YBCO is above 30%. If YBCO volume fraction is below 30%, then there is no continuous network of YBCO in the composite system and YBCO grains become finite and do not belong to the infinite cluster of particles. Thus the superconducting percolation threshold value is around 30 vol% of YBCO in the system, below which the system does not show any superconducting transition.

Normal state resistivity

The normal state resistivity of composite samples was measured as a function of vol % of Ag in the composite. Figure 6.2 shows the normal state resistivity at room temperature for different amount of Ag. Also the temperature coefficient of resistivity at room temperature is plotted in Fig. 6.2. For low vol % of Ag, the composite shows a resistivity almost equal to that for pure

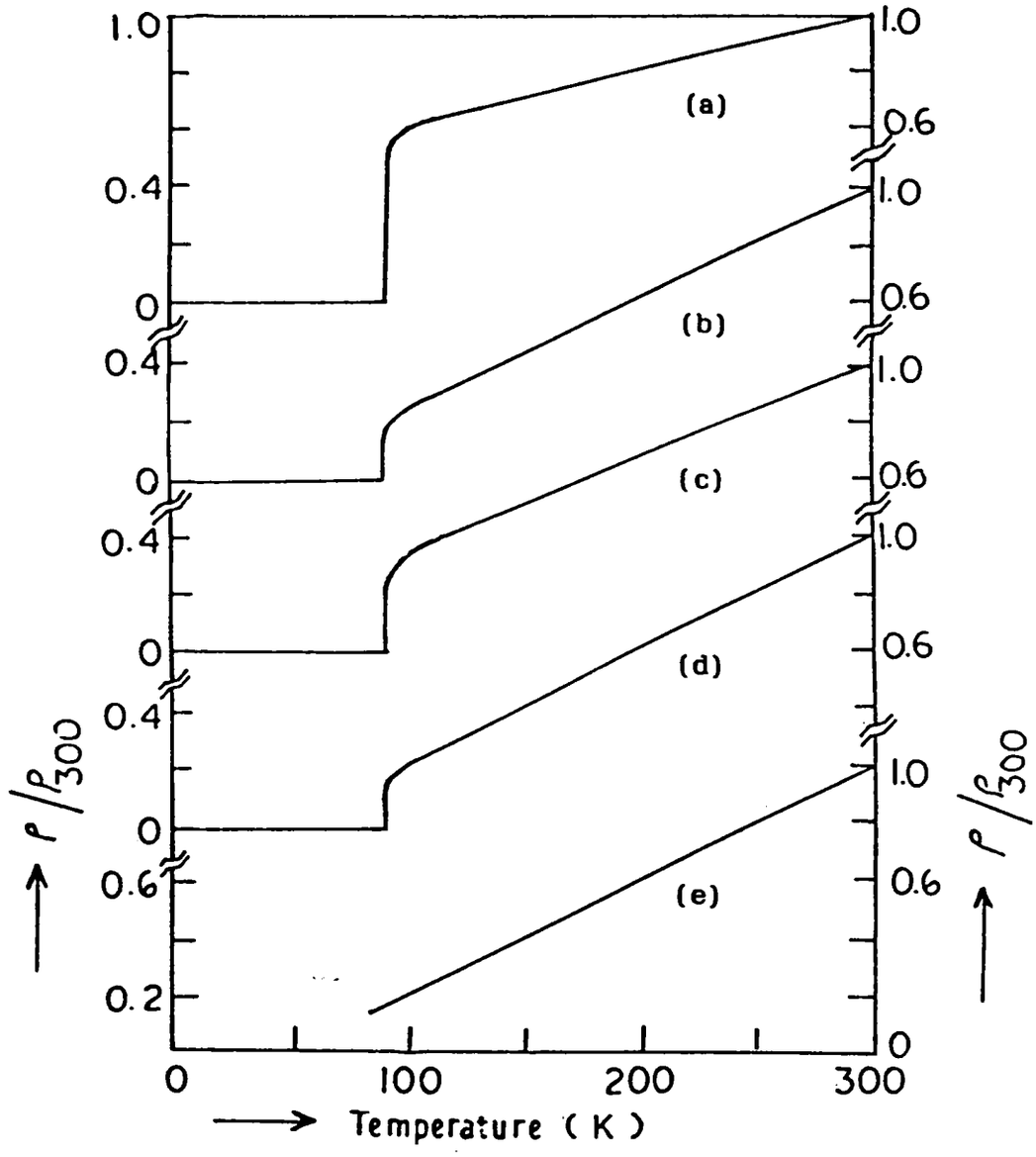

Fig. 6.1: Temperature-resistance curve of Ag-YBCO composites with different vol % of Ag

(a) 0, (b) 20, (c) 30, (d) 60, (e) 70.

For clarity the normalised resistivity is plotted against temperature in figure where the room temperature resistivity

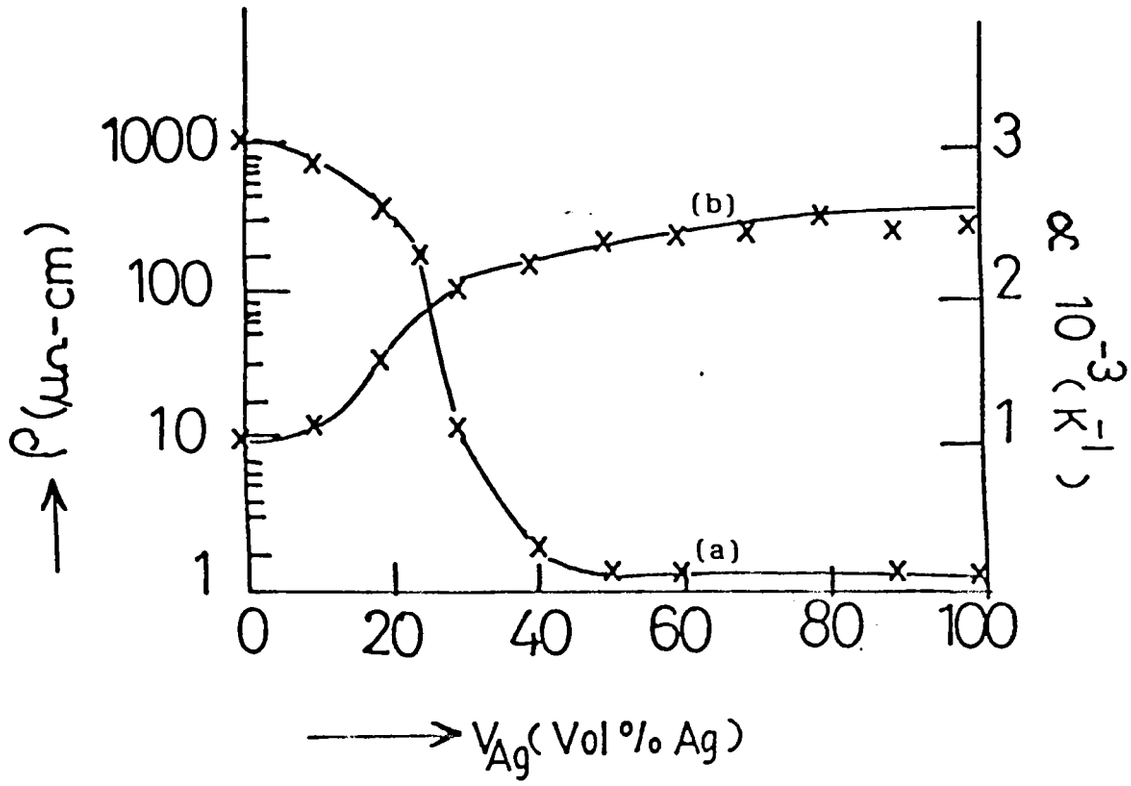

Fig. 6.2: Variation of (a) normal state (room temperature) resistivity (ρ), and (b) temperature coefficient of resistivity $\alpha = \frac{1}{\rho}\frac{d\rho}{dT}$ at room temperature as a function of vol % (V_{Ag}) of Ag in the composite

YBCO. But for higher vol % of Ag, i.e. for more than 30 vol % and above, the normal state resistivity of the composite drastically reduces to the resistivity of pure Ag. For 30 vol % and more of Ag, the silver particles belong to the infinite cluster of particles and do not belong to the finite cluster of particles. There exists a percolation system and the percolation threshold value for the normal state transport properties are around 30 vol % of Ag.

The normal state transport properties of the composite can be represented by the percolation equations (4,7,8)

$$\rho = \rho_o (V_{Ag} - V_c)^{-t} \qquad \text{for } V_{Ag} > V_c$$

$$\rho' = \rho_o' (V_c - V_{Ag})^{u} \qquad \text{for } V_{Ag} < V_c$$

where ρ and ρ' are the resistivities of the composites, V_{Ag} the vol % of Ag, V_c the threshold value at which the resistivity reduces drastically called the percolation threshold value. 't' and 'u' are the critical exponents describing the transport properties. The value of V_c is taken such that log-log plot of ρ versus $(V_{Ag} - V_c)$ and ρ' versus $(V_c - V_{Ag})$ gives straight lines. The values of V_c, t, u, ρ_o, ρ_o' obtained from the log-log plot (Fig. 6.3) are

V_c = 30% of Ag

t = 1.78

u = 0.789

ρ_o = 3.8 $\mu\Omega$-cm

ρ_o' = 2.5 $\mu\Omega$-cm

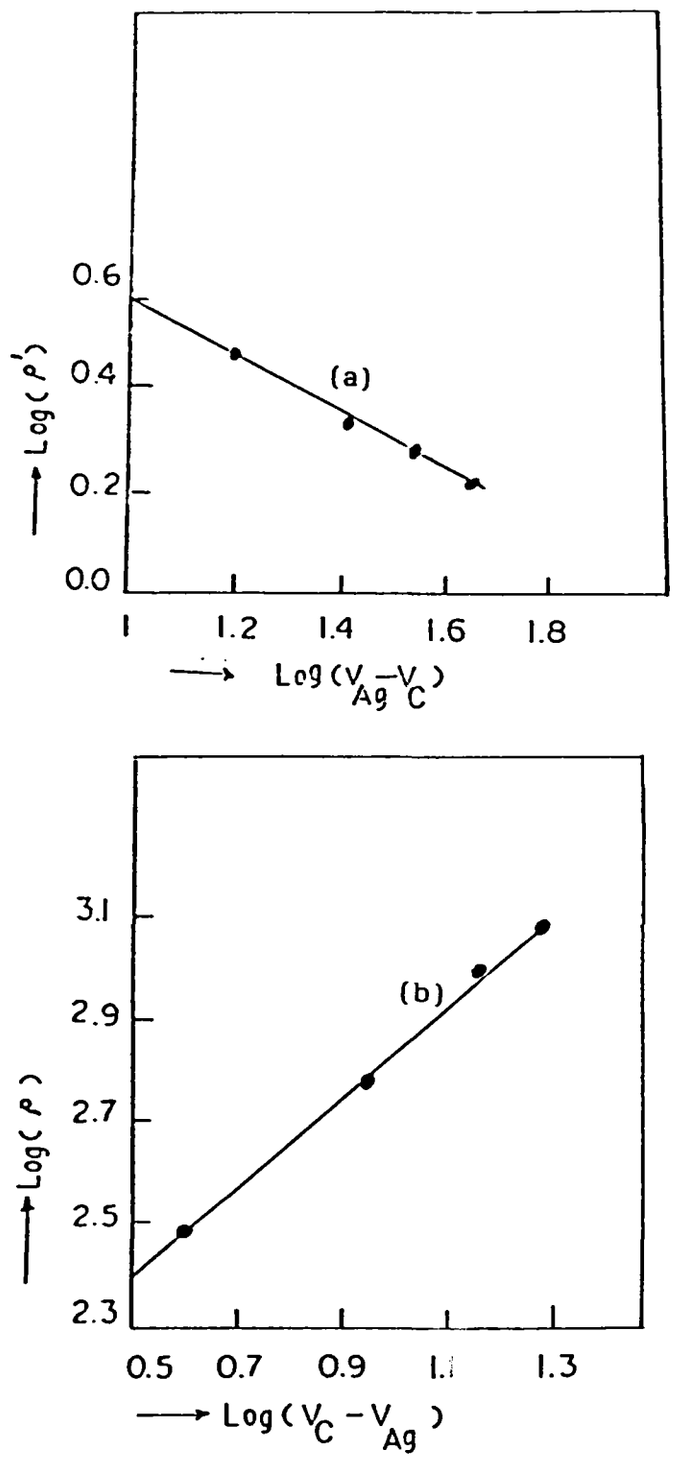

Fig. 6.3: Log-log plot of (a) ρ versus $(V_{Ag} - V_c)$, and (b) ρ' versus $(V_c - V_{Ag})$ where V_c the normal state percolation threshold volume and ρ the resistivity for V_{Ag} vol % of Ag, above and below the percolation threshold volume V_c of the composite Ag-YBCO

The values of t and u obtained for Ag-YBCO composites are nearly equal to the theoretically predicted values for a perfect composite system. The slight deviation in their values can be attributed to the low resistivity ratio between YBCO and Ag compared to insulator-metal composites. The normal state percolation threshold value is about 30 vol % of Ag or 70 vol % of YBCO in the system. Thus the superconducting percolation threshold value and normal state percolation threshold value differs. The reason for the difference is that the superconducting percolation threshold value is given by YBCO particles whereas the normal state percolation threshold value is given by Ag particles. In the normal state, the conductivity is dominated by silver particles compared to YBCO particles. As long as a minimum of 30 vol % of Ag is there in the composites, the system shows conductivity equal to that for Ag, below which the system shows conductivity equal to that for YBCO. At the superconducting state, the conductivity is dominated by YBCO grains compared to Ag particles, and as long as there exists 30 vol % of YBCO in the composite, it shows superconducting transition. Thus the percolation threshold values are dominated by YBCO for superconducting state and by Ag for normal state.

6.4 THERMOELECTRIC POWER

The thermopower of Ag-YBCO composites was measured from room temperature to liquid nitrogen temperature. The details of measurements are described in chapter 2. The variation of thermopower with temperature for different vol % of Ag are shown in Fig.6.4. All the composite samples showed same trend as that of

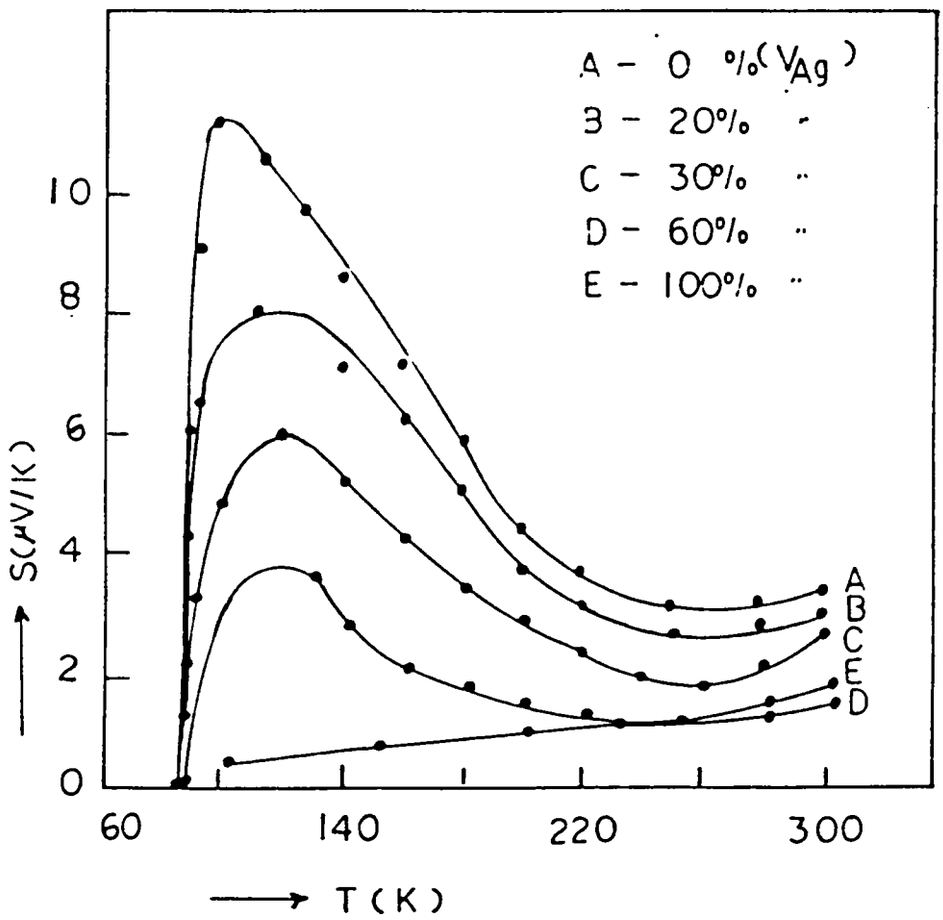

Fig. 6.4: Variation of thermopower with temperature for different vol % of Ag in the composite

pure YBCO upto 70 vol % of Ag, above which the composite does not show any superconducting transition. Thus the thermopower measurements are in agreement with the resistivity measurements. The variation in the normal state thermopower for different vol % of Ag are plotted in Fig. 6.5. The normal state thermopower showed a drastic variation in its value for about 30 vol % of Ag in the composite system. Percolation theory has applied to the normal state thermopower of the composite. The governing relations are

$$S = So\ (V_{Ag} - V_c)^{-t} \qquad \text{for } V_{Ag} > V_c$$

$$S' = So'\ (V_c - V_{Ag})^{u} \qquad \text{for } V_{Ag} < V_c$$

where S and S' are the thermopowers and t and u the critical exponents. The values of V_c, t, u, So, So' are calculated from the log-log plot (Fig. 6.6) of S versus $(V_{Ag} - V_c)$ and S' versus $(V_c - V_{Ag})$. The values obtained are

V_c = 30 vol % of Ag

t = 0.33

u = 0.285

So = 2.57 μV/k

So' = 2.82 μV/k

The values of critical exponents describing the thermopower of the Ag-YBCO composites deviate from those of theoretical values.

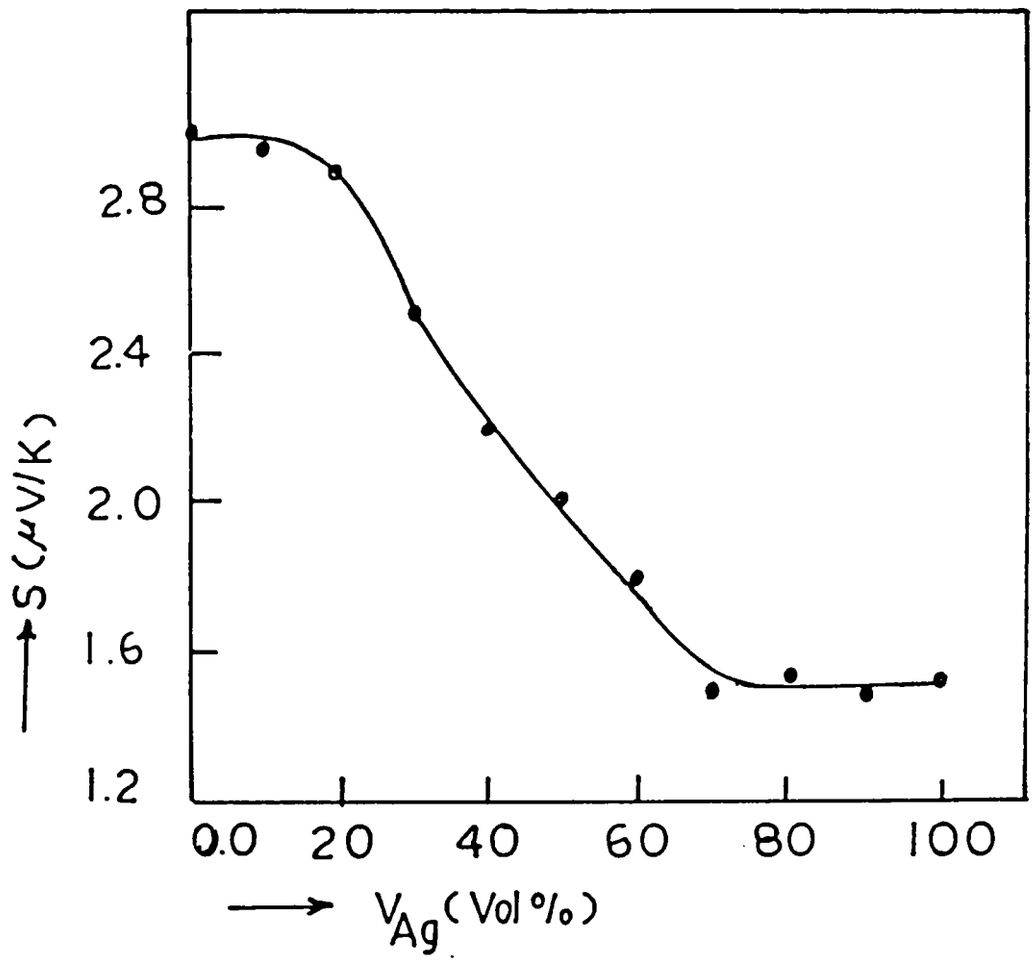

Fig. 6.5: variation of normal state (room temperature) thermopower with different vol % (V_{Ag}) of Ag in the system

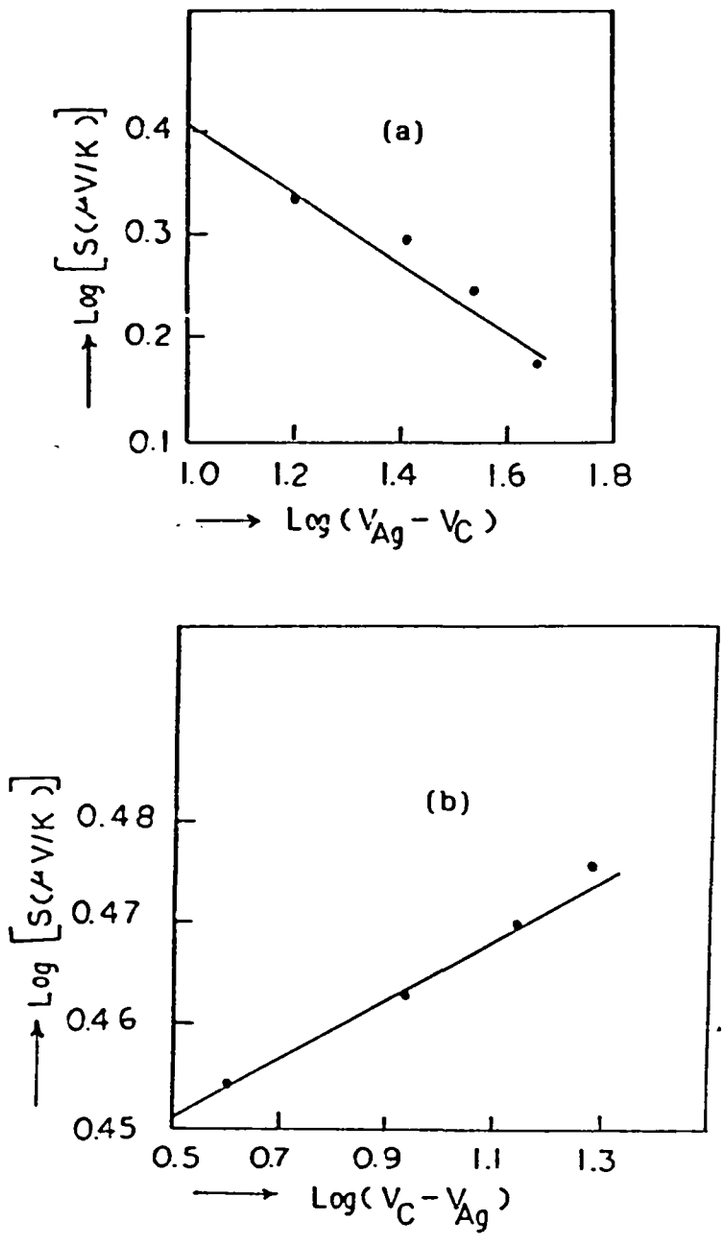

Fig. 6.6: Log-log plot of (a) S versus (V_{Ag} - V_c) and, (b) S' versus (V_c - V_{Ag}) where V_c the threshold volume and S the thermopower for V_{Ag} vol % of Ag, above and below the threshold volume V_c in the composite Ag-YBCO

The deviations in the critical exponents are mainly due to the low ratio of thermopower of YBCO to Ag.

6.5 X-RAY DIFFRACTION STUDIES

X-ray powder diffraction studies were carried out to see the different phases existing in the composite system. Figure 6.7 shows that YBCO forms composite with Ag without any reaction between them. If there is reaction between the two, then the x-ray pattern would have shown additional peaks apart from those for pure YBCO and Ag. Absence of any additional peaks indicates that there is no reaction or interaction between YBCO and Ag and form a composite.

6.6 SILVER-YBCO COMPOSITE SYSTEM: A DISCUSSION

The present investigation shows the formation of a normal metal-ceramic superconductor composite without any reaction or interaction between the two compounds. The composite showed a superconducting percolation threshold value of about 30 vol % of YBCO, both by resistivity and thermopower measurements. The normal state percolation behaviour of the composite could be explained by the percolation theory for a metal insulator composite system. In the present investigation YBCO is considered as an insulator compared to Ag. Since the ratio of resistivities of YBCO to Ag is small compared to that of insulator to metal, the system cannot be considered as a metal-insulator composite, rather it is a metal-metal composite at normal temperatures. But it is possible

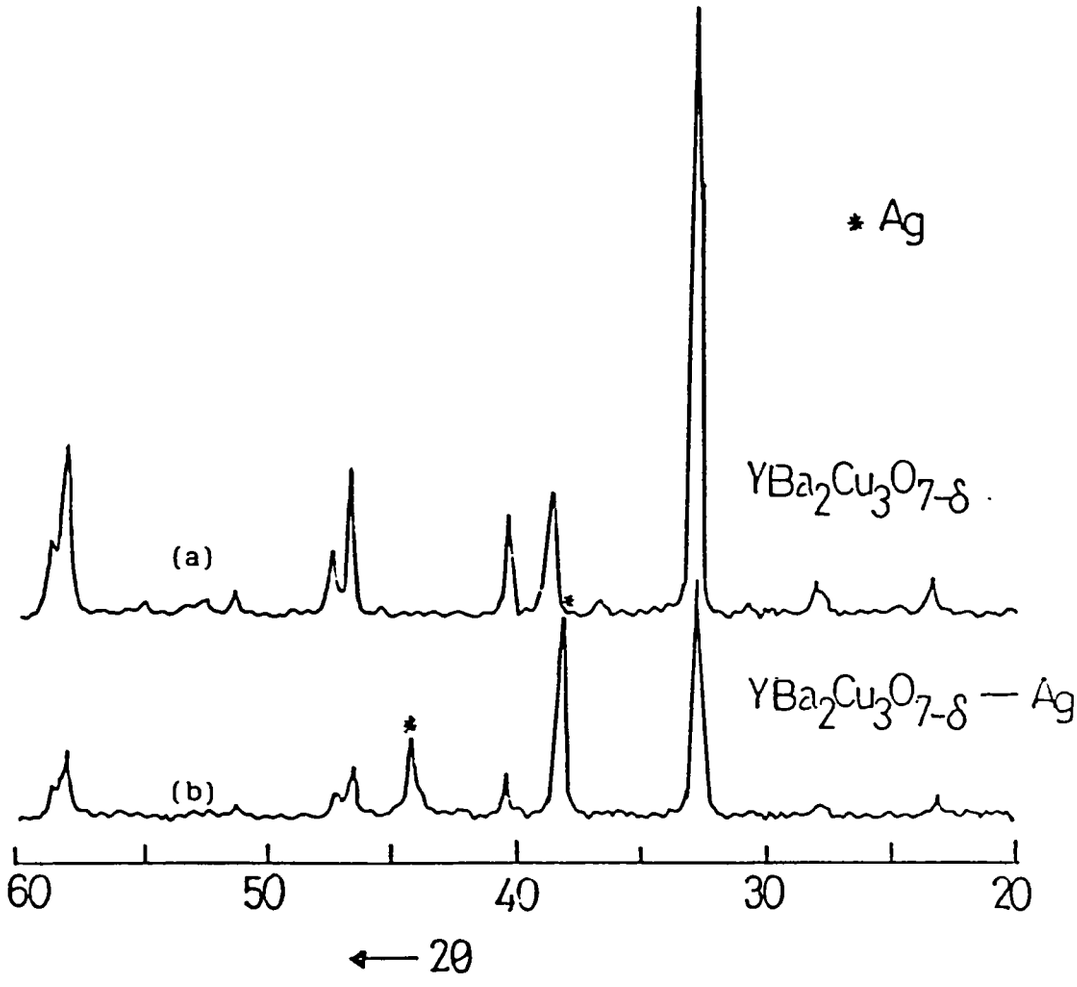

Fig. 6.7: XRD pattern of Ag-YBCO composites, (a) pure YBCO, (b) 50:50 volume ratio of composite

to explain the normal state transport properties with the percolation theory. The values of critical exponents deviate due to low resistivity ratio.

Another aspect is the sintering temperature of Ag-YBCO composites. As the volume percent of Ag increases, the sintering temperature decreases, because the melting temperature of pure silver is less than that for pure YBCO. Hence it is not sure whether there exists actual bond in betwen the superconducting grains for the composite sintered at lower temperatures with high volume % of Ag. The connectivity may be due to the metallic nature of Ag grains. Further studies are required to verify these aspects.

REFERENCES

1. A. Goyal, P.D. Funkenbusch, G.C.S. Chang and S.J. Burns, 'Superconductivity and its applications', (Ed. H.S. Kwok and D.T. Shaw), Elsevier, New York, 213 (1988).

2. S. Jin, R.C. Sherwood, T.H. Tiefel, R.R. Van Dover and D.W. Johnson Jr., Appl. Phys. Lett., 51, 3 (1987).

3. D. Pavuna, H. Berger, J.L. Tholence, M. Affronte, R. Sanjines, A. Dubas, Ph. Bugnon and F. Vasey, Physica C, 153-155, 1339 (1988).

4. G. Xiao, F.H. Streitz, M.Z. Cieplak, A. Bakhashai, A. Garvin and C.L. Chien, Phys. Rev., B 38, 776 (1988).

5. P.N. Peters, R.C. Sisk, E.W. Urban, C.Y. Huang and M.K. Wu, Appl. Phys. Lett., 52, 2066 (1988).

6. J.J. Lin, Phys. Rev., B 44, 789 (1991).

7. D. Stauffer, Phys. Rep., 54, 1 (1979).

8. J. Kerteszi and T. Vicsek, 53 (1982), 'Sintering Theory and Practice' (Ed. D. Kolar, S. Pejovnik and M.M. Ristic), Elsevier, Amsterdam.

CHAPTER 7

CONCLUSION

The thesis describes the studies on the effect of addition of certain oxides such as BeO, Nb_2O_5, Sb_2O_3, SnO_2 or ZrO_2 into the high temperature ceramic superconductor $YBa_2Cu_3O_{7-\delta}$, the resultant variations in superconducting properties like transition temperature, current density etc. and structural and microstructural variations. The studies have shown that the addition of the above oxides does not show any appreciable reduction in the superconducting transition temperature of YBCO and in certain cases the current density is increased. The crystal structure remains the same as that of pure YBCO without any observable variation in lattice parameters and shows that the above dopants are not going into the lattice sites of YBCO to an appreciable extent. Addition of a small amount of oxides (0.2 wt %) results in the formation of a secondary phase due to the reaction between YBCO and the oxides at the sintering temperature $950^{o}C$ (except in the case of BeO). It is found that Beryllium neither goes into the lattice of YBCO nor reacts with YBCO. Also it does not reduce the superconducting transition temperature.

One important observation is the enhanced oxygen absorption of YBCO due to the addition of the above dopants except in the case of BeO. The superconductor YBCO is processed at $950^{o}C$ and

at this temperature, the crystal structure is tetragonal and is a non-superconductor. While cooling from high temperature to room temperature, it absorbs oxygen from atmosphere and transforms to superconducting orthorhombic phase and oxygen absorption is a time dependent process. The doped YBCO absorbs oxygen at a faster rate, thereby even quenching from 950^{o} C to room temperature in oxygen atmosphere results in a superconducting orthorhombic phase.

Another important contribution is the identification of the secondary phases formed in YBCO due to the dopants Nb_2O_5, Sb_2O_3, SnO_2 and ZrO_2. The secondary phases are Ba_2YNbO_6, Ba_2YSbO_6, Ba_2YSnO_6 and Ba_2YZrO_6. All the above compounds are isostructural and can be represented by the formula Ba_2YAO_6 (A = Nb, Sb, Sn or Zr). The compounds Ba_2YZrO_6 and Ba_2YSnO_6 are new and have not been reported earlier and also not indexed in the JCPDS file. The compounds have been synthesised from their constituent oxides and carbonates as single phase materials by solid state reaction method and the crystal structure has been determined. Various electrical, dielectric and other physical properties were also studied. Earlier researchers have reported that the secondary phases formed due to SnO_2 and ZrO_2 as $BaSnO_3$ and $BaZrO_3$. But the present study shows that the secondary phases formed are Ba_2YAO_6 and not $BaAO_6$ and proved by studying the phase compatibility of YBCO and Ba_2YAO_6 at high temperatures (950^{o} C). Equimolar ratio of YBCO and Ba_2YAO_6 are mixed thoroughly and heated to 900-950^{o} C for 10 hours and found that there was no reaction between the two compounds and thus proved that the secondary phase formed in YBCO

due to the addition of the above oxides as Ba_2YAO_6.

Since the new compounds synthesised are found to be non-reactive with YBCO, we prepared ceramic insulator-superconductor composites using Ba_2YAO_6 as insulator. Percolation behaviour of the composites in the normal state and superconducting states have been studied by measuring the transport properties. The composites were characterised by XRD and SEM methods. The percolation studies on ceramic insulator-superconductor (Ba_2YAO_6-$YBa_2Cu_3O_{7-\delta}$) composites again show that the two phases co-exist at 950^oC to 1000^oC without any reaction between them. It again proves that the secondary phases formed in $YBa_2Cu_3O_{7-\delta}$ due to the additives Nb_2O_5, Sb_2O_3, SnO_2 and ZrO_2 are the compounds Ba_2YNbO_6, Ba_2YSbO_6, Ba_2YSnO_6 and Ba_2YZrO_6 respectively.

Almost all the known ceramic insulators react with YBCO at 950^oC when mixed with YBCO. The new compounds prepared in the present investigation are non-reactive with YBCO at 950^oC to 1000^oC. It is possible to fabricate good quality films of YBCO on substrates made of these compounds and these compounds have been suggested as promising substrates for the deposition of YBCO thin and thick films.

The ceramic superconductors are highly brittle and it is very difficult to prepare them in useful forms and shapes. For making it malleable, usually metal-ceramic composites are being prepared. Various properties of Ag-YBCO composites were studied

extensively, primarily because the reactivity is least in Ag-YBCO system. The percolation behaviour of Ag-YBCO composites were studied based on resistivity and thermopower data.

****